BIOCHEMICAL AND MECHANICAL STIMULI FOR IMPROVED MATERIAL PROPERITES AND PRESERVATION OF TISSUE-ENGINEERED CARTILAGE

A Dissertation
Presented to
The Academic Faculty

By

Tanya Mahbuba Farooque

In Partial Fulfillment
Of the Requirements for the Degree
Doctor of Philosophy in Chemical and Biomolecular Engineering

Georgia Institute of Technology

December 2008

Biochemical and Mechanical Stimuli for Improved Material Properties and Preservation of Tissue-Engineered Cartilage

Approved by:

Dr. Barbara Boyan, Advisor
School of Biomedical Engineering
Georgia Institute of Technology

Dr. Timothy Wick, Advisor
School of Biomedical Engineering
University of Alabama at Birmingham

Dr. Athanassios Sambanis
School of Chemical and Biomolecular Engineering
Georgia Institute of Technology

Dr. Athanasios Nenes,
School of Chemical and Biomolecular Engineering
Georgia Institute of Technology

Dr. Kelvin Brockbank,
Parker H. Petit Institute for Bioengineering and Bioscience
Cell & Tissue Systems, Inc.

Date Approved: October 7th, 2008

ACKNOWLEDGEMENTS

In the past five years, I have developed and learned so much that I cannot express fully my gratitude to all the people who have helped me achieve my goal. First, I would like to express my sincere gratitude and appreciation to my advisors, Dr. Wick and Dr. Boyan, as well as to Dr. Schwartz for their guidance and mentoring. Also, to Dr. Brockbank, who provided me with guidance and knowledge on the cryopreservation portion of my project. To the rest of my committee members, Dr. Nenes and Dr. Sambanis, I also wish to express my appreciation for their help in the past five years.

This work could not have been completed without the support and funding from the Georgia Tech and Emory Center for the Engineering of Living Tissues, the National Science Foundation under EEC 9731643, and Children's Healthcare of Atlanta. The code for the CFD modeling was provided by Dr. Nenes at Georgia Institute of Technology, Atlanta, GA 30332. The collagen type II monoclonal antibody developed by Thomas F. Linsenmayer was obtained from the Developmental Studies Hybridoma Bank developed under the auspices of the NICHD and maintained by The University of Iowa, Department of Biological Sciences, Iowa City, IA 52242. The animal surgeries were performed by Dr. Hunter Moyer. The histological analyses were assisted by the Center for Metabolic Bone Disease Core Laboratory at University of Alabama at Birmingham, Birmingham, AL 35294 and by Ms. Sha'Aqua Asberry in the histological lab at IBB at Georgia Institute of Technology, Atlanta, GA 30332. I would especially like to thank Mr. Andrews of the Georgia Tech Machine Shop located in ES&T and the Machine Services Department located in Hinman Building who manufactured the

bioreactors. I want to thank Johnafel Crowe who taught me confocal microscopy and helped me with my live/dead imaging. I also want to thank Dr. Nerem and Steve Woodard for their support, and for not kicking me out of my lab space in 1-D.

Graduate work is never a one-person job. I do not think I could get away without acknowledging the numerous graduate colleagues that have helped and guided me throughout the last five years. Thanks to the former members of Dr. Wick's lab, Padmini Rangamani, Lola Brown, Amanda Owings Amos, and Matt Wagner, who started me on this road and taught me the foundations of cell culture and bioreactor maintenance and provided me with the support that a first year so desperately needs when starting the intimidating process of graduate school. I also greatly appreciated the help from the Sambanis lab, who allowed me to use their mechanical freezer and were a great source of information on everything cryo. To the Nerem, Guldberg, and Levenston lab (basically everyone in wings 1-D and 2-D) who have taught me so much on cell culture and cartilage analysis. And last, but not least, I am very grateful for the support my lab mates, whose number keeps increasing that I've lost count. A special thanks to Sharon Hyzy, Jennifer Hurst-Kennedy, Zhenzhen Chen, and my URS student, Sean Connell, for their help with my numerous bioreactor feedings and cryopreservation experiments.

To Mom and Kaiser, I do not know if you realize how much of a stress reliever you were. You have always kept me grounded and seeing the big picture, even when you humored me as I discussed mathematical formulas and shear stress profiles with you. I did not think that when I entered this program, the quiet person that I was, that I would one day emerge with such confidence and knowledge, that I would get through this and

finish with better skills than when I entered. You helped me to stay focused on that. Thank you.

When I took my quals after my first semester at Georgia Tech, I remember one of the test questions was to describe a cone-and-plate viscometer. My answer? "I have no idea what a cone-and-plate viscometer is, nor how it is used to measure viscosity." Little did I know that the basic foundation of my project was based on such a device. So, with the help of many, many people, I present my thesis.

TABLE OF CONTENTS

LIST OF TABLES

LIST OF FIGURES

LIST OF ABBREVIATIONS

BR	Bioreactor
CC	Concentric Cylinder
CFD	Computational Fluid Dynamics
COMP	Cartilage Oligomeric Matrix Protein
CPAs	Cryoprotectant Agents
DEPC	Diethyl Pyrocarbonate
DI	Deionized Water
DMEM	Dulbecco's Modified Eagle's Medium
DMMB	1,9-Dimethylmethylene Blue
DMSO	Dimethyl Sulfoxide
DNA	Deoxyribonucleic Acid
EC	EuroCollins
ECM	Extracellular Matrix
EDTA	Ethylenediaminetetraacetic Acid
ERT	Estrogen Replacement Therapy
ES&T	Environmental Science and Technology
EtO	Ethylene oxide
FAK	Focal Adhesion Kinases
FBS	Fetal Bovine Serum
GAG	Glycosaminoglycan

GAPDH	Glyceraldehyde 3-Phosphate Dehydrogenase
HEPES	4-(2-hydroxyethyl)-1-Piperazineethanesulfonic Acid
HIF	Hypoxia-Inducible Factor
IACUC	Institutional Animal Care and Use Committee
IBB	Institute for Bioengineering and Biosciences
MAP	Mitogen Activated Protein
MAPK	Mitogen Activated Protein Kinases
MMP	Matrix Metalloproteinases
MSC	Mesenchymal Stem Cells
MTT	3-[4,5-dimethylthiazol-2-yl]-2,5-diphenyl tetrazolium bromide
NASA	National Aeronautics and Space Administration
NMDA	N-Methyl-D-Aspartate
NOS	Nitric Oxide Synthetase
PBE	Phosphate Buffered Saline with EDTA
PBS	Phosphate Buffered Saline
PCC	Perfusion Concentric Cylinder
PCR	Polymerase Chain Reaction
PGA	Poly Glycolic Acid
PKC	Protein Kinase C
PLGA	Poly-Lactic-Co-Glycolic Acid
PLLA	Poly-L-Lactic Acid
RNA	Ribonucleic Acid

RPM	Revolutions per Minute
RWV	Rotating Wall Vessel
TE	Tissue-Engineered
TECCs	Tissue-Engineered Cartilage Constructs
TGF	Transforming Growth Factor
TIMP	Tissue Inhibitor of Metalloproteinases
UV	Ultraviolet
VS	Vitrification Solution

SUMMARY

Articular cartilage on weight-bearing joints experiences three main forces: fluid-induced shear across the surface, perfusion through the cartilage from the surrounding fluid, and compression during motion of the joint. A new bioreactor that employs two of these forces was developed in this lab to study their effect on tissue-engineered cartilage development. The focus of this research and overall hypothesis is that bioreactors that employ both perfusion and shear will improve chondrogenesis and preservation to produce functionally relevant cartilage by modulating shear stress and introducing exogenous preservation factors. Applying both a low shear stress across the surface of cell-seeded scaffolds and perfusion through them in a perfusion concentric cylinder (PCC) bioreactor may stimulate chondrocytes to undergo chondrogenesis. Experimental data showed that the PCC bioreactor stimulated cartilage growth over the course of four weeks, supported by the appearance of glycosaminoglycan (GAG) and collagen type II, which are markers for articular cartilage. Computational fluid dynamics modeling showed that shear stress across the face of the construct was heterogeneous, and that only the center experienced a relatively uniform shear stress of 0.4 dynes/cm^2 when the outer cup of the bioreactor rotated at 38 rpm. When compared to a concentric cylinder (CC) bioreactor that employed only shear stress, the PCC bioreactor caused a significant increase in cellular proliferation, which resulted in a 12-fold increase in cell number per construct compared to 7-fold increase within the CC bioreactor. However, the PCC bioreactor had a less pronounced effect on glycosaminoglycan and collagen content with 1.3 mg of GAG and 1.8 mg of collagen per construct within the CC bioreactor and

0.7 mg of GAG and 0.8 mg of collagen per construct within the PCC bioreactor after 28 days in culture ($p < 0.05$). Our results led to an important observation that the PCC bioreactor affected cellular proliferation significantly but not extracellular matrix synthesis.

The next objective of this study focused on the PCC bioreactor to evaluate the direct role of perfusion and shear on chondrogenesis *in vitro* and *in vivo*. In the presence of perfusion+shear, cellular growth increased by 33 fold, while compared to the presence of shear alone, cellular growth increased by 11 fold ($p < 0.05$). GAG deposition per construct was not affected by either bioreactors, both producing 1.2 mg/construct by Day 28. Total collagen deposition, however, was significantly higher in the perfusion+shear bioreactor with 2.8 mg/construct, while the shear bioreactor produced 1.2 mg/construct by Day 28. The compressive and shear modulus measured showed no difference between the two bioreactors and were approximately 0.15 MPa and 0.33 MPa, respectively. However, the perfusion+shear bioreactor had a significantly higher phase angle compared to the shear bioreactor, due to greater collagen deposition per construct in the perfusion+shear bioreactor. This observation combined with the PCC versus CC study suggests that directional shear stress may influence the proliferation rate of chondrocytes, while the magnitude of shear stress may influence total collagen deposition.

A rat xiphoid chondral defect model was developed to assess *in vivo* chondrogenesis supported by tissue-engineered cartilage constructs (TECCs) grown under perfusion+shear conditions, shear only, or static conditions for 28 days. Implanted into the defect, the tissue-engineered cartilage cultured in the mechanically active

bioreactors resulted in more mature engineered cartilage over static cultured constructs after 28 days *in vivo*. This observation showed the necessity to consider mechanical forces and cell density when culturing engineered cartilage for implantation into cartilage defects.

A major challenge for cartilage tissue engineering is the development of viable preservation methods to ensure long-term "off-the-shelf" availability. The objective of the final study was to identify variables in ice-free cryopreservation by vitrification that affect cell viability of tissue-engineered cartilage and determine whether preservation could be performed in a bioreactor. TECCs were grown in a PCC bioreactor and harvested for cryopreservation studies. Traditional slow-rate freezing cryopreservation was carried out with 1 M DMSO introduced into TECCs. Vitrification experiments consisted of treatments with different formulations of the vitrification solution: VS55, VS70, and VS83, which consisted of DMSO, formamide, and 1,2-propanediol. Vitrification experiments also consisted of different methods of introduction and elution of vitrification solutions into and out of TECCs: 6 or 7 (6/7) sequential discrete steps increasing or decreasing in concentration, respectively, 4/4 sequential discrete steps, and permeation of vitrification solutions using the PCC bioreactor. The final results showed that VS70 preserved 2.2 times more viable cells than VS55 and VS55 preserved 2.8 times more viable cells than VS83. The reduction of steps from VS70 in 6/7 sequential steps to VS70 in 4/4 steps did not alter cell viability, neither did the incorporation of the PCC bioreactor to better permeate VS70 into TECCs. The highest cell viabilities reached were $47.8 \pm 5.6\%$ in the PCC bioreactor treatment, which demonstrated the need to further tailor vitrification protocols to increase cell viability and TECCs function.

CHAPTER 1

INTRODUCTION

Articular cartilage is found at the ends of bones, providing smooth movement and cushioning during movement. Cartilage degradation due to injury or disease poses a serious problem leading to decreased function and quality of life for patients. Pain and stiffness of joints occur as cartilage wears away exposing the underlying bones. The inability of cartilage to self-repair has led to a number of treatments. By the year 2030 the American Society of Orthopedic Surgeons estimates that 3.5 million total knee replacements will be needed (Pearson 2006). Total knee replacement is ultimately a costly and drastic solution to cartilage dysfunction. Alternative treatments before replacement of the joint have been tested (autologous grafts, chondral shaving, and anti-inflammatory drugs). Each has their own advantages and limitations.

A promising and long-term solution to articular cartilage degradation is the implantation of tissue-engineered (TE) cartilage constructs that can repair full thickness defects. Tissue engineering is the combined application of engineering principles and life science to develop functionally relevant tissue that can maintain and restore damaged areas (Langer and Vacanti 1993). The ultimate goal of tissue engineering is to grow healthy functional tissue *in vitro* with suitable structure and properties, which can be implanted into damaged areas, naturally healing the affected region. The challenge lies in finding the appropriate cell source, scaffold material, culture environment, and storage conditions to produce and maintain viable cartilage (Langer and Vacanti 1993; Nerem and Sambanis 1995; Hardingham, Simon et al. 2002; Ochoa and Vacanti 2002).

Biochemical signals, mechanical forces (such as shear stress, perfusion, and compression), and various other environmental cues stimulate the growth, functionality, and preservation of engineered cartilage (Blunk, Sieminski et al. 2002; Shieh and Athanasiou 2003; Saini and Wick 2004; Lee, Grad et al. 2005).

Bioreactors can provide the necessary chemical and mechanical environment to affect the kinetics and material properties of chondrocytes to produce TE cartilage. Bioreactors are systems that provide the appropriate culture and preservation environment to grow three-dimensional (3-D) tissue using biologically relevant scaffolds. The bioreactor environment can be programmed to modulate and preserve cartilage growth, especially when applying mechanical stimuli such as shear and perfusion. Cartilage, due to its avascular structure, depends heavily on mechanical forces to maintain cartilage tissue function and structure; the distribution of nutrients and other regulatory factors also serves an important role to maintain cartilage. Bioreactors also facilitate the introduction of chemical agents such as cryoprotectants for preservation to the fluid environment.

This project studied some of the fundamental issues of the bioreactor environment that will promote the development and preservation of functional cartilage. The main objective of this project was to determine whether the application of orthogonal shear during tissue growth would improve tissue quality. We hypothesized that the addition of perfusion flow orthogonal to fluid-induced surface shear on cell-seeded polymer scaffolds in a perfusion concentric cylinder (PCC) bioreactor will promote construct growth and understanding of mechanical stimulation on cartilage development. Studies include characterizing the fluid regime of the PCC bioreactor and determining the

relationship directional shear stress has on cartilage construct growth. Parallel studies include comparison of cartilage growth between the PCC bioreactor to the previously described concentric cylinder (CC) bioreactor (Saini 2001), as well as comparison of mechanical forces: perfusion and shear to shear only. In addition, methods for preserving cartilage constructs produced in the PCC bioreactor were assessed.

Therefore, the specific aims of this project were:

Aim 1. To compare the development of engineered cartilage constructs produced using two different concentric cylinder bioreactor designs.

The PCC bioreactor was designed and built in our lab (Rangamani 2005), based on a previously characterized CC bioreactor (Saini 2001). Initial studies characterized the pressure gradients, velocity, shear stress, nutrient profile, composition, and structure that occurred within the PCC bioreactor. Properties of cartilage grown in the PCC bioreactor were then characterized and compared to constructs grown in the CC bioreactor.

Aim 2. To assess the direct effects of orthogonal shear via perfusion on engineered cartilage constructs exposed to surface shear.

The PCC bioreactor was designed to employ both perfusion of fluid through the construct thickness and fluid-induced shear stress over the surface of the constructs. Growth of cartilage constructs cultured under both perfusion and shear was compared to growth in a PCC bioreactor that employed only shear. In addition, *in vivo*

chondrogenesis supported by tissue-engineered cartilage constructs (TECCs) grown under these two shear regimes was assessed in a rat xiphoid chondral defect model.

Aim 3. To identify conditions that affect cryopreservation of engineered cartilage constructs grown in a bioreactor.

Clinical use of TECCs requires consideration of long-term storage strategies. TECCs were cultured in the PCC bioreactor and different cryopreservation methods were employed to assess their effect on cell viability upon re-warming. Initial studies varied cryoprotectant agents formulation and step-wise method of introduction and elution of cryoprotectants on the harvested TECCs. The PCC bioreactor was then used to permeate cryoprotectant agents as a means to minimize handling from culture to preservation in a one-step process.

CHAPTER 2

BACKGROUND

2.1 Articular Cartilage

Articular cartilage is found in weight bearing joints. It reduces friction between two opposing bones and supports and distributes loads, relieving any pressure that could be damaging to the bones. The synovial fluid that fills the open cavity between the bones reduces the coefficient of friction over the cartilage aiding the ease of movement for the joint. The tissue is comprised of chondrocytes surrounded by an extracellular matrix (ECM) primarily consisting of proteoglycan and collagen type II (Kuettner, Aydelotte et al. 1991). Organized into a complex three-dimensional structure, cartilage is highly adapted to its mechanical environment where proteoglycan and collagen fibers interact to provide resistance to compressive and shear forces (Mow, Ratcliffe et al. 1992; Muir 1995). Cartilage, due to its avascular structure, depends heavily on mechanical forces, fluid-induced shear across the surface, perfusion of fluid through the cartilage, and compression during motion of the joint, to maintain cartilage tissue function and structure. The lack of blood vessels (which provide oxygen and nutrition), however, contributes to the limited regenerative ability of articular cartilage *in vivo* (Hunziker 2000; Imhof, Sulzbacher et al. 2000; Eyre 2002).

2.1.1 Ultrastructure

The ultrastructure and components of cartilage are responsible for its mechanical properties. Therefore, an understanding of these properties is important for producing

functional tissue-engineered cartilage (Mow, Holmes et al. 1984; Poole, Kojima et al. 2001; Laasanen, Töyräs et al. 2003; Mansour 2004). Seen in Figure 2.1, cartilage is not a homogeneous tissue but can be divided into four zones based on differences in the size, shape, amounts, and distribution of chondrocytes, proteoglycan, and collagen. Water makes up 70 - 85% of the whole tissue depending on the zone. Close to the subchondral bone is the calcified cartilage zone, which serves as the boundary between cartilage and bone. Next is the deep zone containing mostly proteoglycan with tightly packed collagen fibers oriented orthogonal to the surface and relatively little water. Cells here are aligned in columns that are perpendicular to the flow of the fluids across the articular cartilage surface. The middle zone, located between the surface and deep zone, has less proteoglycan and more collagen fibrils arranged in a mesh-like pattern (see inset in Figure 2.1). The surface zone, exposed to the fluid flow from the surrounding synovial fluid, has the least amount of proteoglycan and the most water with densely packed thin collagen fibrils organized into layers. The cells here are oval in shape and are arranged to align with the surface flow (Maroudas and Bullough 1968; Lipshitz, Etheredge et al. 1975; Mow, Holmes et al. 1984; Jeffery, Blunn et al. 1991; Eyre 2002; Mansour 2004). As a result, this zone has the highest tensile properties to accommodate the compressive, shear, and tensile forces experienced on the joints (Krishnan, Park et al. 2003).

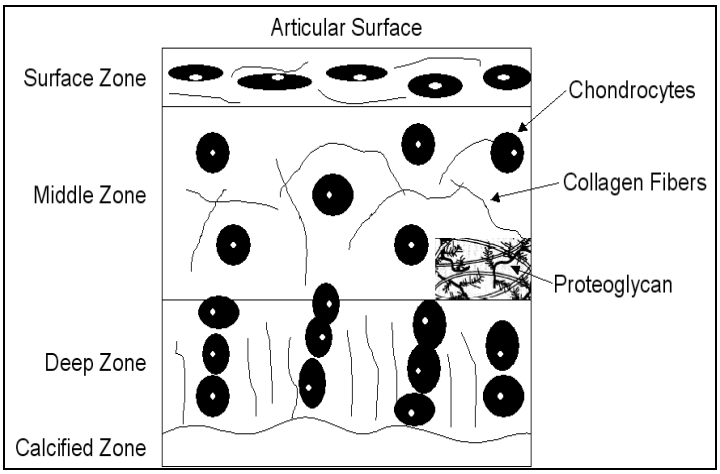

Figure 2.1. Cross section of articular cartilage, showing all zones (Saini 2001). Inset in the middle zone indicates the interaction of the collagen fibers and proteoglycan forming a mesh-like structure.

2.1.2 Chondrocytes

The cells located in cartilage are known as chondrocytes and are normally round in morphology except near the tissue surface. Chondrocytes are a differentiated cell type originating from mesenchymal stem cells (Caplan, Elyaderani et al. 1997; Alsalameh, Amin et al. 2004). Compared to other tissues, the cell density of chondrocytes is low with little cell-to-cell contact and comprises 10% of the tissue volume (Stockwell 1979). Chondrocytes are responsible for the synthesis, secretion, and organization of collagen, glycoprotein, proteoglycan, and hyaluronan composing the extracellular matrix surrounding them (Archer and Francis-West 2003). The large density of the matrix proteins protects chondrocytes from damage due to mechanical forces when cartilage is under loading.

2.1.3 Proteoglycan

Proteoglycan plays a major role in the stiffness, hydration, and pore size of cartilage. Aggrecan is the main type of proteoglycan core protein found in articular cartilage and proteoglycan aggregates comprise up to 30% of the dry weight in native tissue (Mansour 2004). Seen in Figure 2.2, proteoglycan consists of aggrecan to which glycosaminoglycan (GAG) chains attach to form a bottlebrush-like formation. The core protein consists of three disulphide-bonded globular regions (G1, G2, and G3). The G1 region is primarily responsible for interacting with the link protein and the hyaluronan backbone (Roughley 2006). GAG chains (keratan and chondroitin sulfate) covalently link in a region between G2 and G3. Chondroitin sulfate (CS) and keratan sulfate (KS) are the two main forms of glycosaminoglycan, where chondroitin sulfate outnumbers keratan sulfate twelve to one in newborn calf cartilage (Wheeless 2005). Keratan sulfate attachment is adjacent to the G2 region while chondroitin sulfate is adjacent to the keratan sulfate region ending next to the G3 region (Roughley 2006). The sulfated GAG are polysaccharide chains where CS consists of disaccharide units D-glucuronate and N-acetyl-D-galactosamine-4-sulfate or N-acetyl-D-galactosamine-6-sulfate and KS consists of D-galactose and N-acetyl-D-glycosamine-6-sulfate (Voet and Voet 2004). The proteoglycan monomers then aggregate and link to the backbone of a hyaluronic acid chain (a non-sulfated glycosaminoglycan with disaccharide units D-glucuronate and N-acetyl-D-glucosamine) via the link proteins. The resulting macromolecules seen in Figure 2.3 can weigh up to 200 million Daltons (Mow and Lai 1980; Mansour 2004).

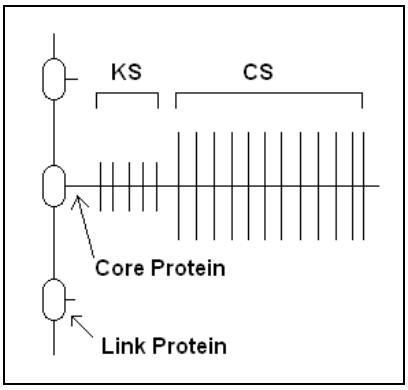

Figure 2.2. Aggrecan bound to a link protein consisting of keratan and chondroitin sulfate chains.

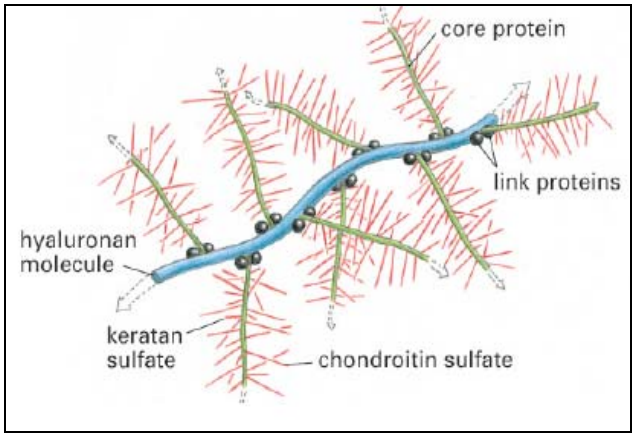

Figure 2.3. Aggrecan chains aggregated to a glycosaminoglycan chain hyaluronan (Currey 2005).

Chondroitin sulfate and keratan sulfate are negatively charged due to the sulfate and carboxyl groups. As tissue is compressed due to loading and water flows out, the resulting high concentration of negatively charged proteoglycan provides resistance to loading and adds to the stiffness in cartilage until equilibrium is achieved (Mansour 2004). Once loading has ceased, the proteoglycan creates a large osmotic swelling pressure drawing back in the water molecules. However, the macromolecular movement

is also restricted by collagen fibrils, preventing free swelling (Kuettner, Aydelotte et al. 1991). Thus, proteoglycan helps the cartilage to expand back to its original shape after loading.

2.1.4 Collagens

Collagen is a major stress-bearing component providing the tensile strength in cartilage, as well as in other collagen containing tissue. In cartilage 60 – 70% of dry weight is collagen, where type II is the dominant form (Eyre 2002; Mansour 2004). Collagen type IX and XI are also present in cartilage, but in smaller amounts (Mow, Ratcliffe et al. 1992; Eyre 2002). Type II collagen serves as a marker for differentiated chondrocytes and mechanically functional articular cartilage (Riesle, Hollander et al. 1998), whereas type I collagen presence is indicative of dedifferentiated chondrocytes into fibroblast-like cells, resulting in fibrocartilage, which cannot support weight-bearing loads. The arrangements and orientation of the collagen fibrils allow cartilage to support stress in all directions, giving the function and stability of articular cartilage.

Seen in Figure 2.4, collagen type II consists of three identical polypeptide α1[II] chains arranged in a triple helix. Collagen is unique in that a third of the amino acids in the chains are glycine (Gly) and 15 - 30% are proline (Pro) and 4-hydroxyproline (Hyp). The hydroxyproline residues are formed after the collagen polypeptides are synthesized; proline residues are catalyzed to hydroxyproline with prolyl hydroxylase, which requires ascorbic acid to maintain the enzyme's activity. The hydroxyproline's hydrogen bonds interact with water molecules to maintain collagen stability, which would otherwise denature at room temperature (denatures instead at 39ºC) (Voet and Voet 2004). Each

chain has the repeating amino acid sequence Gly-X-Y, where position X is usually Pro and Y is usually Hyp (Voet and Voet 2004). The Gly-X-Y motif is responsible for the triple helix conformation through interchain hydrogen bonding, contributing to the rigidity of the entire structure. In type II collagen, these triple helical structures then link and pack themselves in a staggered array into fibrils parallel to the fibrils' axis. This arrangement provides the tensile strength of collagen. Fibrils covalently cross-link to each other using lysine and histidine side chains and collagen type IX in order to increase collagen rigidity. The degree of cross-linking increases due to age (Riesle, Hollander et al. 1998; Voet and Voet 2004).

Figure 2.4. Collagen triple helix structure. Note the repeating Gly-X-Y amino acids (Genitrix).

Collagen type II controls the dynamic tissue response. The fibers are interspersed among the proteoglycan aggregates forming a collagen/proteoglycan network and restricting movement within the matrix, thus providing resistance and maintaining shape and form of cartilage under large forces. Under static conditions, collagen interspersed throughout the proteoglycan mesh, constantly restrains proteoglycan's swelling pressure to stabilize the cartilage matrix (Riesle, Hollander et al. 1998; Mansour 2004).

2.1.5 Cartilage Oligomeric Matrix Protein

Cartilage oligomeric matrix protein (COMP) is a noncollagenous glycoprotein found in the ECM making up approximately 1% of the wet weight of cartilage (Luan, Kong et al. 2008). The protein, 524 kDa, consists of five identical glycoprotein subunits (pentameric) each approximately 110 kDa (Hedbom, Antonsson et al. 1992). Each subunit starts with an amino-terminal domain (stabilized by disulfide bonds and the site of pentamerization) and consists of epidermal growth factor-like domains, then calcium-binding domains, and ending with a COOH-terminal globular domain, which interacts and binds with type I, type II, and type IX collagen (Holden, Meadows et al. 2001; Thur, Rosenberg et al. 2001; Holden, Keene et al. 2005). The glycoprotein consists of N-linked oligosaccharides mainly consisting of glucosamine, galactosamine, glucuronic acid, and galactose (Hedbom, Antonsson et al. 1992). The main function of COMP is in matrix assembly and organization, by influencing collagen fibrils organization and collagen type II cross-linking (Farina, Lemaire et al. 2006). COMP is down regulated when articular cartilage dedifferentiates into fibrocartilage. Fragments of COMP have been detected in the surrounding synovial fluid and cartilage of patients with knee injuries, rheumatoid arthritis, and osteoarthritis, emphasizing its role in ECM structure, maintenance, and stabilization (Zaucke, Dinser et al. 2001).

2.1.6 Cartilage Mechanics

A completely elastic material deforms under stress but returns to its original shape after load is released, while viscous materials do not stretch but flow in response to load and do not return to their original shape. The mechanical behavior of articular cartilage is

dictated by the components in the ECM and their assembly. Cartilage is composed of both solid and fluid materials, allowing the tissue to behave as compressible material, while having incompressible components. This means that under stress the cartilage deforms and "flows" to an extent, but regains its shape once the load is removed, i.e. it is mechanically viscoelastic (Laasanen, Töyräs et al. 2003; Mansour 2004).

The compressive or tensional modulus is defined as deformation of a material due to loading normal to the surface of a material. The compressive modulus for native healthy knee cartilage tissue is around 0.1 - 6 MPa for normal activities such as walking. However, pressures as high as 18 MPa have been measured in the knee joint *in vivo* during high stress activities (Hodge, Fujan et al. 1986; Mow and Guo 2002; Laasanen, Töyräs et al. 2003). Permeability is defined as the measurement of a material's ability to transmit fluids. Cartilage is regarded as impervious, with permeability constants ranging between 10^{-14} and 10^{-16} $m^4/(N*s)$ (Cohen, Chorney et al. 1994; Heneghan and Riches 2008). Dynamic modulus is defined as the deformation of a material due to cyclical loading, which can be calculated from the results of shear, compression, or tension tests. This measurement allows interstitial fluid within the cartilage to exert pressure in response to external loading instead of exuding out due to a constant static load. Physiological frequencies occur between 0.01 and 2 Hz (Park, Hung et al. 2004). Shear modulus is defined as deformation parallel to the surface of a material. For native bovine knee cartilage, the complex shear modulus is approximately 0.16 MPa at 0.01 Hz (Zhu, Mow et al. 1993). Phase angle is defined as the angle between displacement (deformation) and load. The angle is a measure of a material's viscous behavior to elastic behavior, where an elastic material's angle is zero degrees and a viscous material's is

ninety degrees. Viscoelastic materials such as cartilage fall between zero and ninety degrees. For bovine native cartilage the phase angle is approximate 15 degrees at a frequency of 1 Hz, and approximately 30 degrees at 0.1 Hz (Park, Hung et al. 2004). The ability of articular cartilage to handle both compressive and shear loading differently indicates that articular cartilage can handle multi-directional loads (anisotropic).

2.1.7 Mechanotransduction and Biochemical Conditioning

Mechanotransduction is the signaling pathway undertaken as cells respond to an external mechanical load. The mechanical loading can be in the form of hydrostatic pressure, fluid-induced shear, compression, or tension. Chondrocytes make up a small portion of cartilage with little cell-to-cell contact. Their processes do not extend far enough to reach other cells, and therefore, must rely on cell-matrix interaction for cartilage maintenance. Any type of deformation of the tissue can cause changes in pressure, osmolarity, cation concentration, interstitial fluid flow, and cell shape (Wilkins, Browning et al. 2000). In turn, the mechanical forces that cartilage experience modulate the biosynthetic and metabolic activities of chondrocytes. Mechanical stimulation within physiological range can result in increase aggrecan and collagen expression, as well as, decrease in MMP expression (matrix metalloproteinases that degrade cartilage matrix) with a net result in maintaining cartilage structure and function (Salter, Wright et al. 2004). In addition, the variation in cell shape and size throughout the different zones of cartilage are believed to be an important mechanotransducer that regulates the biosynthetic activity in each zone (Urban 2000; Hunziker, Quinn et al. 2002). For example, chondrocytes in the middle zone have up to ten times more synthetic activity

than the surface zone, suggesting variation in the matrix synthesis rate between zones (Wong, Wuethrich et al. 1996). However, little is known about how chondrocytes sense mechanical signals and translate them into a chemical response to maintain cartilage architecture and function.

A number of studies have been done to elucidate possible mechanotransduction pathways as a response to external mechanical loading. Many of the cell surface receptors (Valhmu and Raia 2002), integrins (Loeser 2002), stretch activated channels (Wright, Jobanputra et al. 1996), membrane transporters (ion channels) (Wilkins, Browning et al. 2000; Browning, Saunders et al. 2004), and transmembrane proteins, including G proteins (Erickson, Alexopoulos et al. 2001) and neural associated molecules (Salter, Wright et al. 2004), are responsible for relaying outside signals across the cell membranes (Urban 2000). Inside the cells, signaling cascades occur to regulate gene expression and metabolism for the maintenance of cartilage and its response to load. The pericellular matrix is a zone that immediately surrounds the cell surface and is the location of the cell-matrix interaction. As the extracellular matrix experiences mechanical loading, the force is transmitted to the pericellular matrix to reach the chondrocytes (Urban 2000). The pericellular environment has different amounts and types of ECM components than the matrix experiencing the mechanical loads (Orazizadeh, Lee et al. 2008).

One of the primary mechanoreceptors is the $\alpha_5\beta_1$ integrin (Millward-Sadler, Wright et al. 2000). As mechanical load is detected, this integrin activates downstream intracellular signaling, as well as changes in cytoskeleton and release of cytokines, including interleukin-4 (IL-4), thereby regulating cell shape, function, and metabolism

(Millward-Sadler, Wright et al. 1999; Millward-Sadler, Wright et al. 2000; Millward-Sadler, Wright et al. 2000). Under fluid-induced shear stress, chondrocytes in monolayer culture normally spread out and change morphology and increase proteoglycan and collagen synthesis. However, Spiteri et al. found that when the $\alpha_5\beta_1$ integrin was blocked this effect was negated, with ECM production decreasing by 75%, implicating this integrin's role in signal transduction (Spiteri, Young et al. 2008). The downstream signaling pathways include focal adhesion kinases (FAK) and mitogen activated protein (MAP) kinases, which in turn modulate transcription factors affecting gene expression for proliferation, survival, and matrix remodeling (Loeser 2002). MAP kinases are known to interact with cytokines, including interlukins and tumor necrosis factors (TNF), which can regulate matrix metalloproteinases that assist in cartilage degradation. Fitzgerald et al. showed a link between mechanical stimulation and gene expression through the MAP kinase pathway, where MAP kinase activity, aggrecan expression, and collagen type II expression increased when exposed to dynamic compression (Fitzgerald, Jin et al. 2008).

Despite cartilage's aneural structure, neural associated molecules have been found to act as mechanotransducers under applied load. Salter et al. has found that N-methyl-D-aspartate (NMDA) receptors, which is linked to Substance P (a neuropeptide) is a transmembrane protein. The receptor is activated with protein kinases (PKC and PI3K) and forms a complex to interact with actin cytoskeleton. This leads to influx in calcium and results in increase in nitric oxide synthetase (NOS) activity, which can actually decrease proteoglycan synthesis (Salter, Wright et al. 2004).

Transport pathways that allow ions and nutrients to traverse the cell membrane are influenced by mechanical stress (Mobasheri, Carter et al. 2002). As the ECM

compresses, fluid flows out, concentrating extracellular ions and nutrients, as well as drawing in cations due to the negatively charged proteoglycan. Concentrated calcium, sodium, and hydrogen ions create an electrochemical gradient, which leads to an osmotic imbalance, thus decreasing cell volume to regain osmotic balance. This in turn, can increase intracellular ions and solutes. Guilak et al. showed that changes in intracellular calcium ions occur within seconds due to mechanical deformation on cartilage (Guilak, Zell et al. 1999). Meanwhile, Wilkins et al. showed how applied pressure can stimulate the Na-H pump exchange, where the increase in cation concentration is able to up-regulate gene expression and transporter activity (Wilkins, Browning et al. 2000). Browning et al. showed that by applying hydrostatic pressure, intracellular [Ca^{2+}] increased and by applying osmotic pressure, intracellular [Na^{+}] increased (Browning, Saunders et al. 2004). Inositol triphosphate (IP_3) levels, which are secondary messengers responsible for the release of Ca^{2+} from storage organelle sacs, also increase due to hydrostatic pressure (Valhmu and Raia 2002). This phosphatidylinositol (PtdIns) pathway releases Ca^{2+} from intracellular stores, activating calcium modulated protein-dependent enzymes, which translocates to the nucleus to activate transcriptional complexes such as those on the aggrecan gene (Valhmu and Raia 2002). The end result due to this applied deformation is an increase in GAG synthesis (Valhmu and Raia 2002; Browning, Saunders et al. 2004).

Another characteristic of cartilage mentioned earlier is that the tissue is avascular, where most nutrient and waste transport occurs via diffusion through the tissue from the surrounding synovial membrane and perfusion from the subchondral bone (Imhof, Breitenseher et al. 1999; Imhof, Sulzbacher et al. 2000; Archer and Francis-West 2003).

The lack of blood vessels creates a low oxygen tension (1 - 3%) to which cells have adapted well to by undergoing glycolysis for their energy needs (Brighton and Heppenstall 1971; Rajpurohit, Koch et al. 1996; Archer and Francis-West 2003). Reduced oxygen tension increases GAG production and retention in engineered cartilage (Saini and Wick 2004). Reduced oxygen tension has also been shown to up-regulate aggrecan and collagen type II expression (Murphy and Athanassios 2001; Wernike, Li et al. 2008) and down-regulate collagen type I expression (Wernike, Li et al. 2008). Grimshaw and Mason in particular showed that chondrocytes cultured under low oxygen tension had anabolic genes up-regulated including TGF-β and other growth factors, as well as increased levels of TIMP-1 (inhibits the degradation of the ECM) (Grimshaw and Mason 2001). The pathway to elicit gene expression response (including energy metabolism, cell proliferation, and ECM production) to low oxygen tension is possibly regulated through the activation of the transcriptional complex hypoxia-inducible factor-1 (HIF-1), due to an increased expression of HIF-1α under hypoxic conditions (Coimbra, Jimenez et al. 2004).

Figure 2.5 shows a diagram giving a summary of the possible mechanotransduction pathways that occur within cartilage. The conclusion drawn from these studies suggests that not one single pathway is directly responsible for translating mechanical signals to chemical responses. Instead, the various mechanotransduction pathways most likely act sequentially or parallel with each other, combining at certain steps or acting separately from each other eliciting different biosynthetic responses. Clearly, this is a field of study that needs further expansion. Understanding pathways

allows better control of mechanical stress in order to elicit the regulation of desired biosynthetic and metabolic activities.

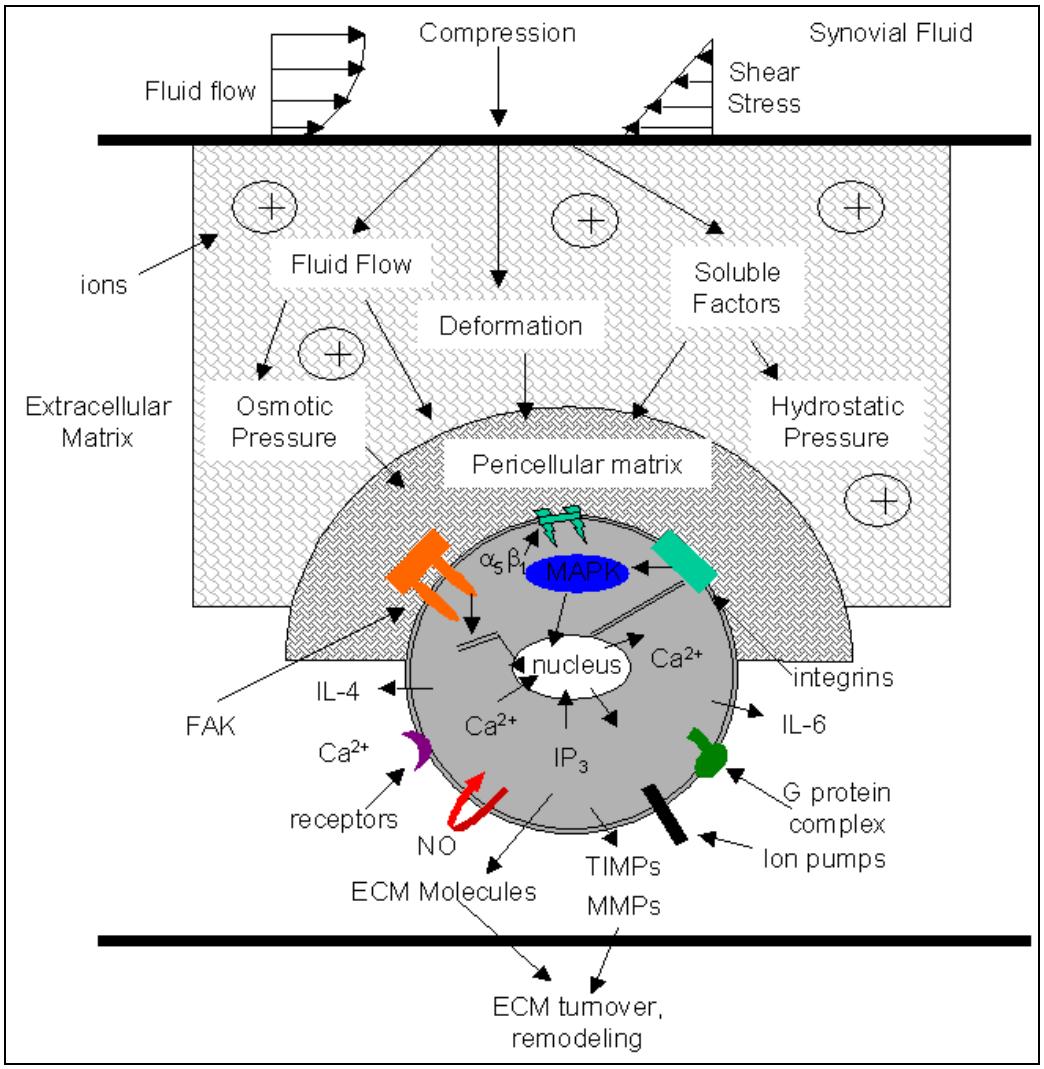

Figure 2.5. Schematic of the mechanotransduction pathways due to loading of the cartilage tissue. Mechanical deformation leads to an increase in fluid flow expulsion creating osmotic imbalances surrounding the cell. Concentration of ions leads to increase in intracellular Ca^{2+}. Load signals are transduced through integrins, receptors, G protein complexes, focal adhesion kinases (FAK), and mitogen activated protein kinases (MAPK). Secondary messengers such as calcium ions and inositol triphosphase (IP_3) affect transcription, regulating ECM and function. Mechanical load can cause release of nitric oxide (NO), ECM components, cytokines (interlukins (IL)-4 and -6), and tissue inhibitors of metalloproteinases (TIMPs) as well matrix metalloproteinases (MMPs). Figure adapted from Urban (2000) and Loeser (2002).

2.2 Cartilage: Injury, Repair, and Treatments

Healthy cartilage is a balance between degradation and synthesis processes. Cartilage injuries and diseases begin when the catabolic pathways overtake synthesis. The most commonly known cartilage disease is the degenerative osteoarthritis. Traumatic injuries such as blunt trauma or cartilage fractures can lead to the degradation of cartilage as well. Cartilage fractures can occur with injuries to the surface or below originating from the subchondral bone and can occur when bones are forced to move under high impact forces. This leads to necrosis in the region of injury, and the inability of cartilage to repair effectively can lead to decrease cartilage function and eventually progress to osteoarthritis (Frenkel and Di Cesare 1999). Sport activities and trauma injuries can be a common source of these blunt traumas and fractures due to repetitive high impact loading.

2.2.1 Osteoarthritis

In 2005 approximately 46.4 million Americans were diagnosed with some form of joint disorder, the most common of which was osteoarthritis (National Center for Health Statistics 2007). After the age of 50 a significant gender disparity exists, where women affected by osteoarthritis outnumber men. The disparity increases further with advancing age (Cecil and Archer 1925; Felson and Nevitt 1998; Richette, Corvol et al. 2003).

Osteoarthritis is characterized by the slow wearing away of the articular cartilage in weight bearing joints, such as the knee or hip. As the cartilage wears away, fibrillations and cracks appear in the once smooth articular surface. Attempts at self-repair are limited by the avascular nature of cartilage, and results in the formation of

fibrocartilage that has poorer mechanical function and lacks long-term stability compared to healthy tissue (Hunziker 2000; Imhof, Sulzbacher et al. 2000; Eyre 2002). The disease starts with the chondrocytes attempting to repair the damaged and frayed extracellular matrix by remodeling the damaged matrix, but the limited regenerative capability hinders such self-repair. By then, pro-inflammatory cytokines such as IL-1 and TNF-α are up-regulated, this in turn releases matrix metalloproteinases responsible for cartilage erosion (Fernandes, Martel-Pelletier et al. 2002). In osteoarthritis patients, nitric oxide levels are higher than average, also indicating degradation, since NO is also responsible for cartilage breakdown (Yasuda 2006). Unable to keep up the matrix synthesis rate to repair the damaged matrix, enzymes, such as the matrix metalloproteinases and aggrecanases that digest the matrix, overtake and result in tissue degradation (Frenkel and Di Cesare 1999; Caterson, Flannery et al. 2000; Roughley 2001). The continuous and eventual wearing away of cartilage leads to full thickness defects. The complete degradation of cartilage exposes the underlying bone, increasing inflammatory responses, painful swelling, thickening of the subchondral bone, and stiffness of the joint for the patient (Brittberg, Lindahl et al. 1994).

2.2.2 Repair and Treatments

Current treatment options include anti-inflammatory drugs, hormone replacement therapy, chondral shaving, mesenchymal cell regeneration, autologous grafts, and total hip or knee replacement. Anti-inflammatory drugs mainly serve as pain relievers without treating the cause, merely blocking the enzymes responsible for pain. A treatment geared towards the gender disparity that exists for osteoarthritis patients is hormone replacement

therapy for post-menopausal women (Zhang, McAlindon et al. 1998). In the Framingham study, some postmenopausal women who partook in estrogen replacement therapy (ERT) showed less symptoms of osteoarthritis compared to women who did not take ERT (Zhang, McAlindon et al. 1998). Chondral shaving refers to shaving down the rough and fibrillated cartilage to a smooth surface to allow friction-free movement. The method can treat large defect areas; however, the treatment provides only temporary relief without regenerating tissue, leaving less cartilage than before to provide normal function. Mesenchymal stem cells are precursors to chondrocytes and have the ability to differentiate into chondrocytes when exposed to the right environment (such as solutions containing transforming growth factor-beta). Implantation of mesenchymal cells into cartilage defects is limited by regenerated tissue that is less stiff and more permeable than native tissue (Kim, Moran et al. 1991; Wakitani, Goto et al. 1994). Osteochondral grafts are transplantations of cartilage and bone typically from the same patient in a non-weight bearing region and grafted to the cartilage defect. But, because this tissue is from a non-weight bearing region, it may not have the same properties and composition as the affected region. Also, implantation of osteochondral allografts risks disease and low cell viability post grafting (Minas and Nehrer 1997). The most drastic treatment of osteoarthritis is total knee or hip replacement with prosthetics. This method is typically reserved for older patients who do not lead an active lifestyle where a prosthetic can limit mobility.

A common treatment especially for the initial stages of osteoarthritis is moderate exercises such as walking. This treatment provides regular mechanical stimulation to the articular joint and improves nutrient transport as fluid is forced through the cartilage,

ultimately slowing degradation. In a four-month trial Roos et al. showed that patients at risk of osteoarthritis who started moderate exercises showed an increase in cartilage GAG content than those who were not given a supervised exercise regiment (Roos and Dahlberg 2005). Even intense exercises for patients showed that within three weeks they improved in mobility, function, and lessened in pain (Bulthuis, Drossaers-Bakker et al. 2007). The role of mechanical stimulation for arthritis highlights the role mechanical forces play in maintaining cartilage function and composition.

Many of these treatment options treat only the painful symptoms and small lesions, but not the underlying cause, nor do they offer any long-term successful repair. Research in tissue engineering to provide cartilage constructs suitable for implantation is seen as a viable long-term treatment for cartilage defects (Freed, Vunjak-Novakovic et al. 1993).

2.3 Tissue Engineering

A promising and long-term solution to cartilage degradation is the implantation of tissue-engineered (TE) cartilage constructs that can repair full thickness defects. The ultimate goal of tissue engineering is to grow healthy functional tissue *in vitro* with suitable structure and properties, which can be implanted and integrate into damaged areas, naturally healing the affected region. The challenge lies in finding the appropriate cell source, scaffold material, culture environment, and storage conditions to produce and maintain viable cartilage (Langer and Vacanti 1993; Nerem and Sambanis 1995; Hardingham, Simon et al. 2002; Ochoa and Vacanti 2002). Biochemical signals, mechanical forces (such as shear stress, compression, and perfusion), and various other

environmental cues stimulate the growth, functionality, and preservation of engineered cartilage. Bioreactors provide the necessary chemical and mechanical environment to affect the kinetics, material properties, and preservation of chondrocytes to produce cartilage. The method for growing tissue-engineered cartilage can be visualized as flow chart, where cells are seeded onto scaffolds implanted into bioreactors. While in the bioreactors, the seeded scaffolds are stimulated under the right environment for a set culture period. After the cartilage is harvested they undergo preservation for long-term storage or implantation into cartilage defects. The bioprocess is illustrated in Figure 2.6 where the end result is to market tissue-engineered cartilage constructs that are suitable for implantation.

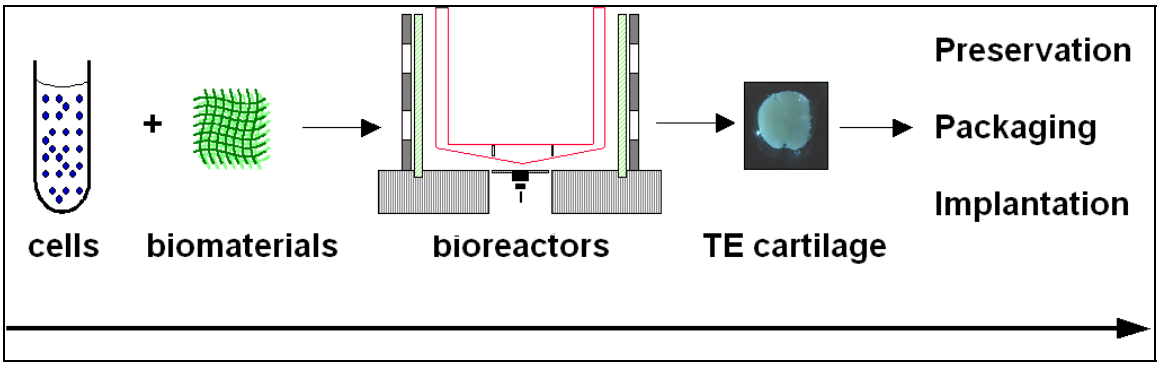

Figure 2.6. Bioprocess schematic for tissue-engineered cartilage constructs. Cells are seeded onto scaffolds and cultured in a bioreactor. Harvested constructs are preserved, packaged, or implanted into defects.

2.3.1 Cell Sourcing

The source of cells used affects the growth, function, and properties of tissue-engineered cartilage. Besides chondrocytes as a cell source for engineering cartilage, mesenchymal progenitor cells, precursors to the differentiated chondrocytes, have also

been studied, and when given the right signals can differentiate into chondrocytes (Martin, Shastri et al. 2001; Sharma and Elisseeff 2004; Marion and Mao 2006). Adult stem cells are seen as a reservoir of cells found in the body and can be removed by minimally invasive means to potentially heal any tissue, such as bone and cartilage.

The age of the chondrocytes is also a concern where adult chondrocytes have slower growth rates and metabolic activity than those from immature sources (Adolphe, Ronot et al. 1983). Even within adult cells, proliferation is affected by the donor's age. Barbero et al. were able to show that between the ages of 20 and 90 cell proliferation rate decrease by 50%. However, by adding a combination of growth factors to the culture media the proliferation rate in the same age range decrease only by 30% (Barbero, Grogan et al. 2004). Thus, while limitations may occur due to the source of cells used, they can possibly be overcome by culturing them under the right environment.

This lab focuses on bovine chondrocytes, but other animals such as pigs and goats have also been used mainly due to the large number of cells harvested from a single source (Passaretti, Silverman et al. 2001; Slivka, Neil C. Leatherbury et al. 2001). However, animals vary in their proliferation and differentiation behavior, which means that using animal models to predict the behavior of human chondrocytes may not be entirely accurate (Giannoni, Crovace et al. 2005).

2.3.2 Biomaterials

Scaffold materials need to provide the three-dimensional support to promote cell attachment, maintain their differentiated phenotype, minimize diffusional constraints for nutrient transfer, promote and support proliferation and matrix growth, and degrade at a

rate comparable to ECM synthesis rate in order to produce cartilage similar in structure and function of native tissue (Saini 2001). Some biomaterials can be woven into a mesh-like structure, which have the advantage of directing cartilage growth into a structure similar to the ultrastructure of native cartilage. Natural polymers such as collagen, fibrin, silk, cellulose, and alginate have advantages such as ease of cell attachment and non-toxic fragments when degraded into the body, lessening the possibility of an inflammatory response. The fibers in collagen scaffolds also provide a matrix similar to native cartilage. Disadvantages in natural polymers lie in finding the right source, maintaining sterility, and difficulty in processing (Stoop 2008). Biodegradable synthetic scaffolds, such as poly-l-lactic acid (PLLA), poly-glycolic acid (PGA), and copolymers of these two (PLGA), have advantages over natural polymers in terms of biocompatibility, controllable degradation rate, strength, and ease of processing (Cima, Vacanti et al. 1991; Temenoff and Mikos 2000). They can be processed into different shapes, composition, strength, and porosity to provide a large surface area for cell attachment and proliferation (Saini 2001). Studies have shown that chondrocytes attached to these polymers retain their differentiated cell function, multiply, and create cartilage in the shape of the scaffold (Vacanti, Langer et al. 1991; Kim, Vacanti et al. 1994). One of the disadvantages in using synthetic scaffolds is the rise in pH when degraded into their acidic fragments causing possible inflammatory responses in the host (Stoop 2008).

High seeding density maintains important cell-to-cell interactions that influence proliferation, matrix synthesis, and differentiation (Watt 1988). Cell seeding density studies showed that scaffolds seeded at high densities maintained their differentiated

phenotype secreting more ECM, while those at low densities contained less ECM (Bruckner, Horler et al. 1989; Vunjak-Novakovic, Obradovic et al. 1998). In another study by Puelacher et al., constructs seeded with less than $20x10^6$ cells/cm^3 created more fibrous and inferior cartilage (Puelacher, Kim et al. 1994). Additional studies in bioreactors showed significantly more ECM content per construct when seeded at $34x10^6$ cells/cm^3 or $43x10^6$ cells/cm^3 than when seeded at $26x10^6$ cells/cm^3 (Saini 2001). With suitable scaffold materials and a high seeding density, the growth of TE cartilage is then influenced mainly by its environment, i.e. bioreactor conditions.

2.3.3 Bioreactors

Bioreactors provide the appropriate culture environment to grow three-dimensional tissue using biologically relevant scaffolds. The bioreactor environment can be programmed to modulate and preserve cartilage growth, especially when applying mechanical stimuli such as shear, perfusion, and compression. The premise that those mechanical and chemical stimuli that modulate chondrocytes' behavior *in vivo* will also influence their behavior *in vitro* (Saini and Wick 2003; Sharma and Elisseeff 2004) has led to a number of studies showing that seeded scaffolds are influenced by their surrounding environment, stimulating chondrogenesis and matrix synthesis (Freed, Vunjak-Novakovic et al. 1993; Vunjak-Novakovic, Freed et al. 1996; Pazzano, Mercier et al. 2000; Davisson, Kunig et al. 2002; van Osch, Mandl et al. 2002; Darling and Athanasiou 2003; Saini and Wick 2003). Bioreactors allow changes in the culture environment to affect the kinetics and properties of the tissue grown, where a well defined fluid regime can elucidate mechanotransduction pathways to understand the

relationship between mechanical forces and kinetics of chondrocytes. To understand and identify the relationship between culture conditions and tissue properties that achieve suitable cartilage growth in a bioreactor requires knowledge of the interaction between cell behaviors and their mechanical and chemical stimuli (Runstadler 1992).

As stated previously, healthy native cartilage is avascular and well suited to carry out normal metabolic activities under low oxygen tension. Such observation has led to a number of *in vitro* studies showing positive effects on chondrogenesis under low oxygen levels compared to normal levels. For example, passaged chondrocytes in alginate lost their characteristic phenotype markers, but regained them when cultured in 5% oxygen with an increase in collagen type II and aggrecan expression when compared to 20% oxygen (Murphy and Athanassios 2001). Additional studies in bioreactors showed that engineered cartilage cultured under 5% oxygen tension demonstrated a significant increase in GAG content (Saini and Wick 2004). These studies demonstrate that an *in vivo* characteristic of cartilage, low oxygen tension, can be an important bioprocessing factor in the *in vitro* development of cartilage.

Monolayer studies have shown that fluid shear at 35 dynes/cm^2 up-regulates chondrocytes proliferation (Malaviya and Nerem 2002). However, when translated to three-dimensional culture, Vunjak-Novakovic et al. showed that the culture of TE cartilage under high shear stresses in bioreactors created elongated cells and collagen fibrils in regions exposed to shear and increased cell content, GAG, and collagen by 70%, 60%, and 125%, respectively, when compared to static cultures (Vunjak-Novakovic, Freed et al. 1996). Davisson et al. seeded ovine chondrocytes under perfusion at 0.05 mL/min and then perfused with culture media at 0.8 mL/min where after nine days

GAG content increased by 40% along with cell content compared to static culture (Davisson, Sah et al. 2002). Some of the reasons speculated as to why bioreactors enhance growth compared to static cultures are that they increase nutrient and oxygen transfer due to increased mixing patterns, that they distribute cells more uniformly due to the design of the bioreactors, and that they stimulate chondrogenesis due to hydrodynamic forces with specified magnitude and type (Freed, Hollander et al. 1998; Lee, Grad et al. 2005). Currently, however, bioreactors engineer cartilage with lower matrix content and inferior material properties compared to native tissue, and little is known of the matrix organization in engineered cartilage (Saini and Wick 2003; Sharma and Elisseeff 2004).

Previous studies of cartilage development in bioreactors have shown that seeded scaffolds can be stimulated to undergo chondrogenesis developing three-dimensional cartilage constructs. Early cartilage bioreactor models include the spinner flasks (Freed, Vunjak-Novakovic et al. 1993; Sucosky, Osorio et al. 2004) and rotating wall vessel bioreactors (Freed and Vunjak-Novakovic 1997). Even though these bioreactors grow cartilage, they produce turbulent or non-uniform fluid environments. Our lab previously developed the concentric cylinder (CC) bioreactor that provides a uniform loading environment to grow tissue-engineered cartilage, but is limited to a one-directional hydrodynamic environment (Saini and Wick 2003).

2.3.3.1 Spinner Flask Bioreactor

One of the more common types and earliest model of bioreactors for TE cartilage is the spinner flask bioreactor. Seen in Figure 2.7A, spinner flasks are containers where scaffolds are attached to needles protruding from the cap. Suspended in culture media, an impeller or magnetic stirbar then mixes the media allowing adequate penetration of nutrients into the scaffolds and creating shear forces on the constructs to stimulate cartilage growth. However, the engineered cartilage has poor mechanical function and low material properties due to non-uniform tissue growth and thickening of tissue in the peripheral edges of the constructs when compared to other types of bioreactors (Vunjak-Novakovic, Martin et al. 1999). Shear stress varies throughout the flask both spatially and temporally, especially with the occurrence of turbulent eddies, making it difficult to quantify the non-uniform shear stress and mass transfer effects on TE cartilage (Freed, Vunjak-Novakovic et al. 1993; Sucosky, Osorio et al. 2004). Another drawback is the complexity in scaling up the design to meet patient demands, limiting the system to bench-top research (Saini 2001).

2.3.3.2 Cone and Plate Bioreactor

The cone and plate bioreactor is based on the geometry of the cone and plate viscometer, which is used in rheological studies to measure the viscosity or shear modulus of a substance. As seen in Figure 2.7B, a cone is placed over a flat plate containing media. The angle between the cone and plate is small and as the cone rotates, the fluid resists in the stationary plate, resulting in a laminar shear stress over the bottom surface (depending on the speed of the cone rotation). Cells are grown in a monolayer

arrangement and respond to the set shear stress created by the cone, where the small angle allows for all the cells, regardless of location, to experience the same shear stress. Dewey et al. was one of the earliest research groups to use the cone and plate apparatus to culture endothelial cells. At a shear stress between 5 and 10 dynes/cm^2 cells elongated in the direction of flow, indicating the response cells had to mechanical stress (Dewey, Bussolari et al. 1981). The cone and plate bioreactor is restricted to monolayer culture and is useful for elucidating mechanotransduction pathways. The CC bioreactor used to culture three-dimensional tissue-engineered cartilage is modeled after the cone and plate bioreactor and is discussed in detail in the Materials and Methods section.

2.3.3.3 Rotating Wall Vessel Bioreactor

Another early bioreactor model is known as the rotating wall vessel (RWV) bioreactor. This bioreactor was developed to create a microgravity environment to stimulate the growth of tissue-engineered cartilage. It has been used to measure long-term growth of cartilage. Developed by NASA and seen in Figure 2.7C, the annulus between two cylinders situated on a horizontal plane is filled with media and cells. Both the inner and outer cylinders rotate independently, and when rotated at the same rate in opposite direction, the cells remain suspended in the media and kept in a stationary location. This effect is replicated in space without the aid of rotating cylinders in order to keep the cells suspended. Long-term growth of tissue-engineered cartilage in a microgravity environment was tested in RWV bioreactors. Freed et al. showed that those cultured in the RWV bioreactors in space had significantly less GAG content and poorer mechanical properties than those cultured on earth; however, even after seven months of

culture the bioreactors could not produced cartilage with ECM content and mechanical properties at level with native cartilage (Freed, Langer et al. 1997).

2.3.3.4 Perfusion Bioreactor

Fluid flow can be manipulated in a bioreactor to flow through a porous scaffold. This type of convective flux increases mass transfer of nutrients and waste removal compared to diffusive flux alone. The pores can be approximated as separate cylindrical tubes. As fluid flows through the tissue at a set rate, it exerts shear stress at the walls of the pores. Thus, perfusion bioreactors apply shear stress on the constructs stimulating growth, just as the spinner flask. The difference lies in the direction of flow. One of the considerations regarding the perfusion bioreactor is ensuring fluid flows through the porous scaffolds and not around, as fluid tends to flow in the path of least resistance. This is usually done by creating a tight seal surrounding and securing the scaffold in place, such that fluid has no choice but to flow through. Another consideration is choosing the right scaffold material, where those with poor mechanical strength like alginate (with a compressive modulus less than 10 kPa) (LeRoux, Guilak et al. 1999) are unable to withstand high flow rates. Typically, a perfusion bioreactor will have a connecting reservoir for media storage and to allow for sufficient gas exchange. As seen in Figure 2.7D, a pump is used to flow fluid from the reservoir to an inlet region of the bioreactor, then pumped out through an exit region, and back to the reservoir creating a closed loop. Multiple perfusion bioreactors can attach to a single reservoir easing the scalability of the system. Thus, perfusion bioreactors can meet patient demands due to its simple geometric design for scaling up.

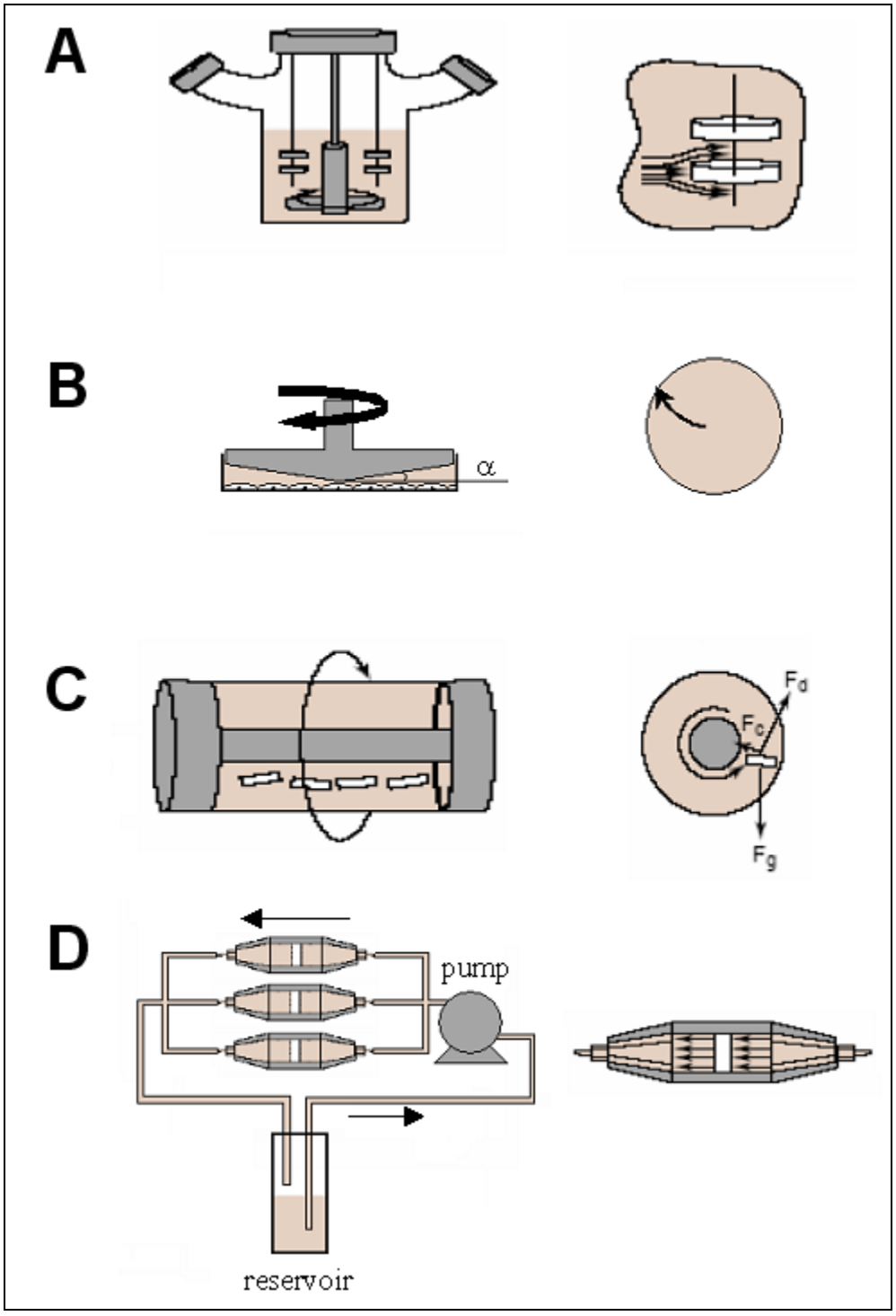

Figure 2.7. Bioreactor models used to culture tissue-engineered cartilage. Images in the second column magnify the fluid profile. (A) Spinner flask bioreactor; (B) cone and plate bioreactor with angle α; (C) rotating wall vessel bioreactor; (D) perfusion bioreactor. Images adapted from Martin et al. (Martin, Wendt et al. 2004)

2.4 Cryopreservation

Long-term success of TE cartilage as a viable treatment option can only be achieved if suitable preservation methods maintain viability and functionality of TE cartilage. Cryobiology is the study of effects of low temperature on cells, tissues, and organs; where as, cryopreservation is the application of subzero temperatures, halting metabolic activity until re-warmed for the storage of such biological systems. Simply lowering the temperature of cells and tissues to below their freezing point invariably destroys them because the ice crystals that form in the water-laden cells and tissues break through the delicate cell membranes. In addition, high salt concentrations inside the cells that result from the ice formation create a toxic imbalance. When thawed the cells and tissues are damaged beyond repair. If the formation of ice crystals can be minimized while still halting metabolic activity of cells at low temperatures, then the viability and functionality of the preserved tissue can be maintained. There are important variables to successful cryopreservation that maximizes cell survival: cryoprotectant agent, cryoprotectant concentration, method of introduction, method of elution, cooling rate, temperature exposure, storage temperature, and warming rate (Brockbank, Covault et al. 2001).

2.4.1 Cryoprotectants

Cryoprotectants can be divided into groups based on their role in protecting cells and tissues during freezing. In 1949, Polge, Smith, and Parkes discovered a significant breakthrough in the role of glycerol as an intracellular cryoprotectant, minimizing ice formation within cells (Polge, Smith et al. 1949). Later on, other cryoprotectant agents

(CPAs) were discovered, such as dimethyl sulfoxide (DMSO) (Lovelock and Bishop 1959), and extracellular CPAs such as starches, sucrose, etc. (Mazur 1981). In 1969 De Vries and Wohlschlag discovered ice blockers such as antifreeze glycoproteins in arctic fish that enabled fish to survive in freezing temperatures (DeVries and Wohlschlag 1969).

Intracellular CPAs suppress high salt concentrations and reduce cell shrinkage during preservation. The ability to protect cells is not so much due to the CPAs individual chemical properties, but rather their colligative properties the solution has due to the presence of the CPAs (Lovelock and Bishop 1959). As the water surrounding the cells or tissues freezes, intracellular water migrates out to freeze, causing high solute concentrations inside the cells, dehydration, and cell shrinkage. DMSO and glycerol have low molecular weights such that at concentrations between 0.5 and 3 M and slow cooling rates they penetrate the cells (Brockbank, Covault et al. 2001). These and other intracellular CPAs slow the migration of water and prevent intracellular ice formation. By replacing the intracellular water such that intracellular ice is minimized, cells are vitrified in ice-free channels of the frozen solution. DMSO and glycerol are common intracellular CPAs and they are traditionally employed for the freezing down of cell stocks. The negatively charged DMSO groups and hydroxyl groups in glycerol most likely form hydrogen bonds with water to prevent water from crystallizing (Muldrew and McGann 1998). Other chemicals, such as formamide and acetamide, reduce the need to have high concentrations of CPAs; by reducing the amount of CPAs, the toxicity of the cryopreservation solution is reduced. Amides in general are weak cryoprotectants, but when combined with CPAs, they improve cell viability (Fahy, Levy et al. 1987).

Known as extracellular CPAs, high molecular weight CPAs such as sugars and starches are used for preserving tissues and organs and protect the cell membranes without penetrating the cells (Brockbank, Covault et al. 2001). The cell membrane is a delicate region of the cell and easily damaged by ice crystals. Upon re-warming, the damaged membranes result in cell death. The CPAs may also play a role in extracellular vitrification; where as, intracellular CPAs guide intracellular vitrification (Brockbank, Covault et al. 2001). Mannitol in particular acts as an osmotic buffer raising the osmolality to balance against intracellular osmotic pressure (Pegg, Wusteman et al. 2006). Another way these extracellular CPAs protect the cells is through their many hydroxyl groups. Through hydrogen bonding, these groups can draw out water from the cells, dehydrating them early in the sub freezing process (Muldrew and McGann 1998), while intracellular CPAs permeate across the membranes, thus protecting them from intracellular ice formation. Combinations of intracellular and extracellular CPAs can result in additive or synergistic effects on cell viability upon re-warming of cryopreserved samples (Brockbank, Covault et al. 2001).

Ice blockers such as antifreeze protein and glycoprotein have been found naturally in plants (Bravo and Griffith 2005), insects (Tomchaney, Morris et al. 1982), and fish (DeVries and Wohlschlag 1969), which allow them to survive subfreezing temperatures. These ice blockers, typically less than 30 kD, work by inhibiting natural ice formation. Water needs a nucleating agent (seed) in order to form the lattice structure characteristic of ice. Ice blockers either direct the plane the ice forms along the c-axis or a-axis or by directly bonding to the nucleating agent halting crystal growth (Muldrew and McGann 1998; Zachariassen and Kristiansen 2000). Synthetic antifreeze compounds such as

ethylene glycol and polyvinyl alcohol can prevent ice crystals from forming by interfering in the lattice array binding to the nucleating agent, similar to antifreeze proteins. The use of ice blockers can reduce the need to have high concentrations of CPAs, reducing toxicity of the cryoprotectant solution (Fahy, Levy et al. 1987).

Table 2.1 lists many of the common cryoprotectants used in cryopreservation of cells, tissues, and organs.

Table 2.1. Chemicals used for cryopreservation

Chemical	Type
Antifreeze proteins and glycoproteins	Natural ice blockers
Ethylene glycol	Synthetic ice blocker
Polyvinyl alcohol	Synthetic ice blocker
1,2-propanediol	Intracellular CPA/ice blocker
Dimethyl sulfoxide	Intracellular CPA
Formamide	Intracellular CPA
Glycerol	Intracellular CPA
Sucrose	Extracellular CPA
Lactose	Extracellular CPA
D-mannitol	Extracellular CPA

CPAs in general are viscous and as temperature drops or their concentration increases, the CPAs solution become more viscous. This increase in viscosity affects the penetration rate through tissues and organs. The time needed for the CPAs to equilibrate with the tissues plays a role in cell viability. Carsi et al. calculated that the diffusivity coefficients of 10% DMSO and 10% glycerol are 0.61×10^{-9} m^2/s and 0.77×10^{-9} m^2/s, respectively, for the penetration into human articular cartilage at 4ºC (Carsi, Lopez-Lacomba et al. 2004). This observation means that equilibration (full penetration) with the CPAs for a 2 mm thick sample would take approximately 20 to 30 minutes, which

may be too long of an exposure to the cytotoxic CPAs. Relying on diffusive flux alone may not be enough to fully penetrate the tissues, instead applying convective flow may better permeate and reduce the total exposure time to CPAs before and after storage. Many of the CPAs are cytotoxic at concentrations often needed for preservation. Introducing or eluting the CPAs at temperatures where metabolic activity has slowed or halted can minimize the lethality of the solutions to the cells. Often this is done by introducing or removing the CPAs at 4ºC. CPAs are also introduced or eluted gradually to tissues and organs to prevent dehydration and maintain osmotic balance between the cells and environment. Seen schematically in Figure 2.8, the CPAs are added initially at a low dosage and increased gradually in discrete steps before fully exposing cells to the full-strength mixture during the cooling stage (before storage). Similarly, when the CPAs are removed during the warming stage (after storage), the dosage is decreased gradually in discrete steps from its full-strength mixture.

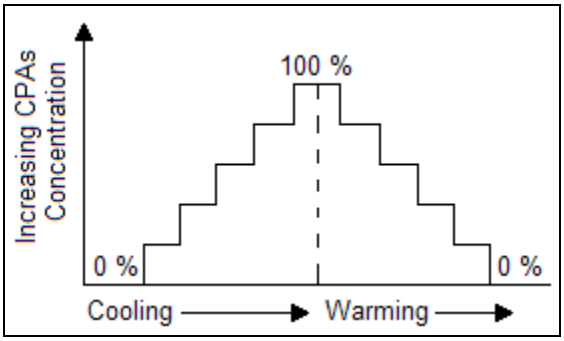

Figure 2.8. Step-wise introduction and elution of CPAs. CPAs are gradually added in discrete steps before cooling down and removed after warming up to maintain equilibrium between the cells and tissues and the surrounding cryoprotectant solution.

2.4.2 Cooling and Re-warming

There are two main approaches to cryopreservation for cells, tissues, and organs. Traditional cryopreservation by freezing techniques, which require the substitution of up to 30% of cell water by a cryoprotective compound (usually DMSO), permits the storage of many types of cells in vitrified channels within ice at deep subzero temperatures (typically lower than -80°C) (Brockbank, Covault et al. 2001). Traditional freezing relies on slow cooling and re-warming rates. In contrast, vitrification is the use of high concentrations of CPAs, resulting in greater than 50% replacement of water in the cell, combined with fast freezing and re-warming rates, thus avoiding both intracellular and extracellular ice formation.

Vitrification, the amorphous solidification of a super-cooled liquid, can be achieved by adjusting the solute composition and the cooling rate such that nucleation and growth of ice crystals is prevented (i.e. fast cooling and warming rates). This method minimizes or prevents formation of ice within the tissues, creating a “glass”, while still halting metabolic activity and maintaining osmotic balance between the cells and environment. The major limitation of vitrification, however, is the potential cytotoxicity of the high concentrations of CPAs (Brockbank, Covault et al. 2001). Seen in Figure 2.9 is a sample of a vitrified compound compared to a traditionally frozen compound.

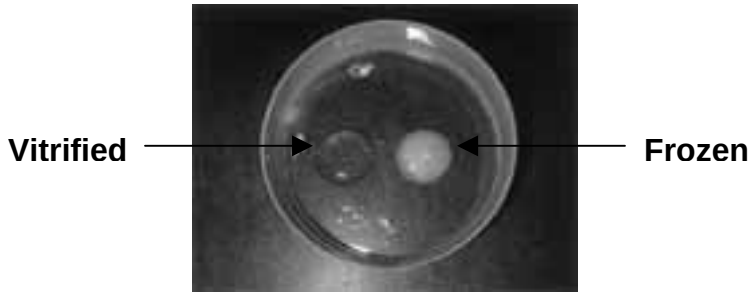

Figure 2.9. Vitrification versus traditional freezing. The sample on the left has been vitrified with a glass-like appearance, while the sample on the right has been frozen and thus has a white appearance due to ice crystals (Nawroth, Rahimi et al. 2005).

Cells are composed of up to 85% water and as water freezes cells react. At room temperature or above water is free-flowing. Metabolic activity is normal and cells maintain an osmotic balance between themselves and surrounding environment. At 4ºC water is at its most dense and metabolic activity begins to decrease. Metabolically-driven pumps have slowed or are inactivated due to the low temperatures; and so, the balance between the intercellular and extracellular environment is regulated mainly by physical means. As temperature is lowered to 0ºC, extracellular water turns to ice given a nucleating agent, expanding and concentrating solutes. As the concentration of extracellular solutes increase, intracellular water migrates out via osmosis to maintain osmotic balance, resulting in cell shrinkage. However, CPAs that permeate cell membranes can adjust the ionic imbalances by substituting for water and non-permeating CPAs (extracellular CPAs) can raise the osmolality to balance against the intracellular osmotic pressure (Pegg, Wusteman et al. 2006). However, Pegg et al. has found that chondrocytes in particular are resistant to osmotic stress (Pegg, Wang et al. 2006), and so the role of extracellular CPAs in preserving cartilage may in fact be minimal.

A phase diagram shown in Figure 2.10 describes the pathway water takes as a sample is either vitrified (red curve) or traditionally frozen (blue curve). With traditional freezing, water changes phase from liquid to solid ice as it passes the melting temperature (T_m). If the fluid is pure, then phase transition does not occur until it is supercooled and passes its temperature of homogenous nucleation (T_h). Nucleation is the seeding agent (ions, salt, etc.) required for ice crystals to form and expand. If the region of nucleation can be avoided as in fast cooling or high concentration of CPAs, then the phase transition from liquid to ice is avoided. This occurs during vitrification where the liquid water reaches its glass transition temperature (T_g) and changes to an amorphous solid instead of ice. Vitrification is achieved when the viscosity of the fluid is so high (~10^{15} P) that molecular movement has ceased (Brockbank, Covault et al. 2001). The glass transition stage is associated with sudden changes in density, which results in high mechanical stresses. This can result in cracking and eventually ice formation. This devitrification problem is avoided by maintaining the sample at or right below the glass transition temperature (Brockbank, Covault et al. 2001). Once vitrified, the storage temperature plays a role to prevent crystallization. As water turns to ice, an exothermic reaction, causing a localized rise in temperature (latent heat of fusion), can start a chain reaction of ice formation. By keeping the storage temperature below –90ºC, this can be avoided (Muldrew and McGann 1998). The glass transition temperature for water is generally accepted at –135ºC (Angell 2002), and storage at -150ºC in a mechanical freezer provides adequate storage without a severe risk of devitrification. Not only does the rate of cooling affect ice crystallization, but the rate of re-warming as well. Generally, fast cooling requires fast warming because seed crystals that formed during cooling process

can have a chance to re-crystallize and expand rapidly if warming is too slow, thus damaging the cells (Best 2006).

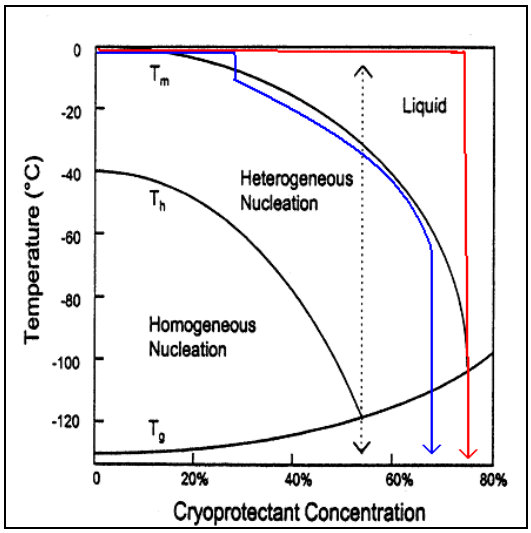

Figure 2.10. Phase diagram of ice formation during freezing. The red curve describes the path of vitrification as fluid bypasses nucleation and thus remains "liquid" as temperature drops. The blue curve describes traditional freezing as ice crystals form during the nucleation stage and water turns solid as temperature drops. In heterogeneous nucleation the nucleating object can be any substance in the fluid mixture for the ice crystals to form, where as in homogeneous nucleation the object is water. Figure adapted from Best (Best 2006).

Guan et al. demonstrated the need for CPAs to preserve tissues. They showed that 51% viability occurred when bovine cartilage was vitrified with CPAs and only 5% viability occurred when bovine cartilage was vitrified without CPAs. The visual damage to cells was also much more pronounced in the cartilage subjected to vitrification without the CPAs (Guan, Urban et al. 2006). In a study conducted by Song et al. on rabbit articular cartilage, vitrification (80.0% viability) proved significantly better than traditional freezing (12.8% viability), leading to the hypothesis that traditionally frozen cells could not move away from extracellular ice formation while confined in the tissue

as isolated cells can in frozen cell solutions (Song, Lightfoot et al. 2003). The cryopreservation studies carried out show that many variables are responsible for affecting cell viability and that protocols for one tissue type does not necessarily apply for other tissue or even the same tissue type from different animals. More studies are needed to measure the factors that affect cell viability of tissue-engineered cartilage to see vitrification as a viable method for long-term storage.

2.5 Research Motivation

These studies show that there is a limited understanding in the direct role of mechanical forces on chondrogenesis. The forces studied that affect cartilage construct development have thus far been limited to one-directional loading and one type of force (shear, perfusion, or compression). A greater understanding of multiple forces in multiple directions, which occur *in vivo*, is needed to understand their role in mechanotransduction pathways and function in cartilage tissue engineering. Furthermore, the effect of chondrogenesis *in vivo*, supported by mechanically stimulated tissue-engineered cartilage constructs, has only recently been explored. In the end, this knowledge can be applied to tailor bioreactor protocols that develop tissue-engineered cartilage with the biochemical and mechanical properties needed for implantation into cartilage defects. To address this gap in understanding, this research project aims to identify multiple mechanical loading variables that influence chondrogenesis. Specifically, a perfusion concentric cylinder bioreactor that was developed in our lab and employs both perfusion and shear orthogonal to each other on scaffolds seeded with chondrocytes, was used to assess the role perfusion and shear had on chondrogenesis.

While tissue-engineered cartilage has emerged as a possible treatment for cartilage defects, few studies have investigated long-term storage of engineered tissues. The investigation of long-term storage is an important field in tissue engineering. To date, most cryopreservation studies have focused on native tissues and organs. Recent studies have also shown that cryopreservation protocols for one type of tissue do not necessarily apply for other tissue types or even the same type from different animals. This research project hopes to address the need to investigate the effectiveness of cryopreservation protocols applicable for tissue-engineered cartilage. Furthermore, the bioprocess scheme for tissue engineering involves multiple steps from cell sourcing to culture to preservation. This research project hopes to simplify this scheme by testing the effectiveness of using a bioreactor to culture and then preserve tissue-engineered cartilage in a one-step process.

CHAPTER 3

MATERIALS AND METHODS

Unless stated otherwise chemicals were purchased from Sigma-Aldrich based in St. Louis, MO and supplies from VWR based in West Chester, PA. The most common solutions used in these experiments were culture media and phosphate buffered saline with EDTA (PBE). Culture media were comprised of Dulbecco's Modified Eagle Medium (DMEM) (containing primarily 4.5 g/L of glucose and L-glutamine), 10% fetal bovine serum, nonessential amino acids (0.1 mM), proline (0.4 mM), 1% penicillin-streptomycin, sodium bicarbonate (44 mM), HEPES buffer (10 mM), ascorbic acid (0.28 mM), and fungizone (0.5 μg/mL) (Invitrogen, Carlsbad, CA) and pH to 7.2. PBE was comprised of 120 mM sodium chloride, 2.7 mM potassium chloride, 10 mM phosphate buffer salts, and 1 mM EDTA and pH to 7.2.

3.1 Scaffold Preparation

Poly-l-lactic acid (PLLA) polymer scaffolds of 90% porosity were prepared by an organic solvent/salt leaching method previously described (Saini and Wick 2003). PLLA crystals (0.5 g) (Polysciences, Inc., Warrington, PA) were dissolved in methylene chloride (5 mL) (Fisher Scientific, Pittsburgh, PA) overnight. Sodium chloride crystals, 106 - 150 μm in diameter (4.5 g), were added to the dissolved PLLA and cast into a 5 cm Teflon Petri dish overnight to allow the solvent (which has a high evaporation rate) to completely evaporate leaving a PLLA-salt disk. The salt crystals were then leached out by placing the scaffold into a beaker of deionized (DI) water for 48 hours, leaving a 90%

porous PLLA scaffold with pore sizes between 106 and 150 μm in diameter. A 10 mm biopsy punch was used to punch out polymer scaffolds used in the bioreactors. Average thickness of the scaffolds was approximately 1.87 mm (Saini 2001). Only scaffolds used in the CC bioreactors were affixed with a plastic shim (8 mm x 8 mm) by a silicone adhesive (CVS, Woonsocket, RI) on one side of the scaffold in order to adhere them to the CC inner bob. All scaffolds were sterilized in triplicate washings 15 minutes each with 70% ethanol then triplicate washings 15 minutes each with sterile DI water. Scaffolds were dried and UV sterilized for 30 minutes and then affixed to the bioreactors before UV sterilized again for 30 minutes. Finally, scaffolds were pre-wetted with culture media in the bioreactors for 48 hours prior to seeding to facilitate cell attachment. All experimental runs used PLLA scaffolds of the same dimension and volume.

3.2 Knee Harvesting, Cartilage Digestion, and Cell Isolation

Male calf knees (2-14 days old) were purchased from an abattoir (Research 87, Boylston, MA). After slaughter the knees were shipped overnight on ice to Georgia Institute of Technology. The knee joints were cleaned of muscle, fat, etc. to expose the articular cartilage. Articular cartilage slices were harvested aseptically from the femoral-patellar groove and femoral condyles and placed in PBE in sterile Petri dishes (Freed, Marquis et al. 1993; Freed, Vunjak-Novakovic et al. 1993). The slices were then cut into 2 - 3 mm^3 cubes in media. The cartilage chunks were spooned into a series of 50 mL centrifuge tubes (approximately 3 g per tube) containing approximately 30 mL per tube of collagenase enzyme solution (1.5 mg/mL of collagenase type II (activity >200 U/mg; Worthington, Lakewood, NJ) in media). The tubes were then wrapped in parafilm and

placed on an orbital shaker at 100 rpm. The enzyme solution cleaved the extracellular collagen matrix in the cartilage chunks overnight (16 - 18 hours) at 37ºC/5% CO_2 to isolate the cells. Longer digestions would compromise cell viability. Afterwards, undigested chunks were removed from the tubes leaving only digested cartilage in collagenase. The cells were spun down in a centrifuge at 600 rpm (70 g_c) for 12 minutes. The supernatant was aspirated and the cells were then washed three times in PBE, spinning down cells between each wash and combining them to completely remove the collagenase and reduce the number of tubes. Repeated pipetting using 10 mL and 5 mL pipettes broke up the pellets. The chondrocytes were then resuspended in approximately 50 mL of media and counted either with a hemacytometer or Vi-Cell Analyzer. Both methods used the trypan blue exclusion method to assess cell concentration and cell viability, where dead cells took up trypan blue. Approximately $200x10^6$ to $400x10^6$ cells was isolated from one knee joint with variations due to the animal source. Cells were then seeded in the bioreactors at a specified concentration for each system. No more than 60 hours passed from the time of slaughter to the seeding of the bioreactors.

3.3 Bioreactor Design and Development

3.3.1 Concentric Cylinder Bioreactor

The CC bioreactor (Figure 3.1) was previously developed and characterized in our lab and modeled after a cone and plate viscometer (Williams, Saini et al. 2002; Saini and Wick 2003). It consisted of an immobile polypropylene inner bob (Professional Plastics, Austin, TX) with scaffolds affixed via silicone adhesives. The 16 scaffolds were arranged in two rows near the bottom of the bob in a staggered array to promote nutrient

transport and efficient seeding. The inner bob was placed in an outer Pyrex glass cup manufactured by Wilmad-Glass, Buena, NJ. The inside of the glass cup had rounded corners to reduce stagnation regions during rotation. The gap between the inner and outer cup was 3 mm and filled with 62 mL of culture media, which covered the scaffolds. The cylinders were covered with a polypropylene cap to prevent contamination and the entire system was placed in a rotating polypropylene base, which was connected to a motor that was mounted on a structural steel support base located inside an incubator. The top of the inner bob was attached to a support bar that was also mounted with screws to the steel base to keep the inner bob immobile as the outer cup rotated. The motor was connected to a control box containing a speed dial, on/off switch, and timer. The outer cup could rotate at variable speeds. For this research project the outer cup was chosen to rotate at a constant speed of 38 rpm based on Dr. Saini's research into the optimum growth of engineered cartilage in the CC bioreactor (Saini 2001). At 38 rpm, a homogeneous laminar flow regime within the gap developed, and changing direction every twelve hours (using the timer) maintained similar shear stress on both sides of the constructs. Numerical simulations have verified that 95% of the construct surface experienced uniform hydrodynamic loading with the average surface shear stress exerted on the constructs at 1.2 dynes/cm^2 (Williams, Saini et al. 2002).

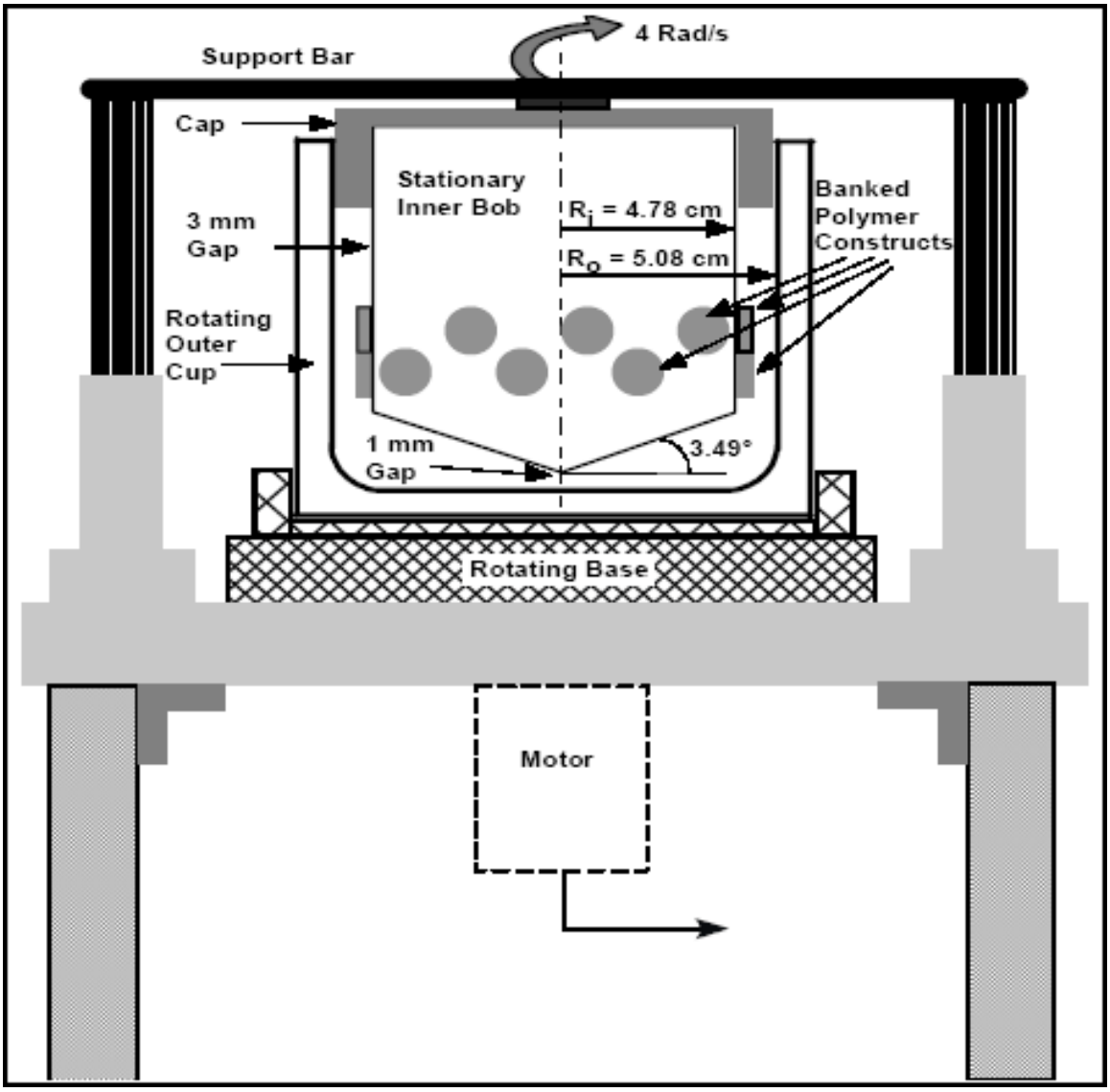

Figure 3.1. Schematic of the concentric cylinder bioreactor (Saini 2001). The CC bioreactor consisted of a stationary inner bob with affixed scaffolds arranged in a staggered array placed inside a glass cup. The gap between the inner bob and outer cup was 3 mm. Not drawn to scale.

3.3.2 Perfusion Concentric Cylinder Bioreactor

The PCC bioreactor (Figure 3.2) was developed in our lab to include fluid perfusion orthogonal to the surface shear created by the outer cup rotation.

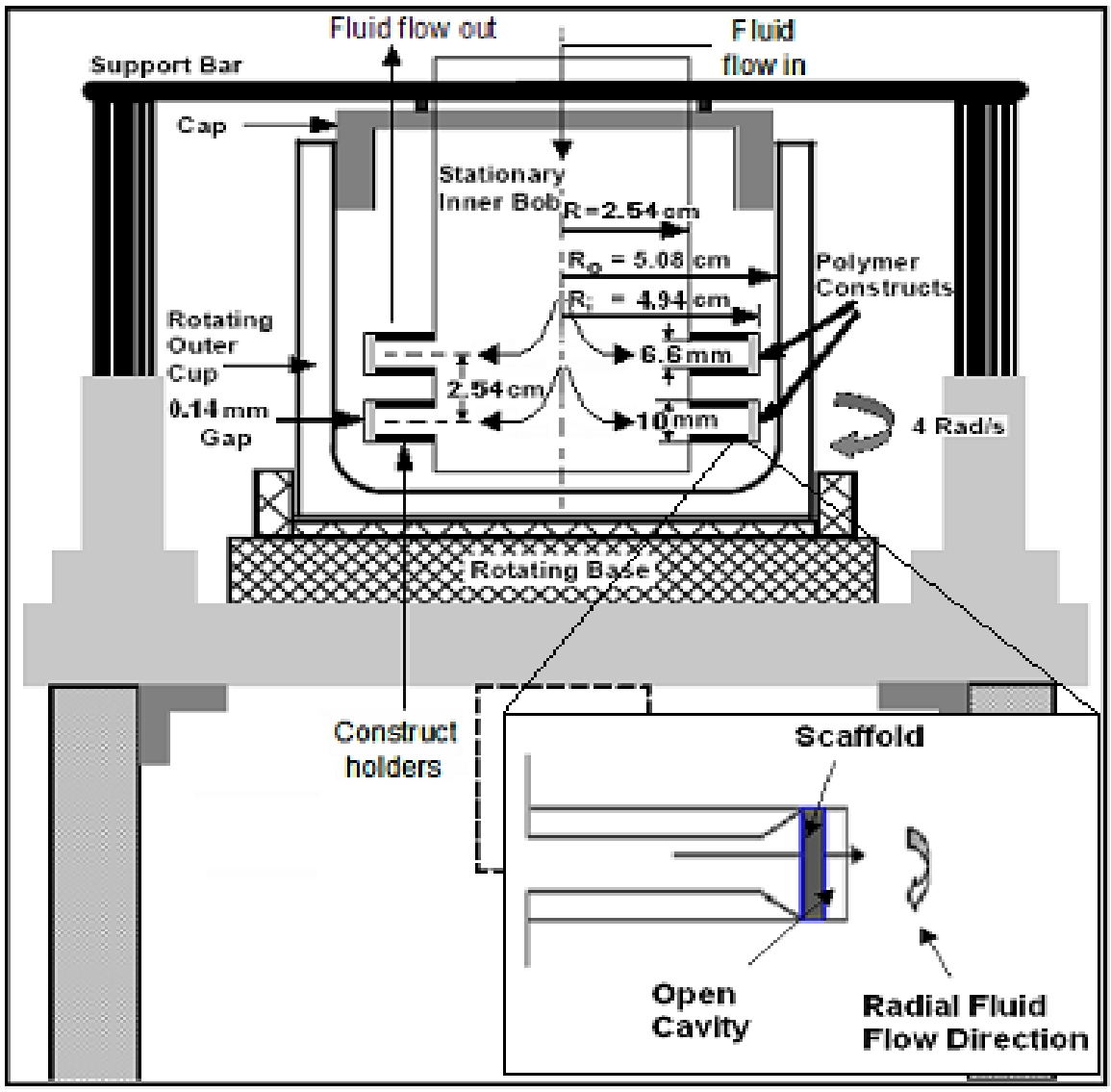

Figure 3.2. Schematic of the perfusion concentric cylinder bioreactor. The PCC bioreactor consisted of a stationary inner bob with 16 spokes (arranged in two rows), which contained embedded constructs radiating from a central hub. The gap between the construct holders and outer cup was 0.14 mm. The peristaltic pump flowed media from the outer cup region to the interior of the central hub to exit radially through the spokes at an average set flow rate of 0.6 mL/min/construct. Inset represents a close-up of construct arm. The diagram is not strictly to scale, but the dimensions are correct.

The clear polycarbonate or acrylic (McMaster Carr, Atlanta, GA) inner bob was redesigned from the CC bioreactor inner bob design to include 16 cylindrical spokes (2 cm in length at 0.66 cm in diameter before increasing in diameter to 1 cm for 0.4 cm)

arranged in two rows radiating from a central hub (5.08 cm in diameter). Like the CC bioreactor, the inner bob was placed in an outer cup and covered with a cap. The system was then mounted on a rotating base and structural steel support base located in the incubator. The bioreactors were machined by Mr. Andrews of the Georgia Tech Machine Shop or by the Machine Services Department.

Scaffolds 1 cm in diameter and approximately 1.87 mm in thickness were embedded 0.4 cm into these construct arms (cylindrical spokes) leaving an open cavity approximately 0.213 cm in height and 1 cm in diameter to surround and affix the embedded scaffolds. Because the diameter of the construct arms and scaffolds were both 1 cm, a tight fit was ensured, which prevented fluid perfusion around the scaffolds during bioreactor operation. Figure 3.3A showed a red dye solution permeating as it flowed through and stained a wet scaffold. (Note the necessity of pre-wetted scaffolds as fluid tried to flow around a dry hydrophobic scaffold, or the path of least resistance in Figure 3.3B.)

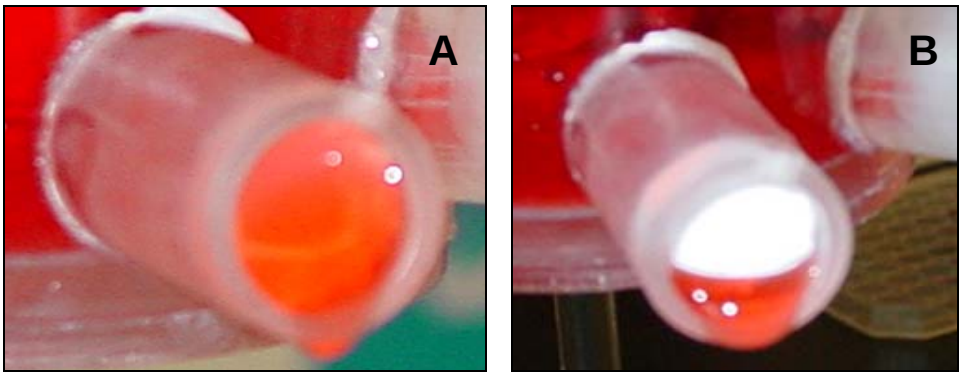

Figure 3.3. Visualization of fluid flow through a scaffold embedded in a construct arm. (A) Wet scaffold; (B) dry scaffold

The clear polycarbonate or acrylic inner bob allowed us to monitor the pressure gradient (between the interior and exterior of the central hub) and fluid regime inside the central hub. Fluid perfusion was introduced via a peristaltic pump (Cole-Parmer Instrument, Vernon Hills, IL) using size #16 tubing (Cole-Parmer) though the central hub and then exited radially through the arms at an average flow rate, Q, of 0.6 mL/min/construct. Fluid was then pumped out from the region between the cylinders at the same rate it was pumped into the central hub. By maintaining a closed loop, fluid was continuously pumped into and out of the bioreactor at the same flow rate. A constant flow rate of 0.6 mL/min/construct was maintained by calibrating the pump to flow at a multiple of the number of constructs in the bioreactor at the time. For example, when 16 constructs were in the bioreactor, the central pump flowed fluid at 10 mL/min; however, when 4 constructs remained, the central pump flowed fluid at 2.5 mL/min with silicone-coated aluminum plugs inserted in vacated arms to prevent fluid flow through the arms not containing a tissue construct. Table 3.1 shows the flow rate into the central hub versus the number of constructs in the PCC bioreactor.

Table 3.1. Fluid flow rate in PCC bioreactor. Flow through the central hub as a function of the number of constructs in the PCC bioreactor.

Constructs in PCC bioreactor	Flow rate into central hub (mL/min)	Flow rate per construct (mL/min/construct)
16	10	0.6
13	8.1	0.6
10	6.3	0.6
7	4.4	0.6
4	2.5	0.6

The Reynolds number, determining laminar or turbulent flow, for flow through a tube was:

$$\mathrm{Re} = \frac{\rho V_m D}{\mu} \qquad \text{Equation 3.1}$$

where,

$$V_m = \frac{Q}{\phi\pi(D/2)^2} \qquad \text{Equation 3.2}$$

For culture media, the density, ρ, was approximated to the density of water (0.99 g/cm^3) and the viscosity, μ, was 0.695 cP at 37ºC. The porosity, ϕ, was 0.9 for flow through the scaffolds and 1 for flow through the arms. The mean velocity, V_m, of fluid through the cylindrical arms (diameter, D, was 0.66 cm) and at a flow rate of 0.6 mL/min was 0.03 cm/s. Therefore, the Reynolds number for flow through the arms was 3, and was much lower than the stability criteria for steady flow (N_{Re} < 2000). The dimensions of the cylindrical arms ensured that parabolic flow was fully developed before perfusing through the scaffolds, assuming inlet velocity was uniform. That is, the entrance length, L_V, (L_V = (D/2)*(1.18+0.112*Re)) (Atkinson, Brocklebank et al. 1969) required for a fully developed flow was 0.5 cm, which was less than the length of the construct arms (2.4 cm). Assuming cylindrical pores with a diameter, d, between 106 and 150 μm and uniform flow distribution across the scaffold surface, with parabolic flow through the pores, the Reynolds number and the shear stress at the wall inside the scaffolds was calculated (Goldstein, Juarez et al. 2001):

$$\mathrm{Re} = \frac{\rho V_m d}{\mu} = 0.01 - 0.07$$ Equation 3.1

$$\tau_w = \frac{8\mu V_m}{d} = 0.13 - 0.18\ dyne/cm^2$$ Equation 3.3

To determine if fluid flowed evenly through the construct arms, a red dye was pumped into the bioreactor system to observe its distribution throughout (Figure 3.4). Without constructs, fluid flowed through the PCC bioreactor construct arms. Figure 3.4A (top view) shows a snapshot of red dye flowing evenly through the radial spokes as fluid was pumped into the central hub. The dye distributed evenly initially through the bottom row of 8 construct arms before radiating evenly through the top row (Figure 3.4B). This demonstrated that pressure gradients greatly affected the flow rate through the extruding construct arms.

Using the inner bob of the PCC bioreactor, the flow rate at various pressure gradients was measured through PLLA scaffolds to calculate the relative difference of volumetric flow rate between the top and bottom rows of the construct holders. The pressure gradient, ΔP, between the two rows was less than 0.25% however flow rate varied by 69% (See Figure 3.5). At an average rate of 0.6 mL/min/construct with a 69% change between the top and bottom row determined that the top row experienced 0.19 mL/min/construct and the bottom row 1.01 mL/min/construct. Despite these observations the PCC bioreactor was run as if the average flow rate through the construct holders was held constant at the assumed rate of 0.6 mL/min/construct to simplify velocity and shear stress calculations.

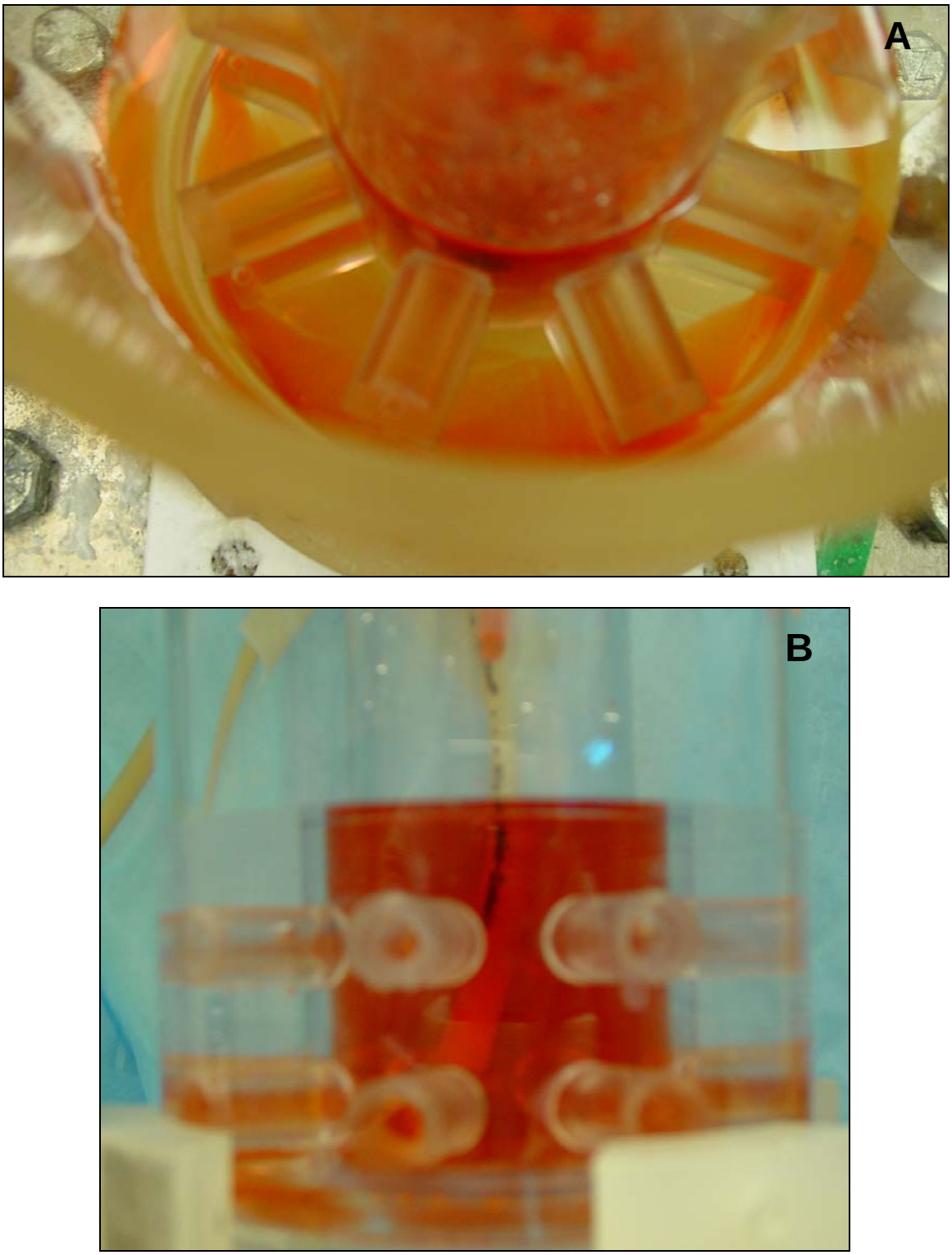

Figure 3.4. Fluid flow distribution through the construct arms of a PCC bioreactor. (A) Top view; (B) side view

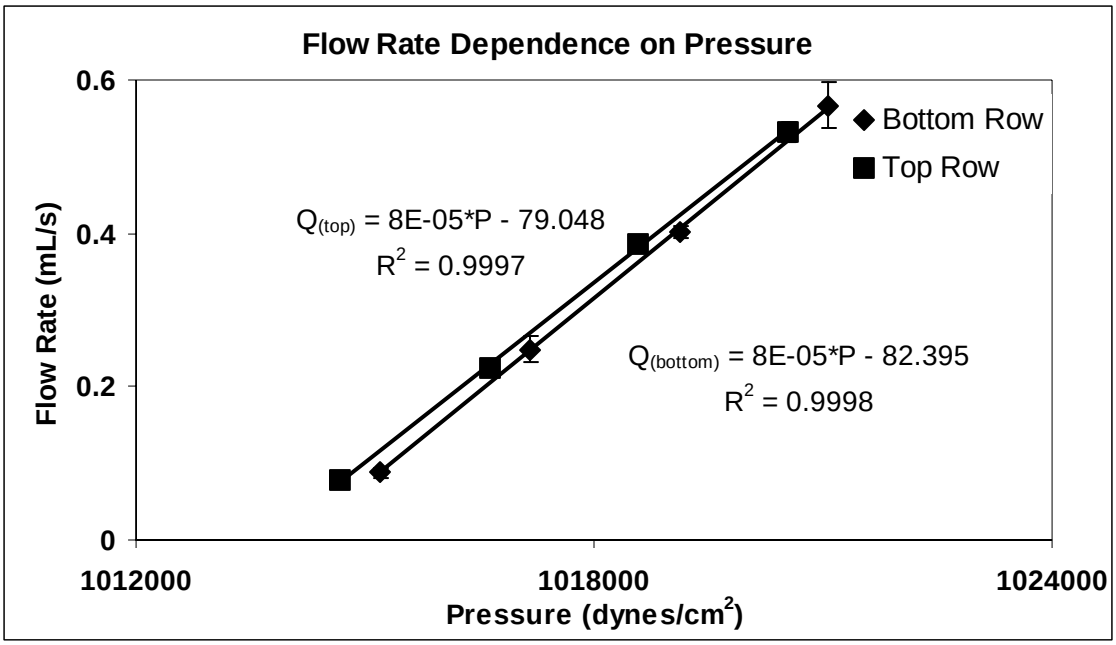

Figure 3.5. Pressure gradient as a function of flow rate between the two rows of a PCC bioreactor.

The gap between the edge of the construct arms and outer cup (10.16 cm diameter) was 0.14 mm and the bioreactor was filled with 350 mL of culture media during the seeding period (4 days) and 400 mL of culture media during the rest of the bioreactor run. The radius ratio, K, defined for this system as the radius of the inner bob's central hub (R_i) divided by the outer cup radius (R_o), was 0.5 for this bioreactor. However, the radius of the inner bob's central hub plus the length of the cylindrical arms was 4.94 cm, which gave a radius ratio of 0.972 for this bioreactor. Values close to 1 ensure stability in flow and constant shear stress at the edge of the construct arms before flowing into the open cavity containing the scaffolds. Like the CC bioreactor, the outer cup rotated at a constant speed, Ω, of 38 rpm, changing direction every twelve hours via a timer. The Reynolds number between annulus of the two concentric cylinders was based on the rotation rate and radius:

$$\mathrm{Re} = \frac{\Omega R^2 \rho}{\mu}$$ Equation 3.4

The Reynolds number for this rotation rate and outer cup radius was 3660 near the wall of the central hub and increased to 14600 near the wall of the outer cup, well below the stability criteria for steady flow ($N_{Re} < 50000$) (Saini 2001). Based on the Navier-Stokes equation, the fluid velocity exposed to the construct arms before entering the open cavity was calculated; assuming that the region between the inner bob and outer cup mimicked two concentric cylinders and that there was no slippage at the walls (Bird, Stewart et al. 2002):

$$v_\theta = \frac{\Omega R_i}{1 - K^2}\left(\frac{r}{R_i} - \frac{R_i}{r}\right) = 19.28 \ \ cm/s$$ Equation 3.5

A more detailed derivation is shown in Appendix A. For comparison, the velocity where the constructs were located in the CC bioreactor was 12.74 cm/s. The velocity profile between the two cylinders can be seen in Figure 3.6 for both the PCC and CC bioreactor.

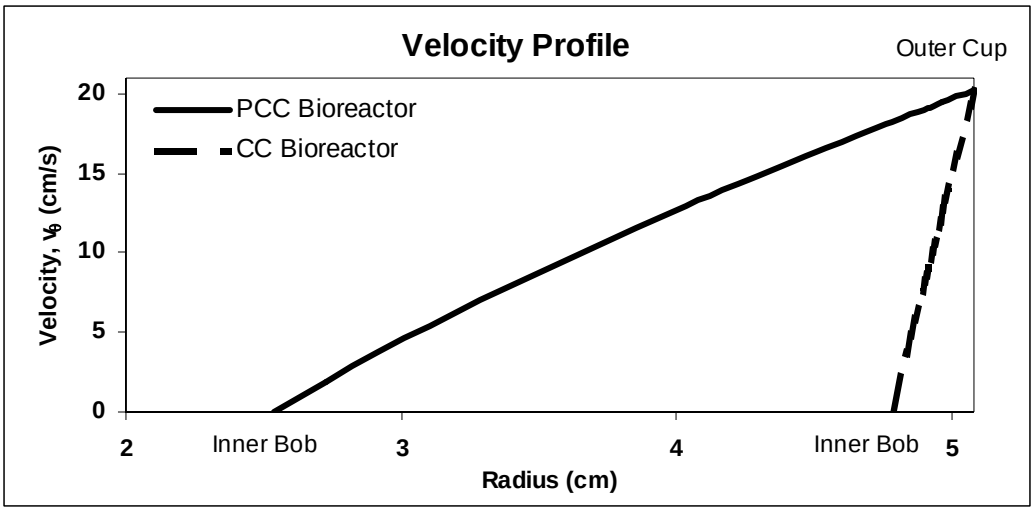

Figure 3.6. Velocity profile within the bioreactor. The velocity profiles between the two cylinders were represented for both the PCC and CC bioreactor as the outer cup rotated at 38 rpm. The gap between the cylinders in the CC bioreactor was smaller and thus showed a steeper increase in speed from the immobile inner cylinder bob to the rotating outer cup.

The oxygen concentration profile within the construct of the PCC bioreactor was based on the species continuity equation (Bird, Stewart et al. 2002) for oxygen with constant density and diffusivity of oxygen, D_{O2}, in media or TE cartilage:

$$\frac{\partial C_{O2}}{\partial t} + \mathbf{v} \bullet \nabla C_{O2} = D_{O2} \nabla^2 C_{O2} + R_{O2} \qquad \text{Equation 3.6}$$

where,

C_{O2} is the concentration of oxygen,

v is the velocity through the constructs,

and R_{O2} is the reaction rate describing the consumption of oxygen by cells.

The diffusivity of oxygen in water was estimated from the Wilke-Change correlation (see Appendix A) at 3.23×10^{-9} m^2/s at 37ºC and the diffusivity of oxygen in tissue was determined from literature at 2.0×10^{-9} m^2/s (Macpherson, O'Hare et al. 1997). The consumption of oxygen by cells was assumed to be fixed at a rate of 0.5 μmol $O_2/10^6$ cells/hr, which was based on the metabolic rates for mammalian cells (Cartwright 1994). This correlated to a zeroth-order reaction (Williams, Saini et al. 2002) where for an average of 10^6 cells per construct and a construct volume of 147 mm^3 the reaction rate was 9.46×10^{-4} mol $O_2/m^3/s$. The time for oxygen to reach steady-state equilibrium with the gas phase in the incubator was calculated from Equation 3.6. However, given the long culture time, media were assumed to be saturated with oxygen and at equilibrium with the gas phase environment in the incubator, which was at 20% O_2, 5% CO_2 and 75% N_2 at 37ºC, for the calculation of the steady-state oxygen profile through the constructs. The equilibrium concentration of oxygen in media was therefore 0.212 mol/m^3, which was based on Henry's Law (see Appendix A) and seen as a boundary condition for Equation 3.6.

The Peclet number describes the ratio between the convective and diffusive flux through a construct of thickness L (1.87 mm):

$$Pe = \frac{V_m L}{D_{O2}} \qquad \text{Equation 3.7}$$

The Peclet number was 316 for perfusion through a construct in the PCC bioreactor, assuming the diffusivity through the construct was the same order of magnitude as the diffusivity of oxygen through tissue. The value indicated that convective flux dominated

and the diffusivity term in Equation 3.6 could be neglected. If there was no convective flow in the PCC bioreactor (i.e. when there was no perfusion) then diffusivity dominated. Taken together the steady-state oxygen profile through the construct was calculated for the entire culture period.

3.3.2.1 Computational Methods

The open cavity of the construct arms after placement of the scaffolds affected the velocity profile and consequently the shear stress experienced on the constructs. The fluid flow profile hence was altered and Equation 3.5 was not an accurate assessment for the velocity experienced on the surface of the constructs. To compensate and determine the shear stress profile a CFD code in FORTRAN provided by Dr. Nenes was used to solve the Navier-Stokes equations for momentum (Nenes 2003):

$$\nabla \bullet \mathbf{v} = 0 \qquad \text{Equation 3.8}$$

$$\frac{\partial \mathbf{v}}{\partial t} + \mathbf{v} \bullet \nabla \mathbf{v} = -\frac{1}{\rho}\nabla p + \frac{\mu}{\rho}\nabla^2 \mathbf{v} \qquad \text{Equation 3.9}$$

The three-dimensional cylindrical cavity was transposed and solved as a discrete two-dimensional rectangular cavity over the surface of the scaffold's diameter (0.00213 m x 0.01 m) with a "moving lid" at a speed of 0.1928 m/s (see Figure 3.7). The assumptions made include an incompressible, Newtonian fluid flow at steady state with no-slip boundary conditions at the "moving lid" and surface of the scaffold. Because of the symmetry and even spacing of the construct arms, the profile generated in one cavity

applied to all construct arms. The Navier-Stokes equations were solved numerically using a finite volume discretization formulation with a rectangular grid with 2304 cells. The spreadsheets generated of the velocity profile in the x and y direction allowed us to calculate the shear stress over the scaffold's surface numerically using Newton's law of viscosity:

$$\boldsymbol{\tau} = -\mu \nabla \mathbf{v} \qquad \text{Equation 3.10}$$

where shear stress was approximated as:

$$\tau_{xy} = -\mu\left[\frac{\partial v_y}{\partial x} + \frac{\partial v_x}{\partial y}\right] \approx -\mu\left[\left.\frac{\Delta v_y}{\Delta x}\right|_y + \left.\frac{\Delta v_x}{\Delta y}\right|_x\right] \qquad \text{Equation 3.11}$$

Both the velocity and shear stress in the open cavity over the surface of the constructs along the diameter were then plotted as a contour map to determine the velocity and shear stress experienced on the surface of the constructs' diameter in the PCC bioreactor.

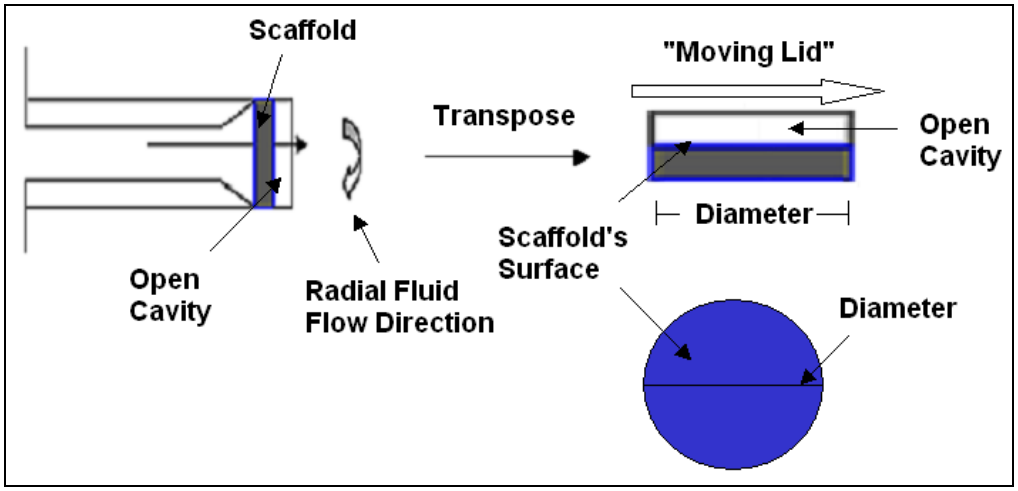

Figure 3.7. Diagram of the transposed two-dimensional open cavity model used for CFD modeling over the surface of the scaffold along its diameter.

3.3.3 Static Bioreactor

The static bioreactors were sterile 6-well polystyrene dishes (low cell binding-treated). One scaffold was placed in each well and filled with 5 mL of culture media. The plates were placed in the incubator at 37ºC/5% CO_2 on an orbital shaker at approximately 50 rpm.

3.4 Bioreactor Sterilization and Assembly

The outer glass cups, the inner bobs of the PCC and CC bioreactor, and the aluminum plugs used for the PCC bioreactors were coated with Sigmacoat. Sigmacoat provided a microscopically thin layer of silicone on the surface of the bioreactor parts to repel water and prevent cell attachment. Because the silicone was suspended in heptane, the bioreactor parts were allowed to dry for 48 hours under a fume hood before washed, wrapped in absorbent paper towels, and placed in sterilization bags. The outer glass cups, the inner bobs for the CC bioreactors, bioreactor caps, plugs, and tubing for the PCC bioreactors were steam sterilized at 121ºC/2.2 atm for 20 minutes. The inner bob of the PCC bioreactor, composed of either acrylic or clear polycarbonate, could not be steam sterilized because of the risk of warping at high temperatures. Therefore, the inner bobs of the PCC bioreactors were washed in triplicates for 15 minutes each with 70% ethanol and then in triplicates for 15 minutes each with sterile DI water, where the inner bobs were placed in sterile 1000 mL beakers to facilitate the washing. Finally, the inner bobs were UV sterilized for 30 minutes. After sterilization all bioreactor pieces for both types of bioreactors were assembled under sterile conditions in a laminar flow hood. Scaffolds were then affixed to the inner bobs and UV sterilized again for 30 minutes.

Silicone adhesives were used to affix the scaffolds with plastic shims to the inner bobs of the CC bioreactors in a staggered array (see Figure 3.1) and allowed to dry for approximately 6 hours. Scaffolds were affixed via tension inside the construct arms of the PCC bioreactors (see Figure 3.2). The outer cups were filled with culture media and the bioreactors were mounted in the incubator for 48 hours prior to seeding to pre-wet the scaffolds.

After experiencing contamination involving the PCC bioreactor, the sterilization method of the PCC bioreactor changed to ethylene oxide (EtO) sterilization. This method provided a safer alternative for the heat sensitive components of the PCC bioreactors. The inner bobs of the PCC bioreactors were exposed to EtO, which is a colorless and odorless gas that kills bacteria, mold, and fungi without the need for heat. Afterwards, the inner bobs of the PCC bioreactors were soaked in sterile DI water for 15 minutes to remove any lingering traces of the toxic gas and UV sterilized for 30 minutes before assembly as mentioned earlier.

3.5 Bioreactor Runs

3.5.1 Concentric Cylinder Bioreactor

The experimental runs involving the CC bioreactor lasted 28 days. On Day 0 $100x10^6$ to $150x10^6$ cells were suspended in media and placed inside the outer cup for a total volume of 62 mL of media. The CC bioreactor was then mounted inside the incubator (37ºC/5% CO_2). Under hydrodynamic forces, cells attached to the scaffolds. After two days, 50% of the culture media were replaced with fresh media. On Day 4 of the run, 100% of the culture media were replaced, which completed the seeding period.

Fresh ascorbic acid (0.28 mM) was added as well. Subsequently, every two days 80% of the media were replaced and every four days ascorbic acid was added to the culture media until the completion of the experimental runs at Day 28. Media samples (three 1 mL samples) were taken from the spent media that were replaced every four days (Day 4, 8, 12, 16, 20, 24, and 28) and stored at –20ºC in Eppendorf tubes for soluble GAG analysis. The pH of the bioreactor was also monitored. After feeding, approximately 30 mL of spent media along with approximately 30 mL of fresh media were stored in the incubator overnight. The next day the pH of spent media was measured and compared to the control. Any significant drop in pH would indicate possible contamination, which was verified microscopically or with gram staining. Constructs were harvested in triplicates on Day 4, 7, 14, and 21 and the final four constructs were harvested on Day 28. All feedings and construct harvestings were handled under sterile conditions in a laminar flow hood. Under the hood the inner bob was removed from the outer cup and placed on a sterile Petri dish. With sterile tweezers the constructs were removed from the inner bob and washed in PBE. The culture media in the outer cup were replaced on feeding days. The inner bob was then placed back inside the outer cup and the system was placed back inside the incubator.

3.5.2. Perfusion Concentric Cylinder Bioreactor

The experimental runs involving the PCC bioreactors lasted 6, 7, or 28 days. On Day 0 $100x10^6$ to $150x10^6$ cells were suspended in media and placed inside the outer cup for a total volume of 350 mL of media. After the PCC bioreactor was mounted in the incubator, no perfusion through the constructs occurred for four days. Instead, the only

hydrodynamic loading during the seeding stage was due to the outer cup rotation, which caused fluid-induced shear on the surface of the constructs. During the seeding period cells attached to the polymer scaffolds. After four days all the media were removed to halt the seeding process and replaced with 400 mL of fresh media and 0.28 mM of ascorbic acid. Except for the shear only conditions in the PCC bioreactor, perfusion of culture media through the constructs also started on Day 4. The shear only studies had no perfusion during the course of the experimental run. All of the culture media were replaced every four days; however, some media in the tubing and inside the central hub, which amounted to approximately 1% of the total volume, were not removed due to risk of contamination. Like the CC bioreactor, media samples were taken from the spent media that were replaced every four days and stored at –20ºC in Eppendorf tubes for soluble GAG analysis. The pH of the bioreactor was also monitored in the same way as the CC bioreactor. Experimental runs continued for 6, 7, or 28 days depending on the study. All feedings occurred under sterile conditions in a laminar flow hood and treated in a manner similar to the CC bioreactor mentioned above. On month-long experimental runs constructs were harvested in triplicates on Day 4, 7, 14, and 21 and four were harvested on Day 28. For cryopreservation studies, all 16 constructs were harvested the day the cryopreservation experiments started (Day 6, 7, 14, or 28). All constructs were harvested under the hood using sterile tweezers to twist the constructs out from the construct arms and washed in PBE. Sterile silicone-coated plugs were placed inside the vacated arms to retard fluid flow through them before placing the inner bob back inside the outer cup and the system back inside the incubator to continue the experimental run.

3.5.3 Static Bioreactor

Cells were suspended at a density of $9.38x10^6$ cells per 5 mL of culture media and added to a scaffold located in a well of a 6-well plate dish on Day 0. A total of 16 scaffolds were used in a static bioreactor and thus a total of $150x10^6$ cells were seeded to the scaffolds. Culture media were changed completely every two days and ascorbic acid (0.28 mM) was added to the culture media every four days until the completion of the experimental run (28 days total). Media samples and the pH of the spent media were taken in the similar manner as the PCC and CC bioreactor mentioned above. Constructs were harvested and washed in PBE in triplicates on Day 4, 7, 14, and 21 and four constructs were harvested and washed on Day 28. All feedings and construct harvestings occurred under sterile conditions in a laminar flow hood, where media were aspirated out of each well and 5 mL of fresh media were added on feeding days, and where sterile tweezers were used to remove the constructs on harvesting days.

3.6 Tissue-Engineered Cartilage Construct (TECC) Growth Studies

Different studies were performed to characterize the growth of TECCs in the PCC bioreactor and to optimize the viability of cryopreserved TECCs. The studies can be divided into four main groups. The PCC validation studies included biochemical, histological, and viability analysis of constructs cultured in the PCC bioreactor over the course of 28 days after seeded with $150x10^6$ cells. Velocity, shear stress, and oxygen transport profiles were also calculated for constructs in the PCC bioreactor. The PCC versus CC studies consisted of one PCC bioreactor and one CC bioreactor seeded with $100x10^6$ to $150x10^6$ cells with chondrocytes from the same animal source. Over the

course of 28 days, the constructs were analyzed for biochemical composition, biochemical distribution, gene expression, and cell viability. The perfusion+shear versus shear studies consisted of two PCC bioreactors seeded with $100x10^6$ to $150x10^6$ cells with chondrocytes from the same animal source. After four days, one PCC bioreactor exposed constructs to both perfusion and shear (perfusion+shear bioreactor), while the other PCC bioreactor exposed construct to shear only forces (shear bioreactor). Over the course of 28 days, the constructs were analyzed for biochemical composition, biochemical distribution, mechanical properties, and cell viability. With regards to the animal studies, a static bioreactor was included in the perfusion+shear versus shear comparison. The cryopreservation studies had seven experiments, which can be seen in detail in Table 3.2. Constructs were cultured in the PCC bioreactor with $150x10^6$ cells and after 6, 7, 14, or 28 days were harvested for the cryopreservation study. Each experiment divided the constructs into two treatment groups, one of which served as the control. Constructs were analyzed for cell viability and cellular content after each treatment. The experimental studies are outlined in Table 3.2.

Table 3.2. Lists of experiments

Experiment Name	Bioreactors	Culture Time	Number of Experiments
PCC Validation			
CFD Modeling and Oxygen Transport Calculation	PCC	N/A	1
Biochemical Analysis	PCC	28 days	1
Live/Dead	PCC	28 days	1
Histological	PCC	28 days	1
PCC vs. CC Comparison			
Biochemical Analysis	PCC, CC	28 days	2
Live/Dead	PCC, CC	28 days	1
Histology	PCC, CC	28 days	1
Gene Expression	PCC, CC	28 days	2
Perfusion+Shear vs. Shear Comparison			
Biochemical Analysis	PCC	28 days	2
Live/Dead	PCC	28 days	1
Histology	PCC	28 days	1
Mechanical Testing	PCC	28 days	1
Animal Study	PCC, Static	28 days post implantation	1
Cryopreservation Optimization			
Frozen vs. VS55 6/7	PCC	7 days	1
VS55 6/7 vs. VS83 6/7	PCC	6 days	1
VS55 6/7 vs. VS70 6/7	PCC	6, 7, 14 or 28 days	5
VS55 6/7 vs. VS70 6/7 no vitrification	PCC	7 days	4
VS55 vs. VS70 on native tissue	PCC	N/A	1
VS70 6/7 vs. VS70 4/4	PCC	6 or 7 days	4
Orbital Shaker vs. PCC Bioreactor	PCC	7 days	3

3.7 Animal Surgeries

TECCs were cultured under three types of mechanical stimulation: perfusion and shear (in the PCC bioreactor), shear (in the PCC bioreactor), and no mechanical stimulation (static bioreactor). After 28 days the TECCs were harvested and washed in PBE. A 3 mm biopsy was punched out of the center of each construct and implanted into a xiphoid chondral defect in a rat model.

All procedures involving the rat model were performed under the Georgia Tech Institutional Animal Care and Use Committee (IACUC) guidelines. All animal surgeries and euthanasia were performed in the Physiological Research Laboratory at Georgia Institute of Technology. The animals used were 5 weeks old athymic nude male rats and purchased from Harlan Sprague Dawley, Inc., Indianapolis, IN. The rats had a reduced immune system to prevent rejection of the bovine implants. A total of 30 rats were used, divided evenly into six groups. Each group was treated according to the Table 3.3.

Table 3.3. Animal study groups

Group	Xiphoid Treatment
Group A	Xiphoid defect only
Group B	PLLA scaffold, no cells
Group C	TECC from static bioreactor
Group D	TECC from perfusion+shear (in the PCC bioreactor)
Group E	TECC from shear (in the PCC bioreactor)
Group F	$5x10^6$ cells with no PLLA scaffold

The rats were anesthetized with inhalation of 5% isoflurane and maintained with 2 - 3% isoflurane while undergoing the surgery. Their skin covering the xiphoid region was cleaned and sterilely prepared for surgery. A standard parasagittal incision and sharp dissection was made left of the xiphoid region such that the integrity of the ribs was not violated. The xiphoid cartilage (located at the base of the sternum) was exposed. A cartilage defect was created in the center of the xiphoid of the rats by using a biopsy punch out to create a 3 mm circular hole. The TECCs, PLLA scaffolds, or $5x10^6$ cells (the cells were in pellet form and were not embedded into scaffolds) were implanted into the defect (see Figure 3.8) or otherwise left empty (Group A). The inferior and superior

margins were covered with SepraFilm (Genzyme Biosurgery, Cambridge, MA). The incision through the muscle was sutured (4.0 absorbable suture) and the skin was sealed with wound clips. The rats were monitored for pain and administered buprenorphine (0.03 mg/kg) via a subcutaneous injection on their dorsal side post surgery.

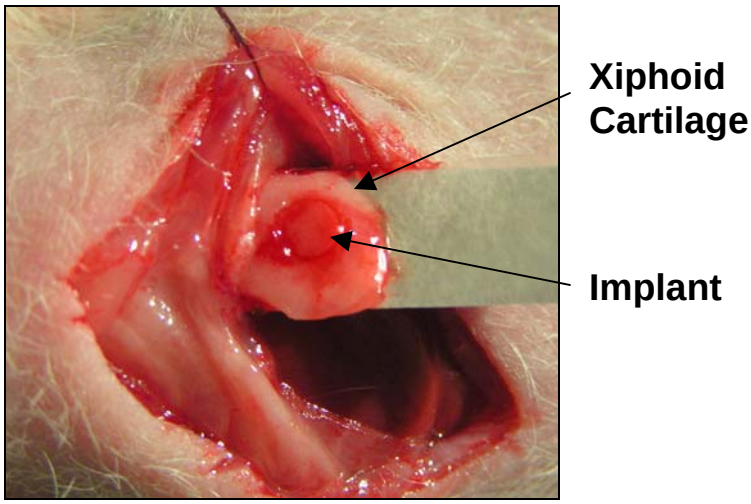

Figure 3.8. Implant location in an athymic nude male rat xiphoid chondral defect.

Ten days after surgery the wound clips were removed. At four weeks the rats were euthanized with CO_2 asphyxiation in covered animal containers. The xiphoid and implant were excised from each animal for histological analysis. Dr. Hunter Moyer performed both the surgeries and the removal of the xiphoid and implant after euthanasia.

3.8 Cryopreservation

Vitrification solutions (VS) used in the cryopreservation studies consisted of dimethyl sulfoxide (DMSO), formamide, and 1,2-propanediol as the cryoprotectant agents (CPAs) in 5xEuroCollins (5xEC) solution (0.97 M dextrose, 0.07 M potassium

phosphate monobasic (KH_2PO_4), 0.21 M potassium phosphate dibasic (K_2HPO_4), 0.08 M potassium chloride (KCl), and 0.05 M sodium bicarbonate ($NaHCO_3$)) and 0.01 M HEPES buffer with pH between 7.9 and 8.1. The solution used for traditional freezing contained 1 M DMSO in culture media. The three vitrification solutions, VS55, VS70, and VS83, used in this study varied in concentration (8.4 - 12.6 M) of the CPAs and their formulations are listed in Table 3.4. The full-strength removal solutions (solutions added to the TECCs after vitrification) contained half the CPAs in the formulations listed in Table 3.4 and mannitol (400 mM). Thus, the full-strength mixture of the removal solutions contained 50% VS, 20% 5xEC, and 400 mM mannitol in DI water, and pH to 7.9-8.1. The mannitol had to be dissolved on a hot plate in 5xEC before the addition of the CPAs to make the formulations.

Table 3.4. Vitrification solution formulations

Vitrification Solution	DMSO	formamide	1,2-propanediol	HEPES	Total
VS55	3.1 M	3.1 M	2.21 M	0.01 M	8.4 M
VS70	3.97 M	3.97 M	2.83 M	0.01 M	10.8 M
VS83	4.65 M	4.65 M	3.3 M	0.01 M	12.6 M

The viability (see section 3.10.4 AlamarBlue Assay) of the harvested TECCs was tested before the cryopreservation process began. The full-strength mixture of each vitrification solution (both the addition and removal solutions) was introduced/eluted into/out of the TECCs at 4ºC in a step-wise method consisting of discrete steps 15 minutes each of exposure to the vitrification solution increasing (addition solutions) or decreasing (removal solutions) in strength. The solution used for traditional freezing was introduced and eluted in one step. The step-wise method of introducing addition

solutions gradually exposed the TECCs to the CPAs to equilibrate with the surrounding solution and to maintain osmotic balance. Table 3.5 shows the percentage of vitrification solution in 1xEC solution (0.19 M dextrose, 0.01 M potassium phosphate monobasic (KH_2PO_4), 0.04 M potassium phosphate dibasic (K_2HPO_4), 0.02 M potassium chloride (KCl), and 0.01 M sodium bicarbonate ($NaHCO_3$) with a pH between 7.9 and 8.1) for each addition solution increasing in strength from A1 to A6. Studies that involved six steps introduction method included all six solutions, whereas, studies that involved four steps included A1, A3, A5, and A6 solutions only.

Table 3.5. Solutions for the step-wise introduction of CPAs

Vitrification Solution	CPA Volume	1xEC Volume
A1	0%	100%
A2	18.7%	81.3%
A3	25%	75%
A4	50%	50%
A5	75%	25%
A6	100%	0%

In a similar manner, the step-wise method of introducing removal solutions gradually removed the CPAs from the TECCs. Table 3.6 shows the percentage of the vitrification solutions in 1xEC solution for each removal solution decreasing in strength from R1 to R7. Studies that involved seven steps eluting method included all seven solutions, whereas, studies that involved only four steps included R1, R4, R6, and R7. The 1xEC solution used in the removal method contained 200 mM of mannitol for solutions R1 to R6 and R7 solution contained 1xEC with 0 M of mannitol. After the R7 solution was removed, culture media was added for 15 minutes before removal. Finally,

more culture media was added to each TECC and stored in the incubator (37ºC) for a one-hour recovery before the viability was tested.

Table 3.6. Solutions for the step-wise removal of CPAs

Vitrification Solution	CPA Volume	1xEC Volume
R1	100%	0%*
R2	75%	25%*
R3	50%	50%*
R4	25%	75%*
R5	12.5%	87.5%*
R6	0%	100%*
R7	0%	100%

* 1xEC with 200 mM of mannitol

In the step-wise introduction method, TECCs were exposed to 5 mL of each addition solution in 6-well dishes on ice (4ºC) on an orbital shaker (approximately 100 rpm) to facilitate diffusion. The TECCs were then placed in scintillation vials filled with 5 mL of A6 (the full-strength mixture) solution and 0.8 mL of isopentane (EMD Chemicals Inc., Darmstadt, Germany) to limit direct air contact (Song, Lightfoot et al. 2003). Samples, along with a blank vial filled with VS55 and a thermocouple, were loaded into a tube rack and then placed in a pre-cooled isopentane bath located in a -150ºC mechanical storage freezer (Thermo Fisher Scientific, Inc., Waltham, MA or Sanyo Moriguchi, Japan) or in a small-scale bench-top apparatus (53 cm x 34 cm x 30 cm) which contained approximately 7 L of liquid nitrogen. The temperature was monitored via the thermocouple. When samples went from 4ºC to -100ºC they were removed from the isopentane bath and placed on a shelf in the mechanical freezer or in the vapor phase of the liquid nitrogen to slowly drop from

-100ºC to -135ºC. After samples reached -135ºC they were stored in the freezer overnight or in the case of the bench-top system, were removed immediately to begin the re-warming process. Vitrification occurred when drop in temperature from 4ºC to -100ºC occurred at approximately -40ºC per minute. The traditional freezing method occurred at a slow cooling rate of approximately -1ºC per minute to -180ºC.

Samples were re-warmed slowly by removing the vials from the freezer to room temperature. The temperature went from -135ºC to -100ºC and then quickly re-warmed from -100ºC to 4ºC when the vials were placed in a 37ºC water bath. Fast re-warming was at a rate approximately 40ºC per minute. TECCs were then removed from the vials and placed in 6-well dishes filled with 5 mL of the first of the removal solutions (R1) on an orbital shaker at 4ºC. The removal solutions were then introduced in a step-wise manner, which decreased in strength of CPAs. The traditional freezing method occurred at a slow warming rate similar to the cooling rate. The freezing solution was removed in one-step.

In the no vitrification study, TECCs were not subjected to vitrification to -150°C. Instead, TECCs were kept at 4°C in the full-strength mixture of VS55 or VS70 for approximately 30 minutes. Thirty minutes was chosen because the total time for samples to vitrify from 4°C to -135°C and to re-warm back to 4°C took approximately 30 minutes (without overnight storage at -150°C).

While the step-wise method introduced/eluted the CPAs in discrete steps on the orbital shaker the bioreactor introduced/eluted the CPAs gradually. Three reservoirs filled with 150 mL of A3, A5, and A6 were connected via tubing to pump the solution into the central hub of the PCC bioreactor, which contained the TECCs at 4ºC. The

TECCs were harvested from the PCC bioreactor and tested for viability and then eight TECCs were placed back into the bottom row of the inner bob of the PCC bioreactor. The top row was not utilized in this study. The outer cup was filled with 150 mL of A1 solution, which was not enough to penetrate the top row, but permeated the constructs only (due to a pressure gradient between the inner hub and outer cup region) when the inner bob was placed inside the outer cup. After 15 minutes the A3 solution from the first reservoir was pumped at 10 mL/min (or a perfusion rate of 1.25 mL/min/construct) into the PCC bioreactor as the A1 solution was pumped out into a waste beaker at the same rate. A5 solution was pumped in as A1 was pumped out after 15 minutes. A6 solution was then pumped in as A5 was pumped out after 15 minutes. After 10 minutes of the A6 solution pumping in, the TECCs were removed from the PCC bioreactor and placed in scintillation vials containing A6 solution and isopentane as mentioned earlier. Vitrification and re-warming proceeded in the method described earlier. The TECCs were then placed back into the bottom row of the inner bob of the PCC bioreactor and the removal solutions were pumped in using the reservoir method, where four reservoirs containing 150 mL of R4, R6, R7, and culture media at 4ºC were used. The TECCs were harvested after the last of the media perfused through the constructs and placed in 6-well dishes containing media and stored in the incubator for a one-hour recovery. The viability of the TECCs were then measured and compared to their viability before the cryopreservation process began. A flow chart in Figure 3.9 shows the diagrams of the bioreactor introduction/elution method.

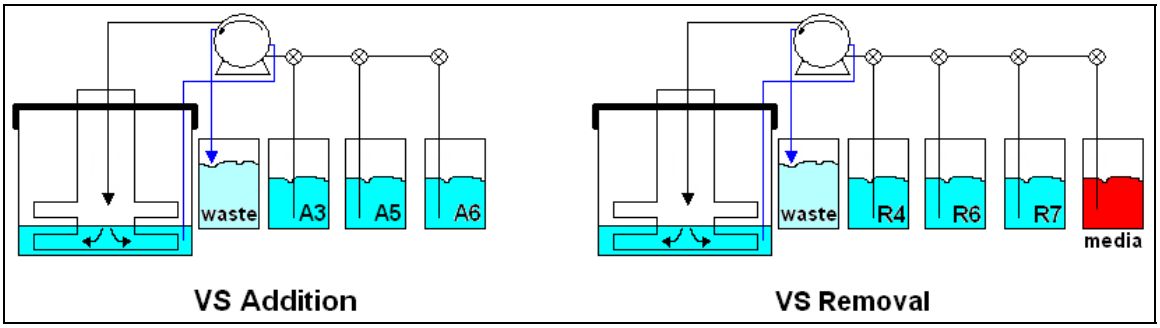

Figure 3.9. Bioreactor introduction/elution diagram for the addition and removal of vitrification solutions.

The viscosity of the vitrification solutions, VS55 and VS70, were measured with a viscometer. The solutions were prepared and allowed to equilibrate in the viscometer at 4ºC. The efflux time was recorded in a size 50 M710 Cannon-Fenske viscometer, which had the viscometer constant 0.004 centistokes per second. Multiplication of the constant to the efflux time determined the kinematic viscosity, ν. The average density of the components of the vitrification solution was 1.09 g/mL. The viscosity of the vitrification solution was calculated using Equation 3.12:

$$\nu = \frac{\mu}{\rho} \qquad \text{Equation 3.12}$$

By knowing the viscosity and the perfusion flow rate through the PCC bioreactor, the shear stress exerted on the construct during the introduction and elution of the vitrification solution was derived according to Equation 3.3.

3.9 Construct Harvesting and Digestion

Harvested constructs were washed in PBE in 50 mm sterile Petri dishes and stored in Eppendorf tubes at –20ºC for biochemical analysis. After all the constructs were harvested from each experimental run they were then dried overnight in a speed vacuum system (Labconco Corporation, Kansas City, MO), which dehydrated the samples under vacuum pressure. Each sample was then digested in 1 mL of 0.5% papain (v/v) (activity 23.2 U/mg) (Worthington) in PBE containing 1.75 mg/mL cysteine overnight (16 - 18 hours) at 60ºC. The papain enzymes broke down cellular and extracellular components within the TECCs, releasing them from the scaffold for biochemical analysis. Samples were then stored at –20ºC and used for various biochemical composition assays. Samples tested for mechanical properties were washed in PBE and stored in PBE with 1x protease inhibitor cocktail I (Calbiochem, Darmstadt, Germany) at –20ºC to prevent the breakdown of the cartilage extracellular matrix before they were tested. Those used for histological analysis (including the animal implants) were washed in PBE and stored in 10% formalin for fixation in 15 mL centrifuge tubes at 4ºC until processed. Samples used for live/dead analysis under the confocal microscope were washed in PBE and immediately viewed before stored in Eppendorf tubes at -20ºC, lyophilized, and papain digested as mentioned in the procedure for samples analyzed for biochemical composition. Samples tested for gene expression were chopped into cubes 1 - 2 mm^3 in size before treated with Trizol reagent (Invitrogen) for RNA extraction and stored at -80ºC until analyzed.

3.10 Construct Analysis

3.10.1 DNA Assessment

DNA content was determined from a PicoGreen DNA determination kit (Invitrogen). The PicoGreen reagent was a sensitive fluorescent nucleic acid stain and was used to quantify double-stranded DNA strands. A DNA stock solution was prepared from calf thymus DNA (100 μg/mL) provided by the kit. The stock solution of 2 μg/mL was prepared using a TE buffer solution (10 mM Tris·Cl, 1 mM EDTA, and pH 7.5). A standard curve was made from diluting the DNA stock solution in accordance to Table 3.7.

Table 3.7. DNA standard formulations

DNA Stock Solution	TE Solution	Final Concentration
1000 μL	0 μL	2 μg/mL
500 μL	500 μL	1 μg/mL
300 μL	700 μL	0.6 μg/mL
100 μL	900 μL	0.2 μg/mL
10 μL	990 μL	0.02 μg/mL
1 μL	999 μL	0.002 μg/mL
0 μL	1000 μL	0 μg/mL

Samples were typically diluted 1:80 v/v in order for samples to fall within range of the standard curve. Aliquots of the diluted samples and controls were measured with the PicoGreen reagent. In accordance with the kit's protocol, the reagent was diluted 200-fold with TE buffer and added in a 1:1 ratio to the samples in black 96-well plates. Fluorescence was read in a fluorescence plate reader at an excitation of 480 nm and emission of 520 nm. Correlated to the standard curve, DNA content per construct was

determined. Cell number was determined by correlating 7.7 pg of DNA per cell for chondrocytes (Kim, Sah et al. 1988).

3.10.2 Glycosaminoglycan Assessment

Glycosaminoglycan (GAG) concentration in harvested TECCs and spent media samples was measured using a dimethylmethylene blue (DMMB) spectrophotometric assay (Farndale, Sayers et al. 1982). DMMB binds to the sulfate groups located on chondroitin sulfate and keratan sulfate to result in a detectable color shift. The absorbance was measured in a spectrophotometer at 525 nm. A stock solution of chondroitin sulfate A (CS) from bovine trachea was prepared at a concentration of 200 μg/mL. Table 3.8 lists the formulations for the GAG standard curve where the diluent was either PBE for measuring GAG in TECCs or media for measuring GAG in spent media.

Table 3.8. GAG standard formulations

CS Stock Solution	Diluent*	Final Concentration
0 μL	1000 μL	0 μg/mL
125 μL	875 μL	25 μg/mL
250 μL	750 μL	50 μg/mL
375 μL	625 μL	75 μg/mL
500 μL	500 μL	100 μg/m L
625 μL	375 μL	125 μg/mL
750 μL	250 μL	150 μg/mL
875 μL	125 μL	175 μg/mL
1000 μL	0 μL	200 μg/mL

* PBE or media

Typical dilution for measuring GAG concentration in TECCs was 1:10 and 1:1 for spent media samples. The DMMB dye solution (46.0 mM DMMB, 40.5 mM NaCl, 40.5 mM glycine, 8.7 mM HCl, and pH 3.0) was added in a 26:1 ratio to aliquots of the diluted samples and controls in 96-well plates. Soluble GAG in media released per construct was determined from knowing the total volume of media in the bioreactor and the number of constructs in the bioreactor when media samples were taken.

3.10.3 Collagen Assessment

Total collagen concentration in TECCs was determined via hydroxyproline quantification. The ratio of total collagen to hydroxyproline content was 9:1 (Woessner 1961). A stock solution of cis-4-hyroxyproline was prepared at a concentration of 100 μg/mL. Table 3.9 lists the formulations for the hydroxyproline standard curve.

Table 3.9. Hydroxyproline standard formulations

Hydroxyproline Stock Solution	DI Water	Final Concentration
0 μL	1000 μL	0 μg/mL
100 μL	900 μL	10 μg/mL
200 μL	800 μL	20 μg/mL
400 μL	600 μL	40 μg/mL
500 μL	500 μL	50 μg/mL
600 μL	400 μL	60 μg/mL
800 μL	200 μL	80 μg/mL
900 μL	100 μL	90 μg/mL
1000 μL	0 μL	100 μg/mL

The collagen in the samples, controls, and standards were hydrolyzed with 6 N HCl in a 1:1 ratio at 110ºC for 3 - 4 hours and at 95ºC for 18 hours or until dried in glass tubes

capped loosely with glass covers. A stock buffer (0.24 M monohydrate citric acid, 0.85 M NaOH, 0.12 g/mL sodium acetate trihydrate, and 1.2% v/v acetic acid) and working buffer (66.7% v/v stock buffer, 13.3% v/v DI water, 20% v/v isopropanol, and pH 6.0) were prepared beforehand to make a chloramine-T solution (0.05 M chloramines-T, 20% v/v DI water, 20% v/v isopropanol, and 80% v/v working buffer). After samples, controls, and standards were hydrolyzed, they were resuspended in 1 mL of water. 50 μL of each sample, control, or standard was plated in a 96-well plate, then 50 μL of the chloramine-T solution was added to each sample, control, or standard and incubated at room temperature in the dark for 20 minutes to oxidize the hydroxyproline. Next, a p-dimethylaminobenzaldehyde (pDAB) solution was prepared (60% v/v isopropanol, 0.15 g/mL pDAB, 26% v/v 60% perchloric acid, and 14% v/v n-propanol) and added (50 μL) to each sample, control, and standard. The pDAB reacted with the intermediate pyrrole to produce a color change (Stegemann and Stalder 1967). The solution was then incubated for 30 minutes at 60ºC, and absorbance was read at 550 nm on a spectrophotometer. Typically, samples were diluted 2-fold to fall within the standard curve.

3.10.4 AlamarBlue Assay

The cell viability in TECCs treated in the cryopreservation studies was quantitatively determined from an alamarBlue dye (Invitrogen). The alamarBlue dye was both fluorometric and spectrometric and was used to measure the metabolic activity of cells. During incubation, metabolically active cells converted the oxidized form of alamarBlue (non-fluorescent and blue) to its reduced form (fluorescent and red) with

mitochondrial and cytosolic enzymes (Gonzalez and Tarloff 2001). Aliquots of the media and alamarBlue solution were measured in a 96-well plate on a fluorescence plate reader at an excitation of 544 nm and emission of 590 nm. Each TECC was incubated with 2.5 mL of media and 250 μL of alamarBlue and allowed to incubate for 3 hours at 37ºC/5% CO_2. Controls were media and alamarBlue with no cells. Because the dye was non-cytotoxic the assay was performed on the TECCs just before cryopreservation and again right after cryopreservation to determine the percentage of cells that survived the various preservation treatments, thus giving quantifiable cell viability levels.

3.10.5 Live/Dead Assay

The cell viability in TECCs was qualitatively determined from a fluorescent live/dead viability kit (Invitrogen). The live/dead solution contained calcein AM (1 μM) and ethidium homodimer-1 (EthD-1) (2 μM) in PBE. Nonfluorescent calcein AM was converted to green fluorescent calcein (excitation/emission 495 nm/515 nm) by intracellular esterase, where esterase activity was characteristic of live cells. EthD-1 stains for dead cells by entering cells through damaged cell membranes and then producing a 40-fold enhancement of red fluorescence (excitation/emission 495 nm/635 nm) upon binding to nucleic acids. Immediately after harvesting TECCs from the bioreactor or after finishing the alamarBlue assays the samples were washed in PBE for 30 minutes to remove media or alamarBlue. Samples were then treated with 150 μL of the live/dead solution and incubated at 37ºC/5% CO_2 for 30 minutes before viewed under a laser scanning confocal microscope (Carl Zeiss Inc., Thornwood, NY) to assess cell viability and distribution in the constructs. Images were taken at the center of

the construct and imaged approximately 1% of the whole construct. Fluorescent intensity (red or green) of the cells and fragments in the images taken was measured using ImageJ software (National Institutes of Health, Bethesda, MD). The relative intensity of the live and dead cells was then used to determine relative cell viability levels.

3.10.6 Histology

All samples for histological analysis were fixed in 10% neutral buffered formalin and stored at 4ºC prior to embedding. Samples were then dehydrated with a series of graded ethanol stations to be replaced with xylene in order to be miscible with paraffin. Liquefied paraffin (60ºC) infiltrated into the samples to penetrate all interstitial spaces in the TECCs. The paraffin wax provided the support needed for thin sectioning. The paraffin-infiltrated samples were further embedded into a liquid mold of paraffin, which solidified at room temperature. After solidification, the blocks containing the samples were cut with a microtome into thin sections (5 μm in thickness) and positioned onto slides for staining. All sections were cut across the thickness of the TECCs.

Sections were stained with hematoxylin and eosin (H&E) for cells, fast green/Safranin-O for cytoplasm/GAG, and immunostained for collagen type II and collagen type I. Immunohistochemical staining was carried out with the primary monoclonal antibody for type II collagen (II-II6B3, Developmental Hybridoma Studies Bank, Iowa City, IA), for type I collagen (MAB3391, Chemicon, Inc. Temecula, CA), and a biotintylated anti-mouse secondary antibody (BA2020, Vector Laboratories, Burlingame, CA). Prior to staining the sections were deparaffinized and rehydrated to be miscible with the water-soluble dye or antibody used. After staining the samples were

dehydrated with ethanol, cleared with xylene, and coverslipped with mounted media for long-term preservation. Tables 3.10 - 3.12 lists the protocols for each of the stains used on the TECCs.

Table 3.10. Hematoxylin and eosin protocol

Step	Procedure	Number of washes	Duration
1	Xylene	3	3 minutes
2	100% alcohol	3	2 minutes
3	95% alcohol	2	2 minutes
4	70% alcohol	1	2 minutes
5	DI water	1	2 minutes
6	Hematoxylin	1	0.5-1 minute
7	0.5% acid alcohol	1	1 dip
8	Water	1	1 minute
9	Bluing reagent	1	30 seconds
10	Water	1	1 minute
11	95% alcohol	1	1 minute
12	1% alcoholic eosin	1	30 seconds
13	95% alcohol	1	30 seconds
14	100% alcohol	3	1 minute
15	Xylene	3	1 minute
16	Coverslip and mount media	--	--

Table 3.11. Safranin-O protocol

Step	Procedure	Number of washes	Duration
1	Xylene	3	3 minutes
2	100% alcohol	3	2 minutes
3	95% alcohol	2	2 minutes
4	70% alcohol	1	2 minutes
5	DI water	1	1 minute
6	Weigert's hematoxylin	1	15-30 seconds
7	Tap water	1	2 minutes
8	1% acid alcohol	1	Dip
9	Tap water	1	2 minutes
10	0.2% aqueous fast green	1	1 minute
11	1% acetic acid	1	3 seconds
12	0.5% Safranin-O	1	5 minutes

Table 3.11. Safranin-O protocol (continued)

13	95% alcohol	1	1 minute
14	Reagent alcohol	3	1 minute
15	Xylene	2	1 minute
16	Coverslip and mount media	--	--

Table 3.12. Immunohistochemical staining for collagen type II and collagen type I procedure

Step	Procedure	Number of washes	Duration
1	Xylene	3	3 minutes
2	100% alcohol	3	2 minutes
3	95% alcohol	2	2 minutes
4	70% alcohol	1	2 minutes
5	Rehydrate in PBS	2	5 minutes
6	Antigen retrieval with pepsin (37°C)	1	20 minutes
7	PBS	2	5 minutes
8	Block 1% gelatin in PBS	1	20 minutes
9	Primary antibody (1:1 for collagen type II, 1:80 for collagen type I) dilution in 1% BSA in PBS	1	1 hour
10	PBS	2	5 minutes
11	Secondary antibody (1:400) dilution in 1% BSA in PBS	1	30 minutes
12	PBS	2	5 minutes
13	Vector ABC Reagent (Vector Laboratories, Burlingame, CA)	1	30 minutes
14	PBS	2	5 minutes
15	DAB* peroxidase substrate	1	Until stain develops
16	Tap water rinse	1	--
17	Counter stain with Hematoxylin	1	2 minutes
18	Tap water rinse	1	--
19	95% alcohol	1	30 seconds
20	100% alcohol	3	1 minute
21	Xylene	3	1 minute
22	Coverslip and mount media	--	--

* 3,3’-diaminobenzidine tetrahydrochloride

All slides were viewed under a light microscope (Nikon's Eclipse E600) at 4x, 10x, or 20x magnification and images were taken at the center of the constructs using a Retiga 1300 Q imaging camera. Histology was performed at the histology lab located in the Institute of Bioengineering and Bioscience (IBB) at the Georgia Institute of Technology or by the Center for Metabolic Bone Disease Core Laboratory at the University of Alabama at Birmingham, Birmingham, AL.

3.10.7 Gene Expression

Reverse-transcription polymerase chain reaction (RT-PCR) was used to evaluate the gene expression of tissue-engineered cartilage harvested from the bioreactors by measuring mRNA expression for collagen type II, collagen type I, aggrecan, COMP, and glyceraldehyde 3-phosphate dehydrogenase (GAPDH). Primary bovine articular chondrocytes were used as positive controls for collagen type II, aggrecan, and COMP. Primary bovine osteoblasts were used as positive controls for collagen type I. The primary sequences, annealing temperatures, and product size for each gene marker were as follows:

Table 3.13. Gene sequences for reverse transcriptase PCR

Accession Number	Forward Primer Reverse Primer	Annealing Temperature	Product size
Collagen Type II			
AF138957	5'-GAA GGT GGA AAA CCA GGT GA-3' 5'-CAT TCC CTG AAG ACC TGG AG-3'	57ºC	228 bp
Collagen Type I			
AB098910	5'-GAA GAG CGG AGA ATA CTG G-3' 5'-GTG GTA GGT GAT GTT CTG G-3'	59.8ºC	301 bp
Aggrecan			
AF019755	5'-TGC TAC ACA GGT GAA GAC-3' 5'-TGG ACT CTC TGG GAA AGG-3'	54.5ºC	307 bp
COMP*			
X74326	5'-TTC GGA ACG CAC TGT GG-3' 5'-TGC AGG AAC CAG CGG TA-3'	58.1ºC	302 bp
GAPDH			
U85042	5'-CGA GAA GTA TAA CAA CAC C-3' 5'-GGT AGA AGA GTG AGT ATC G-3'	54ºC	472 bp

* (Bosnakovski, Mizuno et al. 2006)

After TECCs were harvested from the bioreactors, washed, and chopped into 1 - 2 mm^3 cubes, each sample was stored in 4 mL of Trizol reagent (a mixture of phenol, guanidine isothiocyanate, red dye, and other proprietary components which disrupted the cells and isolated the RNA) in a 15 mL centrifuge tube at -80ºC until the end of the experimental run. At the end of each run, each sample was treated with 0.8 mL of chloroform for 2 - 3 minutes and centrifuged (Sorvall, SH-3000 rotor) at 4700 rpm (4575 g_c) for 30 minutes to separate the aqueous and organic phases. The RNA, located in the aqueous phase was removed and precipitated out with isopropanol (2 mL). After incubation at room temperature for 10 minutes, the RNA was spun down at 4700 rpm for 20 minutes to pellet form. The supernatant was decanted and the RNA pellet was washed and mixed in 8 mL of cold 75% ethanol. The RNA was spun down to pellet form again (4700 rpm for 12 minutes) and the ethanol decanted. Before dissolution in 60 μL of

diethyl pyrocarbonate (DEPC)-treated water (RNase free water), the RNA pellet was air-dried for approximately 20 minutes. The RNA was quantified by UV spectrophotometer, which required a 1:10 dilution of the samples with DEPC-water before measurement. The RNA/DNA ratios (absorbance 260/280 nm) for all the samples were above 1.5 as an indicator of RNA purity. The RNA concentration per construct was recorded. The mean concentration was then determined for each day (Day 4, 7, 14, 21, and 28). The construct whose RNA value was closest to its mean value (the smallest variance) was chosen to use for gene expression analysis for collagen type II, collagen type I, aggrecan, COMP, and GAPDH.

Reverse transcription using a PCR machine (iCycler, Bio-Rad Laboratories, Hercules, CA) was performed on the RNA to make cDNA (complementary DNA). Unless otherwise noted materials used for PCR were purchased from Qiagen, Duesseldorf, Germany and primers were purchased from VWR. Samples were diluted with DEPC-water to a total volume of 8 μL (DEPC-water volume = 8 μL - $[RNA]^{-1}$) before placed in the PCR machine. The RNA was denatured at 65ºC for 10 minutes and cooled to 4ºC for 5 minutes. Then to each sample the following was added: 2 μL of 10X Buffer RT, 2 μL of dNTP (5 mM), 1 μL of Omniscript RT, 5 μL DEPC-water, and 2 μL of their respective reverse primer. The mixed samples were then placed back into the PCR machine for one hour at 37ºC to finish the first set of cDNA.

To amplify the cDNA content, 1 μL of the cDNA was added to the following: 2.5 μL 10X PCR Buffer, 17.375 μL of DEPC-water, 1 μL dNTP (5 mM), 1 μL of $MgCl_2$, 0.125 μL of Taq DNA polymerase (Fisher), 1 μL of the forward primer, and 1 μL of the reverse primer. Placed back into the PCR machine and after activation of the Taq

polymerase for four minutes at 95ºC, the sample mixture was allowed to reach 95ºC to separate DNA strands for 30 seconds, then cooled to the respective annealing temperature for 1 minute for the attachment of primers to single DNA strands, and then heated to 72ºC for 30 seconds to elongate the DNA, all before repeating the cycle again. Approximately 30 cycles were performed to produce enough cDNA for gel electrophoresis.

Gel electrophoresis allowed visualization of the amplified cDNA for the gene tested. To each agarose gel, a mixture of 10 μL of the PCR product or DNA ladder standard (BioVentures, Inc., Murfreesboro, TN) and 2 μL of loading dye (BioVentures) was added to each well of a pre-made Ready Gel (Bio-Rad). Placed in a gel electrophoresis apparatus (Bio-Rad) and filled with 300 mL of 1x TBE Buffer (0.89 M Tris Base, 0.89 M boric acid (Bio-Rad), 20 mM EDTA, and pH to 8.0), the gel was exposed to 100 V for 55 minutes for the migration of the cDNA through the gel. Afterwards, the gel was covered with 50 mL of DI water and 5 μL of ethidium bromide (Bio-Rad) for 5 minutes on a shaker (ethidium bromide fluoresces when bound to DNA). After rinsing with DI water for 25 minutes, the gel was read on a Versadoc machine (Bio-Rad), which exposed the gel to UV light and imaged the florescent cDNA throughout the gel. The cDNA from the samples and controls were imaged (Quantity One 4.41 software, Bio-Rad) and compared to the ladder gradient to verify the correct product size. The intensity of the bands on each harvest day was measured and compared to each other for an increase or decrease in gene expression.

3.10.8 Mechanical Testing

In one experimental run, TECCs harvested and stored at –20°C with protease inhibitors from the PCC bioreactor were tested for mechanical properties. The protease inhibitors prevented the breakdown of ECM during storage and testing. The samples were thawed to room temperature for 30 minutes prior to testing. From each TECC a biopsy punch was used to punch out one 5 mm disk, and two 4 mm disks. The 5 mm sample was tested for its compressive modulus and permeability, while the two 4 mm disks were tested for its dynamic modulus and phase angle. The thickness of each sample, h_0, was measured with digital calipers prior to testing to calculate the appropriate strain required in the tests.

3.10.8.1 Confined Compression

The compressive modulus for each TECC grown in the PCC bioreactor was measured via a confined compression chamber loaded onto an ELF uniaxial loading machine (ELF 3200, Bose, Eden Prairie, MN) located in the mechanical testing lab in IBB. The chamber (Figure 3.10A) was filled with PBE containing protease inhibitors and the 5 mm TECC was placed inside the chamber's confining chamber section (5 mm in diameter). A non-permeable indenter was loaded onto the sample until the load read 0.01 N (where stress, σ, was defined as load over the cross-sectional area of the sample). WinTest software was used to program the stress relaxation tests. Each stress relaxation test was programmed to apply strains at 5, 10, 15, and 20% on each sample. The strains were reached at a rate, V_0, of 0.0005 mm per second (dynamic loading) and the software recorded the resulting load. After reaching each strain the samples were allowed to relax

for 15 minutes. During relaxation, resulting equilibrium loads were recorded. The compressive modulus was determined from plotting the equilibrium stress values (the mean of the last ten seconds of the relaxation portion of the test) versus the applied strain. A linear fit using regression analysis was used to calculate the slope between the stress and strain, and thus, the equilibrium modulus, H_A, for each TECC.

From the dynamic portion of the confined compression test, the permeability constant, k_0, of the TECCs was determined. The dynamic portion preceded the relaxation portion of the test and measured the stress-strain relationship before the equilibrium strain was reached. The TECCs were modeled as a nonlinear biphasic material consisting of both solid and fluid that interacted to provide resistance to load. The strain-dependent permeability relationship for an isotropic homogeneous tissue was described by the following (Lai, Mow et al. 1981; Holmes and Mow 1990; Heneghan and Riches 2008):

$$k = k_0 e^{M(\lambda - 1)} \qquad \text{Equation 3.13}$$

where,

$$\lambda = \frac{h}{h_0} \qquad \text{Equation 3.14}$$

$$k = \frac{vh}{\Delta P} = \frac{vh}{\sigma} \qquad \text{Equation 3.15}$$

The displacement height, h, and resulting bulk stress, σ, were measured from the confined compression test. We assumed that bulk stress, σ, was equivalent to the pressure difference across the thickness of the sample, given that the pressure was zero at the boundary of the porous platen (when z = h in Figure 3.10A) (Soltz and Ateshian

1998). The fluid velocity, v, was determined from the ramp strain rate selected, V_0, for the dynamic portion of the compression test. That is, fluid was forced in one direction at a rate of 0.0005 mm/s through the confined constructs. Curve-fitting the dynamic portion of the stress-strain curve resulted in the determination of the permeability constant and the strain dependent coefficient, M. Four dynamic stress-strain relationships were measured before reaching equilibrium at 5, 10, 15 and 20% strain. The stress-strain curve before 5% strain was reached was not included in the permeability calculations. This was due to the large lag time in stress resulting from strain displacement, which resulted in poor fitting. The three permeability constants calculated before each strain was average together as the final value for the permeability constant. An example calculation for the compressive modulus and permeability constant is seen in Appendix A.

3.10.8.2 Rheology

The dynamic/shear modulus and phase angle for each TECC was determined from an oscillation test that was performed on a CVO 120 rheometer (Bohlin Instruments, Malvern Instruments Ltd., Worcestershire, UK) located in the mechanical testing lab in IBB. The 4 mm samples were loaded onto the rheometer (Figure 3.10B) and immersed in PBE containing protease inhibitors to keep the samples hydrated. The indenter (upper platen), 4mm in diameter, was lowered to a 10% uniaxial strain and the sample was allowed to equilibrate for 30 minutes before testing. As the upper platen rotated at a 0.5% strain, a frequency sweep between 0.01 and 1 Hz was carried out with a logarithmic increase in frequency. The three frequencies used were 0.01, 0.1, and 1 Hz.

The final outcome resulted in a frequency-dependent dynamic shear modulus, G*, and phase angle, δ. The phase angle defined the ratio of the viscous response to deformation of the sample to its elastic response, thus measuring the viscoelastic behavior of each TECC.

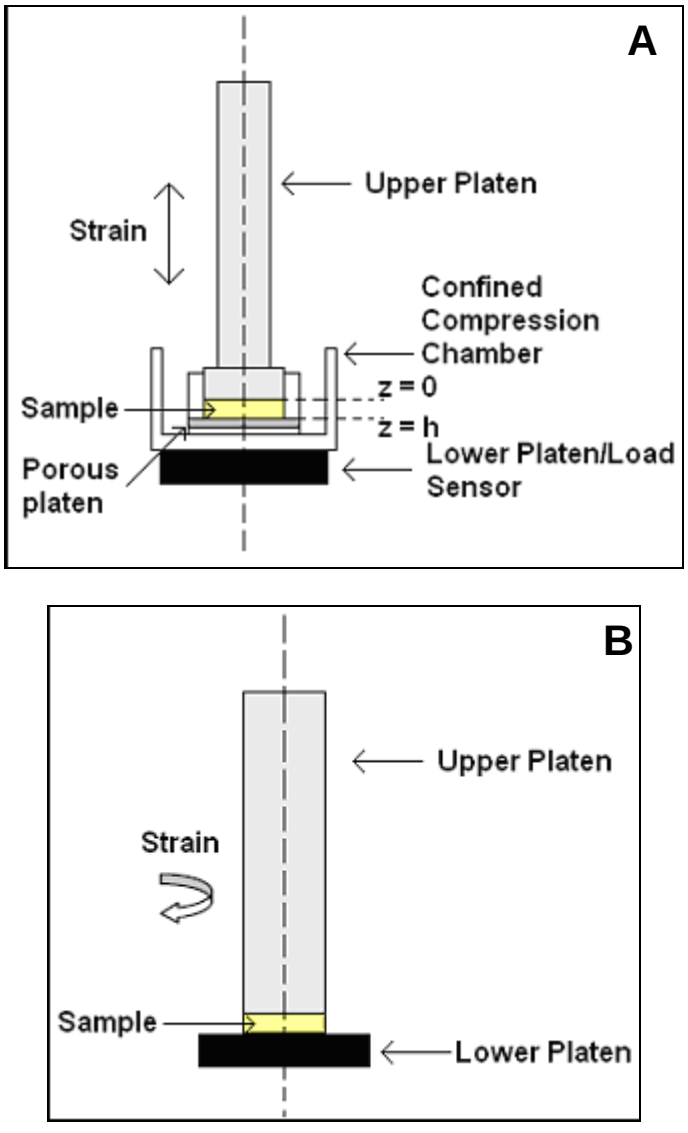

Figure 3.10. Schematic of the mechanical testing apparatus. (A) Confined compression apparatus; (B) rheometer

3.11 Statistical Analysis

For each data set, values were represented as mean ± standard error mean (SEM) for n constructs or N experimental trials. Comparison was made within each bioreactor in cartilage growth studies. That is, for 28-day long experiments, Student's t-test (two-tailed) was performed between each day compared to Day 4 values. Comparison between different bioreactor treatments was also carried out, where Student's t-test was performed between each bioreactor treatment (for example, between the CC and PCC bioreactor) for each day measured. Most experimental trials in which statistics were performed were repeated but not averaged together to confirm similar trend in each run. This was partially due to the large variation that occurred in construct development from using separate animal sources for each experiment, where each experimental trial had chondrocytes harvested from a single animal source (Saini and Wick 2003). Significance was achieved for p-values less than 0.05.

Student's t-test was also performed between each cryopreservation treatment method for the study that was carried out. In each study, treatment was normalized to a control within the experiment to measure relative difference in viability. Repeated experimental trials that were normalized were then pooled and averaged together for statistical analysis. The p-values were stated for each cryopreservation comparison study.

CHAPTER 4

RESULTS

4.1 Characterization of the Perfusion Concentric Cylinder Bioreactor

4.1.1 Momentum Transport across Construct in the Perfusion Concentric Cylinder Bioreactor

Computational fluid dynamics (CFD) calculations with the parameters mentioned in the Materials and Methods section were carried out over the diameter of the constructs embedded in the cylindrical spokes. Velocity contours (Figure 4.1A) inside the open cavity revealed that 80% of the scaffold diameter experienced a flow rate between 0.02 and 0.04 cm/s and approximately 20% at the edge experienced recirculation with an average flow rate of 0.6 cm/s. The fluid recirculation zone can be seen on the right-hand side of the open cavity in Figure 4.1A. The shear stress profile (Figure 4.1B) revealed distinct regions of varying shear stress across the diameter of the scaffold. Between 0 and 0.4 cm the average shear stress was 0.02 dynes/cm^2, between 0.4 cm and 0.8 cm the average was 0.4 dynes/cm^2, and between 0.8 cm and 1 cm where recirculation of fluid occurred, the average shear stress was 3 dynes/cm^2. Since fluid flow changed direction every twelve hours across the diameter, the center of the scaffolds experienced a constant shear stress of 0.4 dynes/cm^2, while the edges were exposed to oscillations between high and low shear stresses.

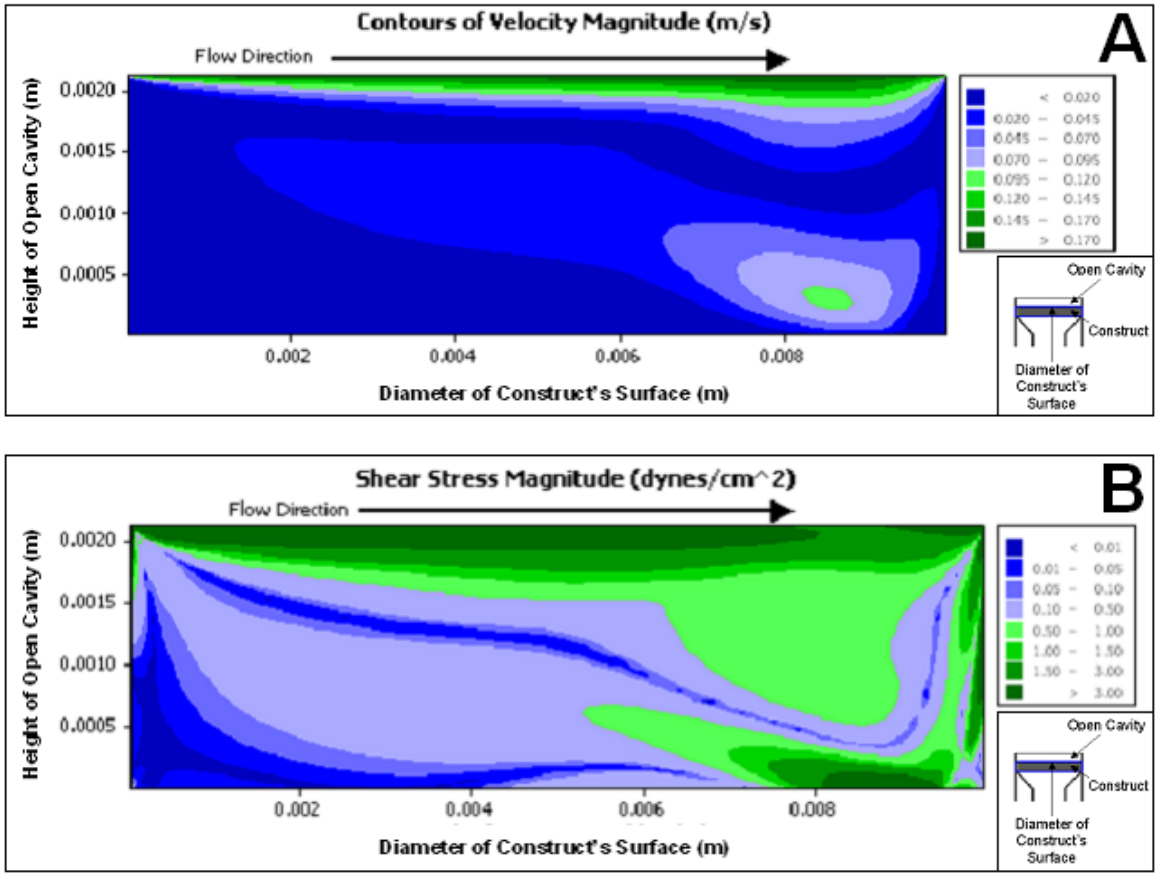

Figure 4.1. Fluid modeling of open cavity within the PCC bioreactor. (A) Velocity profile within the open cavity located over scaffold diameter; (B) shear stress profile within the open cavity located over scaffold diameter. Insets represent a diagram of the open cavity in the construct arm.

4.1.2 Oxygen Transport within the Perfusion Concentric Cylinder Bioreactor

The oxygen transport profile within the PCC bioreactor was modeled after the species continuity equation. The time taken to reach equilibrium levels based on diffusivity alone for oxygen in water was less than 24 hours (see Appendix A). Therefore, a steady-state profile was assumed and that the oxygen in media was at equilibrium with the oxygen in the incubator for all calculations, $C_{O2} = 0.212$ mol/m^3.

Before Day 4, when there was no perfusion, the oxygen transport through the thickness of the construct depended solely on diffusion in one direction. This reduced the species continuity equation to:

$$0 = D_{O2}\frac{d^2C_{O2}}{dx^2} - R_{O2} \qquad \text{Equation 4.1}$$

By assuming 10^6 cells per construct (volume 147 mm^3) the reaction rate was calculated at $R_{O2} = 9.46x10^{-4}$ mol $O_2/m^3/s$. The boundary conditions were:

$C_{O2}(0) = C_{O2}(L) = C_{O2}^0 = 0.212\ mol/m^3$, where L was the thickness of the construct.

Thus, the oxygen profile up to Day 4 followed a parabolic distribution:

$$C_{O2} = \frac{R_{O2}x}{2D_{O2}}(x - L) + C_{O2}^0 \qquad \text{Equation 4.2}$$

After Day 4, convective transport dominated in one direction and reduced the species continuity equation to:

$$V_m\frac{dC_{O2}}{dx} + R_{O2} = 0 \qquad \text{Equation 4.3}$$

By assuming $5x10^6$ cells per construct on Day 14 the reaction rate was calculated at $4.73x10^{-3}$ mol $O_2/m^3/s$. Also, by assuming approximately $10x10^6$ cells per construct on Day 28 the reaction rate was calculated at $9.46x10^{-3}$ mol $O_2/m^3/s$. With the boundary conditions the same as for when diffusivity dominated, the oxygen profile thus followed a linear dependence on position through the thickness of the construct:

$$C_{O2} = -\frac{R_{O2}}{V_m}x + C_{O2}^0 \qquad \text{Equation 4.4}$$

Figure 4.2 plots the oxygen concentration through the thickness of the construct, showing that oxygen reached the interior with a 97.4% drop from equilibrium oxygen levels in the media to the center of the construct for Day 4. In contrast, the drop in oxygen levels in media was 6.9% for Day 14 and 13.9% for Day 28 at the center of the construct.

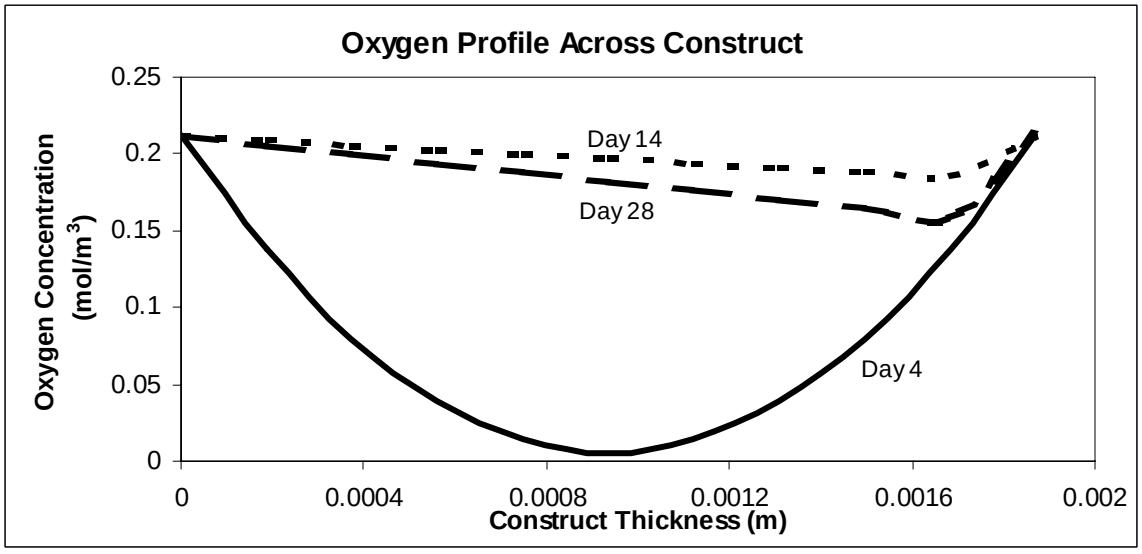

Figure 4.2. Oxygen profile through the thickness of the construct. On Day 4 diffusion dominated and followed a parabolic distribution. After Day 4, convection dominated and followed a linear distribution.

4.1.3 Construct Growth in the Perfusion Concentric Cylinder Bioreactor

The cell seeding efficiency, measured from Day 4 values, was low compared to the number of cells initially loaded into the bioreactor at 2.1 ± 1.3% ($0.2x10^6 \pm 0.1x10^6$ cells per construct). However, by Day 28 cell number increased to $7.1x10^6 \pm 0.6x10^6$ cells per construct (Figure 4.3A). Cell number had increased by 37 ± 3 fold from initial Day 4 values. Glycosaminoglycan content increased to 0.31 ± 0.03 mg/construct (Figure 4.3B) and total collagen content increased to 1.3 ± 0.1 mg/construct after 28 days in culture (Figure 4.3C). Total collagen production continued to increase over the course of 28 days, while GAG content leveled out by Day 14. There was an increase in resistance to flow as a function of time. The increase in the pressure gradient across the constructs was due to the decrease in porosity and pore size as extracellular matrix deposition into the scaffolds increased. By maintaining the overall flow rate and accounting for the decrease in porosity and pore size, the increase in shear stress exerted on the scaffolds due to perfusion over the course of 28 days was noted but not determined in this study. Bioreactor pH levels varied between 7.1 and 7.5 over the course of the run, which was within range considered physiologically relevant for cartilage (Razaq, Wilkins et al. 2003). To determine overall GAG synthesis, soluble GAG levels were measured in media samples taken from spent media and combined with GAG content retained by the constructs. Over the course of 28 days, about 92 - 99% of total GAG produced was released into the media.

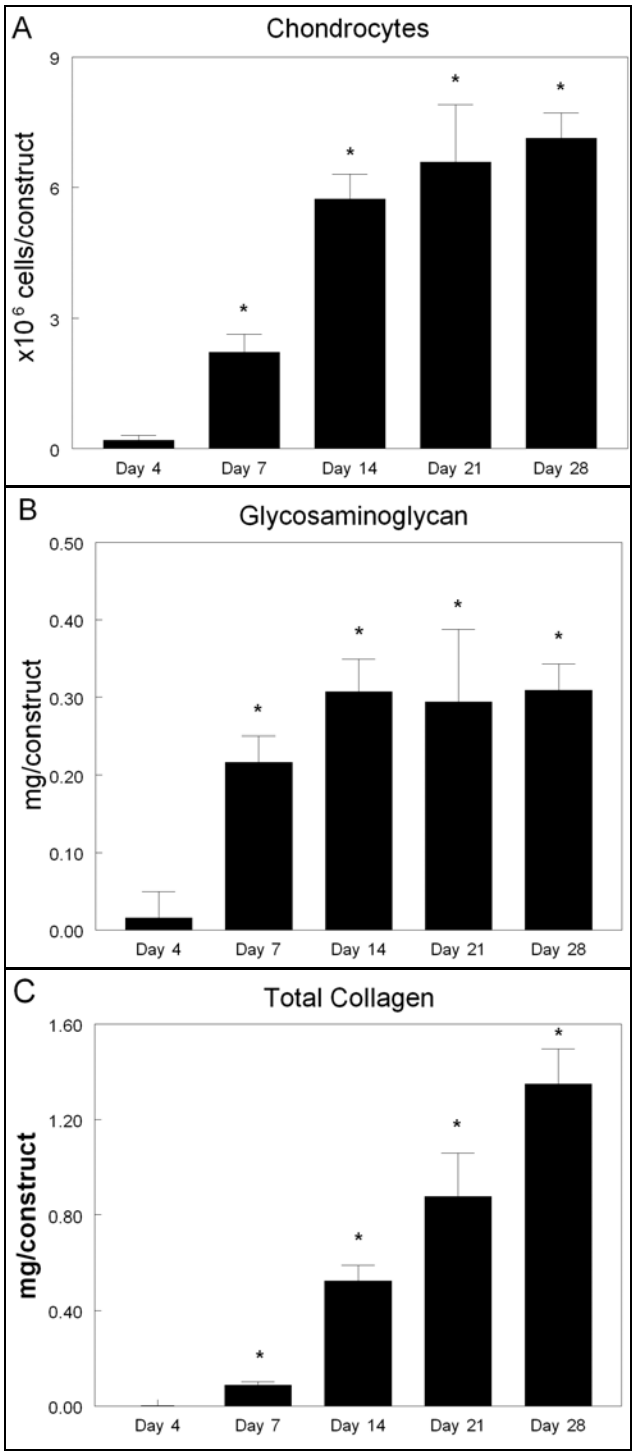

Figure 4.3. Cartilage growth in the PCC bioreactor. Data are presented for one experimental run and are presented as mean ± SEM (n = 3 constructs). (A) Cells/construct; (B) GAG/construct; (C) total collagen/construct. By Day 28 PCC bioreactor had significantly more ECM deposition with a 37-fold increase in cell number per construct. (* $p < 0.05$ vs. Day 4)

Histologically, over the course of 28 days, cells and matrix growth propagated preferentiality on the construct face that experienced surface shear (Figure 4.4). However, growth also occurred on the face that experienced bulk perfusion albeit less so than the surface shear face. By Day 28, histological analyses determined that most of the cartilage development occurred on the shear face of the constructs, whereas some extracellular matrix deposition occurred on the perfusion face. Immunohistochemical staining showed presence of collagen type II indicating cells expressed articular cartilage phenotype. Positive staining for GAG (red stain) was not present at the surface exposed to shear, but was detected in the interior away from direct exposure to surface shear forces. Seen in Figure 4.5, at higher magnification (20x) cartilage lacunae were seen surrounding cells, further indicating cartilage formation. Lack of staining for cells and extracellular matrix in the center of the constructs and presence of polymer indicated lack of cartilage development at the center of the cross-section of the constructs.

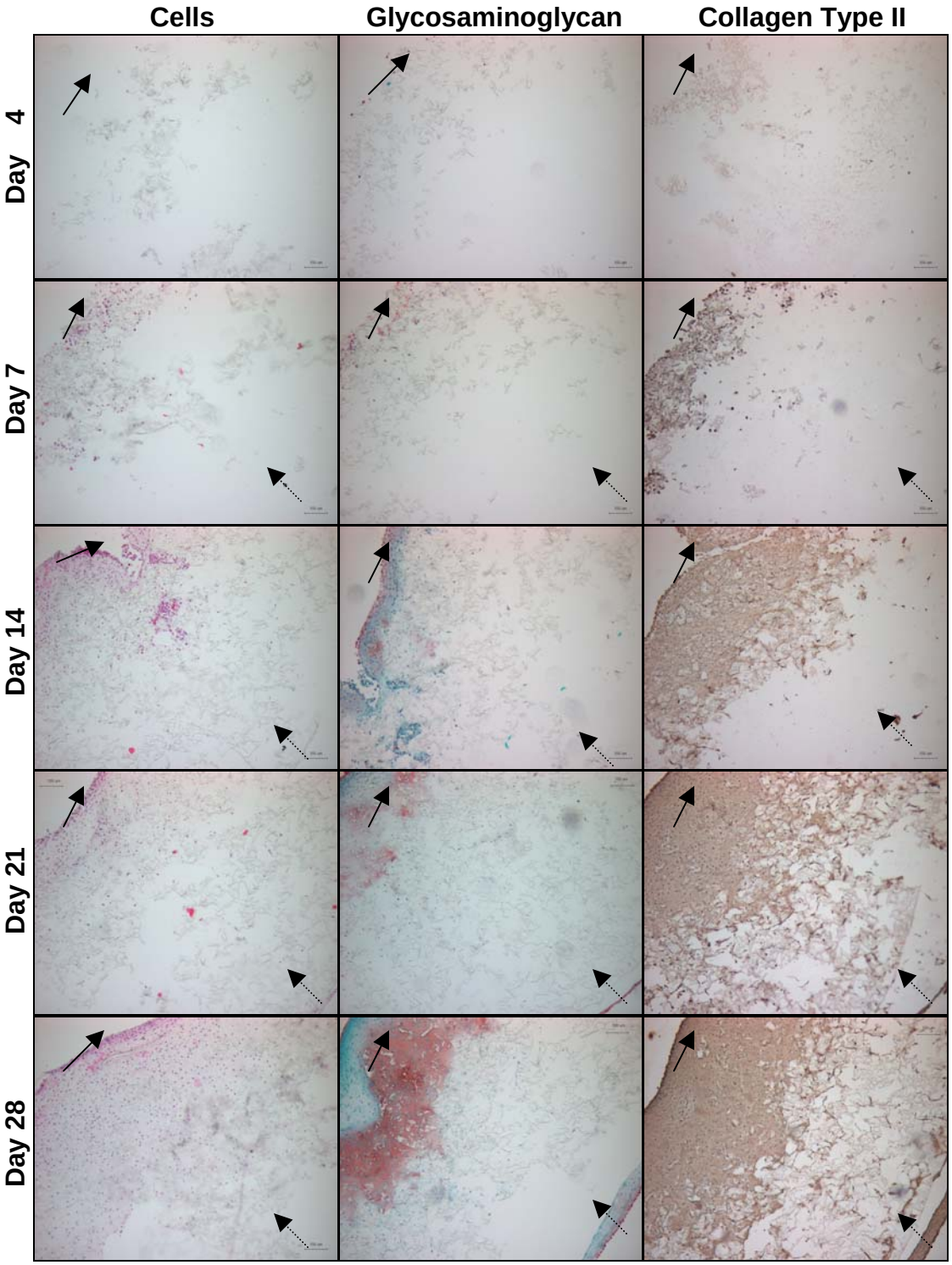

Figure 4.4. Histological images, taken at 10x, over a 4 week run. Upper left corner is the "front side" of the construct exposed to surface shear (solid arrow), while lower right corner is the "back side" of the construct exposed to perfusion (dashed arrow).

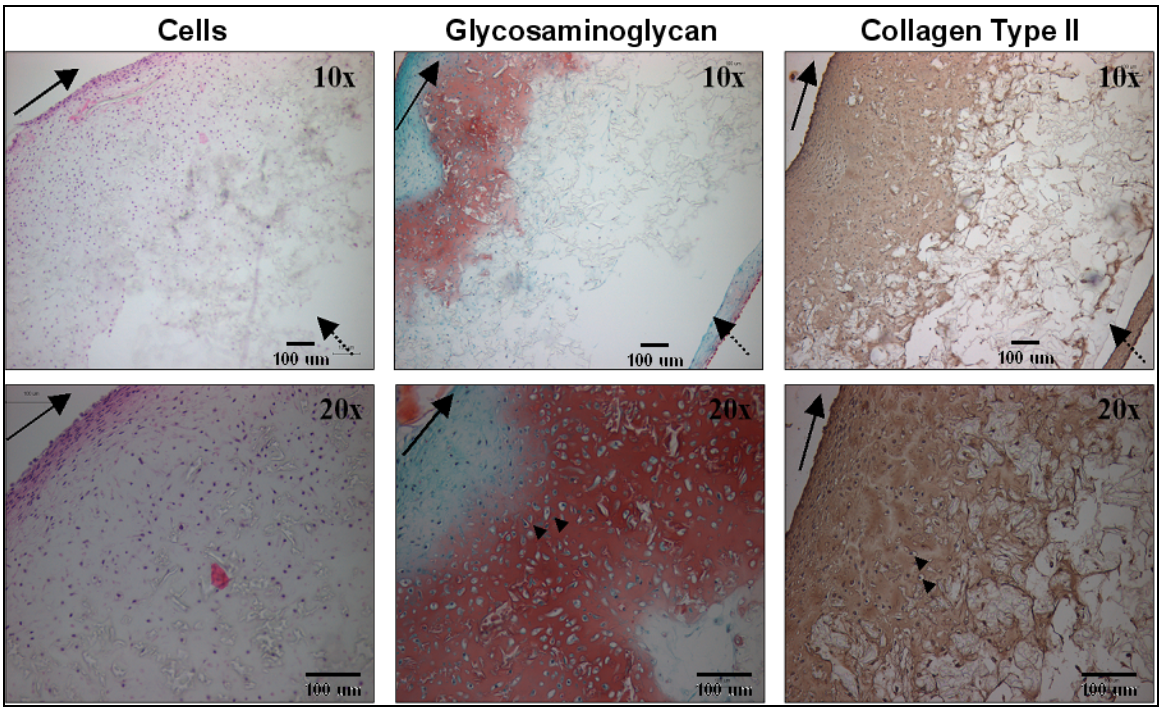

Figure 4.5. Histology for Day 28 tissue-engineered cartilage constructs from the perfusion concentric cylinder bioreactor. Constructs were sectioned through the thickness and viewed at the center. Arrows indicate direction of fluid flow in relation to construct. Solid arrows indicate fluid flowed over the top surface of the constructs (shear) and dashed arrows indicate fluid flowed through the constructs from the backside (perfusion). Constructs were stained with hematoxylin and eosin for cells, safranin-O for GAG (stained red), and immunostained for collagen type II. At higher magnification (20x) lacunae were seen surrounding cells (indicated by the small triangles) and then surrounded by ECM. Scale bar represents 100 μm.

Seen in Figure 4.6, by Day 28, cells were 82 ± 1% viable. Confocal images showed that live and dead cells were distributed over the surface of the TECCs when cultured over the course of 28 days. By Day 21, most cells were viable as seen in Figure 4.6, indicated by the green fluorescent cells. Dead cells were present throughout the constructs. The three-dimensional compilation indicated that cells grew along the rough surface of the scaffold adopting its three-dimensional shape.

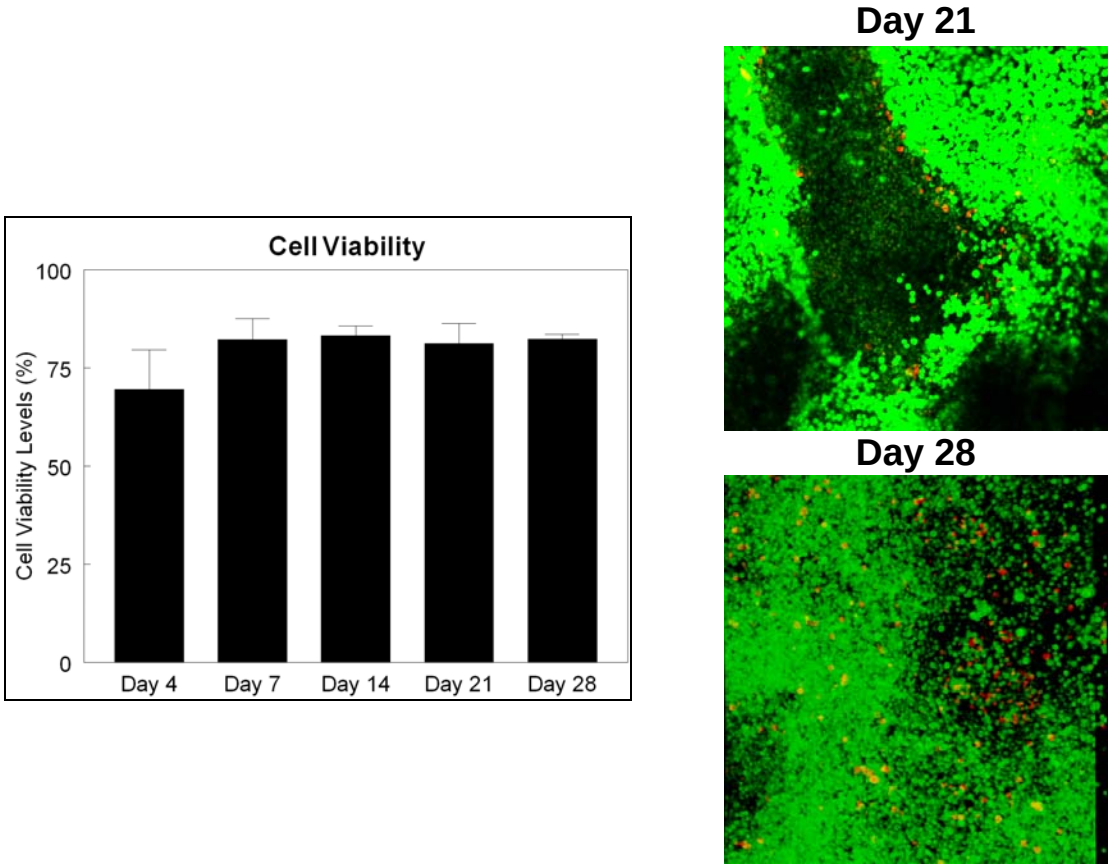

Figure 4.6. Live/dead analysis of constructs grown in the PCC bioreactor. Data are presented for one experimental run and are presented as mean ± SEM (n = 3 constructs). Confocal fluorescence images are constructs grown in the PCC bioreactor after 21 and 28 days. Cells grew along the rough surface of the PLLA scaffold. Images represent the front surface of the constructs that experienced shear. Green fluorescent indicated live cells, while red indicated dead cells or fragments.

4.2 Comparison of Construct Growth between the Concentric Cylinder and Perfusion Concentric Cylinder Bioreactor

Both bioreactors had low seeding efficiencies. By Day 4 the CC bioreactor had $1.8 \pm 0.5 \times 10^6$ cells per construct (seeding efficiency 27 ± 8%), while the PCC bioreactor had $0.8 \pm 0.2 \times 10^6$ cells per construct (seeding efficiency 11 ± 2%) (Figure 4.6A). After 28 days in culture the PCC bioreactor increased in cell number by 12 ± 1 fold, whereas the CC bioreactor increased by 7.1 ± 0.9 fold ($p < 0.05$). However, both bioreactors by

Day 28 had about 10 million cells per construct (Figure 4.7A). After the seeding period, the CC bioreactor continuously produced significantly more GAG per construct than the PCC bioreactor. By Day 28 the CC bioreactor had 1.3 ± 0.1 mg of GAG per construct while the PCC produced 0.7 ± 0.1 mg/construct ($p < 0.05$) (Figure 4.7B). GAG production reached peak levels by Day 14 in the PCC while by Day 7 in the CC bioreactor before leveling off. By Day 28 the CC bioreactor produced 1.8 ± 0.3 mg of total collagen per construct, significantly more than the PCC bioreactor at 0.8 ± 0.1 mg/construct ($p< 0.05$) (Figure 4.7C). As with GAG production, the production for total collagen reached peak levels by Day 7 for the CC bioreactor and Day 14 for the PCC bioreactor. However, total collagen content for the CC bioreactor continued to increase after Day 7, whereas after Day 21 total collagen content leveled out for the PCC bioreactor. By Day 28 little variation existed between harvested constructs from the PCC bioreactor and CC bioreactor in their cell number and extracellular matrix content (Table 4.1). Bioreactor pH levels varied between 7.1 and 7.5 over the course of the run for the PCC bioreactor; and though still mostly in physiological range, the CC bioreactor varied between 6.7 and 7.5. Over the course of 28 days, 79 - 91% of GAG was released into the media for the PCC bioreactor while only 40 - 58% of GAG was released into the media for the CC bioreactor. Repeat of this study showed the same trend with the CC bioreactor producing significantly more extracellular matrix than the PCC bioreactor, but with roughly equal number of cells per construct by Day 28 (Table 4.1). The PCC bioreactor also repeated the significantly higher fold increase in cell number per construct than the CC bioreactor. Results of this second study can be seen in detail in Appendix B.

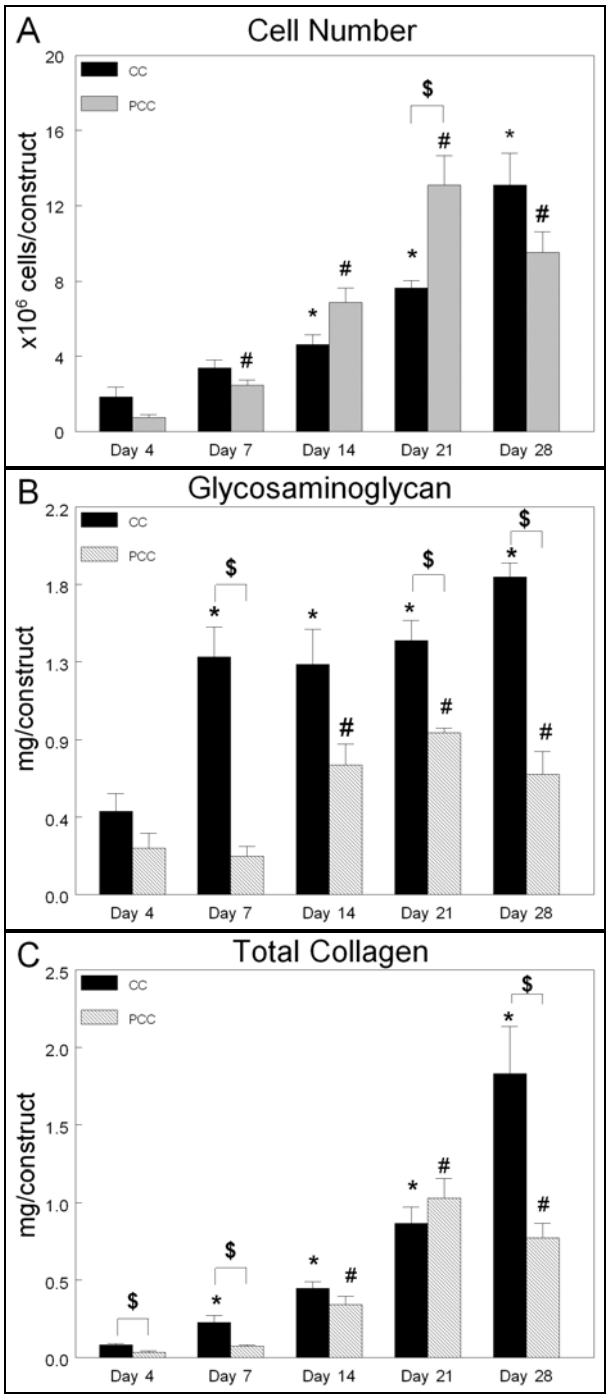

Figure 4.7. Chondrocyte proliferation and matrix deposition in the PCC bioreactor compared to the CC bioreactor. Data are presented for one experimental run and are presented as mean ± SEM (n = 3 constructs for Day 4 - 21 and n = 4 for Day 28). (A) Cells/construct; (B) GAG/construct; (C) total collagen/construct. By Day 28, constructs from the CC bioreactor had significantly more extracellular matrix deposition than the PCC while both bioreactors had roughly the same number of cells per construct. (* $p < 0.05$ vs. CC Day 4; # $p < 0.05$ vs. PCC Day 4; and $ $p < 0.05$ between PCC and CC)

Table 4.1. Individual construct composition for two experimental runs: PCC versus CC

	First Experimental Run		Second Experimental Run	
CC Bioreactor	Day 4	Day 28	Day 4	Day 28
Cells/construct ($x10^6$/construct)	1.37	10.7	2.65	7.68
	1.23	10.1	2.26	7.24
	2.89	14.5	2.18	6.79
		17.2		
mean ± SEM	1.83 ± 0.53	13.1 ± 1.7	2.37 ± 0.15	7.24 ± 0.26
Glycosaminoglycan (mg/construct)	0.36	1.70	0.29	1.14
	0.38	1.86	0.49	1.52
	0.68	1.65	0.33	1.33
		2.00		
mean ± SEM	0.47 ± 0.10	1.80 ± 0.08	0.37 ± 0.06	1.33 ± 0.11
Collagen (mg/construct)	0.10	1.36	0.07	1.83
	0.07	1.25	0.06	1.93
	0.07	2.31	0.09	1.64
		2.41		
mean ± SEM	0.08 ± 0.01	1.83 ± 0.31	0.07 ± 0.01	1.80 ± 0.09
PCC Bioreactor	Day 4	Day 28	Day 4	Day 28
Cells/construct ($x10^6$/construct)	0.78	9.76	0.19	10.81
	0.99	11.85	0.41	9.56
	0.49	9.90	0.07	7.10
		6.63		
mean ± SEM	0.75 ± 0.15	9.5 ± 1.1	0.22 ± 0.10	9.16 ± 1.09
Glycosaminoglycan (mg/construct)	0.31	0.54	0.31	0.80
	0.38	0.98	0.23	0.79
	0.10	0.82	0.28	0.44
		0.39		
mean ± SEM	0.26 ± 0.08	0.68 ± 0.13	0.28 ± 0.02	0.67 ± 0.12
Collagen (mg/construct)	0.05	0.81	0.04	1.64
	0.02	1.00	0.03	1.48
	0.04	0.76	0.03	1.48
		0.54		
mean ± SEM	0.03 ± 0.01	0.77 ± 0.10	0.03 ± 0.00	1.54 ± 0.05

Data are cells, glycosaminoglycan, and collagen content for individual constructs harvested after 4 (n = 3) or 28 (n = 3 or 4) days in culture from the indicated bioreactor. Comparisons within bioreactors indicated relatively uniform construct composition.

Seen in Figure 4.8, by Day 28, cells were approximately 52% viable with no difference between the two bioreactors. Confocal images showed no discernable difference in viability between the two bioreactors and by Day 28, most cells were viable, indicated by the green fluorescent cells. Dead cells were present throughout the constructs.

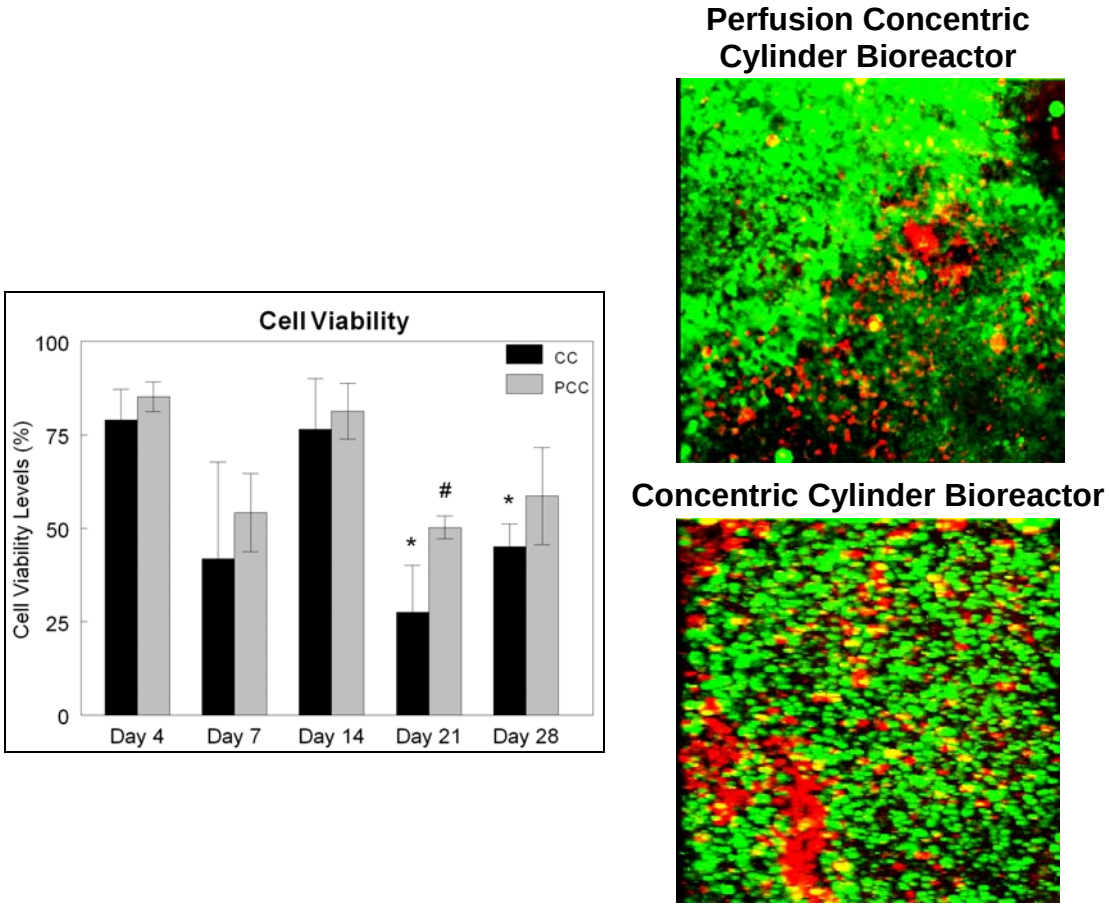

Figure 4.8. Live/dead analysis of constructs grown in the PCC or CC bioreactor. Data are presented for one experimental run and are presented as mean ± SEM (n = 3 constructs) (* $p < 0.05$ vs. CC Day 4; # $p < 0.05$ vs. PCC Day 4). Confocal fluorescence images are constructs grown in the PCC or CC bioreactor after 28 days. Live cells fluoresced green and dead cells or fragments fluoresced red.

By Day 28 extracellular matrix stained more intensely from constructs harvested from the CC bioreactor than the PCC bioreactor (Figure 4.9). The constructs from the CC bioreactor produced more intense staining for collagen type II than the PCC bioreactor, which correlated to the biochemical analysis that the CC bioreactor produced more collagen and GAG. However, cells and deposition of collagen type II and GAG were restricted to the surface shear face of the constructs from the CC bioreactor, whereas, while preferentially deposited on the surface shear face, cells and extracellular matrix were also found on the perfusion face of the constructs from the PCC bioreactor.

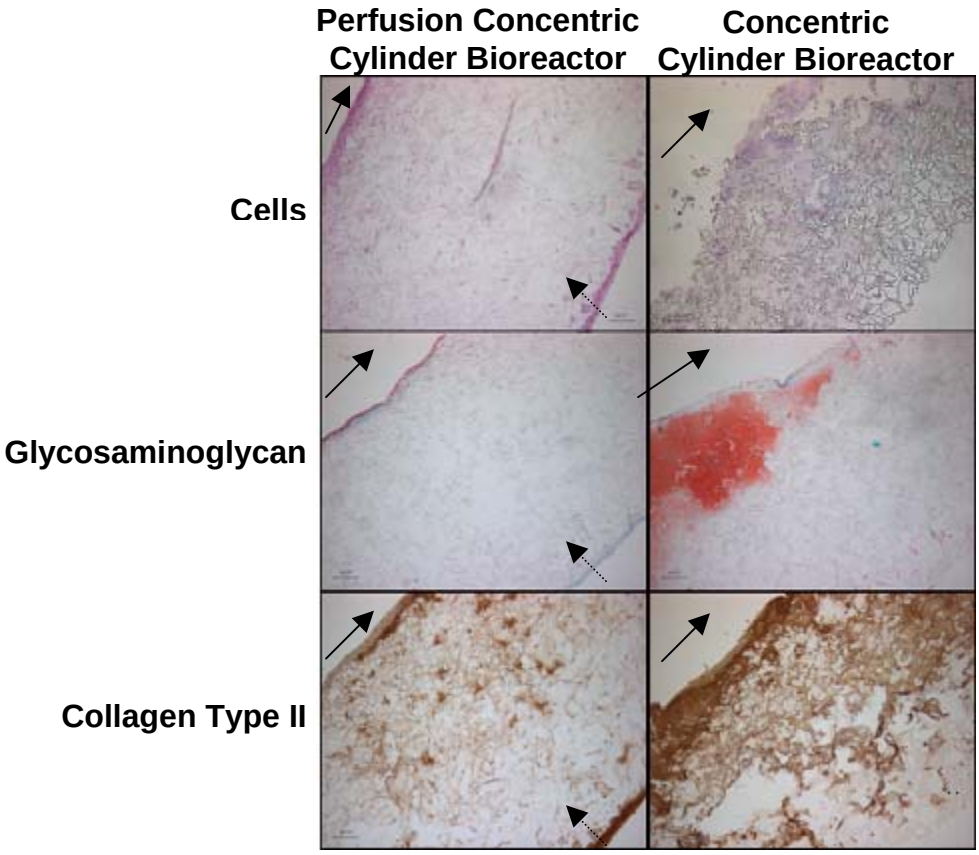

Figure 4.9. Histology for tissue-engineered cartilage constructs at 10x magnification. Constructs cultured for 28 days were harvested and stained with hematoxylin and eosin for cells, safranin-O for GAG (stained red), and immunostained for collagen type II. Column labeled samples represent constructs grown in either the CC or PCC bioreactor. Arrows indicate direction of fluid flow exerted on the constructs. All sections show construct face experienced surface shear (solid arrows) on the upper left-hand side and perfusion (dashed arrows) on the lower right-hand side (for the PCC bioreactor only). Open areas indicate presence of polymer.

Both the CC and PCC bioreactor expressed articular cartilage markers, aggrecan, collagen type II, and COMP (Figure 4.10). Neither bioreactors showed definitive increase or decrease in aggrecan and collagen type II gene expression over the course of 28 days. Seen in Table 4.2, both bioreactors showed a decrease in COMP expression by Day 21 with a 40% decrease for the PCC bioreactor and 60% decrease for the CC

bioreactor compared to Day 14 values. Both bioreactors also expressed collagen type I mRNA, indicative of possible dedifferentiation or fibroblastic cells. However, constructs from the PCC bioreactor expressed a 30% decrease in collagen type I by Day 21 compared to Day 14 values, while constructs from the CC bioreactor neither increased nor decreased in collagen type I expression by more than 18%.

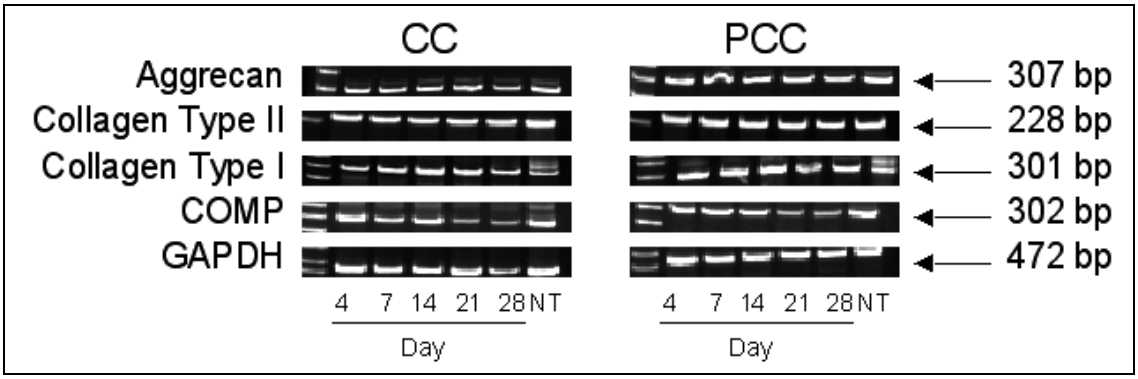

Figure 4.10. Characterization of tissue-engineered cartilage cultured in either CC or PCC bioreactor using RT-PCR. NT: Native Tissue. The phenotype of the chondrocytes cultured in the bioreactor was measured by mRNA expression for aggrecan, collagen type II, collagen type I, COMP, and GAPDH. Throughout the 28 day culture, both bioreactors showed expression for aggrecan, collagen type II, collagen type I, COMP, and GAPDH. Presence of collagen type I indicate that cells have partially dedifferentiated towards fibroblastic tissue, however collagen type II presence indicated some retention of articular cartilage tissue.

Table 4.2. Gene expression normalized to GAPDH*

CC	Collagen Type I	Collagen Type II	COMP	Aggrecan
Day 4	1.18	1.10	1933.62	1.11
Day 7	0.96	1.03	1013.17	1.03
Day 14	0.89	1.08	1638.11	1.03
Day 21	1.02	1.13	657.50	1.08
Day 28	0.94	0.96	516.79	0.99
Native Tissue	1.12	1.11	1762.99	1.06
PCC	Collagen Type I	Collagen Type II	COMP	Aggrecan
Day 4	1.28	103.86	9.09	49.08
Day 7	1.48	118.97	11.39	61.60
Day 14	1.44	113.91	9.05	48.98
Day 21	1.01	107.00	5.10	55.03
Day 28	1.13	93.37	5.19	46.17
Native Tissue	1.34	110.28	9.79	66.13

* Values are ratio of specified gene intensity to GAPDH

4.3 Effect of Mechanical Stimulation on Tissue-Engineered Cartilage Growth

4.3.1 Perfusion and Shear versus Shear Cartilage Construct Growth: Biochemical Composition

After four days in culture, both bioreactors had equivalent low seeding efficiency with the perfusion+shear bioreactor having 4.1 ± 0.7% efficiency at $0.4 \pm 0.1 \times 10^6$ cells/construct and the shear bioreactor 3.9 ± 1.1% efficiency at $0.4 \pm 0.1 \times 10^6$ cells/construct (Figure 4.11A). However, by Day 28 the difference between the two bioreactors was more noticeable. After 28 days in culture, the perfusion+shear bioreactor increased in cell number by 33 ± 1 fold to $13.4 \pm 0.3 \times 10^6$ cells/construct, whereas the shear bioreactor increased by 11 ± 4 fold to $4.0 \pm 1.7 \times 10^6$ cells/construct ($p < 0.05$) (Figure 4.11A). From Figure 4.11B, GAG deposition was the same in either bioreactor by Day 28, where the perfusion+shear

bioreactor produced 1.2 ± 0.1 mg/construct and the shear bioreactor produced 1.2 ± 0.3 mg/construct. GAG production rate peaked by Day 14 for the perfusion+shear bioreactor and by Day 7 in the shear bioreactor before the rates leveled out by Day 21. By Day 28 total collagen production in the perfusion+shear bioreactor was 2.8 ± 0.2 mg/construct, which was significantly greater than the 1.2 ± 0.1 mg/construct produced in the shear bioreactor (Figure 4.11C) ($p < 0.05$). Total collagen production continued to increase over the course of 28 days in the perfusion+shear bioreactor, while in the shear bioreactor collagen production leveled out by Day 14. Bioreactor pH levels varied between 7.0 and 7.5 over the course of the run for both bioreactors, which were within physiological range for cartilage. Over the course of 28 days, 71 - 91% of GAG were released into the media for the perfusion+shear bioreactor while 62 - 94% of GAG were released into the media for the shear bioreactor. Repeat of this study showed the same trend with the perfusion+shear bioreactor producing significantly more cells and total collagen than the shear bioreactor, but with roughly equal number of GAG per construct by Day 28 (Table 4.3). The perfusion+shear bioreactor also repeated a significantly higher fold increase in cell number per construct from Day 4 values than the shear bioreactor.

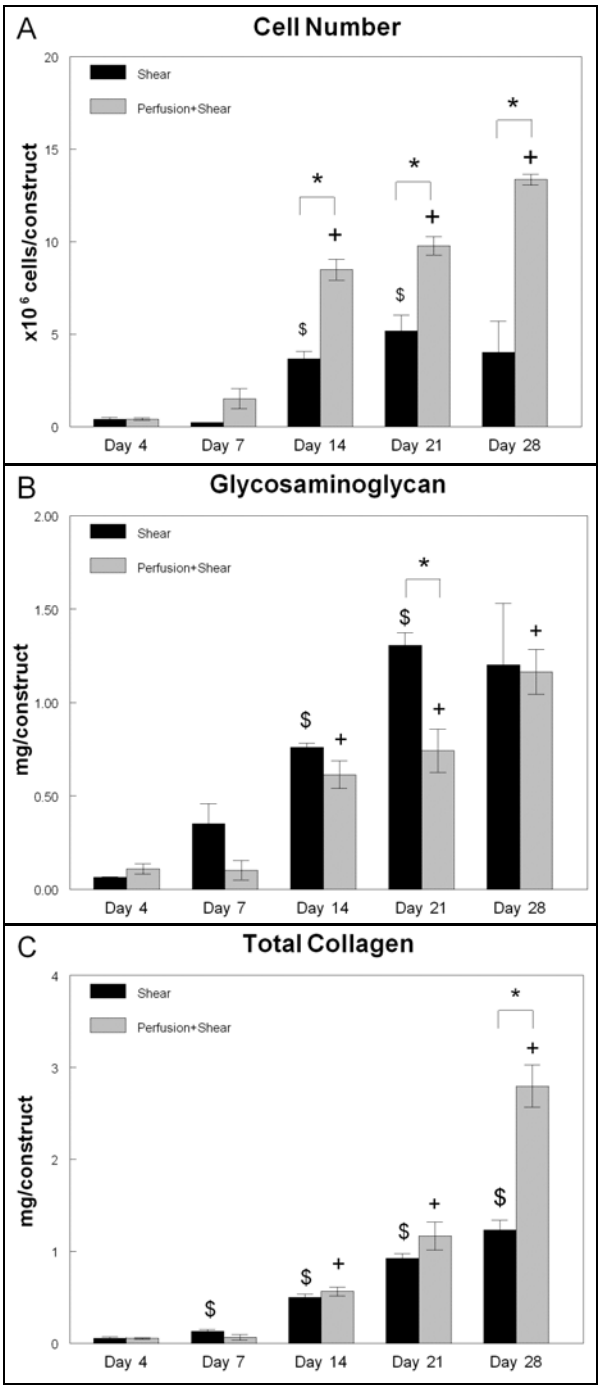

Figure 4.11. Chondrocyte proliferation and matrix deposition in the perfusion+shear PCC bioreactor compared to the shear only PCC bioreactor. Data are presented as mean ± SEM (n = 3 constructs). (A) Cells/construct; (B) GAG/construct; (C) total collagen/construct. By Day 28, constructs from the perfusion+shear bioreactor had significantly more cells and total collagen than the shear bioreactor while both bioreactors had roughly the same amount of GAG per construct. ($ $p < 0.05$ vs. Shear Day 4; + $p < 0.05$ vs. Perfusion+Shear Day 4; and * $p < 0.05$ between Perfusion+Shear and Shear)

Table 4.3. Individual construct composition for two experimental runs: perfusion+shear versus shear

	First Experimental Run		Second Experimental Run	
Perfusion+Shear	Day 4	Day 28	Day 4	Day 28
Cells/construct ($x10^6$/construct)	0.47	13.8	0.19	10.8
	0.47	12.8	0.41	9.56
	0.27	13.4	0.07	7.10
mean ± SEM	0.40 ± 0.07	13.4 ± 0.3	0.22 ± 0.10	9.16 ± 1.09
Glycosaminoglycan (mg/construct)	0.15	1.36	0.31	0.80
	0.12	0.94	0.23	0.79
	0.06	1.19	0.28	0.44
mean ± SEM	0.11 ± 0.03	1.16 ± 0.12	0.28 ± 0.02	0.67 ± 0.12
Collagen (mg/construct)	0.04	2.88	0.04	1.64
	0.05	2.36	0.03	1.48
	0.07	3.15	0.03	1.48
mean ± SEM	0.05 ± 0.01	2.80 ± 0.23	0.03 ± 0.00	1.54 ± 0.05
Shear	Day 4	Day 28	Day 4	Day 28
Cells/construct ($x10^6$/construct)	0.59	4.89	0.38	4.55
	0.27	6.40	0.05	3.47
	0.28	0.77	0.05	3.39
mean ± SEM	0.38 ± 0.11	4.02 ± 1.68	0.16 ± 0.110	3.80 ± 0.38
Glycosaminoglycan (mg/construct)	0.07	1.30	0.27	0.46
	0.07	1.71	0.27	0.52
	0.06	0.58	0.27	0.38
mean ± SEM	0.06 ± 0.00	1.20 ± 0.33	0.27 ± 0.00	0.46 ± 0.04
Collagen (mg/construct)	0.08	1.20	0.04	0.83
	0.05	1.43	0.04	0.87
	0.03	1.07	0.05	0.67
mean ± SEM	0.06 ± 0.01	1.23 ± 0.11	0.04 ± 0.00	0.79 ± 0.06

Data are cells, glycosaminoglycan, and collagen content for individual constructs harvested after 4 or 28 days in culture from the indicated bioreactor (n = 3). Comparisons within bioreactors indicated relatively uniform construct composition.

Histologically, over the course of 28 days in bioreactor culture, cells and matrix growth propagated preferentiality on the construct face that experienced surface shear.

However, growth also occurred on the backside of the constructs, away from surface shear in both bioreactors. Even though no perfusion occurred for the shear bioreactor, the constructs cultured in the shear bioreactor showed no discernable difference in cell growth and extracellular matrix deposition compared to the perfusion+shear bioreactor. Seen in Figure 4.12, by Day 28 histological analyses determined that most of the cartilage development occurred on the shear face of the constructs, whereas some extracellular matrix deposition occurred on the backside (perfusion face for the perfusion+shear bioreactor). Positive staining for GAG (red stain) was not present at the surface exposed to shear, but was detected in the interior away from direct exposure to surface shear forces. Immunohistochemical staining showed presence of collagen type II, which indicated cells expressed articular cartilage phenotype. The presence of collagen type I was also detected and indicated possible dedifferentiation and fibroblast-like tissue. Lack of staining for cells and extracellular matrix in the center of the constructs and presence of polymer indicated lack of cartilage development at the center of the cross-section of the constructs.

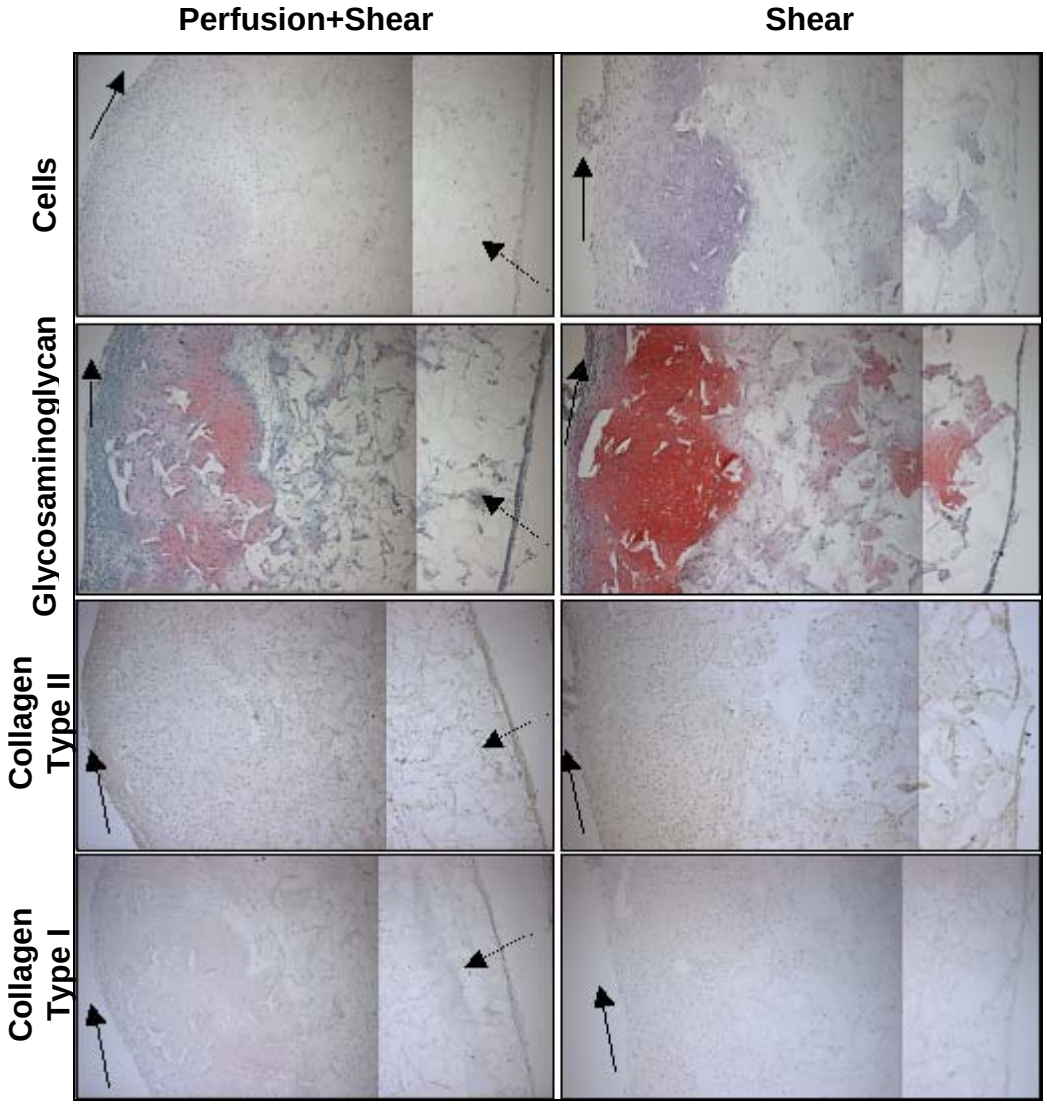

Figure 4.12. Histological analysis of TECCs cultured either in the perfusion+shear bioreactor or the shear bioreactor at 10x magnification. Constructs cultured for 28 days were harvested and stained with hematoxylin and eosin for cells, safranin-O for GAG (stained red), and immunostained for collagen type II (stained brown) and collagen type I (stained brown). Arrows indicate direction of fluid flow exerted on the constructs. All sections show construct face experiencing surface shear (solid arrows) on the left-hand side and perfusion (dashed arrows) on the right-hand side (for the perfusion+shear bioreactor only). Open unstained areas indicated presence of polymer. The cross-sectional area of the constructs at 10x was larger than the field of view. As such, two images across the thickness of the construct were imaged and cropped together to give one image representative of the cross-sectional area.

Seen in Figure 4.13, by Day 28, cells were approximately 51% viable with no difference between the two bioreactors. Confocal images showed no discernable difference in viability between the two bioreactors; however, the perfusion+shear bioreactor showed more cells than the shear bioreactor. By Day 28, most cells were viable, indicated by the green fluorescent cells and dead cells were present throughout the constructs (Figure 4.13).

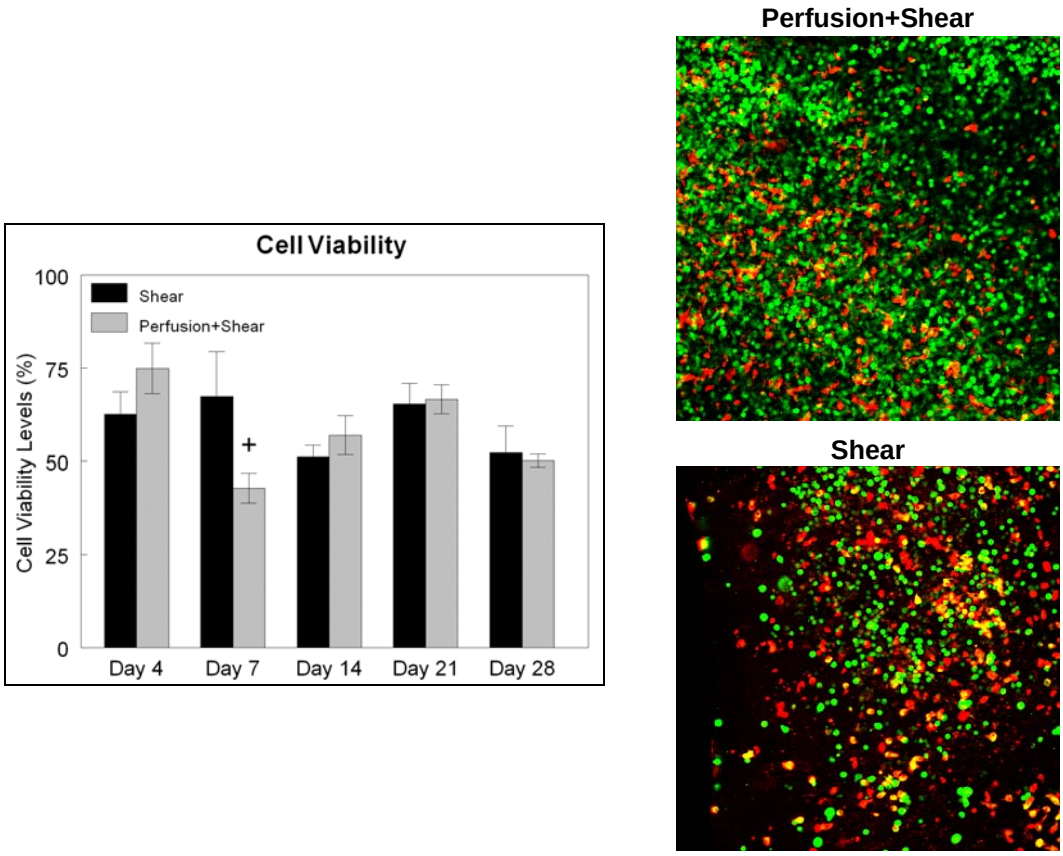

Figure 4.13. Live/dead analysis of constructs grown in the perfusion+shear or shear only PCC bioreactor. Data are presented for one experimental run and are presented as mean ± SEM (n = 3 constructs) (+ $p < 0.05$ vs. Perfusion+Shear Day 4). Confocal fluorescence images are constructs grown in the perfusion+shear or shear bioreactor after 28 days. Live cells fluoresced green and dead cells or fragments fluoresced red.

4.3.2 Perfusion and Shear versus Shear Cartilage Construct Growth: Mechanical Properties

In Figure 4.14 the aggregate modulus over the course of 28 days were not significantly different from Day 4 values for either bioreactor. In addition, there was no difference in stiffness between the perfusion+shear and shear bioreactor. By Day 28 the bioreactors produced TECCs with a compressive modulus of 0.15 ± 0.02 MPa. In comparison, the compressive modulus of native cartilage was significantly greater at 0.57 ± 0.10 MPa ($p < 0.05$), while the PLLA scaffold's compressive modulus (cultured for 28 days in media with no cells) was equivalent to the TECCs at 0.10 ± 0.04 MPa.

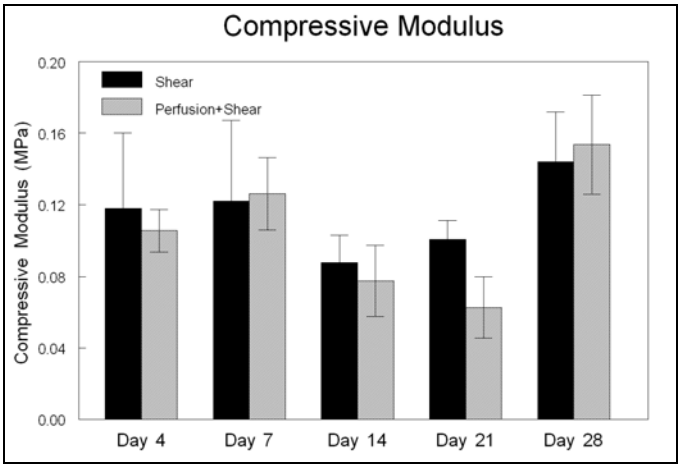

Figure 4.14. Compressive modulus of TECCs cultured in PCC bioreactor. Data are presented as mean ± SEM (n = 3 constructs).

Figure 4.15 shows the variability in permeability over the course of 28 days and between the perfusion+shear and shear bioreactor. There was no significant difference in permeability over the course of 28 days for either bioreactor conditions or between the two bioreactors. By Day 28 the bioreactors produced TECCs with a permeability

constant of 2.0 ± 0.5 x10^{-13} m^4/(N*s). In comparison, the permeability constant of native cartilage was on the same order of magnitude as the TECCs at 1.2 ± 0.8 x10^{-13} m^4/(N*s). However, the permeability constant for PLLA scaffolds after 28 days in culture media (0.6 ± 0.2 x10^{-13} m^4/(N*s)) was significantly less permeable than Day 7 and Day 28 samples from the perfusion+shear bioreactor and Day 14 and Day 21 samples in the shear bioreactor ($p < 0.05$).

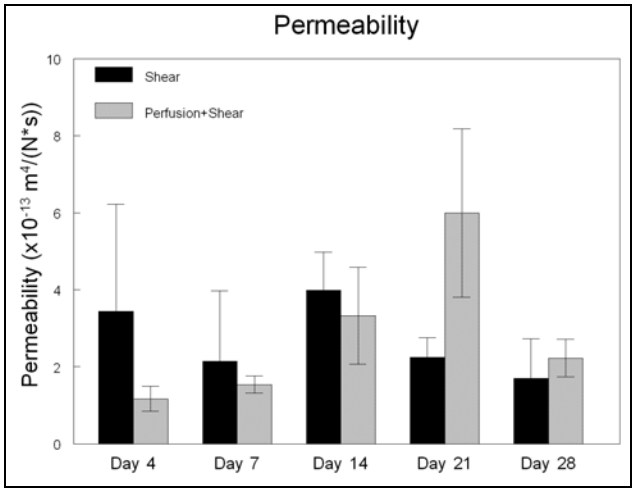

Figure 4.15. Permeability constant of TECCs over the course of 28 days cultured in the PCC bioreactor. Data are presented as mean ± SEM (n = 3 constructs).

No significant difference in the shear and dynamic modulus was detected between the perfusion+shear and shear bioreactor. For either bioreactor, at 28 days the dynamic modulus increased as frequency increased from 0.01 Hz to 1 Hz, which indicated viscoelastic behavior (Figure 4.16A). Over the course of the experiment the shear modulus at 1 Hz decreased over time from Day 4 values (Figure 4.16B); where the perfusion+shear bioreactor decreased from 1.2 ± 0.2 MPa on Day 4 to 0.3 ± 0.1 MPa on Day 28 and the shear bioreactor went from 0.9 ± 0.2 MPa on Day 4 to 0.4 ± 0.1 MPa. By

Day 14 there was a significant drop in the perfusion+shear modulus compared to Day 4 values ($p < 0.05$). In comparison, the shear modulus of native cartilage was measured at 0.7 ± 0.2 MPa at 1 Hz, while PLLA scaffolds after 28 days in culture media (no cells) had a shear modulus of 1.8 ± 0.7 MPa.

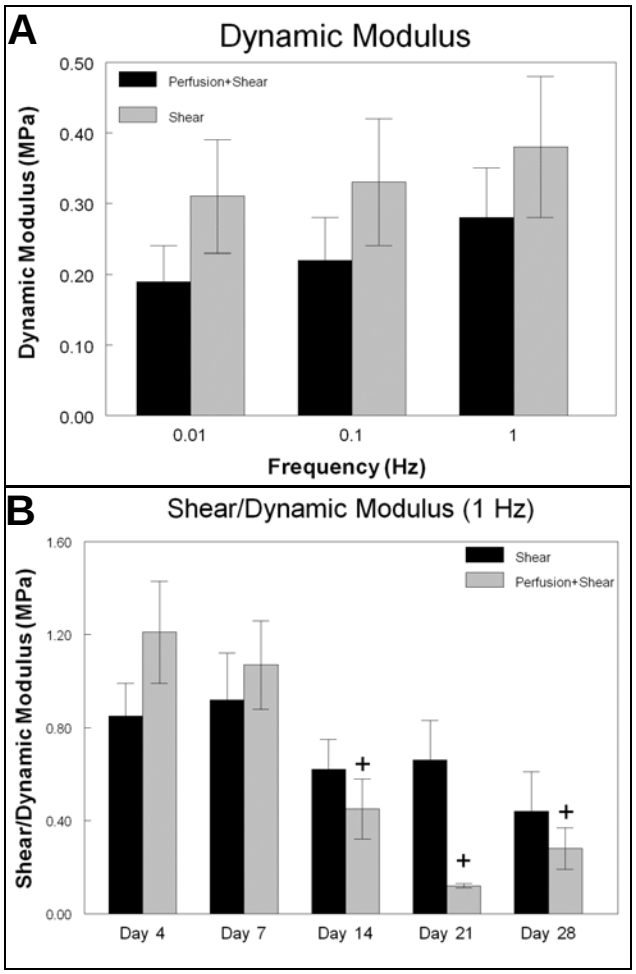

Figure 4.16. Shear/Dynamic modulus of TECCs cultured in PCC bioreactor for 28 days. Data are presented as mean ± SEM (n = 3 constructs). (A) Dynamic modulus between 0.01-1 Hz; (B) shear modulus at 1 Hz over the course of 28 days. (+ $p < 0.05$ vs. Perfusion+Shear Day 4)

Seen in Figure 4.17 for a frequency of 1 Hz, the perfusion+shear bioreactor had a significant increase in phase angle from 4.2 ± 0.1 º at Day 4 to 15 ± 1 º at Day 28; as well as, the shear bioreactor, which increased from 5.1 ± 0.3 º at Day 4 to 11 ± 1 º at Day 28 ($p < 0.05$). In addition, there was a significant difference between the two bioreactors by Day 21 ($p < 0.05$). In comparison, the phase angle of native cartilage was greater than Day 28 TECCs measured at 29 ± 6 º ($p < 0.06$), while the phase angle of PLLA was significantly lower than Day 28 TECCs measured at 6.2 ± 0.8 º ($p < 0.05$).

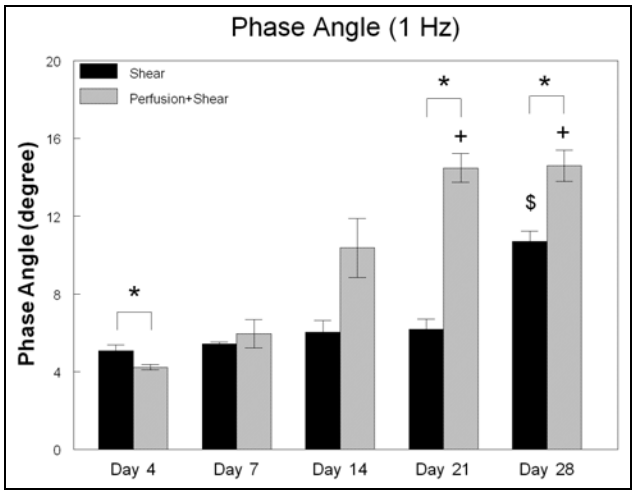

Figure 4.17. Phase angle measured at 1 Hz for TECCs cultured over 28 days. Data are presented as mean ± SEM (n = 3 constructs). (* $p < 0.05$ vs. Shear, + $p < 0.05$ vs. Perfusion+Shear Day 4, $ $p < 0.05$ vs. Shear Day 4)

4.4 Effect of Mechanical Stimulation on Tissue-Engineered Cartilage Growth *In Vivo*

After 28 days in bioreactor culture and before implantation, constructs in the perfusion+shear bioreactor had 11 ± 1 million cells per construct, which was significantly greater than the shear bioreactor at 7.9 ± 0.8 million cells per construct and the static

bioreactor at 5.7 ± 1.5 million cells per construct ($p < 0.05$) (Figure 4.18A). Seen in Figure 4.18B, GAG content per construct between the perfusion+shear and shear bioreactor prior to implantation was equivalent, in which the perfusion+shear bioreactor produced 0.8 ± 0.2 mg/construct and the shear bioreactor 1.2 ± 0.2 mg/construct. The static bioreactor produced 0.3 ± 0.2 mg of GAG per construct, which was significantly less than the shear bioreactor of 1.2 ± 0.2 mg of GAG per construct ($p < 0.05$). Total collagen production per construct before implantation showed significantly more total collagen between the mechanically active bioreactors and the static bioreactor, where the perfusion+shear bioreactor produced 0.47 ± 0.03 mg/construct, the shear bioreactor 0.50 ± 0.04 mg/construct, and the static bioreactor 0.17 ± 0.08 mg/construct ($p < 0.05$) (Figure 4.18C).

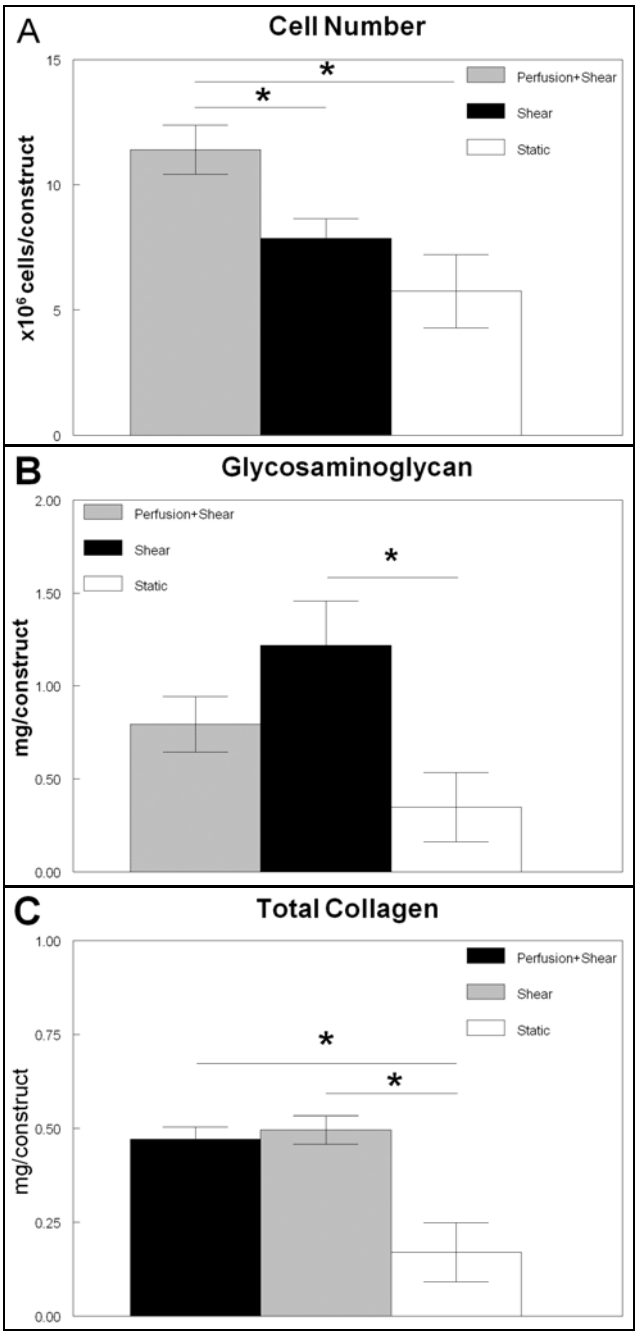

Figure 4.18. Cell number and matrix deposition in the perfusion+shear bioreactor, shear bioreactor, and static bioreactor prior to implantation. Data are presented as mean ± SEM (n = 5 constructs). (A) Cells/construct; (B) GAG/construct; (C) total collagen/construct. By Day 28 constructs from the perfusion+shear bioreactor had significantly more cells and total collagen than the static bioreactor (* $p < 0.05$)

The 3 mm in diameter implants were punched out of the 10 mm TECCs harvested from the bioreactors. Assuming an even distribution, the relative concentration of cells, GAG, and total collagen for a 3 mm construct implant with a volume of 13.2 mm^3 for each bioreactor was derived and is summarized in Table 4.4 along with the control groups. The assumption of an even distribution of cells and extracellular matrix was not accurate based on histological analysis (see Figure 4.12); however, the derivation allowed us to make a relative comparison of the TECCs cultured in the bioreactors to the implants in the control groups (Group A, B, and F)

Table 4.4. Biochemical composition of implants on day of surgery

	Implant	Cells	GAG	Total collagen
Group A	Xiphoid defect	0 cells	0 mg	0 mg
Group B	PLLA scaffold	0 cells/cm^3	0 mg/cm^3	0 mg/cm^3
Group C	Static bioreactor	$0.5 \pm 0.1 \times 10^6$ cells/cm^3	0.03 ± 0.02 mg/cm^3	0.015 ± 0.007 mg/cm^3
Group D	Perfusion+shear bioreactor	$1.0 \pm 0.1 \times 10^6$ cells/cm^3	0.07 ± 0.01 mg/cm^3	0.042 ± 0.003 mg/cm^3
Group E	Shear bioreactor	$0.7 \pm 0.1 \times 10^6$ cells/cm^3	0.11 ± 0.02 mg/cm^3	0.045 ± 0.003 mg/cm^3
Group F	Cells	5×10^6 cells	0 mg	0 mg

All of the animals survived the surgery and post-surgical stage. No complications were observed post-implantation and through the course of the experimental run. After 28 days post-implantation, the xiphoids and TECCs were excised and imaged. Samples were stained for cells, GAG, collagen type II, and collagen type I. Figures 4.19 - 4.23 show the cross-section of the implant surrounded by the xiphoid.

Except for the empty defect model, all implants supported cell growth and extracellular matrix deposition. Compared to the other five groups, the empty defect had

the least amount of healing in terms of cellular and extracellular matrix deposition into the defect region. Even when no cells were present in the implant (Group B: PLLA scaffold), cells and extracellular matrix deposition occurred after 28 days *in vivo*. Compared to Figure 4.12 of TECCs prior to implantation, after 28 days *in vivo* Groups D and E (shear bioreactor and perfusion+shear bioreactor, respectively) showed increase amounts of cells and extracellular matrix deposition in the implant. In Figure 4.21, which stained for GAG (red stain), only the shear bioreactor, perfusion+shear bioreactor, and cells group showed any retention of GAG. The static bioreactor showed no presence of GAG. This observation indicated increased maturation occurred after implantation for TECCs cultured in mechanically active bioreactors, i.e. the shear and perfusion+shear bioreactor. There was no discernable difference between the two mechanically active bioreactors in cellular and extracellular matrix deposition. The greatest intensity of GAG occurred in the cells only control group. This group also had significantly higher amounts of cells when implanted compared to any of the other groups, which may have increased the maturation of the cartilage implants. However, seen in Figure 4.19F, at 4x magnification, the structural integrity of the xiphoid was compromised in the cells only group; whereas, with the implant, the shape of the xiphoid remained more linear compared to the cells only group (Figure 4.19). Finally, all implants stained for both collagen type II (Figure 4.22) and collagen type I (Figure 4.23) (brown stain). Type I collagen was mainly located around the edges of the implants or at the interface between the implants and xiphoids. This indicated that the implants maintained cartilage phenotype, but that fibroblast-like tissue (scar tissue) was also present, indicative of healing mechanisms.

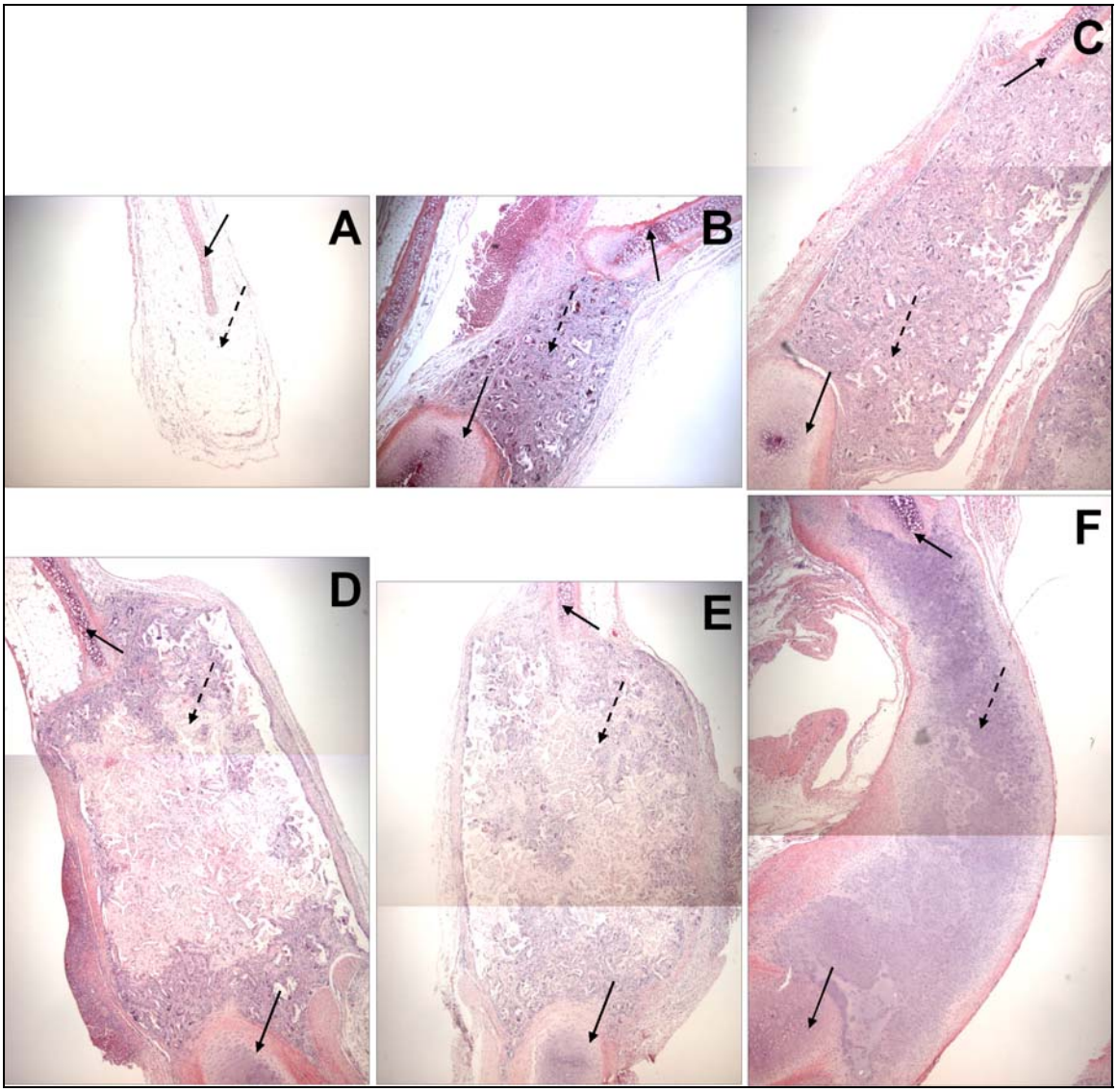

Figure 4.19. Cellular histological analysis at 4x magnification of implants in a xiphoid chondral defect model. (A) Xiphoid defect; (B) PLLA scaffold; (C) static bioreactor; (D) perfusion+shear bioreactor; (E) shear bioreactor; (F) cells. Arrows indicate either implant (dashed arrows) or native xiphoid cartilage (solid arrows). Open unstained areas indicated presence of polymer. The cross-sectional area of the implant and surrounding cartilage at 4x was larger than the field of view. As such, two images across the thickness of the implant were imaged and cropped together to give one image representative of the cross-sectional area.

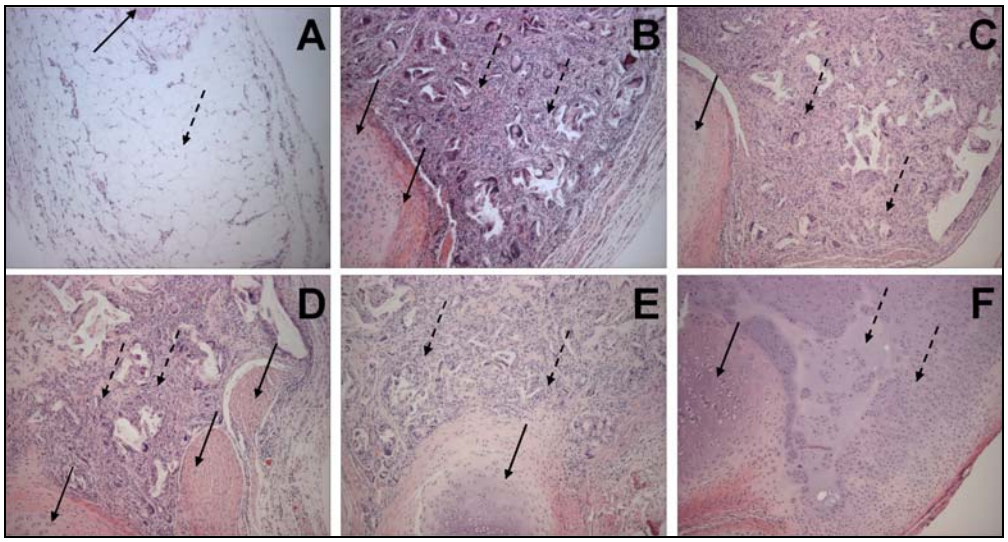

Figure 4.20. Cellular histological analysis at 10x magnification of implants in a xiphoid chondral defect model. (A) Xiphoid defect; (B) PLLA scaffold; (C) static bioreactor; (D) perfusion+shear bioreactor; (E) shear bioreactor; (F) cells. Arrows indicate either implant (dashed arrows) or native xiphoid cartilage (solid arrows). Open unstained areas indicated presence of polymer.

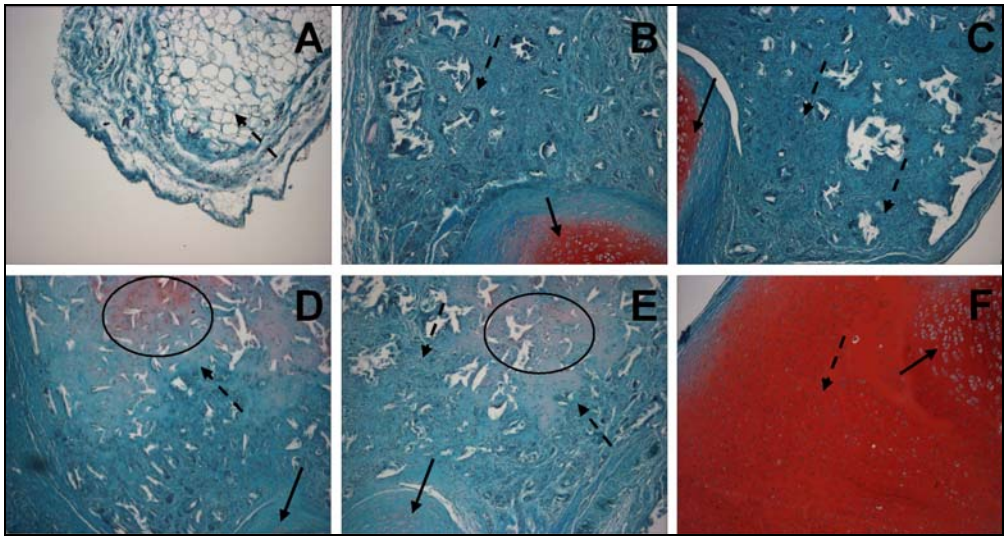

Figure 4.21. GAG (red stain) histological analysis at 10x magnification of implants in a xiphoid chondral defect model. (A) Xiphoid defect; (B) PLLA scaffold; (C) static bioreactor; (D) perfusion+shear bioreactor; (E) shear bioreactor; (F) cells. Arrows indicate either implant (dashed arrows) or native xiphoid cartilage (solid arrows). GAG in the implant region is circled for Group D and E. Open unstained areas indicated presence of polymer.

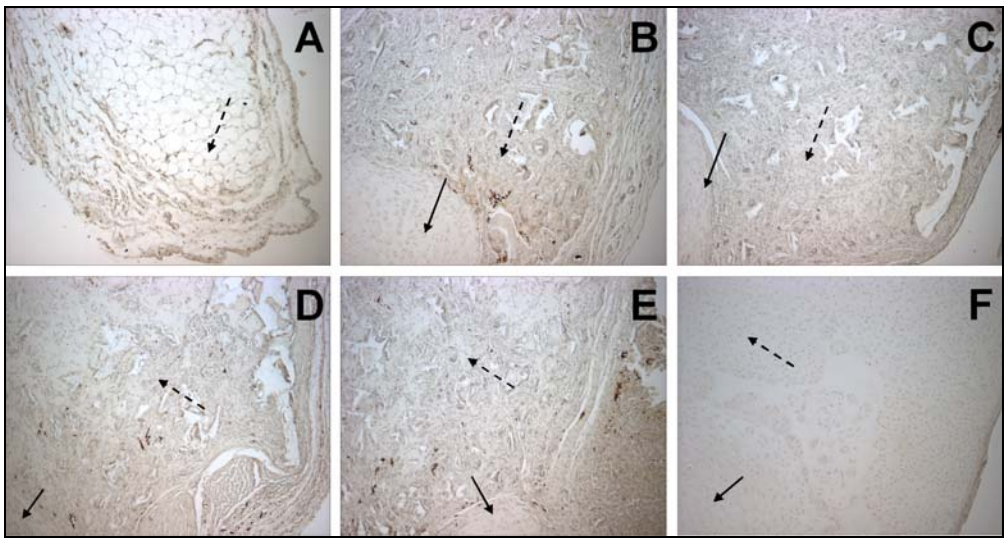

Figure 4.22. Collagen type II (brown stain) histological analysis at 10x magnification of implants in a xiphoid chondral defect model. (A) Xiphoid defect; (B) PLLA scaffold; (C) static bioreactor; (D) perfusion+shear bioreactor; (E) shear bioreactor; (F) cells. Arrows indicate either implant (dashed arrows) or native xiphoid cartilage (solid arrows). Open unstained areas indicated presence of polymer.

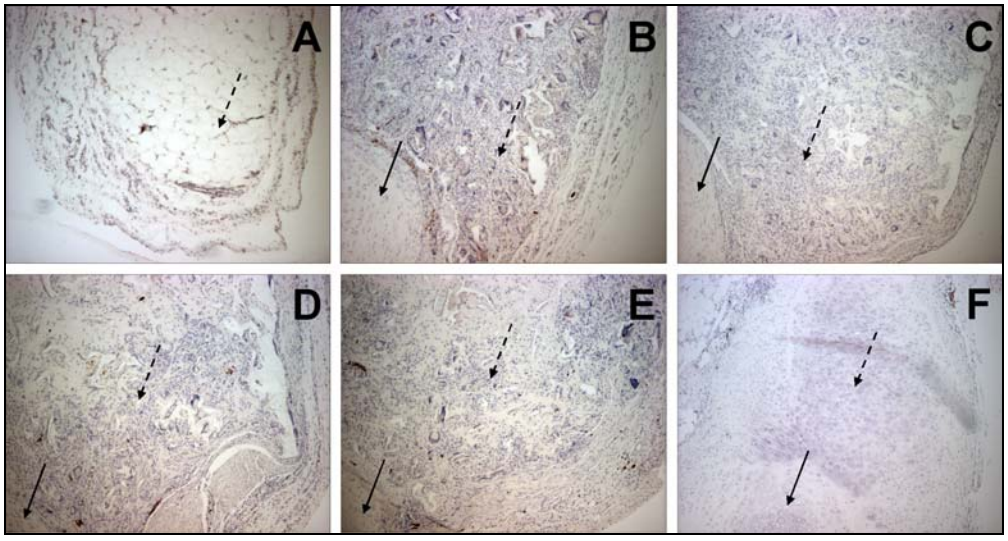

Figure 4.23. Collagen type I (brown stain) histological analysis at 10x magnification of implants in a xiphoid chondral defect model. (A) Xiphoid defect; (B) PLLA scaffold; (C) static bioreactor; (D) perfusion+shear bioreactor; (E) shear bioreactor; (F) cells. Arrows indicate either implant (dashed arrows) or native xiphoid cartilage (solid arrows). Open unstained areas indicated presence of polymer.

4.5 Cryopreservation of Tissue-Engineered Cartilage Constructs

There was considerable variability from experiment to experiment. For this reason, multiple experimental trials on the same cryopreservation study were normalized to a control within the trial and then grouped and average together to determine the overall result. Values for each experiment are provided in Appendix B. This was due to the inconsistency in achieving successful vitrification during each experimental trial. Further discussion on unsuccessful vitrification is discussed in Chapter 5. Successful vitrification was achieved when the drop in temperature from 4°C to –100°C occurred at a rapid rate of approximately -40°C per minute. However, some trials showed that the temperature drop instead occurred at a rate of approximately -10°C per minute, which resulted in visible ice formation. A comparison between successful and unsuccessful vitrification showed that the trend between the cryopreservation methods studied remained the same. The differences lie in the relative cell viability levels. For example, in Table 4.5 the cryopreservation method studied was between VS70 in 6/7 steps and VS70 in 4/4 steps. In the fourth trial, successful vitrification occurred when the temperature dropped from 4°C to -100°C occurred at -38.5 °C/min minutes and resulted in approximately 47% relative cell viability levels for both VS70 in 6/7 steps and VS70 in 4/4 steps. In the third trial, unsuccessful vitrification occurred when the temperature dropped from 4°C to -100°C occurred at -7.3 °C/min minutes and resulted in approximately 9% relative cell viability levels for both VS70 in 6/7 steps and VS70 in 4/4 steps. Thus, while there was a noticeable difference in cell viability levels between successful and unsuccessful vitrification, there was no noticeable difference between VS70 in 6/7 steps and VS70 in 4/4 steps.

Table 4.5. Relative cell viability levels after vitrification

Experimental Trial	Cell Viability Levels		Cooling Rate from 4°C to -100°C
	VS70 in 6/7 steps	VS70 in 4/4 steps	
1 [s]	39.6 ± 9.7%	42.1 ± 4.2%	-47.6 °C/min
2 [u]	11.5 ± 2.2%	20.8 ± 5.4%	-5.4 °C/min
3 [u]	10.8 ± 1.4%	7.3 ± 1.3%	-7.3 °C/min
4 [s]	44.5 ± 6.0%	50.0 ± 2.5%	-38.5 °C/min

Data are presented as mean ± SEM (n = 4 constructs).
s: successful vitrification; u: unsuccessful vitrification

4.5.1 Cryopreservation of Native Cartilage

Native articular cartilage was harvested from bovine calves and punched into 10 mm diameter plugs. Cell viability levels were normalized to VS55 in 6/7 steps. For the one trial, native cartilage treated with VS70 in 6/7 steps retained a 2.8 ± 0.1 -fold increase in cell viability levels over VS55 in 6/7 steps (see Figure 4.24) (p = 0.0005).

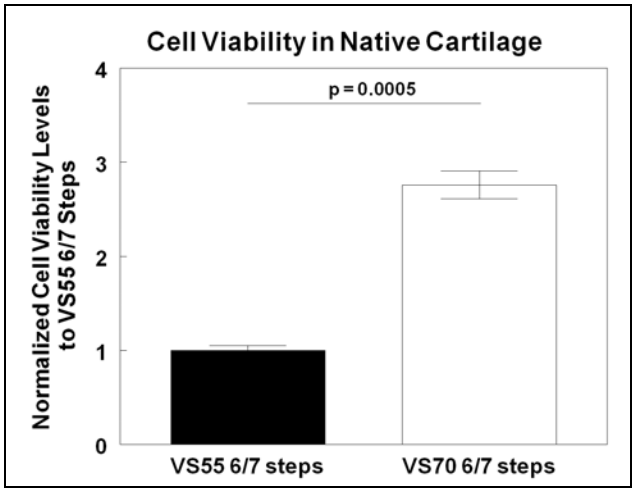

Figure 4.24. Cell viability levels for native cartilage treated with VS55 in 6/7 steps and VS70 in 6/7 steps. VS70 retained a 2.8 ± 0.1-fold increase in cell viability levels over VS55 in 6/7 steps (p = 0.0005 vs. VS55 in 6/7 steps) (n = 4 cartilage plugs). This was an unsuccessful vitrification experiment; therefore, the highest cell viability levels were 8.1 ± 0.5% for VS55 in 6/7 steps and 22.0 ± 1.2% for VS70 in 6/7 steps.

Confocal images, seen in Figure 4.25, showed the distribution of live and dead cells throughout the thickness of cartilage. Because this experimental trial was an example of unsuccessful vitrification, most cells did not survive this cryopreservation experiment. However, cell that did survive were visible along the surface of the native cartilage (located along the right-hand side of the images).

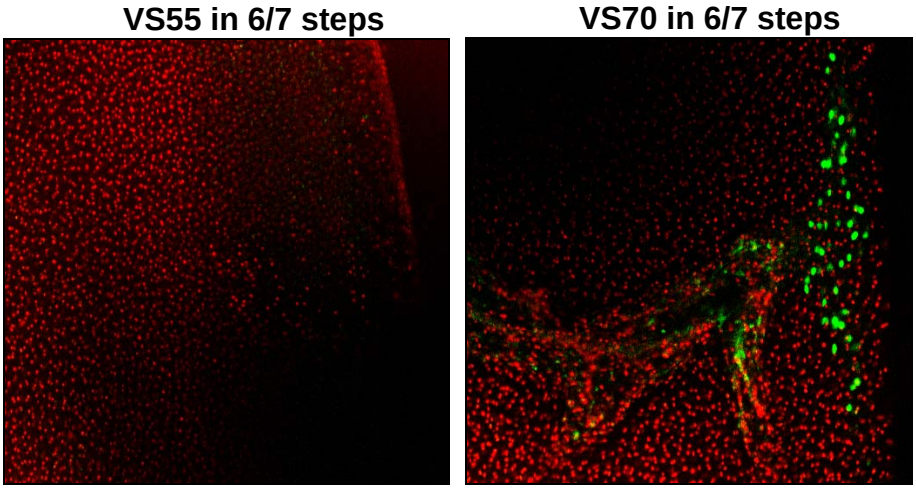

Figure 4.25. Confocal images of live and dead cells throughout the thickness of cryopreserved native cartilage. Live cells (green) were located along the surface (right-hand side) of the cartilage, while dead cells and fragments (red) were found in the interior. For these sample images, VS70 in 6/7 steps retained more live cells (23.5%) than VS55 in 6/7 steps (8.1%).

4.5.2 Traditional Freezing versus Vitrification on the Effect of Cell Viability

TECCs used in this study were cultured for 7 days in the PCC bioreactor and contained 1.2 ± 0.1 million cells per construct. Traditionally frozen samples actually fared better in maintaining cell viability levels at 32.8 ± 5.9%, while vitrified samples treated with VS55 in 6/7 steps maintained only 18.7 ± 2.9% cell viability levels

(p = 0.08). Seen in Figure 4.26, traditionally frozen samples normalized to VS55 in 6/7 steps had a 1.8 ± 0.3 -fold increase over VS55 in 6/7 steps.

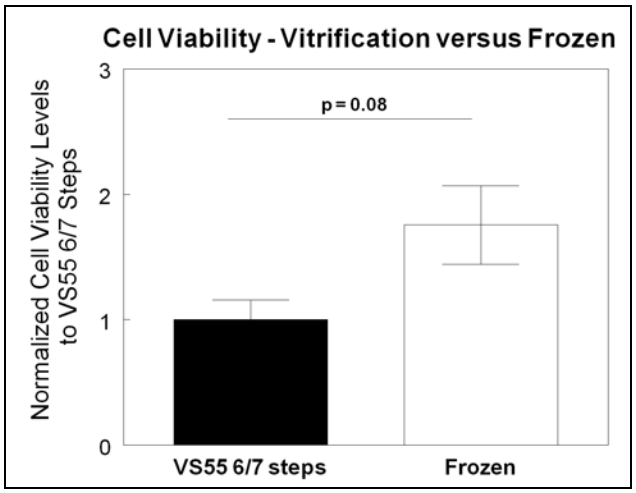

Figure 4.26. Cell viability levels for TECCs treated with VS55 in 6/7 steps and 1 M DMSO. Frozen samples retained a 1.8 ± 0.3 -fold increase in cell viability levels over vitrified samples treated with VS55 in 6/7 steps (p = 0.08 vs. VS55 in 6/7 steps) (n = 4 constructs for VS55 in 6/7 steps and n = 5 constructs for traditionally frozen constructs). This was a successful vitrification experiment; therefore, the highest cell viability levels were 32.8 ± 5.9% for frozen samples and 18.7 ± 2.9% for VS55 in 6/7 steps.

Confocal images, seen in Figure 4.27, showed the distribution of live and dead cell over the surface of TECCs. Though this experimental trial was an example of successful vitrification, most cells did not survive this cryopreservation experiment. However, cells that did survive were visible and distributed over the surface of the TECCs.

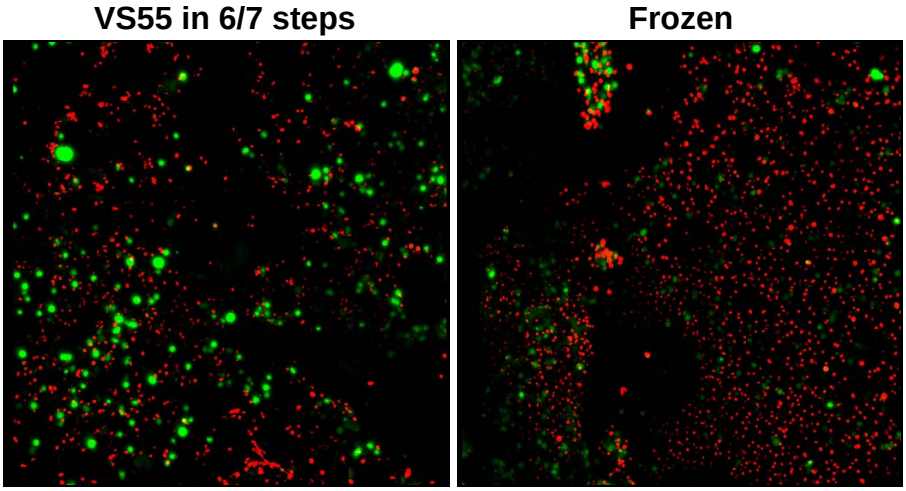

Figure 4.27. Confocal images of live and dead cells over the surface (not over the cross-section) of cryopreserved TECCs. Live cells (green) and dead cells and fragments (red) were distributed over the surface of the TECCs.

4.5.3 Cytotoxicity of Vitrification Solution

Seen in Figure 4.28, non-vitrified samples treated with VS70 in 6/7 steps normalized to VS55 in 6/7 steps had a 36.0 ± 11.3% decrease in cell viability levels compared to VS55 in 6/7 steps ($p = 0.05$). The highest cell viability levels reached for non-vitrified samples were 58.8 ± 4.8% for TECCs treated with VS55 in 6/7 steps and 29.4 ± 3.7% for TECCs treated with VS70 in 6/7 steps ($p = 0.003$).

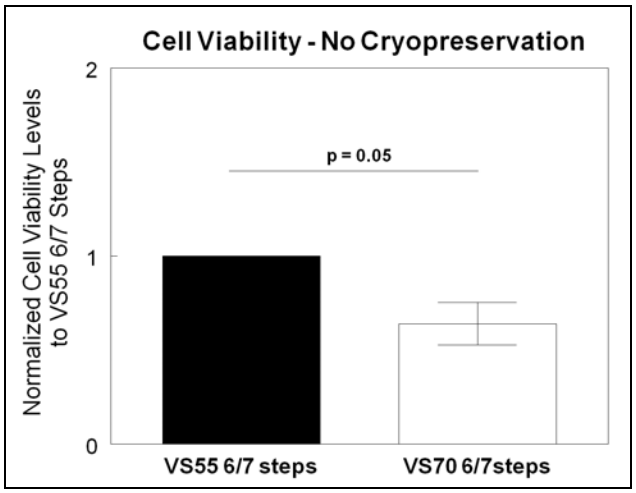

Figure 4.28. VS55 in 6/7 steps compared to VS70 in 6/7 steps without cryopreservation. VS70 in 6/7 steps maintained 36.0 ± 11.3% less viable cells than VS55 in 6/7 steps ($p = 0.05$ vs. VS55 in 6/7 steps) ($N = 4$ experimental trials). The highest cell viability levels reached were 58.8 ± 4.8% for VS55 in 6/7 steps and 29.4 ± 3.7% for VS70 in 6/7 steps.

The confocal images presented showed no noticeable difference in cells viability even though VS55 in 6/7 steps maintained more viable cells than VS70 in 6/7 steps. Figure 4.29 shows the cell distribution and viability throughout the thickness of the TECCs. Live cells were noticeably visible along the surface of the constructs.

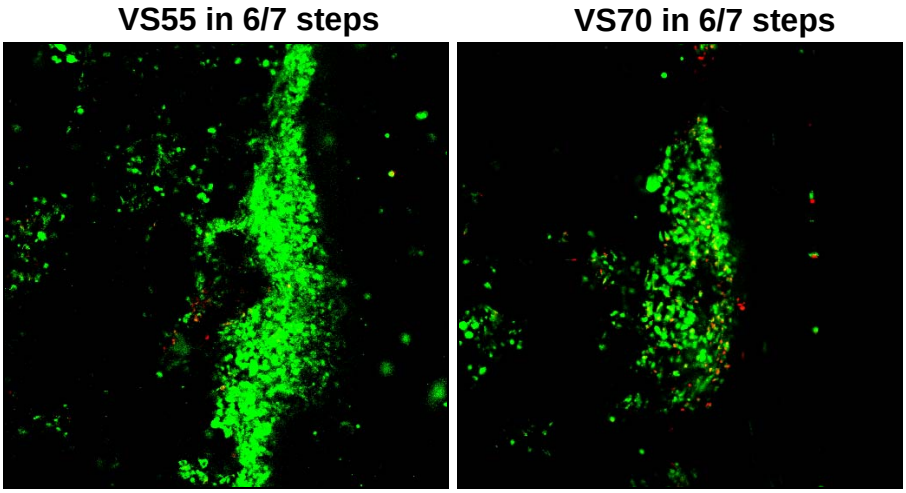

Figure 4.29. Confocal images of live and dead cells throughout the thickness of non-vitrified TECCs. The surface (right-hand side) showed a concentration of densely packed cells. Live cells (green) were located throughout the thickness of the cartilage, while dead cells and fragments (red) were sparsely distributed. For these sample images of TECCs containing 6.0 ± 0.4 million cells per construct, VS55 in 6/7 steps retained more live cells (40.1%) than VS70 in 6/7 steps (26.2%). The viability levels of the entire construct were measured quantitatively via the alamarBlue assay, while the confocal images was a single-plane image at the center of the construct.

4.5.4 Effect of Cryopreservation Formulations on Cell Viability Levels

Seen in Figure 4.30, VS70 in 6/7 steps normalized to VS55 in 6/7 steps maintained a 2.2 ± 0.4 -fold increase in cell viability levels over VS55 in 6/7 steps after cryopreserved ($p = 0.08$). The highest cell viability levels reached for vitrified TECCs with 1.0 ± 0.2 million cells per construct for VS55 in 6/7 steps was 20.9 ± 2.7%, while VS70 in 6/7 steps maintained 39.7 ± 9.7% relative cell viability levels ($p = 0.15$).

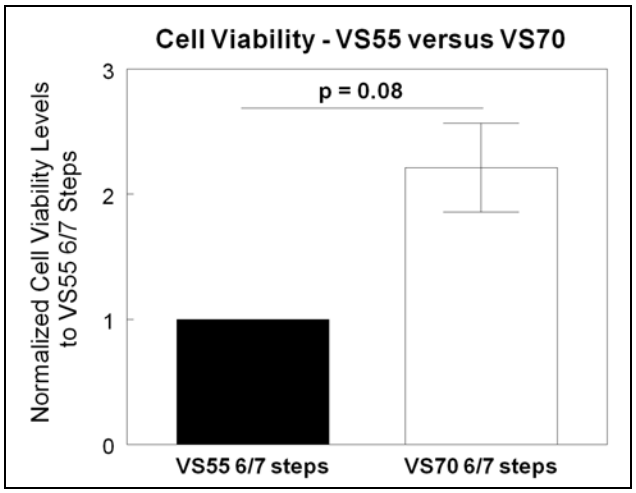

Figure 4.30. VS55 in 6/7 steps compared to VS70 in 6/7 steps. VS70 in 6/7 steps maintained twice as many viable cells than VS55 in 6/7 steps ($p = 0.08$ vs. VS55 in 6/7 steps) ($N = 3$ experimental trials). TECCs were cultured 6 or 7 days before cryopreserved. The highest cell viability levels reached were 20.9 ± 2.7% for VS55 in 6/7 steps and 39.7 ± 9.7% for VS70 in 6/7 steps ($p = 0.15$).

The TECCs cultured for 14 days contained 8.3 ± 1.2 million cells per construct. The TECCs treated with VS70 in 6/7 steps normalized to VS55 in 6/7 steps had a 2.6 ± 0.3 -fold increase in viable cells over VS55 in 6/7 steps (Figure 4.31A) ($p = 0.01$). In Figure 4.31B, TECCs cultured to 28 days (6.4 ± 0.7 million cells per construct) also showed a difference between VS70 in 6/7 steps to VS55 in 6/7 steps, where VS70 in 6/7 steps maintained a 2.2 ± 0.4 -fold increase in viable cells over VS55 in 6/7 steps after cryopreserved ($p = 0.04$). Each of these experimental trials was conducted once and was an example of unsuccessful vitrification. This resulted in low cell viability levels overall. However, given the similar trend between successful and unsuccessful vitrification (see Table 4.5), VS70 in 6/7 steps would likely still maintain significantly greater cell viability levels over VS55 in 6/7 steps during successful vitrification.

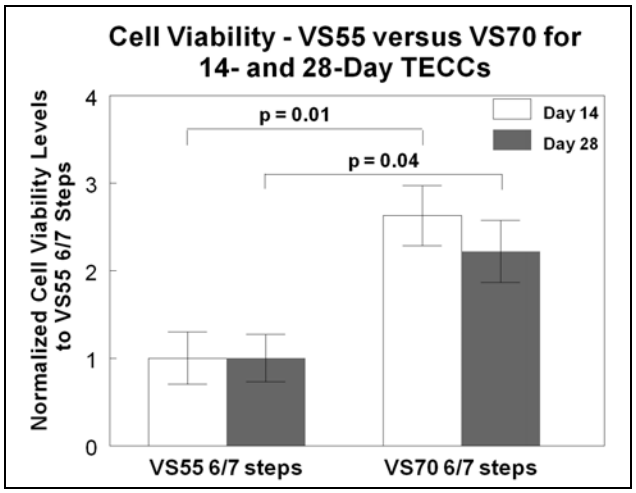

Figure 4.31. VS55 in 6/7 steps compared to VS70 in 6/7 steps for Day 14 and Day 28 TECCs. VS70 in 6/7 steps maintained twice as many viable cells than VS55 in 6/7 steps ($p < 0.05$ vs. VS55 in 6/7 steps) ($n = 4$ constructs). TECCs cultured for 14 days before cryopreserved maintained 10.9 ± 1.6% viability when treated with VS55 in 6/7 steps, while VS70 in 6/7 steps maintained 28.6 ± 1.6% viability. TECCs cultured for 28 days before cryopreserved maintained 9.8 ± 2.7% viability when treated with VS55 in 6/7 steps, while VS70 in 6/7 steps maintained 21.7 ± 3.5% viability.

Seen in Figure 4.32, VS83 in 6/7 steps normalized to VS55 in 6/7 steps maintained 64.7 ± 1.5% less viable cells over VS55 in 6/7 steps ($p = 0.08$). The TECCs cultured for 6 days in the PCC bioreactor had 0.7 ± 0.3 million cells per construct when vitrified. This experimental trial was an example of successful vitrification, and thus, cell viability levels for vitrified TECCs treated with VS55 in 6/7 steps was 18.5 ± 3.7%, while VS83 in 6/7 steps maintained only 6.5 ± 0.3%.

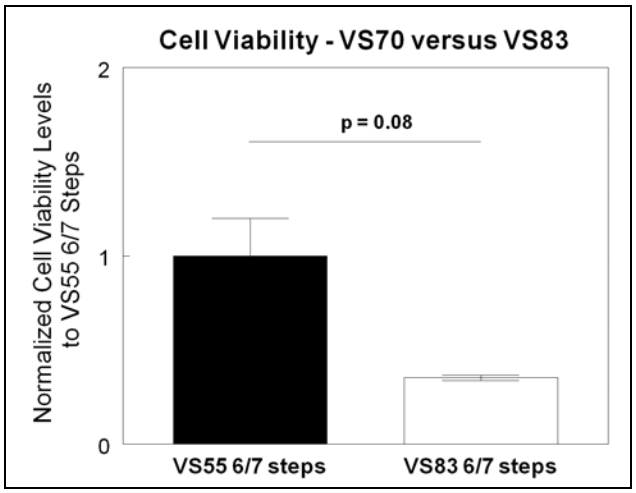

Figure 4.32. VS55 in 6/7 steps compared to VS83 in 6/7 steps. VS83 in 6/7 steps maintained less than half as many viable cells than VS55 in 6/7 steps ($p = 0.08$ vs. VS55 in 6/7 steps) ($n = 3$ constructs). This was a successful vitrification experiment; therefore, the highest cell viability levels were 18.5 ± 3.7% for VS55 in 6/7 steps and 6.5 ± 0.3% for VS83 in 6/7 steps.

Confocal images showed that after vitrification most of the cells died in the interior of the constructs. Seen in Figure 4.33, most cells within the TECCs treated with VS83 in 6/7 steps were dead, while those treated with VS55 in 6/7 steps or VS70 in 6/7 steps showed that cells along the surface of the constructs remained viable after vitrification. Though overall, vitrification in all three solutions resulted in low cell viability with the maximum viability levels at 39.6 ± 9.7% with VS70 in 6/7 steps.

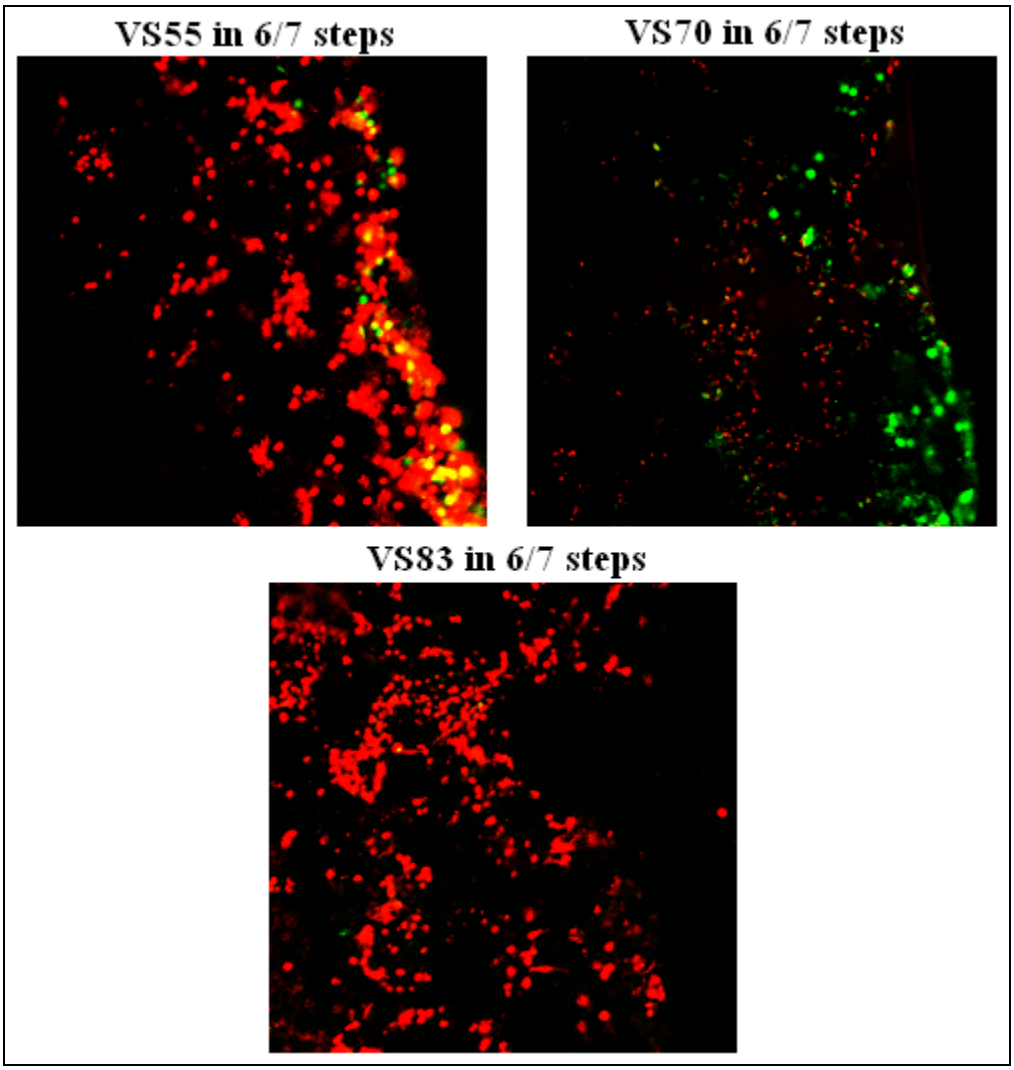

Figure 4.33. Live and dead staining across the thickness of the constructs for cryopreserved TECCs treated with VS55 in 6/7 steps, VS70 in 6/7 steps, or VS83 in 6/7 steps. Live cells fluoresced green and dead cells or fragments fluoresced red. For these sample images, the surface of the constructs (right-hand side) showed presence of live cells for VS55 (20.8% viable) and VS70 (30.4% viable), while the interior and VS83 (6.2% viable) showed mostly dead cells and fragments.

4.5.5 Reduction of Steps in Introduction/Elution of CPAs

Compared to VS55 and VS83, VS70 maintained the highest cell viability levels of approximately 40%. Thus, the next study focused on the number of steps the CPAs in VS70 were introduced and eluted, which was changed to reduce exposure time and

simplify the cryopreservation process. The six discrete steps of introduction of CPAs that gradually increased to the full-strength mixture were reduced to four discrete steps. Similarly, the seven steps of elution of CPAs that gradually reduced the strength of the CPAs were reduced to four steps. Total time to introduce the TECCs to 6 or 7 steps took 90 or 105 minutes, respectively, whereas 4 steps took 60 minutes. Seen in Figure 4.34, VS70 in 4/4 steps normalized to VS70 in 6/7 steps maintained only a 1.2 ± 0.2 -fold increase in cell viability levels over VS70 in 6/7 steps after cryopreserved ($p = 0.53$). The highest cell viability levels reached for vitrified TECCs with 2.6 ± 0.2 million cells per construct for VS70 in 4/4 steps was 50.0 ± 2.5%, while VS70 in 6/7 steps maintained an equivalent of 44.5 ± 6.0% relative cell viability levels.

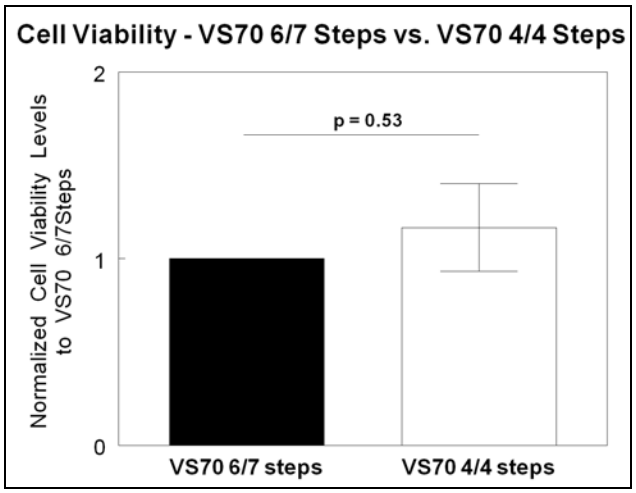

Figure 4.34. VS70 in 6/7 steps compared to VS70 in 4/4 steps. VS70 in 4/4 steps maintained equivalent amounts of viable cells compared to VS70 in 6/7 steps ($p = 0.53$) ($N = 4$ experimental trials). The highest cell viability levels reached were 44.5 ± 6.0% for VS70 in 6/7 steps and 50.0 ± 2.5% for VS70 in 4/4 steps.

Confocal images across the thickness of the constructs showed the distribution of live and dead cells, with dead cells found mainly in the interior of the constructs after vitrification. Seen in Figure 4.35, most cells within the TECCs in VS70 in 6/7 steps treated constructs were dead. However, along the surface of the constructs live cells were prevalent. Similar behavior was noticed after vitrification of TECCs treated with VS70 in 4/4 steps.

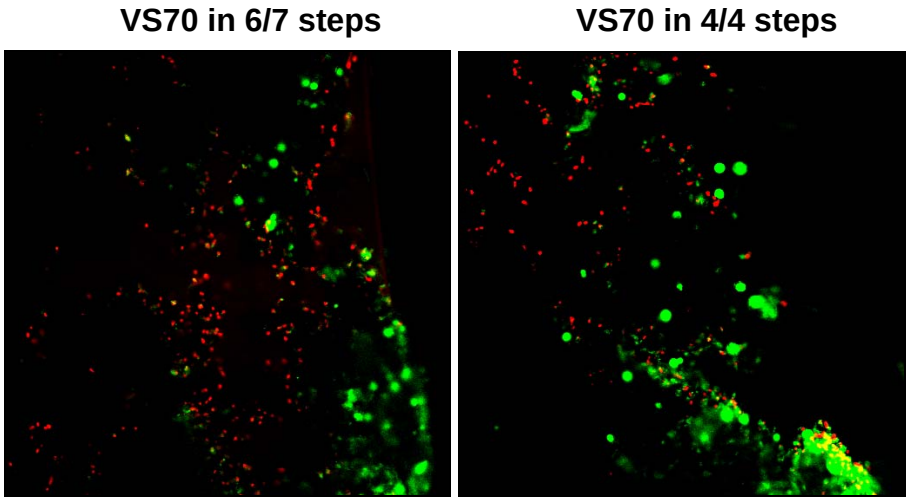

Figure 4.35. Live and dead staining across the thickness of the constructs for cryopreserved TECCs treated with VS70 in 6/7 steps or VS70 in 4/4 steps. The surface (right-hand side) showed prevalence of live (green) cells. Dead cells or fragments (red) were also detected throughout the thickness of the constructs. For these sample images, VS70 in 6/7 steps maintained 30.4% viable cells and VS70 in 4/4 steps maintained 51.7% viable cells for constructs with 2.6 ± 0.2 million cells per construct.

4.5.6 Introduction of CPAs via the PCC Bioreactor

Before utilizing the PCC bioreactor to pump the vitrification solution, the shear stress exerted on the TECCs was determined according to Equation 3.3 described in Chapter 3:

$$\tau_w = \frac{8\mu V_m}{d}$$ Equation 3.3

The vitrification solution pumped into the PCC bioreactor at a rate of 10 mL/min. This correlated to a rate of 1.25 mL/min/construct for 8 constructs embedded in the bottom row of the PCC bioreactor or 0.07 cm/s/construct. At 4°C the viscosity of VS55 was measured at 2.55 ± 0.01 cP and the viscosity of VS70 was 2.31 ± 0.00 cP ($p < 0.05$). Thus, the shear stress at the wall exerted in the TECCs as the vitrification solution was pumped through the constructs was between 0.9 and 1.3 dynes/cm^2 for VS55 and 0.8 and 1.2 dynes/cm^2 for VS70. However, this calculation assumed that the pore density size remained the same, between 106 and 150 μm. In actuality, the pore size most likely decreased as cellular and extracellular matrix deposition increased over the course of 7 days in bioreactor culture.

From the previous studies, VS70 was chosen over VS55 to pump into the PCC bioreactor due to higher cell viability results. In addition, because VS70 in 4/4 steps was not detrimental to cell viability compared to VS70 in 6/7 steps, VS70 in 4/4 steps was modified to pump into the PCC bioreactor (see Section 3.8 for set-up). Seen in Figure 4.36, VS70 in 4/4 steps using the PCC bioreactor normalized to VS70 in 4/4 steps using the orbital shaker maintained only 1.0 ± 0.1 -fold increase in cell viability levels over VS70 with the orbital shaker after cryopreserved ($p = 0.97$). The highest cell viability levels reached for successfully vitrified TECCs (cultured for seven days) with 2.6 ± 0.2 million cells per construct for VS70 with the orbital shaker was 56.0 ± 3.3%,

while VS70 in the PCC bioreactor maintained an equivalent amount at 47.8 ± 5.6% ($p = 0.23$).

.

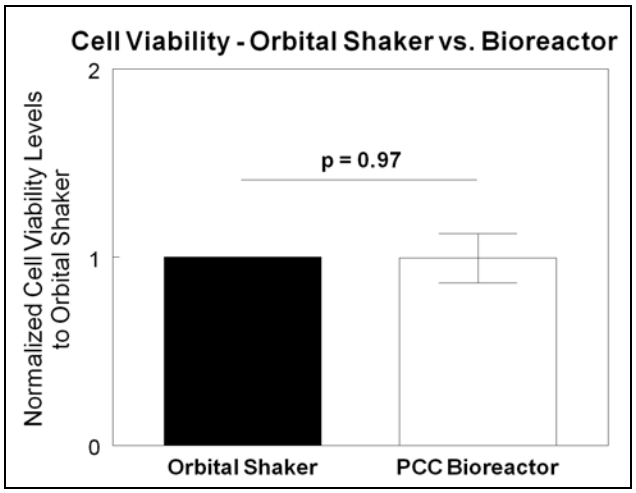

Figure 4.36. VS70 in 4/4 steps using the PCC bioreactor method compared to the orbital shaker method. The PCC bioreactor method maintained equivalent amounts of viable cells compared to the orbital shaker method (N = 3 experimental trials). The highest cell viability levels reached were 56.0 ± 3.3% for VS70 in 4/4 steps and 47.8 ± 5.6% for VS70 in the PCC bioreactor.

Confocal images of vitrified TECCs treated with either the orbital shaker method or the PCC bioreactor method showed a distribution of live and dead cells throughout the thickness of the constructs. Seen in Figure 4.37, TECCs treated with the orbital shaker or with the PCC bioreactor had live cells primarily on the surface of the construct. However, live cells were also visible in the interior of the constructs, but no discernable difference was seen between the two treatments.

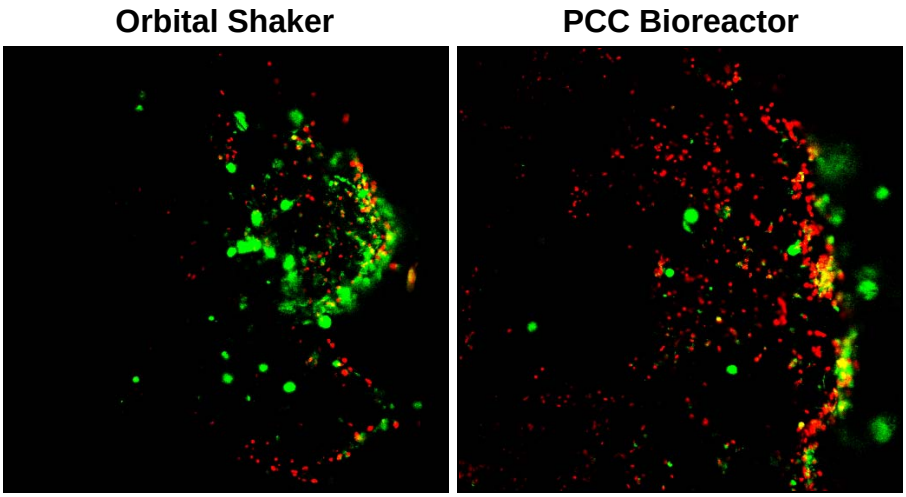

Figure 4.37. Live and dead staining across the thickness of the constructs for cryopreserved TECCs treated with VS70 in 4/4 steps using the orbital shaker or the PCC bioreactor. The surface (right-hand side) showed prevalence of live (green) cells. Live cells were also found in the interior of the constructs. Dead cells and fragments fluoresced red. For these sample images, the orbital shaker method maintained 50.1% viable cells and the PCC bioreactor method maintained 44.1% viable cells for constructs with 2.6 ± 0.2 million cells per construct.

4.6 Summary of Cell Viability after Cryopreservation

The separate cryopreservation studies taken together showed that overall VS70 was the best vitrification formulation compared to VS55 and VS83. VS70 maintained almost twice as many viable cells over the standard VS55, while VS83 maintained less than half as many viable cells than VS55. VS70 was introduced and eluted in 6 and 7 steps, respectively. By reducing the number of steps to 4 for introduction and 4 for elution, the cell viability levels remained unchanged from the baseline of VS70 in 6/7 steps. Thus, the reduction of steps had no effect on cell viability while simplifying the vitrification process. Finally, by introducing and eluting VS70 through the TECCs using the PCC bioreactor, the cell viability levels remained unchanged from the baseline of VS70 in 4/4 steps using the orbital shaker. The highest cell viability levels reached after

vitrification of the TECCs was approximately 50% when treated with VS70 in 6/7 steps, in 4/4 steps, and in the PCC bioreactor. Table 4.6 summarizes the highest cell viability levels reached for each successful vitrification study.

Table 4.6. Highest cell viability levels reached in each cryopreservation study

Cryopreservation Study	Cell Viability Levels (%)
Traditional vs. VS55 6/7	32.8 ± 5.9 vs. 18.7 ± 2.9
VS55 6/7 vs. VS83 6/7	18.5 ± 3.7 vs. 6.5 ± 0.3
VS55 6/7 vs. VS70 6/7	20.9 ± 2.7 vs. 39.7 ± 9.7
VS55 6/7 vs. VS70 6/7 no vitrification	58.8 ± 4.8 vs. 29.4 ± 3.7
VS70 6/7 vs. VS70 4/4	44.5 ± 6.0 vs. 50.0 ± 2.5
VS70 4/4: Orbital Shaker vs. PCC Bioreactor	56.0 ± 3.3 vs. 47.8 ± 5.6

Data are presented as mean ± SEM for n constructs

CHAPTER 5

DISCUSSION

These results show for the first time the importance of fluid-induced shear in the production of tissue-engineered cartilage constructs in a bioreactor environment. We used two model systems for this study: the concentric cylinder bioreactor, which exposed the TECCs to surface shear, and the perfusion concentric cylinder bioreactor, which exposed the TECCs to orthogonal shear forces in addition to surface shear via the addition of perfusion. We found that the proliferation and distribution of cells within the construct and the quality of their extracellular matrix were impacted by the direction of shear and the magnitude of shear that they experienced. We also showed that the PCC bioreactor could be used to introduce and elute cryoprotectant agents, but the variability inherent in the system precluded identification of an optimal cryopreservation protocol. These experiments are discussed below.

5.1 Effects of Mechanical Stimulation on TECC Development

The premise that mechanical forces that modulates chondrocytes' behavior *in vivo* will also influence their behavior *in vitro* (Saini and Wick 2003; Sharma and Elisseeff 2004) has led to a number of studies that showed that cell-seeded scaffolds are influenced by their environment, stimulating chondrogenesis and matrix synthesis (Freed, Vunjak-Novakovic et al. 1993; Vunjak-Novakovic, Freed et al. 1996; Davisson, Kunig et al. 2002; Darling and Athanasiou 2003; Saini and Wick 2003; Xu, Urban et al. 2006). Culture of tissue-engineered cartilage under high shear stresses (turbulent flow) in

bioreactors created elongated cells and collagen fibrils in regions exposed to shear and increased cell content, GAG, and collagen by 70%, 60%, and 125%, respectively, when compared to static cultures (Vunjak-Novakovic, Freed et al. 1996). Davisson et al. seeded ovine chondrocytes under perfusion at 0.05 mL/min and then perfused with culture media at 0.8 mL/min. After nine days GAG content increased by 40% along with cell content compared to static cultures (Davisson, Sah et al. 2002). Some of the reasons speculated as to why mechanically active bioreactors enhance growth compared to static cultures are that they increase nutrient and oxygen transfer due to increased mixing patterns, that they distribute cells more uniformly due to the design of the bioreactors, and that they stimulate chondrogenesis due to hydrodynamic forces with specified magnitude and type (Freed, Hollander et al. 1998; Lee, Grad et al. 2005). These studies led to the motivation for the development of the PCC bioreactor, in which multi-directional forces were hypothesized to influence cartilage growth.

5.2 Perfusion Concentric Cylinder Bioreactor for the Production of Tissue-Engineered Cartilage: Effect of Perfusion Coupled with Shear on Construct Development

The PCC bioreactor was designed to incorporate convective flow of fluid through the cell-seeded scaffolds while fluid also flowed over the surface of the scaffolds. This bioreactor system was used to understand how mechanical forces enhance the growth and structure of tissue-engineered cartilage grown over the course of 28 days. The inner bob of the PCC bioreactor was designed to closely imitate the inner bob of the CC bioreactor, however significant changes had to be made for perfusion through the scaffolds to occur.

Many of the operating parameters for the PCC bioreactor were based on the studies carried out in the CC bioreactor, which determined that 38 rpm and 90% porous PLLA were optimum culturing conditions. Saini determined that at 38 rpm, as opposed to 76 rpm, maximum cell growth and significantly more GAG was deposited per construct. In addition, maximum collagen deposition occurred at 38 and 76 rpm compared to static and 19 rpm (Saini 2001). At this rotation, constructs in the CC bioreactor experienced a surface shear stress of 1.2 dynes/cm^2. These observations led to the final selection of 38 rpm for the rotation speed of the outer cup in the PCC bioreactor. In addition, 90% porous PLLA was chosen over PGA (poly glycolic acid) due to higher cell number and GAG deposition per construct (Saini 2001). The perfusion flow rate of 0.6 mL/min/construct, which started at Day 4 of culture, was chosen by Rangamani, the original inventor of the PCC bioreactor. The addition of perfusion prior to Day 4 may have been detrimental to cell viability, and thus was eliminated during the seeding period (Rangamani 2005).

The PCC inner bob did not conform to the shape of a cylindrical bob due to the extruding construct arms. However, at 38 rpm the Reynolds number indicated laminar flow, and thus discrete steady path lines from the rotating outer cup to at least the edge of the construct arms. By assuming that flow was not angularly dependent, the velocity exerted on the top of the open cavity could be calculated with the simplified model of two concentric cylinders, in which the inner central hub minus the construct arms represented the inner radius. The open cavity model for CFD calculations that was used to calculate the shear stress profile over the construct indicated that along the surface, the center of the construct experienced a relatively uniform shear stress between 0.1 and 0.5 dynes/cm^2

and an average stress of 3 dynes/cm^2 near one edge (Figure 4.1B). This result was markedly different from the homogeneous shear stress (1.2 dynes/cm^2) exerted on the constructs in the CC bioreactor (Williams, Saini et al. 2002). Had the constructs not been embedded into the arms, but aligned to the edge of the arms (i.e. no open cavities), the shear stress experienced on the surface of the construct would have been nearly homogeneous. The shear stress, based on Newton's law of viscosity, and derived from Navier-Stokes equations for the annulus region between two concentric cylinders (Saini 2001), would have been 0.99 dynes/cm^2. This open cavity design indicated a limitation in the PCC bioreactor, where the constructs overall experienced multi-directional flow and heterogeneous surface shear stress; however, it is important to note that the first aim of this project focused on the comparison of the different types of bioreactors and not mechanical forces.

The CFD model for flow over the constructs in the open cavity was done as a two-dimensional cavity over the diameter of the construct. Recirculation was evident and a homogeneous flow and shear stress did not occur for the PCC bioreactor except at the center of the construct at 0.4 dyne/cm^2. Other sections on the surface of the construct were not evaluated, but CFD modeling would have shown recirculation as well. The shear stress profile could be further evaluated in future studies over the entire surface of the construct as discrete cavities of varying lengths.

The fluid perfusion orthogonal to the surface shear exerted a shear stress between 0.13 and 0.18 dynes/cm^2 on cells in the construct. Fluid perfusion may also have occurred in the CC bioreactor, especially early in culture when the relatively large pores (106 – 150 μm in diameter) were not filled with cells and extracellular matrix, such that

shear stress was exerted in the pores of the scaffolds. The affixed scaffolds are banked along the surface of the inner bob. Thus, fluid could permeate through the side of the porous scaffolds at 38 rpm (10.44 cm/s). At this speed the shear stress, calculated from Equation 3.3, through the porous scaffolds was between 39 and 55 dynes/cm^2. Though this is a high shear stress value, fluid also has a tendency to flow in the path of least resistance, and flowing around the scaffolds is less work than flowing through the scaffolds. Thus, while some fluid perfusion may have occurred through the side of the scaffolds in the CC bioreactor, the shear stress exerted via perfusion may have been less than the shear stress that occurred on the surface of the scaffolds. Fluid perfusion itself was not a different mechanical force than from shear stress, but rather, the PCC bioreactor exerted shear stresses of different magnitudes on the constructs in directions orthogonal to each other. So while this research refers to perfusion and shear as separate mechanical forces, in reality, both forces employed shear stress.

In the PCC bioreactor, cells seeded, proliferated, and deposited extracellular matrix on PLLA scaffolds. The choice of PLLA scaffolds was decided because of the ease in synthesis and inexpensiveness of the material. Other scaffolds such as poly-glycolic acid (PGA), which would have produced more uniform tissue (Saini 2001), would not have been an ideal choice because of the poor material properties. That is, the addition of perfusion adds an additional load that would force the PGA scaffolds out of the construct arms, while PLLA has the stiffness to withstand perfusion. Hybrid polymer scaffolds, such as poly-lactic-co-glycolic acid (PLGA), may have the stiffness needed while producing uniform tissues. The ideal scaffold for the culture of TECCs would fully maximize the potential for the PCC bioreactor.

Diffusion flux was eliminated when perfusion occurred (i.e. when convective flux dominated), which led to a linear dependence for the transport of oxygen across the thickness of the construct (Equation 4.4). When this assumption was not made, the oxygen concentration profile from the species continuity equation followed an exponential and linear profile (see Appendix A for derivation):

$$C_{O2} = \frac{R_{O2}L}{V_m(e^{V_m L/D_{O2}} - 1)}(e^{V_m x/D_{O2}} - 1) - \frac{R_{O2}x}{V_m} + C_{O2}^0 \qquad \text{Equation 5.1}$$

However, when plotted, the oxygen profile showed that the linear dependence of oxygen across the thickness of the construct still dominated and that there was less than a 0.13% difference between the profiles plotted from Equation 4.4 (Figure 4.2) and Equation 5.1.

To rely on diffusion alone, the oxygen concentration within the constructs would have reached zero by Day 28. Thus, perfusion dramatically increased oxygen transport within the constructs. This result had the potential to improve cell growth within the center of the constructs by preventing oxygen depletion. Cells propagated towards the interior of the constructs from the surface shear face because cells were initially seeded under shear forces only, without the aid of perfusion. This observation was made evident in the histological images. Over time, however, cells and extracellular matrix did deposit on the perfusion face of the constructs. Though histological images showed lack of cells within the central-interior of the constructs, this could be explained by the low initial seeding of the scaffolds and thus, low overall cell number in the constructs. Higher cell density would further penetrate the constructs and the nutrient transport calculations have

shown that the cell growth would not have been limited by oxygen availability for constructs cultured in the PCC bioreactor.

The initial low seeding of the constructs was due to the low cell density in media prior to seeding. 150 million cells were suspended in 350 mL of media (0.4 million cells/mL) for the PCC bioreactor. In comparison, the CC bioreactor had a cell density of 2.4 million cells/mL prior to seeding. The high volume requirements in the PCC bioreactor (400 mL) compared to the CC bioreactor (62 mL) also were a factor in the low seeding efficiency. The geometric design of the PCC bioreactor left regions of "dead space" near the central hub and between the construct arms. These empty regions never came into contact with scaffolds; and thus, cells located in those regions aggregated together lowering the overall seeding efficiency of the PCC bioreactor. Cells also permeated through the scaffolds without attaching to the matrix and settled at the bottom of the central hub. Though the cells did not attach to the bottom surface because of the silicone coating, after 28 days a thin biofilm layer of cartilage was found inside the central hub. This tissue-engineered cartilage (without a scaffold matrix) adopted the central hub's dimensions (5.08 cm diameter) to form a thin circular piece of cartilage. The lack of disturbance in the central hub made the environment ideal for growth of tissue-engineered cartilage and lowered the overall seeding efficiency of the PCC bioreactor. Another reason for the low seeding efficiency was that the scaffolds were embedded inside the arms, whereas, in the CC bioreactor the scaffolds were not. The decreased surface area of the scaffolds in the PCC bioreactor provided less cell-attachment sites, lowering overall seeding efficiency.

The low seeding efficiency of the PCC bioreactor was determined by cell content from Day 4 samples. However, chondrocytes remained viable, proliferated, and synthesized GAG and collagen in the PLLA scaffolds over the course of 28 days, which demonstrated that the bioreactor was conducive to cartilage growth. No statistics could be performed between the constructs harvested from the top row and bottom row because three constructs were harvested at each time point (two from one row and one from the other). Yet, the general observation in construct composition showed no noticeable difference between those harvested from the top or bottom row, which indicated that variance between the perfusion flow rate (69%) between the top and bottom row of the PCC bioreactor had little effect on cartilage composition. In fact, the variances were similar between constructs harvested from the PCC bioreactor and from the CC bioreactor. This observation led more credibility to use the average flow rate of 0.6 mL/min/construct to calculate the shear stress (0.13 - 0.18 dynes/cm^2) through the construct regardless of its position.

While the PCC bioreactor was conducive to cartilage growth, the bioreactor was compared to the previously characterized CC bioreactor to gauge its effectiveness. Constructs from the CC bioreactor had about twice as much ECM than the PCC bioreactor, yet did not proliferate as fast as the PCC bioreactor (Figure 4.7). The multi-directional stresses in the PCC bioreactor may have affected the proliferation rate as opposed to the CC bioreactor, which experienced only surface shear stress. Initial cell density is also an important variable in tissue-engineered cartilage production and can influence cellular proliferation, phenotypic stability, structure, and matrix deposition. Cell seeding studies showed that scaffolds seeded at high densities

(e.g. 30 - 40 $x10^6$ cells/cm^3) maintained their differentiated phenotype and secreted more ECM, while those at low densities produced less ECM (Bruckner, Horler et al. 1989; Vunjak-Novakovic, Obradovic et al. 1998; Mauck, Wang et al. 2003; Saini and Wick 2003). In another study by Puelacher et al., constructs seeded with less than $20x10^6$ cells/cm^3 created more fibrous and inferior cartilage (Puelacher, Kim et al. 1994). Mandl et al. showed that seeding at low cell density increased the proliferation rate due to lack of cell-to-cell contact inhibition (Mandl, van der Veen et al. 2004). Therefore, a high seeding density would have maintained important cell-to-cell interaction influencing proliferation, matrix synthesis, and differentiation (Watt 1988) in the bioreactors. That the constructs from the CC bioreactor produced more ECM could have been due to the higher initial cell density, 12 ± 4 million cells/cm^3, compared to the PCC bioreactor, at 5 ± 1 million cells/cm^3, which enhanced cell-to-cell contact. However, the difference between the initial cell densities was not significant. As such, the most likely reason for the higher ECM content was because of the higher shear stress in the CC bioreactor. That both bioreactors expressed collagen type I was also indicative of possible dedifferentiation of some chondrocytes to more fibroblastic structure and attributed to the low cell seeding of the scaffolds, in agreement to previous studies (Puelacher, Kim et al. 1994). From histological images in Figure 4.9, constructs from the PCC bioreactor showed a more even distribution of cells and extracellular matrix than the CC bioreactor. This could be attributed to the orthogonal fluid regime in the PCC bioreactor, which distributed cells to both sides of the constructs surfaces more than the one-directional CC bioreactor fluid regime, which had constructs affixed to a non-permeable inner bob.

Derived from Freed et al., the growth curve of tissue-engineered cartilage constructs to describe proliferation could be modeled after a polynomial equation that accounted for initial cell density, α (cells/construct), the initial cell growth rate, β (cells/construct/day), and the decrease in growth rate over time, $-\gamma$ (cells/construct/day^2). The proliferation of cells, X (cells/construct), in the PCC and CC bioreactor was fitted to the quadratic equation as a function of time, t (days) (Freed, Vunjak-Novakovic et al. 1993):

$$X(t) = \alpha + \beta t - \gamma t^2 \qquad \text{Equation 5.2}$$

Table 5.1 lists the coefficients and R^2 value extrapolated from fitting the experimental data to the growth curve for the bioreactors. The extrapolated negative initial cell density coefficient was due to the low seeding density for the PCC bioreactor. The PCC bioreactor had a higher initial growth rate (β) and a decrease in growth (γ) compared to the CC bioreactor. The growth curve predicted that the PCC bioreactor would culture cells to a maximum of 11 million cells per construct by Day 23, while the maximum growth occurred in the CC bioreactor at Day 2 with 2.2 million cells per construct. However, this was due to the observation cell in the CC bioreactor had not yet entered log phase and that in the cells in the PCC bioreactor for this experimental run had entered death phase by Day 28. Repeat of this experimental run, however, showed that the PCC bioreactor extended cell growth up to 37 days, while CC bioreactor only reached maximum cell growth by Day 23. These calculations showed that the addition of perfusion extended the growth time in the PCC bioreactor over the CC bioreactor.

Table 5.1. Cell growth kinetics as a function of time in the PCC and CC bioreactor

Bioreactor	α (cells/construct)	β (cells/construct/day)	γ (cells/construct/day^2)	R^2
PCC	-5.19×10^6	1.40×10^6	3.00×10^4	0.910
CC	2.27×10^6	-4.71×10^4	-1.53×10^4	0.989

In terms of ECM growth, new GAG synthesis leveled off by Day 14 for the PCC bioreactor and by Day 7 for the CC bioreactor. Continuous production of GAG could not be maintained for prolong periods. This may have occurred because cells became accustomed to the steady shear environment signaling them to a more quiescent state, which inhibited GAG synthesis. The PCC bioreactor, however, appeared to prolong new GAG synthesis a week longer than the CC bioreactor. This observation was seen again when the experimental trial was repeated. That GAG production leveled off or decreased as a result of steady mechanical loading over a prolong growth period has been shown in literature (Saini and Wick 2003; Seidel, Pei et al. 2004; Gemmiti and Guldberg 2006). However, by introducing a new mechanical stimulation after Day 4, it was possible that the cells responded to the more dynamic loading environment in the PCC bioreactor, which prolonged GAG synthesis. The CC bioreactor, which had greater shear stress values, continued to produce more total collagen than the PCC bioreactor after 28 days, which indicated that collagen was dependent on the magnitude of the mechanical loading. The primary focus of this experiment was to compare the growth in two different bioreactors. By Day 28, samples in both bioreactors had roughly the same amount of cells. However, by Day 28 the CC bioreactor produced $1.4 \pm 0.17 \times 10^{-4}$ μg of GAG per cell and $0.69 \pm 0.08 \times 10^{-4}$ μg of total collagen per cell, which was significantly greater than the PCC bioreactor, which produced $0.70 \pm 0.07 \times 10^{-4}$ μg of GAG per cell and

$0.40 \pm 0.02 \times 10^{-4}$ μg of total collagen per cell, respectively ($p < 0.05$). This observation indicated that the incorporation of perfusion through the constructs in the PCC bioreactor had little role in ECM growth and was most likely governed by the higher surface shear forces in the CC bioreactor. This was more clearly seen in histological images where ECM deposition was primarily regulated to the surface shear face in the CC bioreactor (Figure 4.9).

Articular cartilage is an avascular tissue, with low oxygen tension (1 - 3%). Cells have adapted to this low oxygen tension by undergoing glycolysis for their energy needs (Brighton and Heppenstall 1971; Rajpurohit, Koch et al. 1996; Archer and Francis-West 2003). In literature, studies have shown that chondrocytes respond favorably to low physiologic oxygen tension (less than 5% compared to 20% oxygen), with increased ECM expression, specifically up-regulation of aggrecan and collagen type II, and down-regulation of collagen type I (Murphy and Athanassios 2001; Saini and Wick 2004; Wernike, Li et al. 2008), but no significant difference in cellular proliferation (Malda, van den Brink et al. 2004). However, Lewis et al. were able to model oxygen availability to cell density and speculated that chondrocytes increased their proliferative behavior in scaffolds during the first 14 days in regions where there were no oxygen limitations (Malda, van den Brink et al. 2004; Lewis, Macarthur et al. 2005). The PCC bioreactor incorporated convective flow, which increased oxygen transport across the thickness of the constructs, while the CC bioreactor relied on diffusion of oxygen through the constructs (Williams, Saini et al. 2002). The increase in oxygen availability may have been responsible for the increase in cellular proliferation in constructs cultured in the PCC bioreactor. In turn, the decrease in oxygen availability in constructs cultured in the

CC bioreactor may have been responsible for the overall increase in ECM synthesis per cell compared to the PCC bioreactor. Indeed, the limited oxygen availability in the CC bioreactor may have been more ideal for chondrocytes to behave as they would *in vivo*, while the increased availability of oxygen may have triggered cellular proliferation in the PCC bioreactor.

Tissue development was non-uniform for both bioreactors and showed preferential growth on the surface shear face. This was partially due to the seeding period, which was governed by surface shear forces only and low seeding efficiency. Some growth was seen in the constructs on the face affixed to the inner bob of the CC bioreactor, however more intense staining of cells and ECM was detected on the perfusion face of constructs from the PCC bioreactor. Tissue development from the CC bioreactor has stagnant regions with no stimulation while the PCC bioreactor had multi-directional mechanical loading on both faces, which contributed to the distribution of cells and ECM. No GAG was seen on the direct surface of the constructs, but detected towards the interior away from the high shear stresses. The lack of GAG on the surface indicated that small molecular weight glycosaminoglycans were unable to adhere to the constructs and were likely sheared off due to the high shear stresses. Detection of soluble GAG in the media supported this hypothesis, where up to 58% of the GAG produced was released in the CC bioreactor and up to 91% of the GAG produced was released in the PCC bioreactor. The addition of perfusion in the PCC bioreactor may have forced small molecular weight glycosaminoglycans from the interior of the constructs into the media, hence more GAG was detected in the media of the PCC bioreactor than the CC bioreactor. Other studies have supported this observation; in particular, Seidel et al.

showed that tissue-engineered cartilage lacked GAG along the edges of the constructs exposed to fluid, but retained GAG in the interior of the constructs away from direct exposure (Seidel, Pei et al. 2004).

The cell viability of TECCs was viewed under the confocal using live/dead analysis. Quantification of live and dead cells visualized under the confocal was not accurate due to the inhomogeneity of the cells throughout the constructs and the fact that only a small sample size at the center of the construct was imaged. These images also amounted to only 1% of the total construct area and thus, were not representative of the entire construct. Time constraints limited confocal visualization of the entire construct. Thus, the measurements stating that the cell viability of the constructs was approximately 52% by Day 28 for constructs from the CC or PCC bioreactor (and 51% for constructs from the perfusion+shear and shear bioreactor) were not accurate. If more images were taken of each construct, cell viability levels would most likely have been higher and more accurate, and any differences in cell viability between the two bioreactors would have been noticeable.

The PCC versus CC study (and perfusion+shear versus shear study) were each evaluated for one experimental trial. Statistics using the Student's t-test assumed that the samples harvested were independent of each other. However, constructs within the bioreactor could have influenced the growth of other constructs within the same bioreactor, and thus be dependent upon each other. This would have affected the significance of our results. Therefore, the entire experimental run was repeated and evaluated once more for each study. The same trend was observed as the first trial and can be seen in Appendix B. However, major differences in cellular and ECM content

existed between the first and second independent runs due to variations in the animal source. As such, the two runs could not be grouped and statistically evaluated together for each bioreactor's effect on cellular growth and ECM deposition because the variations between the two runs were greater than the variations between constructs.

One of the main goals in tissue engineering is the development of bioreactor technology, which can be used to promote the growth of functional tissues for human implantation. This study demonstrated the growth of tissue-engineered cartilage cultured in a perfusion concentric cylinder bioreactor that incorporated orthogonal fluid regimes with a quantifiable hydrodynamic environment to mechanically stimulate cell-seeded scaffolds. One of the advantages of the PCC bioreactor over the CC bioreactor was the opportunity for implantation of constructs into cartilage defects. The CC bioreactor constructs required silicone and plastic adhesives that when removed damaged the constructs. This level of destruction made them unusable for implantation. Whereas, the PCC bioreactor constructs were affixed via tension into the construct arms and were easily removed without damage. Our results indicated that the PCC bioreactor greatly affected cellular proliferation and prolonged new extracellular matrix synthesis, but produced less ECM than the previously characterized CC bioreactor. This bioreactor was useful to study construct development and the role of hydrodynamic loading. These results have important applications in tailoring the growth of tissue-engineered cartilage. By allowing focus on cellular proliferation as opposed to ECM deposition, we address issues related to the optimization of cartilage development in cartilage bioprocess engineering. Thus far, cartilage constructs cultured in bioreactors have lower ECM composition than native cartilage (containing 60 - 70% collagen and 15 - 20% GAG)

(Mansour 2004), which suggests improvements in strategies to increase matrix production are necessary. The biomechanical environment controls cellular proliferation and ECM development, addressing the need for research into an optimal bioreactor design for cartilage tissue engineering.

5.3 Mechanical Stimulation for Improved Properties of Tissue-Engineered Cartilage: Effect of Perfusion and Shear Cartilage Growth

Native articular cartilage experiences a number of mechanical forces, perfusion of fluid through the permeable cartilage, compression due to motion of the joint, hydrostatic pressure, and fluid-induced shear over the surface of the cartilage. Two of these mechanical forces, perfusion and shear, were adapted to the bioreactor environment and applied to constructs cultured in the PCC bioreactor. The first aim of this project focused on the characterization of the PCC bioreactor and compared the new bioreactor to the previously characterized CC bioreactor. Because the two bioreactors had different culture environments and geometric designs, which resulted in different surface shear stresses, a comparison between the effect mechanical forces had on construct growth could not be determined. This led to the motivation of the second aim of this project, where mechanical forces, perfusion and shear, were applied to constructs cultured in the PCC bioreactor. Perfusion and shear were applied to one PCC bioreactor, while only shear was applied to another. A perfusion only application in the PCC bioreactor would have completed this study; however, the aim of this study focused instead on the effect multi-directional fluid flow had on construct growth. In addition, the risk of contamination increased when more than two PCC bioreactors were in use in each

experimental run because of the increased handling of the bioreactors. A perfusion only application in the PCC bioreactor would also have been detrimental to growth, simulating a static culture due to the low shear stress from fluid perfusion (0.14 dynes/cm^2). The focus of this aim was to understand the effect mechanical forces had on construct cartilage growth both *in vitro* and *in vivo*.

From nutrient transport calculations for oxygen, a shear only application in the PCC bioreactor relied on diffusion alone for oxygen transport through the thickness of the constructs. This resulted in a severe drop in oxygen levels (to 0 mol/m^3) from equilibrium values by Day 28 in the PCC bioreactor in the interior of the constructs, which contained approximately 4 million cells per construct. In contrast, the perfusion+shear bioreactor had only a 13.9% drop in oxygen levels across the thickness of the constructs, which contained approximately 10 million cells per construct. Though oxygen depletion was more pronounced in the shear bioreactor and may have had limited transport of cells to the interior of the TECCs, the live/dead staining showed no discernable pattern of dead cells (see Figure 4.13). Most cells on the surface of the TECCs were alive and proliferating. Improved oxygen transport, however, may have been one of the reasons for the increase in cellular and ECM deposition in the perfusion+shear bioreactor over the shear bioreactor.

Sikavitsas et al. demonstrated that though mass transfer of nutrients and waste removal increased as perfusion rate increased, the response to increased shear stress was the primary factor in improving mineralization of osteoblasts. Their study demonstrated that by varying viscosity (hence shear stress) of the perfusing culture media with dextran, without increasing mass transfer, that mineralized matrix deposition increased as shear

stress increased from 0.1 to 0.3 dynes/cm^2 (Sikavitsas, Bancroft et al. 2003). This reasoning, if applied to the PCC bioreactor with chondrocytes, which had a magnitude shear stress of approximately 0.42 dynes/cm^2 (assuming 0.4 dynes/cm^2 from the surface shear calculations), would also explain the increase in ECM deposition in the perfusion+shear bioreactor, which had more mechanical forces than the shear bioreactor. The multi-directional flow in the perfusion+shear bioreactor increased the shear stress exerted on the constructs both in magnitude and direction. Collagen, in particular, showed a definite increase in the perfusion+shear bioreactor compared to the shear bioreactor.

Collagen production may have also increased, in response, as a protective measure to the increase in mechanical loading over the shear bioreactor. The collagen matrix provided a barrier to direct interaction between cells and mechanical loading. In turn, the collagen matrix deformation, as a result of mechanical loading, relayed signals to chondrocytes in a variety of mechanotransduction pathways to affect chondrogenesis. In contrast, by Day 28, GAG deposition per construct showed no significant difference between the perfusion+shear bioreactor (1.2 ± 0.1 mg/construct) and shear bioreactor (1.2 ± 0.3 mg/construct). GAG production rate in the perfusion+shear bioreactor peaked a week later the shear bioreactor. This observation could be explained by the addition of perfusion as a new mechanical force, whereas, the shear bioreactor experienced a constant mechanical environment. Other studies have shown that a dynamic culture environment was needed to maintain GAG synthesis. Saini showed that a dynamic culture environment that oscillated from 19 rpm (0.6 dynes/cm^2) to 38 rpm (1.2 dynes/cm^2) was needed for continuous production of glycosaminoglycan, while still

maintaining collagen synthesis. Otherwise, GAG synthesis rate entered a quiescent state (Saini 2001). This would explain why the GAG production rate slowed and leveled out after 21 days in culture for the perfusion+shear bioreactor (after 14 days for the shear bioreactor) and why no significant difference between the two bioreactors existed after 28 days in GAG content. Thus, a constant fluid-induced shear may not be able to stimulate GAG synthesis for long-term culture. Both bioreactors released a large percentage of GAG into the culture media, where small glycosaminoglycan chains were sheared off of the PLLA scaffolds.

The effects of continuous and dynamic loading on matrix synthesis seen in our studies have been observed in a number of other bioreactor studies in literature (Kisiday, Jin et al. 2004; Seidel, Pei et al. 2004; Gemmiti and Guldberg 2006; Xie, Han et al. 2007). In a parallel plate flow chamber bioreactor developed by Gemmiti et al., chondrocytes were subjected to fluid-induced shear (1 dynes/cm^2) for three days after two weeks under static culture. The results showed that after three days of shear, collagen content increased significantly, but not GAG or cell number, when compared to static culture. This suggested that collagen, responsible for tensile properties, responded to shear, while GAG, responsible for compressive properties, did not (Gemmiti and Guldberg 2006). Kisiday et al. compared proteoglycan and collagen synthesis in tissue-engineered cartilage cultured either under continuous compression (2.5% strain superimposed on a 5% static compression offset at 1 Hz) for 45 minutes every six hours or intermittent compression (where continuous compression was applied every other day). Their study determined that while short-term culture (less than 48 hours) of compression increased proteoglycan and collagen synthesis, long-term culture (greater

than 14 days) of intermittent compression, as opposed to continuous compression, increased proteoglycan synthesis, but had no effect on collagen synthesis. The speculation was that cells responded to the intermittent dynamic environment by synthesizing macromolecules to resist compressive forces (i.e. proteoglycan) (Kisiday, Jin et al. 2004). In a similar study carried out by Xie et al., continuous compression (10% strain at 0.1 Hz) on tissue-engineered cartilage constructs also resulted in a decreased expression of both aggrecan and collagen type II expression over intermittent loading (where continuous compression was applied every other day) after three days in culture (Xie, Han et al. 2007).

When cartilage growth was normalized to cell content for Day 28 samples, the perfusion+shear bioreactor produced 0.9 ± 0.1 $x10^{-4}$ μg of GAG per cell and 2.1 ± 0.2 $x10^{-4}$ μg of total collagen per cell, which was not significantly different from the shear bioreactor at 4.3 ± 1.6 $x10^{-4}$ μg of GAG per cell and 6.2 ± 3.9 $x10^{-4}$ μg of total collagen per cell, respectively. This observation showed that increase in ECM production was due more to the increase in mechanical loading in the perfusion+shear bioreactor than to the increase in cell number or decrease in oxygen availability in the shear bioreactor. Table 5.2 shows the ratio of ECM content per cell for both bioreactors as well as the ratio of collagen to GAG per construct. When compared to native cartilage, the percentage of GAG and collagen produced per cell in the bioreactor was less than 0.01%. However, the ratio of collagen to GAG in the perfusion+shear bioreactor (2.42 ± 0.15) was greater than native cartilage (1.5), while the shear bioreactor had a ratio of 1.19 ± 0.32. This observation suggested that improvement was needed in GAG synthesis

in the perfusion+shear bioreactor and collagen synthesis in the shear bioreactor to match native cartilage composition and produce functionally relevant articular cartilage.

Table 5.2. Effect of mechanical stimulation on extracellular matrix production on Day 28 samples

	Perfusion+Shear	Shear	Native Cartilage [a]
GAG (μg/cell)	$0.9 \pm 0.1 \times 10^{-4}$	$4.3 \pm 1.6 \times 10^{-4}$	1.4
Total Collagen (μg/cell)	$2.1 \pm 0.2 \times 10^{-4}$	$6.2 \pm 3.9 \times 10^{-4}$	2.1
Collagen/GAG	2.4 ± 0.2*	1.2 ± 0.3*	1.5

* $p < 0.05$ between perfusion+shear and shear bioreactor
a. (Saini and Wick 2003)

The significant increase in cell proliferation in the perfusion+shear bioreactor indicated chondrocytes dependence on mechanical stimulation. The effect of shear stress on the up-regulation of cell proliferation has been discussed in literature (Bancroft, Sikavitsas et al. 2002; Malaviya and Nerem 2002; Raimondi, Moretti et al. 2006). Raimondi et al. showed a dose-dependent response, where increasing the shear stress through the scaffold from 0.05 to 0.6 dynes/cm^2, caused an increase in cell number by 1.7 fold compared to static controls (Raimondi, Moretti et al. 2006). When constructs in the PCC bioreactor were exposed to both perfusion and shear, cell growth was significantly affected by the multi-directional flow than when compared to constructs exposed to only shear. Both et al. showed that low cell seeding density influenced the proliferation rate of mesenchymal stems cells cultured in monolayer. Cells seeded at 100 cells/cm^2 reached 200×10^6 cells 4.1 days earlier than those seeded with 5000 cells/cm^2 (Both, van der Muijsenberg et al. 2007). This indicated higher proliferation rates when cells were seeded at lower densities. Despite that the PCC

bioreactor had low initial cell density, both bioreactors were seeded with approximately the same number of cells at Day 4 and demonstrated that the increase in cellular proliferation was likely due to the addition of perfusion in the perfusion+shear bioreactor. This increase in proliferation behavior matched the results obtained when the PCC bioreactor was compared to the CC bioreactor, which only employed surface shear over the constructs. Even though the CC bioreactor had higher shear stress than the PCC bioreactor and few nutrient limitations (Williams, Saini et al. 2002), the PCC bioreactor still caused higher proliferation rates.

Derived from Freed et al., the growth curve of tissue-engineered cartilage constructs to describe proliferation could be modeled after a polynomial equation that accounted for initial cell density, α (cells/construct), the initial cell growth rate, β (cells/construct/day), and the decrease in growth rate over time, $-\gamma$ (cells/construct/day^2). The proliferation of cells, X (cells/construct), in the PCC bioreactor was fitted to the quadratic equation as a function of time, t (days) (Freed, Vunjak-Novakovic et al. 1993):

$$X(t) = \alpha + \beta t - \gamma t^2 \qquad \text{Equation 5.2}$$

Table 5.3 lists the coefficients and R^2 value extrapolated from fitting the experimental data to the growth curve for the perfusion+shear bioreactor and shear bioreactor. The extrapolated negative initial cell density coefficient was due to the low seeding density for both bioreactors. The perfusion+shear bioreactor had a higher initial growth rate (β) and slower decrease in growth (γ) over the shear bioreactor. The growth curve predicted

that the perfusion+shear bioreactor would culture cells to a maximum of 14 million cells per construct by Day 38, while the shear bioreactor already reached a maximum by Day 22 at 4.7 million cells per construct. Repeat of this experimental run showed the same trend where perfusion+shear extended cell growth up to 37 days, while shear only reached maximum cell growth by Day 17. These calculations further showed that the addition of perfusion extended the growth time in the PCC bioreactor.

Table 5.3. Cell growth kinetics as a function of time in the perfusion+shear and shear bioreactor

Bioreactor	α (cells/construct)	β (cells/construct/day)	γ (cells/construct/day^2)	R^2
Perfusion +Shear	-3.55×10^6	9.45×10^5	1.26×10^4	0.970
Shear	-2.74×10^6	6.63×10^5	1.47×10^4	0.914

Bovine cartilage was chosen because large amounts of cells can be extracted from a single source. Variations exist, however, between animal sources, and affect the goal to develop consistent results in cartilage growth in the PCC bioreactor. Mesenchymal stem cells (MSC) as a primary source would alleviate this problem. Ideally, this type of system could be used to implant TECCs into human cartilage defects. The source and amount of cells would be of concern, where MSC and human chondrocytes would have to be expanded first to a high cell density (greater than $20 \times 10^6/cm^3$) before seeded into the bioreactor. More studies on the examination of the growth curve of the PCC bioreactor with human chondrocytes or MSC would elucidate the minimum number of cells needed to seed the bioreactors, shortening the wait time for patients.

That proliferation was affected by directional shear stress may be attributed to the mechanotransduction pathways. This result highlighted that mechanoreceptors in the cells may be sensitive to not only the magnitude of the stresses, but also the direction of the stress vectors. The exact mechanism for translating shear stress due to perfusion to pathways that induce proliferation is not well understood. Though not a directional study of stress vectors, Malaviya and Nerem were able to demonstrate that chondrocytes cultured in a parallel plate flow chamber and exposed to 35 dynes/cm^2 proliferated and increased by 6 fold compared to 4 fold in static culture. They were also able to show that the effect of shear stress on proliferation was partially mediated by transforming growth factor beta 1 (TGF-β1), a known mitogen for chondrocytes, which was up-regulated 3.5 fold compared to static culture (Malaviya and Nerem 2002).

Histological images showed tissue development with cellular and extracellular matrix deposition across the thickness of the constructs (see Figure 4.12). Despite the addition of perfusion in the perfusion+shear bioreactor, the shear bioreactor also showed cartilage development on the backside of the constructs. This was the result of "static culture" on the backside of the constructs in the shear bioreactor (where perfusion occurred in the perfusion+shear bioreactor). Diffusion of culture media from the backside through the constructs aided cartilage development in the shear bioreactor. In fact, the addition of perfusion on the backside of the constructs had no visible role in the distribution of cells and extracellular matrix throughout the constructs. Seen in Figure 4.12, GAG staining in the shear bioreactor was more intense than the pefusion+shear bioreactor. GAG deposition was also seen near the backside of the constructs in the shear bioreactor, whereas, the addition of perfusion in the

perfusion+shear bioreactor possibly decreased GAG attachment to the scaffolds. Thus, the addition of perfusion resulted in less intense staining for GAG at the center. Both bioreactors stained equally for collagen type II and type I. The presence of collagen type I was not surprising due to the presence of collagen type I gene expression in the perfusion+shear bioreactor (see Figure 4.10). The presence of collagen type I was due to possible dedifferentiation of chondrocytes and the result of the formation of fibrous tissue to protect cells from direct mechanical loading.

The compressive modulus measured the bulk stiffness of the TECCs. Primarily, GAG chains provided resistance to compressive forces by drawing in water to resist loading and providing stiffness (Mansour 2004). In this study, there was no significant difference in the modulus over the course of the experimental run, nor between the two bioreactors. After 28 days the modulus measured 0.15 MPa, which was only 25% of native cartilage. Based on biochemical composition, the relatively low GAG content in the constructs cultured in the perfusion+shear and shear bioreactor may have accounted for the low modulus. In addition, the negatively charged PLLA scaffolds may have provided the main resistance to compressive forces.

The permeability constants describe the ease of fluid permeation through TECCs. Generally, native cartilage has permeability constants between 10^{-14} and 10^{-16} $m^4/(N*s)$ (Cohen, Chorney et al. 1994; Heneghan and Riches 2008). The permeability constant measured for native cartilage using the confined compression testing apparatus seen in Figure 3.10A was $1.16 \pm 0.78 \times 10^{-13}$ $m^4/(N*s)$. This measurement was at least one order of magnitude greater than found in literature (Holmes and Mow 1990; Soltz and Ateshian 1998; Chen, Bae et al. 2001). The discrepancy may be due to the age of the cartilage

tested, where samples measured in literature were from mature bovines. Our samples were from newborn calves. Immature cartilage has less cross-linkages in the extracellular matrix, and thus possibly more permeable than adult samples. In this study, the permeability constants measured from the dynamic portions of the confined compression test showed no significant difference over the course of 28 days, nor between the two bioreactors. After 28 days the permeability constant measured $2.0x10^{-13}$ $m^4/(N*s)$ and was equivalent to native juvenile cartilage, but 220% more permeable than PLLA scaffolds (0.61 ± 0.23 $x10^{-13}$) ($p < 0.05$). This observation may be explained by the breakdown of the PLLA polymer, which increased the negative charge of the PLLA scaffold. This increase in negative charge retarded fluid flow, and thus decreased permeability in the confined chamber. Overall, the permeability constants were higher than those found in literature. The nonlinear biphasic theoretical equation, Equation 3.13, was used to calculate the permeability constants. The permeability calculations assumed that the fluid velocity through the constructs was the same as the set ramp rate of 0.0005 mm/s. In actuality, fluid flow may have been lower if resistance to flow was considered (as in the PLLA scaffolds), which would have decreased the permeability constants. This was not assumed because the compression apparatus did not have the means to measure interstitial fluid flow rates. Instead, we assumed that fluid flow was based on forced convection from the non-permeable indenter. The biphasic theory also assumed a homogenous tissue; however, based on histological analysis, the TECCs were not homogeneous and had regions where PLLA dominated. Taken together, these major assumptions may have contributed to the higher than normal permeability constants for native juvenile cartilage and TECCs.

The permeability constant could also have been calculated from a permeability-strain relationship equation based on the linear biphasic theory which was derived from mass and momentum balances (Mow, Kuei et al. 1980):

$$\sigma(h,t) = H_A \left.\frac{\partial u}{\partial z}\right|_{z=h} = -\frac{V_0 H_A t}{h} - \frac{2V_0 h}{k_0 \pi^2}\sum_{n=1}^{\infty}\frac{1}{n^2}\left(1 - e^{-n^2\pi^2 H_A k_0 t / h^2}\right) \qquad \text{Equation 5.3}$$

where,

V_0 is the strain rate,

t is time

This equation did not require the knowledge of the fluid rate and could have been used to fit the dynamic portion of the experimental data to calculate the permeability constant. The simplicity of the non-linear biphasic equation was chosen over the linear biphasic equation to calculate the permeability constant. However, Heneghan and Riches compared the two theories and showed that the permeability constants calculated had the same order of magnitude (between 10^{-14} and 10^{-16} $m^4/(N*s)$) regardless of the permeability-strain equation used, and were also within the same order of magnitude of the permeability constants measured from direct permeation experiments (Heneghan and Riches 2008).

The shear modulus measured resistance due to deformation parallel to the load and took in account the amount and interaction of the ECM network. This in turn, provided a more accurate assessment of the mechanical properties of TECCs. The collagen fibrils provided the main resistance to tensile (stretching) loading (Mansour 2004), which was applicable to shear deformation. However, the orientation of the fibrils

and the degree of cross-linking in the matrix between the collagen and GAG also determined the shear properties of the cartilage (Stading and Langer 1999; Silver, Christiansen et al. 2001). In this study, the shear modulus for both bioreactors decreased over the course of 28 days, which was surprising due to the increase in ECM deposition in the TECCs. However, the phase angle increased over the course of 28 days, and the perfusion+shear bioreactor had a significantly higher phase angle than the shear bioreactor. The complex shear modulus is a combination of the elastic modulus (storage) and viscous modulus (loss) and the phase angle measures the ratio of the viscous behavior to the elastic behavior. Based on the biochemical composition, the total collagen in the perfusion+shear bioreactor was significantly greater than the shear bioreactor. Because collagen is the primary component responsible for viscous behavior, this would explain why the phase angle was greater as well. Yet, the decrease in the shear modulus indicated that the interaction between the collagen and GAG was lacking, i.e. low amounts of cross-linking (immature cartilage) that provide the resistance to loading, which allowed the viscous sliding of uninhibited collagen fibrils. The high shear modulus (1.83 MPa) and low phase angle (6.15°) of the PLLA scaffolds supported this observation, in which the stiff scaffold had no collagen to contribute to the viscous behavior. Stading and Langer have demonstrated that over time the ECM composition and structure influence the shear modulus of the TECCs and that mature cartilage with high collagen and GAG (and high levels of cross-linking) showed an increase in stiffness over time (Stading and Langer 1999). However, Raimondi et al. were able to show that collagen scaffolds seeded with chondrocytes, decreased in their storage modulus and

increased in phase angle over time, which is in agreement with our results (Raimondi, Colombo et al. 2003).

We created a xiphoid chondral defect in a nude rat model to observe cartilage healing. The purpose of this study was to evaluate this new technique and the role of mechanically stimulated tissue-engineered cartilage to heal cartilage defects. This was the next logical step in the bioprocess scheme: to evaluate the necessity of bioreactors that employ mechanical forces in order to heal cartilage defects. Though not articular cartilage, the xiphoid had similar composition as hyaline cartilage and served as a model for these cartilage studies. One problem with the nude rat model had to do with the thickness of the xiphoid. The 5-week old rats had thin xiphoids (less than 2 mm in thickness), while the TECCs had an average thickness of 1.87 mm. This resulted in an uneven fit and healing between the implant and defect, which is easily seen in Figure 4.19. Nevertheless, the implant was lined up on one side of the cartilage defect and sealed with SepraFilm during the surgery. Prior to implantation, constructs from the perfusion+shear and shear bioreactor had twice as many cells and ECM compared to those in the static bioreactor. The implants, however, had significantly less cells than the cells only implants (Group F). The results from the histology showed more differentiation and mature cartilage in the TECCs cultured in either the perfusion+shear or shear bioreactor, which was evidenced by the presence of GAG in the implants. TECCs cultured in the static bioreactor and the PLLA scaffolds showed only cells. No detection of GAG was seen throughout the implants. These results highlighted the importance and necessity of mechanically active environments to culture TECCs before

implantation in order to prolong maturation and extend cartilage growth after implantation.

Group F contained implants that had only cells, but no scaffold or ECM. This control group also had significantly higher amounts of cells than any other implant group ($5x10^6$ cells). Group F showed the most maturation than any of the other implant groups, with intense staining for cells and GAG. This observation showed the necessity to consider cell density in implants, in which the higher the cell density, the greater the maturation and healing. This was further verified when constructs from the perfusion+shear and shear bioreactor showed more maturation than the static bioreactor and PLLA scaffold group, which had a significantly lower cell density or none in the case of the PLLA scaffold. Even though Group F showed the most positive result compared to the implants from the bioreactors, the structural integrity was compromised in this cells only group. The xiphoid cartilage was unable to maintain its original shape without the aid of the scaffolds as seen in Figure 4.19. Therefore, both cell density and structural support has to be considered for tissue-engineering cartilage for the purpose of healing cartilage defects. Collagen type I was detected in all implant groups. Collagen type I is a marker for scar tissue and indicated that while articular cartilage was detected by the presence of type II collagen, the detection of type I collagen at the interfaces and edges of the implants indicated that the xiphoid was attempting to heal the defect with fibrous scar tissue. The empty defect model indicated that without the aid of an implant, poor healing occurred and little to no cells or ECM was present in the defect region. The results from this animal study indicated that cell density as oppose to ECM content was the primary factor in the success of engineered cartilage maturation. Mechanically active bioreactors

could still play a role in tissue engineering by expanding cell number in a scaffold to a critical cell density (in this case $5x10^6$) to promote maturation.

Some studies have been carried out on the implantation of TECCs into cartilage defects. The animal models most commonly used were subcutaneous implants into nude rats or mice (Jin, Park et al. 2007; Jung, Kim et al. 2008). Jung et al. implanted mechanically stimulated cartilage constructs (cultured for either 10 days or 24 days) subcutaneously into nude mice models. Their results showed that these mechanically stimulated constructs increased in maturity and formed well-developed cartilage over those cultured under static conditions. This was in agreement with our results. They also noted, however, that TECCs stimulated for 24 days became more hypertropic compared to the 10 day old implanted constructs (Jung, Kim et al. 2008). This study suggested that while mechanically stimulated constructs were beneficial to growth upon implantation and enhanced chondrogenesis, the age of the cells also had to be considered in optimizing growth after implantation.

The improved maturation of implanted tissue-engineered cartilage cultured in the PCC bioreactor necessitated the role for mechanically active bioreactors to heal cartilage defects. The perfusion+shear bioreactor may play an important role in the future of tissue engineering, given that the biochemical composition showed that the addition of perfusion greatly improved cellular proliferation from a low cell-seeding density. The perfusion+shear bioreactor could provide the mechanical environment to expand a small amount of cells extracted from patients in a relatively short culture period compared to a shear only bioreactor. The mechanical properties indicated that the TECCs grown in either bioreactor provided less than ideal behavior to native cartilage. The increase in

phase angle in the perfusion+shear bioreactor and decrease in shear modulus indicated that high collagen content over GAG was not enough to improve the stiffness of the TECCs. More improvement in the culture conditions to increase GAG content and maturation to increase cross-linking would improve the compressive and shear modulus of the TECCs. This study created a better understanding of hydrodynamic forces on the growth of cells and extracellular matrix deposition. A proposed new model extrapolated from these results would be to use directional perfusion to increase proliferation rates, surface shear to increase collagen synthesis, and intermittent dynamic compression or dynamic fluid-induced shear to increase GAG synthesis. Taken together, the growth of tissue-engineered cartilage could be tailored by these mechanical forces to produce constructs with the desired composition and properties prior to implantation into cartilage defects.

5.4 Cryopreservation of Tissue-Engineered Cartilage

The long-term success of implanted tissue-engineered cartilage constructs for osteoarthritis and other cartilage-damaged injuries depends on suitable storage methods. Long-term storage that maintains cartilage viability and function can provide an “off-the-shelf” availability for patients without the need to wait for cells to grow and make TECCs. To date most research in cryopreservation has been on native tissues and cells. The interaction between newly formed tissue and the scaffold matrix during vitrification is not well understood and as such, few studies have been carried out on preservation of tissue-engineered constructs. The focus of this study was to investigate the factors that regulate the preservation of tissue-engineered cartilage by studying cell viability levels as

a result of vitrification methods that have previously been effective for native articular cartilage. The use of different vitrification formulations and introduction and elution methods provides insight into the cytotoxicity of cryoprotectant agents as well as their mass transfer properties through TECCs.

The method to quantify cell viability was assessed by the measurement of the metabolic activity of cells. Similar to the cytotoxic MTT (3-[4,5-dimethylthiazol-2-yl]-2,5-diphenyl tetrazolium bromide) assay, the non-cytotoxic alamarBlue assay measured the color change as the dye is reduced by mitochondrial and cytosolic enzymes characteristic of metabolic activity. In addition, cells are quantified (DNA assay) to give a perspective of the viability levels detected. For example, TECCs that had contamination or less than $0.5x10^6$ cells per construct had unusually high cell viability levels (between 80% and 110% viability). This demonstrated not only a lower limit to the effectiveness of the viability assay, but also allowed us to discount the data gathered from these experimental runs. Cell viability was re-tested four hours after the cryopreservation studies. However, cells have been shown to undergo apoptosis 24 hours after thawing from traditional freezing methods even when cell viability levels were high immediately after thawing. Milosevic et al. has shown that even after a week, cell viability levels decreased 50 - 60% after thawing from traditional freezing (Milosevic, Storch et al. 2005). These observations show that the viability assessments may not be entirely accurate and that viability at least 24 hours after preservation or apoptosis assays needs to be assessed to fully gauge the effectiveness of different preservation methods. Live/dead confocal images supplemented the alamarBlue assay in order to view the orientation of live and dead cells throughout the thickness of the constructs.

Quantification of live and dead cells visualized under the confocal was not accurate, as they did not match viability levels measured from the alamarBlue assay (data not shown). The inaccuracy stemmed from the single images taken at one plane along the z-axis at the center of the construct and due to the inhomogeneity of the cells throughout the constructs. These images also amounted to only 1% of the total construct area and thus, were not representative of the entire construct. Time constraints also limited confocal visualization of the entire construct.

The largest hindrance to the viability studies was the risk of ice formation as the temperature of the TECCs dropped from 4°C to -100°C. Vitrification is defined as fast cooling of approximately -40°C per minute for tissues. Glass formation was critical because ice crystals damaged delicate cell membranes. In many of the experimental trials, unsuccessful vitrification occurred, which is defined as slow cooling and visualization of ice crystals and resulted in low cell viability levels in the TECCs. The temperature gradient played a large role in the success of vitrification. The mechanical freezer was maintained at -150°C and the initial temperature of the TECCs was 4°C. The temperature change initiated from a pre-cooled isopentane bath located in the mechanical freezer or the small-scale bench-top system to the aluminum mesh vitrification canister (that held the vials), which then proceeded through the borosilicate glass, the vitrification solution, and finally to the TECCs. Table 5.4 lists the estimated thermal conductivity, the density multiplied by the heat capacity value, and the thermal diffusivity found in literature, for the materials mentioned.

Table 5.4. Thermal properties of the materials used in vitrification

Material	Thermal Conductivity (W/(m*K))	Heat Capacity x Density ($J/(m^3*K)$)	Thermal Diffusivity (m^2/s)
Isopentane [a]	0.17	$1.07x10^6$	$1.57x10^{-7}$
Aluminum [b]	236.09	$2.39x10^6$	$9.86x10^{-5}$
Glass [c]	1.11	$2.10x10^6$	$5.29x10^{-7}$
Vitrification Solution [d]	0.36	$2.98x10^6$	$1.21x10^{-7}$
TECCs [e]	0.48	$3.73x10^6$	$1.28x10^{-7}$

a. Linearly extrapolated to –150°C (Schumann, Aston et al. 1942; U.S.CoastGuard 1999)
b. Measured at 4°C (Giauque and Meads 1941; Steele and Pinsky 2008)
c. Measured at 4°C (Carwile and Hoge 1966; Yamashita, Tojo et al. 2001)
d. Fitted to the energy equation for temperature change (Mukherjee 2008)
e. Measured at 27°C for native cartilage (Youn, Telenkov et al. 2000)

Aluminum had the largest conductivity and diffusivity; however, given its wire mesh configuration, most of the glass vials came in contact with liquid isopentane. Based on Fourier's law of heat conduction, the largest heat flux occurred through the aluminum and glass materials. The vitrification solution (VS55) had the smallest diffusivity and could be seen as the limiting factor to temperature change for the system. VS70 had a higher concentration of CPAs than VS55, which may have resulted in a smaller thermal diffusivity and thus longer temperature change than VS55. However, except for the aluminum canister, the diffusivities were on the same order of magnitude, and thus would have had roughly equal thermal transport times. The mass properties and path length of the aluminum, glass, and vitrification solutions was constant. This left the isopentane bath as a possible reason for unsuccessful vitrification. Based on Newton's law of cooling, increasing the contact surface area of the isopentane bath to the glass vials would increase the heat flow. Khirabadi et al. found that the cooling rate of the VS55 occurred faster if vials were immersed deeper into an isopentane bath. For example, an immersion

of vials 3 cm into the pre-cooled isopentane bath had a cooling rate of -43°C per minute, while 6 cm resulted in -71°C per minute (Khirabadi, Song et al. 2001). In our experiments, vials were immersed anywhere between 2 to 6 cm in the pre-cooled bath, in which the isopentane level was always above the level of the vitrification solution inside the vials. Successful vitrification, however, would still occur sporadically in vials immersed in 2 cm or 6 cm of isopentane. Nevertheless, isopentane served as a better conduit for cooling than cooled air at –150°C, which had a thermal conductivity of approximately 0.01 W/(m*K) (Bird, Stewart et al. 2002).

The ability to maintain a stable pre-cooled isopentane bath varied as well, especially in regards to the small-scale bench-top method, which affected the success of vitrification. The closed insulated system maintained a stable temperature in the vapor phase of the liquid nitrogen. When opened to room temperature, temperature fluctuations inside the system occurred, which affected the temperature of the isopentane and thus the heat transfer rate. The temperature of liquid nitrogen is -196°C, while the melting temperature of isopentane is -160°C. The isopentane would begin to solidify in the small-scale bench-top system after a prolong period in liquid nitrogen, which affected its thermal diffusivity. In our experimental trials, the isopentane was allowed to equilibrate with the vapor phase of the liquid nitrogen inside the bench-top system for at least 30 minutes before used for vitrification. When the mechanical freezer (set at -150°C) was available the isopentane bath remained stable. The mechanical freezer had a larger volume compared to the small-scale bench-top system, which created a stable temperature environment. Samples could be stored overnight in the freezer and maintained at -150°C. Whereas, liquid nitrogen in the small-scale bench-top system

would evaporate overtime, raising the temperature of the system. When vitrification occurred in the small-scale bench-top system, we assumed that most cell damage was caused by ice crystal formation, which only occurred during the cooling and re-warming stage from the glass transition temperature (-135°C). Thus, eliminating storage of the samples overnight when we used the small-scale bench-top system should not have affected the resulting cell viability levels.

Ideally, the storage of the TECCs at -196°C in liquid nitrogen would have been more preferable and easier than storage at -150°C. Yet, the storage of the samples were kept at -150°C instead of -196°C to prevent thermal cracking. The further the samples were in temperature from their glass transition temperature, the higher the risk was for thermal cracking and ice formation.

In this study, VS70 was determined as the optimum vitrification solution over VS55 and VS83. VS83 proved to be highly cytotoxic under conditions of exposure, due to its high concentration of cryoprotectant agents. VS55, in contrast, could not adequately maintain cell viability levels equivalent to VS70. VS70, which was more cytotoxic than VS55, preserved twice as many cells as VS55. This pattern of cell viability was constant even when cell number in the TECCs increased (as in Day 14 and Day 28 samples), which determined that using a short-term culture period may adequately represent results for TECCs cultured for longer periods. The toxicity of the vitrification solution was evident when TECCs exposed to VS70 for approximately 30 minutes at 4ºC, had a third less viable cells than VS55. But then, the protective effect of VS70 was observed when twice as many cells survived over VS55 after vitrification. The highest viability level measured with VS70 without vitrification was 29.4%, while

the highest viability level measured with VS70 with vitrification was 39.7%. The discrepancy was due to the prolonged exposure of VS70 at 4ºC when samples were not vitrified. When samples were vitrified, metabolic activity ceased; and thus, the toxic behavior of VS70 could not affect the cell viability levels, which occurred at 4ºC. However, a parallel study directly comparing cytotoxicity and vitrification would better elucidate the full effect of VS70 on cell viability levels.

The more concentrated VS70 solution (compared to VS55) provided the best balance of CPAs to protect cells from ice damage without becoming too cytotoxic. Fahy et al. hypothesized that solutions with higher hydrogen bonding energy could vitrify solutions with high water concentration, but were also more toxic than solutions with low hydrogen bonding energy between water and the hydrogen bonding groups in cryoprotectant agents. The suggestion was that there existed a threshold concentration, C_T, in which CPAs below the C_T was not cytotoxic. As such, the toxicity could be reduced more severely than the ability of the CPAs to prevent ice formation, which may explain VS70's performance over VS55 (Fahy, Wowk et al. 2004). Only three formulations of DMSO, formamide, and 1,2-propanediol were tested. Further variations in formulation or conditions of exposure could further increase cell viability by reducing CPAs toxicity while preventing ice formation during vitrification.

The maximum cell viability in TECCs retained for VS70 in 6/7 steps was 39.7%. In native bovine cartilage tissues, VS70 in 6/7 steps still retained more viable cells than VS55 in 6/7 steps. In comparison, Song et al. were able to preserve up to 80% viability of vitrified rabbit articular cartilage with VS55 in 6/7 steps (Song, Lightfoot et al. 2003). Pegg et al. preserved ovine cartilage with 10% DMSO in 5/4 steps to –196°C, but only

recovered 11% of functional [^{35}S]sulfate incorporation into GAG (Pegg, Wusteman et al. 2006). The difference in viability levels highlighted that separate protocols are needed between native animal tissues and for tissue-engineered constructs, in which the interaction between cells and scaffolds have to be considered.

In one study, VS55 in 6/7 steps was compared to traditionally frozen samples. Traditionally frozen samples maintained 32.8% viability compared to 18.7% of VS55 in 6/7 steps. Although VS70 could maintain 40 - 50% viability, it was not directly compared to frozen samples. Traditionally frozen samples in 1 M of DMSO was less cytotoxic than the vitrification solutions. DMSO, which blocks ice formation, was the main contributor to successful cryopreservation. The low cytotoxicity and the prevalence of cells along the surface of the constructs may have resulted in the higher viability levels over the fast vitrification. Though clearly more studies on traditional freezing treatments are needed, this particular study primarily focused the effect of vitrification solutions on cell viability in TECCs. As such, optimization of the slow cooling method with 1 M DMSO was not investigated further.

The next study focused on the number of steps used to gradually introduce and elute the full-strength mixture of VS70. The highest cell viability levels reached for VS70 in 4/4 steps was 50.0%, and 45.5% for VS70 in 6/7 steps. Initially 6 steps introduction and 7 steps elution was used and full exposure time was 90 and 105 minutes, respectively. Reduction of steps (4 introduction and 4 elution) reduced exposure time to 60 minutes each. This simplified and shortened the CPAs exposure process. Pegg et al, found that chondrocytes were particularly resistant to and were more able to withstand osmotic imbalances than other cells (Pegg, Wang et al. 2006). Though reduction of steps

increased the concentration gradient and thus osmotic imbalances, our results showed that reduction of steps had no detrimental effects on cell viability levels. The higher concentration gradients in the 4/4 steps method, however, may have under-exposed the TECCs to the CPAs because only 15 minutes was given for diffusion of the CPAs, in each step, which would have reduced cell viability levels. The 6/7 steps method, in turn, may have over-exposed the TECCs to the CPAs because of the additional steps required, which also would have reduced cell viability levels.

The final study utilized the result that 4/4 steps method was not detrimental to cell viability and modified the method to the PCC bioreactor. The hypothesis was that increasing mass transport of the CPAs through the TECCs would improve cell viability levels. The highest cell viability levels reached for VS70 in the PCC bioreactor was 47.8%, while VS70 in 4/4 steps using the orbital shaker to introduce and elute the CPAs maintained 56.0%. This was surprising when mass transfer estimations were made. The step-wise introduction and elution methods were carried out on an orbital shaker at 4°C at approximately 100 rpm. Diffusion of DMSO, formamide, and 1,2-propanediol were the main limitation to mass transfer. Measured by Mukherjee et al. the diffusivity for DMSO, formamide, and 1,2-propanediol into cartilage tissue at room temperature were 4.63×10^{-10} m^2/s, 3.47×10^{-10} m^2/s, and 6.67×10^{-10} m^2/s, respectively. Based on Fick's second law of diffusion, the time for VS55 to permeate native cartilage and equilibrate with the surrounding bulk VS55 solution took approximately 2 - 3 hours (Mukherjee, Li et al. 2008). If these diffusivity constants were applied to TECCs, then the 15-minute exposures to vitrification solutions using the orbital shaker method were not adequate for complete permeation of CPAs. However, this assumption did not account for convection

due to the orbital shaker and increased porosity of the TECCs over native cartilage (65 - 85% porous), which would have shortened the equilibrium time. Also, this assumption did not take in account that our system was at 4°C, which would have extended equilibrium time. During introduction and elution of the vitrification solution, media remained inside the constructs (observed by a red coloring in the white constructs), but was not quantified. This observation, however, confirmed that CPAs did not permeate completely into the constructs. Therefore, we hypothesized that using convective flow in the PCC bioreactor as the main transport of the CPAs through the TECCs, would have overcome these transport limitations and improved cell viability.

The Peclet number (Equation 3.7), which was estimated from the diffusivity of the CPAs and a path length of 1.87 mm, exceeded 1800, which indicated that convective transport dominated when CPAs perfused through the constructs inside the PCC bioreactor. The shear stress exerted on the constructs due to perfusion fell within physiological range. Thus, the stresses were not detrimental to cell viability, and any protective or detrimental effects of the vitrification solution were due to permeation of the cryoprotectants. During the introduction and elution of the CPAs using the PCC bioreactor, media was removed from the constructs (observed by no red coloring in the white constructs). This observation indicated that CPAs did permeate completely into the constructs. Mass transfer estimations indicated that there were limitations to the penetration of CPAs in the orbital shaker method. However, the quantitative cell viability analysis of constructs preserved indicated that possible mass transfer limitations due to the orbital shaker method or that increased permeation due to the PCC bioreactor

method had no effect on cell viability, given that there were no noticeable differences in viability levels between the two treatments.

All the vitrification studies were supplemented with confocal images that showed the distribution of live and dead cells across the thickness of the constructs after preservation. The confocal images of live and dead cells seemed to indicate that there were some limitations to reach the interior of the TECCs. Most live cells were limited to the surface of the constructs within easy access of the CPAs. There also may have been an unavoidable bias because most cells cultured on the TECCs after 7 days were also primarily located on the constructs' surface. Even though Day 14 and Day 28 samples for VS55 and VS70 comparison did not show differences to Day 6 and Day 7 samples, extended growth studies for the orbital shaker method and the PCC bioreactor method comparison may show differences. This was reasoned because confocal images showed some cells in the interior (not quantified) preserved in the PCC bioreactor method (see Figure 4.37). Another explanation for the lack of difference between the orbital shaker and PCC bioreactor method was that convective flow may have over-exposed TECCs to CPAs, lowing cell viability levels. The reduction of exposure time may increase cell viability while still fully exposing TECCs to CPAs. Nevertheless, the introduction of the PCC bioreactor was not detrimental to cell viability in comparison to the orbital shaker method. This result could be further utilized and taken advantage of by streamlining the bioprocess scheme from cell culture to preservation in one-step.

The PCC bioreactor method was not detrimental to cell viability when used to perfuse vitrification solution through TECCs. This advantage allows for future studies where cells can be cultured in the PCC bioreactor and preserved in the same system. In

turn, this reduces handling and possible contamination risks, as well as, providing a one-step process from culture to preservation, streamlining the bioprocess scheme from culture to market. One disadvantage, thus far, was that the TECCs had to be removed for the vitrification process (4°C to –100°C) and re-warming process (-150°C to 4°C). Currently, the design of the PCC bioreactor prevents removal of the construct arms from the central hub, nor can the polycarbonate PCC bioreactor be exposed to –150°C without warping or cracking the material. (Polycarbonate is stable between -40°C and 95°C.) If the PCC bioreactor had easily removable arms that held the TECCs or was made out of a durable material (i.e. borosilicate glass or polypropylene) that withstood low storage temperatures, then the vitrification process could be further simplified by simply lowering the bioreactor system into the mechanical freezer for vitrification. However, the thickness of the material would affect the rate of cooling and re-warming of the TECCs, and thus, more research into this method would have to be explored.

In conclusion, VS70 affected cell viability levels after vitrification, more so than VS55 or VS83. The protective effect of this formulation showed that cells were sensitive to the concentration of DMSO, 1,2-propanediol, and formamide. DMSO probably played an important role in protecting cells during vitrification, given that traditionally frozen samples in 1 M DMSO also fared well. The reduction of steps did not affect cell viability levels because even though osmotic stress increased, chondrocytes, which are fairly resistant to osmotic stress, were better able to handle larger concentration gradients in shorter steps. However, the reduction of exposure time due to reduction of steps may have also under-exposed the TECCs to the CPAs, reducing overall cell viability levels. The addition of convective flow did not alter cell viability levels and offered the

opportunity to streamline the bioprocess scheme from culture to preservation in one-step. The PCC bioreactor method was not detrimental to cell viability when used to perfuse the CPAs, but may also have over-exposed TECCs to the CPAs, reducing cell viability levels. These results and the variability in cell viability levels due to the success rate of vitrification showed that vitrification protocols and temperature exposure has a critical role in maintaining high cell viability levels. The use of the PCC bioreactor method allows for future studies where cells can be cultured in the PCC bioreactor and preserved in the same system. In turn, this reduces handling of samples and possible contamination risks and provides a one-step process from culture to preservation. The difference in cell viability levels reached for TECCs and rabbit native cartilage and other tissues indicate that TECCs require different protocols than those for native tissues. The interaction between engineered tissue and the scaffold matrix may play an as yet unknown role in the success of vitrification. The highest cell viability levels reached were 50%, which indicated that more research into the vitrification method need to be investigated for improvement in the cell viability levels of TECCs.

CHAPTER 6

CONCLUSIONS AND FUTURE DIRECTIONS

The main goal of tissue engineering is to develop replacement tissues and organs. The challenge is to find the right combination of cells, scaffolds, and environment that improves the growth of tissue to produce functionally relevant constructs suitable for implantation into defects, as well as finding long-term storage solutions for "off-the-shelf" availability. In this work, the perfusion concentric cylinder bioreactor was characterized and evaluated for its ability to grow tissue-engineered cartilage. Key mechanical forces were evaluated, perfusion and shear, to determine their effect on chondrogenesis. The final aspect of this work evaluated construct preservation methods in order to meet market demands for tissue-engineered cartilage. This research gave insight into factors that may be important for the culture and preservation of tissue-engineered cartilage. From our observations, we found that the addition of perfusion orthogonal to surface shear increased the proliferation rate of cells, while the magnitude of shear stress controlled collagen deposition in constructs cultured in the PCC bioreactor. We also observed that the PCC bioreactor could be used to permeate CPAs through TECCs cultured in the bioreactor without affecting cell viability, thus streamlining the bioprocess scheme from culture to preservation.

The comparison of the PCC bioreactor to the CC bioreactor showed that overall the original bioreactor produced more ECM over the course of 28 days. What was interesting to note was the high rate of proliferation that occurred in the PCC bioreactor, despite that cells were seeded at approximately the same concentration in both the CC

and PCC bioreactor. The high ECM deposition was attributed to the higher shear stress in the CC bioreactor over the PCC bioreactor. Though this study alone could not confirm that perfusion was partially responsible for cell growth and not a function of low seeding density (which increases the proliferation rate of cells due to limited cell-to-cell contact (Mandl, van der Veen et al. 2004)), the second aim of this research project did, which investigated the role of mechanical forces on chondrogenesis.

The second aim of this study was to investigate the role of mechanical forces *in vitro* by utilizing the PCC bioreactor as a bench-top model. From the perfusion+shear versus shear studies, the proliferation rate and total collagen deposition in the perfusion+shear bioreactor was significantly higher than the shear bioreactor, while GAG deposition remained the same in either bioreactor. Because the proliferation rate was greater in the PCC bioreactor when compared to the CC bioreactor, despite the higher shear stress in the CC bioreactor, the results from the perfusion+shear versus shear studies indicated that perfusion was the main contributor to the increase in cell growth for TECCs. This observation thus indicated that directional shear stress was mainly responsible for cellular proliferation while the magnitude of shear was responsible for total collagen production. Another possible reason was that perfusion increased oxygen transport through the constructs, thus increasing the proliferation rate of cells. The prolonged GAG synthesis in the perfusion+shear bioreactor over the shear bioreactor, i.e. with the addition of a new mechanical force, was responsible for prolonged GAG deposition. Based on literature, intermittent perfusion flow or compression would prolong GAG synthesis (Kisiday, Jin et al. 2004; Gemmiti and Guldberg 2006). Taken together, these observations lead to a proposed model to consider for the growth of

TECCs: perfusion to increase cellular proliferation, surface shear to increase collagen production, and intermittent compression or fluid flow to increase GAG production. This information can be applied to tailor the growth of TECCs for patients by first expanding the small amount of cells extracted from them with perfusion, and then focusing on the growth and deposition of ECM with shear and intermittent perfusion or compression. The end result could maximize cartilage growth in a time-efficient manner to meet market demands.

One advantage of this PCC bioreactor bench-top model is that mechanotransduction pathways can be further investigated. Because directional shear may be responsible for proliferation, studies inhibiting membrane receptors, integrins, or ion channels may suppress proliferation despite the addition of perfusion. Studies focused on the blocking of G-proteins, growth factors, calcium channels, or kinases with inhibitors in the culture media would elucidate possible pathways activated by the mechanical loads.

The animal study involved one trial with TECCs cultured either with mechanical forces or under static forces for 28 days prior to implantation. The histological results showed that the mechanically stimulated samples prolonged cartilage growth and induced maturation *in vivo*, which was observed via the presence of GAG over the static samples. The mechanically stimulated samples also had more cells and ECM than the static culture samples before implantation. This demonstrated the necessity to consider mechanical loads and cell density in the culture of TECCs before implantation to heal cartilage defects. Combined with the results from the perfusion+shear versus shear studies, a proposed model to tailor the growth of TECCs prior to implantation would be to use

perfusion and shear in the PCC bioreactor to not only stimulate chondrogenesis, but to expand cells to a desired density suitable for implantation.

A weakness in this study was that there was no direct relation of perfusion to cellular proliferation without the addition of shear to the bioreactor. The ideal experiment would have been to run four PCC bioreactors in parallel: perfusion, shear, perfusion+shear, and static. The low perfusion rate (0.6 mL/min/construct) indicated that there might not have been any significant difference between the perfusion bioreactor and static bioreactor, and that the combination of the two forces, perfusion and shear, had to act together to affect proliferation and collagen synthesis. The risk of contamination would have increased as well because three or more bioreactors in use at the same time increases handling and exposure to a non-sterile environment. Future studies of this ideal experiment though, would be able to confirm the direct effect of perfusion on the proliferation rate of cells.

The final aim of this study was to assess the effect different cryopreservation protocols had on TECCs. The most noticeable result was that an increase in the concentration of cryoprotectant agents in VS70 from the baseline VS55 preserved twice as many cells. However, also noticeable was that the reduction of steps to introduce and elute vitrification solutions did not affect the viability, nor did the perfusion of the solution through the constructs using the PCC bioreactor. The conclusions that could be drawn from these observations was that chondrocytes in TECCs were neither affected by the increase in osmotic stresses due to the higher concentration changes in the shorten steps method nor by the increase in permeation of CPAs in the PCC bioreactor method. The cryopreservation studies showed that even with successful vitrification (fast cooling),

the highest cell viability levels reached were 50%. Clearly, further methods should be explored to increase and maximize cell viability levels. The orbital shaker method and PCC bioreactor method did not affect cell viability levels, but did reduce total introduction and eluting time, as well as, simplified the process from culture to vitrification. The role of DMSO, 1,2-propanediol, and formamide should be investigated further. DMSO plays a large part in the success of vitrification, while formamide is cytotoxic. Increasing DMSO concentration and reducing formamide in VS70 could be investigated in future studies. Other variables beside CPA formulations could be investigated on their role in cell viability levels, such as temperature storage and temperature exposure during introduction and elution of CPAs. The storage of samples at –196°C (liquid nitrogen) would ease transport cost, but may be detrimental to cell viability due to the risk of devitrification. TECCs were exposed to the vitrification solution at 4°C, where metabolic activity had slowed. Exposing TECCs to the full-strength vitrification solution (last addition step and first removal step) at approximately -15°C, where metabolic activity has halted and ice has not formed yet, may decrease the cytotoxic effect of the vitrification solution. Maintaining consistent fast cooling and re-warming rates would also increase cell viability levels. Another aspect to investigate is not only cell viability levels, but also cartilage functionality. There is a need to determine that cells could continue to proliferate and produce ECM after vitrification. One way to do this is to measure [^{35}S]sulfate incorporation or [^{3}H]proline incorporation after preservation to determine if cells are synthesizing GAG or collagen, respectively. The result from the cryopreservation studies demonstrates that vitrification protocols can be manipulated to affect cell viability levels. The interaction of scaffolds and cells need to

be considered, as successful vitrification of native cartilage cannot always be applied to achieve successful vitrification of TECCs.

In summary, the perfusion concentric cylinder bioreactor is conducive to cartilage growth and identifies possible regions where perfusion and shear affects cartilage growth. In addition, storage protocols for the preservation of TECCs show that cell viability levels are dependent on cryoprotectant formulations, cooling and re-warming rates, and not affected by the method of introduction and elution of CPAs investigated in this study. This allows for streamlining the bioprocess scheme for tissue engineering from culture to preservation. Despite these results, there are opportunities to improve cartilage growth and vitrification, mainly surrounding the geometry and design of the inner bob of the PCC bioreactor.

6.1 Recommendations for the Improvement of the Design of the PCC Bioreactor

The current design of the PCC bioreactor demonstrates possible methods to increase seeding efficiency, reduce nutrient requirements, and simplify the vitrification process, without losing the ability to perfuse fluid through the constructs. Currently, the bioreactor is seeded with $150x10^6$ cells per 350 mL, which translates to $0.43x10^6$ cells/mL. In comparison, the CC bioreactor is seeded with $2.4x10^6$ cells/mL. Reduction of the culture media in the PCC bioreactor would increase the seeding density and efficiency. This can be achieved by reducing the amount of "dead space" between the central hub and outer cup region. Starting from an inner bob of the CC bioreactor, a cylindrical hole could be drilled axially though the bob to represent the central hub of the inner bob of the PCC bioreactor. The dimensions would be 5.08 cm in diameter and

11.8 cm long for an inner bob 12.8 cm in length. From the radial position, two rows of 8 construct arms would be drilled 45 degrees apart. The two rows would be separated by 2.54 cm in height, the same as the PCC bioreactor. The length of the arms would be less than the PCC bioreactor construct arms (2.4 cm) at 2.2 cm, but still have a large entrance length for a full parabolic flow to develop. The reduction in culture media is estimated to be approximately 50% (about 150 mL may still be required to completely cover the construct arms). The cell-seeding density would increase to approximately $1.0x10^6$ cells/mL. The media requirements also would reduce drastically without impeding nutrient limitations, saving cost for the month-long experimental runs.

Another redesign element to consider is the height of the open cavity. The construct was set into the construct arm, which resulted in a 2.13 mm in height open region, and which ensured that the construct was tightly embedded into the arm forcing fluid through the construct. However, this height also resulted in considerable recirculation of fluid flow and heterogeneous shear stress over the surface of the construct. Reduction of height would limit recirculation, but limit the tight fit needed for perfusion. CFD modeling could be performed to see what the minimum height of the open cavity would have to be to increase homogeneity of shear stress, while still maintaining perfusion through the constructs.

The PCC bioreactor has the advantage of simple scale-up to increase the number of constructs cultured in one system. Scale up of the system would occur by increasing the amount of rows of construct arms. However, the pressure gradient would be considerably less in the top rows as oppose to the bottom rows. Having individual perfusion tubing to pump fluid into each of construct arms would alleviate pressure

gradients. This would require engineering a system designed to connect tubing to each of the construct arms from the central hub to a single reservoir. Not only would this method ensure equal perfusion flow rates to all of the construct arms regardless of their position, but also eliminate fluid in the central hub. This would eliminate cartilage formation away from the scaffolds, increase seeding efficiency, and decrease nutrient depletion of culture media.

The next recommended change on the design of the PCC bioreactor is the choice of material for the inner bob. Polycarbonate is a clear material, which allows ease of checking on the perfusion aspect of the PCC bioreactor; however, it is not easily steam sterilized, nor can it handle extremely low temperatures used for vitrification. Steam sterilization provides a simple, fast, and inexpensive method of sterilization, while ethylene oxide sterilization is costly and has a lengthy sterilization time. Polypropylene or borosilicate glass could be manufactured as the inner bob of the PCC bioreactor to ease sterilization methods. Though polypropylene would reduce the visibility of the interior of the central hub, individual perfusion tubing to each of the construct arms would negate the need to do so. Polypropylene or glass materials could also withstand low temperatures used in vitrification. The system, after perfused with the vitrification solution would be immersed into an isopentane bath and cooled to –100°C. This would also eliminate the need for individual glass vials in tube racks. A thermocouple could be inserted in the gap region to monitor the temperature change. One consideration though, is determining if the thickness of the outer glass cup affects the cooling and re-warming rates of the system, but given that glass has a low thermal conductivity of 1.1 W/(m*K) at 4°C (Carwile and Hoge 1966), the rates should not be affected greatly.

Contamination within the PCC bioreactor was a major delay in the experimental runs. The most common contaminant was yeast, which thrived in humid warm environments, like the incubator. This high risk of contamination also limited the number of experimental runs and studies that could be performed at one time. The inner bob of the PCC bioreactor was most likely the source of contamination because of its alternative sterilization method. Ethanol rinse and UV sterilization was the initial sterilization method, but was then switched to ethylene oxide sterilization, which was less abrasive to the polycarbonate material. Over time however, the polycarbonate material has degraded and is currently showing signs of cracking and warping. This is due to the fact that the material is not durable or suited for repetitive long-term cell culture. The suggestions made in this section lead to possible paths for improvements in the design of the PCC bioreactor that can be made if future studies assessing the role of perfusion and shear on chondrogenesis are carried out.

APPENDIX A

DEVELOPMENT OF BIOREACTOR THEORY AND MECHANICAL PROPERTIES

The PCC bioreactor consisted of an immobile inner cylindrical bob and a rotating outer cup. Scaffolds were embedded into protruding construct arms that radiated from the inner bob. The following section describes the derivation for the calculation of the velocity profile between the two cylinders of the PCC bioreactor and the fluid velocity over the construct arms. The solution was based on the derivation shown by Saini and Bird et al. (Saini 2001; Bird, Stewart et al. 2002). Figure A.1 shows a schematic of the PCC bioreactor (top view) listing coordinates used in the calculation of velocity in the PCC bioreactor.

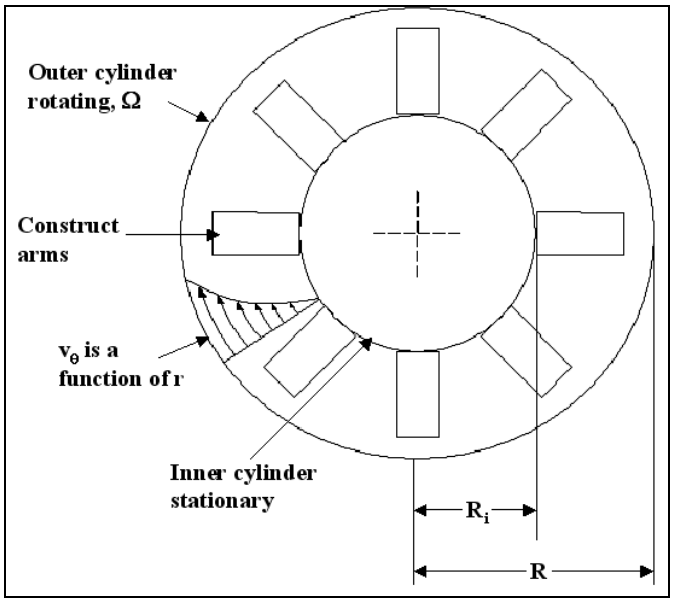

Figure A.1. Schematic of the perfusion concentric cylinder region in the bioreactor (Top View).

Navier-Stokes equation for motion:

$$\rho \frac{D}{Dt}\mathbf{v} = -\nabla p + \mu \nabla^2 \mathbf{v} + \rho \mathbf{g} \qquad \text{Equation A.1}$$

where,

r-component: $$-\rho \frac{v_\theta^2}{r} = -\frac{\partial p}{\partial r} \qquad \text{Equation A.2}$$

θ-component: $$0 = \frac{\partial}{\partial r}\left(\frac{1}{r}\frac{\partial}{\partial r}\left(r v_\theta\right)\right) \qquad \text{Equation A.3}$$

z-component: $$0 = -\frac{\partial p}{\partial z} + \rho g_z \qquad \text{Equation A.4}$$

Assuming no slip at the walls, the boundary conditions are:

B.C.1. $v_\theta = 0 \quad at\ r = KR$

B.C.2. $v_\theta = \Omega R \quad at\ r = R$

Equation A.3 can be integrated to obtain:

$$v_\theta = \frac{C_1 r}{2} + \frac{C_2}{r} \qquad \text{Equation A.5}$$

The boundary condition solutions are:

$$C_1 = \frac{2\Omega}{1-K^2} \qquad \text{Equation A.6}$$

$$C_2 = -\frac{\Omega K^2 R^2}{1-K^2} \qquad \text{Equation A.7}$$

When boundary conditions are substituted into Equation A.5:

$$v_\theta = \frac{\Omega KR}{1-K^2}\left(\frac{r}{KR} - \frac{KR}{r}\right) \qquad \text{Equation A.8}$$

where,

$$KR = R_i \qquad \text{Equation A.9}$$

The following section calculates the diffusivity of oxygen and the equilibrium concentration of oxygen in media. The Wilke-Change equation (Equation A.10) was used to calculate the diffusivity of oxygen in water. Culture media were composed of mainly water, and thus the Wilke-Change correlation was an adequate estimate for diffusivity into liquids. The equation assumed that oxygen was dilute in water at 37°C (Bird, Stewart et al. 2002). Henry's Law (Equation A.11) was used to calculate the equilibrium concentration of oxygen into water as water was in equilibrium with the gas phase in the incubator (Hines and Maddox 1985).

$$D_{O2-H20} = 7.4 \times 10^{-8} \frac{(\psi_{H20} M_{H20})^{1/2} T}{\mu V_{O2}^{0.6}} = 3.23x10^{-9}\ m^2 / s$$ Equation A.10

where,

ψ_{H20} = 2.6

M_{H20} = 18 g/gmol

T = 310.15 K

μ = 0.695 cP

V_{O2} = 25.6 cm^3/gmol

$$C_{O2} = \left(\frac{\rho_{H20}}{M_{H20}} \right) \frac{P_{O2}}{H_A} = 0.212\ mol / m^3$$ Equation A.11

where,

P_{O2} = 0.2 atm

H_A (37°C) = 5.17x10^4 atm (Hines and Maddox 1985)

ρ_{H2O} = 0.99 g/cm^3

The following section calculates the equilibrium time for oxygen in media to reach the saturated oxygen level of 0.212 mol/m^3. The derivation started from the species continuity equation and assumed that no perfusion occurred. The total volume in the PCC bioreactor was 350 mL, which correlated to approximately 5 cm in height from the liquid-to-air interface. The solution assumed that oxygen diffusion occurred in the axial direction only from the liquid-to-air interface, that diffusivity of oxygen in media was constant at 3.23x10^{-9} m^2/s, and that there was no metabolic consumption of oxygen in the media. At the liquid-to-air interface the concentration of oxygen in the gas phase was

derived from the ideal gas law for oxygen in the incubator (20% O_2/5% CO_2) at 37°C. Thus, the solution to the species continuity equation for non-steady state diffusion of oxygen in media was calculated as follows:

Species continuity equation for oxygen:

$$\frac{\partial C_{O2}}{\partial t} + \mathbf{v} \bullet \nabla C_{O2} = D_{O2-H2O} \nabla^2 C_{O2} + R_{O2} \qquad \text{Equation A.12}$$

where,

z-component: $$\frac{\partial C_{O2}}{\partial t} = D_{O2-H2O} \frac{\partial^2 C_{O2}}{\partial z^2} \qquad \text{Equation A.13}$$

The boundary and initial conditions are:

B.C.1. $C_{O2} = C_{O2}^1 = 7.859\ mol/m^3 \quad at\ z = 0\ \ for\ t > 0$

B.C.2. $C_{O2} = 0\ mol/m^3 \quad at\ z = \infty\ \ for\ all\ t$

I.C.1. $C_{O2} = 0\ mol/m^3 \quad at\ t = 0\ \ for\ z > 0$

Substituting the boundary and initial conditions, the solution to Equation A.13 is:

$$\frac{C_{O2}}{C_{O2}^1} = 1 - erf\left(\frac{z}{\sqrt{4D_{O2-H2O}t}}\right) \qquad \text{Equation A.14}$$

The equilibrium time for media to reach saturated oxygen levels of 0.212 mol/m^3 at z = 5 cm was calculated by solving the error function in Equation A.14. Thus, the time to reach equilibrium was 21.9 hours. If the assumption that fresh media were already saturated with oxygen when prepared, and that perfusion after four days in the PCC bioreactor increased oxygen transport within the bioreactor, then the time to reach oxygen saturation levels in media would be less than the estimated 21.9 hours. Thus, the concentration of oxygen in media before transport through the constructs was held steady at 0.212 mol/m^3.

The following section derives the nutrient transport profile across the thickness of the constructs when both diffusivity and convective transport were considered. The equation originated from the species continuity equation, Equation A.12, for steady-state oxygen transport in one direction, where the x component is as follows:

x-component: $$D_{O2}\frac{d^2C_{O2}}{dx^2} - V_m\frac{dC_{O2}}{dx} - R_{O2} = 0 \qquad \text{Equation A.15}$$

Equation A.15 can be integrated to obtain:

$$C_{O2} = \left(\frac{D_{O2}}{V_m}\right)^2 \times e^{\frac{V_m(C_1+x)}{D_{O2}}} - \frac{R_{O2}x}{V_m} + C_2 \qquad \text{Equation A.16}$$

The boundary conditions are:

$$C_{O2}(0) = C_{O2}(L) = C_{O2}^0 = 0.212\ mol/m^3$$

Substituting the boundary conditions, the solution to Equation A.16 is:

$$C_{O2} = \frac{R_{O2}L}{V_m(e^{V_m L/D_{O2}} - 1)}(e^{V_m x/D_{O2}} - 1) - \frac{R_{O2}x}{V_m} + C^0_{O2} \qquad \text{Equation A.17}$$

The following section is an example of the calculation of the compressive modulus and permeability constant from a confined compression test. Four compression tests were carried out on each sample at 5, 10, 15, and 20 % strain seen in Figure A.2. The applied strain and subsequent equilibrium stress were plotted in Figure A.3 to calculate the compressive modulus, H_A.

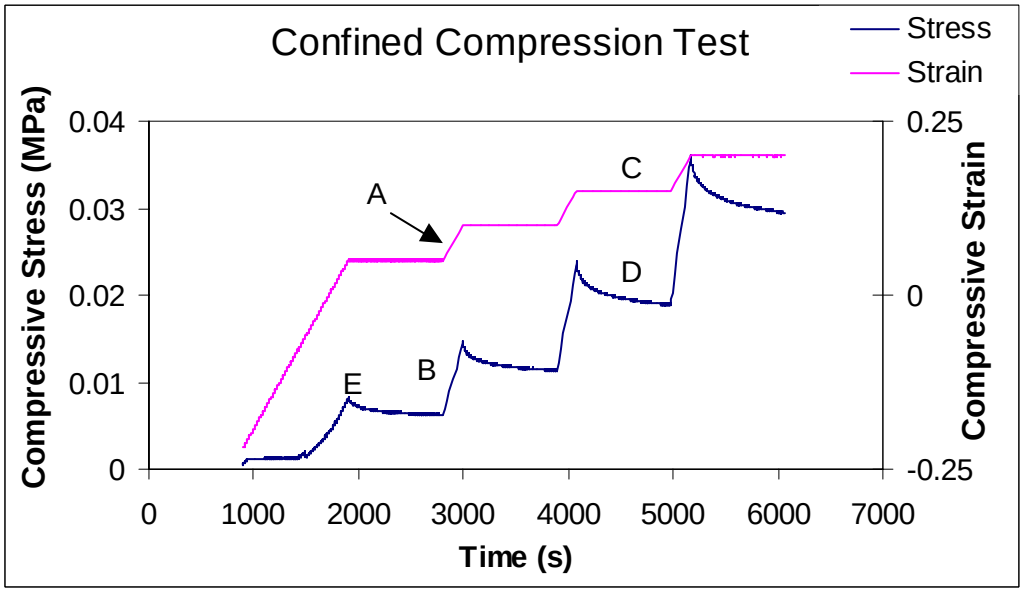

Figure A.2. Confined compression curve for a Day 28 perfusion+shear sample. Test represents stress-strain relationship during dynamic and relaxation times, as indicated. (A) One of the four dynamic strains tested; (B) one of the four dynamic stresses measured, which corresponded to the dynamic strain indicated by A; (C) one of the four relaxation strains held for 15 minutes; (D) one of the four relaxation stresses measured, which corresponded to the relaxation strain indicated by C; (E) one of the four peak stresses measured at the end of the dynamic portion of the compression test

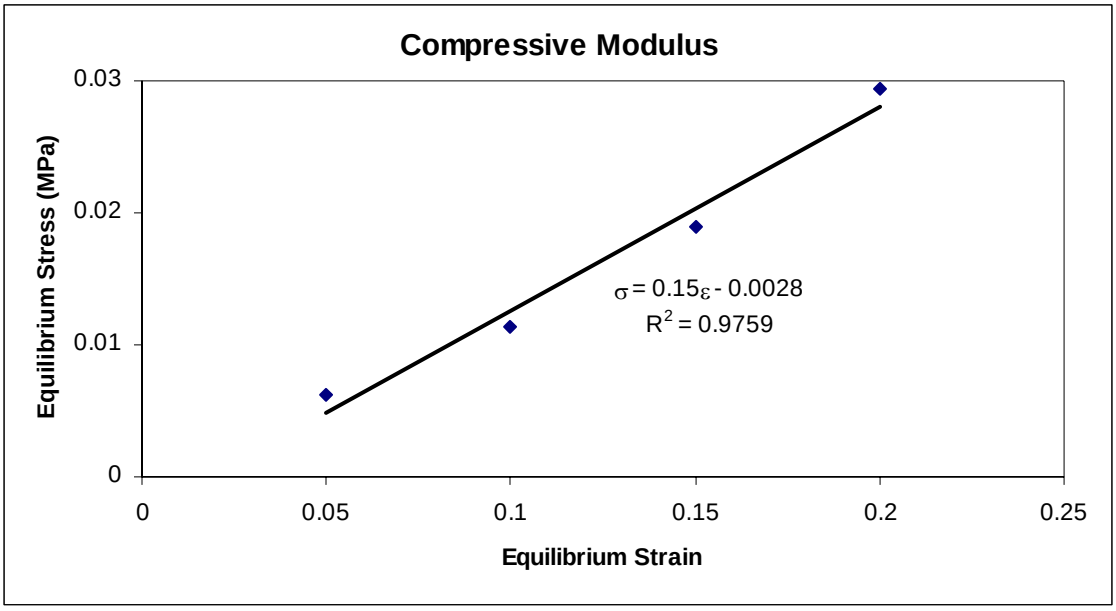

Figure A.3. Equilibrium modulus for a Day 28 perfusion+shear sample. Data from the relaxation portion of the compression test were plotted to calculate the compressive modulus of tissue-engineered cartilage samples. The last ten seconds of the compressive strain values for each relaxation curve (four curves total) were plotted against the corresponding measured relaxation stress. The linear fit revealed the slope, which corresponded to the equilibrium modulus of the sample tested, 0.15 MPa.

Data from the dynamic portion of the compression test were plotted to calculate the permeability constant of tissue-engineered cartilage samples. The negative of the compressive strain values for each dynamic curve (four curves total) were plotted against the corresponding measured permeability, k, which was inversely related to the dynamic stress (see Equation 3.15). The data was fitted to an exponential curve ($k = k_0 e^{-M\varepsilon}$, Equation 3.13) to give the permeability parameters, k_0 and M. Table A.1 shows an example measurement for a Day 28 sample harvested from a perfusion+shear bioreactor along with the R^2 value. The poor fit at 5% strain resulted in its elimination for the calculated average permeability constant.

Table A.1. Permeability constant for Day 28 perfusion+shear sample

Equilibrium Strain	k_0 (m^4/(N*s))	M	R^2
0.05	2.52E-13	8.54	0.86
0.1	2.72E-13	16.11	0.97
0.15	2.69E-13	14.26	0.96
0.2	2.59E-13	12.89	0.97
Average	2.67E-13	14.42	0.97
SEM	3.66E-15	0.93	0.00

APPENDIX B

EXPERIMENTAL DATA

Table B.1. PCC experiment 1

PCC Bioreactor	Day 4	Day 7	Day 14	Day 21	Day 28
	351815	2950180	4966285	4084615	8146154
Cells/construct	266497	2204096	6854539	8518434	7096310
	0	1511076	5379266	7157040	6152428
Average	194425	2221784	5733363	6586696	7131631
SEM	117345	415528	573124	1311317	575810
	0	265.09	230.79	351.87	350.45
μg GAG/construct	0	151.11	375.59	110.91	334.77
	83.29	233.01	315.07	419.57	242.37
Average	15.45	216.40	307.15	294.11	309.20
SEM	33.93	33.94	41.99	93.66	33.72
	0	67.65	424.76	1026.16	1091.61
μg collagen/construct	0	113.42	644.27	513.53	1608.03
	0	83.69	508.43	1088.69	1344.35
Average	0	88.25	525.82	876.13	1348.00
SEM	1.89	13.41	63.96	182.20	149.09

Table B.2. PCC versus CC experiment 1

CC Bioreactor	Day 4	Day 7	Day 14	Day 21	Day 28
	1374495	3801195	4804106	8266564	10703962
Cells/construct	1231109	3822770	5424496	7733852	10057694
	2894366	2500213	3642563	6923547	14505837
					17169141
Average	1833323	3374726	4623722	7641321	13109158
SEM	532134	437301	522247	390446	1201698
	360.97	1522.76	1395.98	1571.00	1695.54
μg GAG/construct	382.85	1514.35	1595.13	1215.34	1862.15
	676.80	1008.90	923.63	1536.78	1652.91
					1997.91
Average	473.54	1348.67	1304.91	1441.04	1802.13
SEM	101.83	169.90	199.12	113.28	55.29
	102.05	291.32	360.08	1025.93	1356.21
μg collagen/construct	67.60	252.13	502.34	667.76	1246.72
	71.65	140.69	477.10	907.66	2306.50
					2407.06
Average	80.43	228.04	446.51	867.12	1829.12
SEM	10.87	45.12	43.82	105.36	291.42
PCC Bioreactor	Day 4	Day 7	Day 14	Day 21	Day 28
	783044	2011494	7645405	13975599	9756454
Cells/construct	988517	2885104	5331812	15288776	11846357
	489554	2525130	7645405	10028712	9897311
					6628736
Average	753705	2473910	6874208	13097696	9532214
SEM	144783	253486	771198	1580623	584035
	311.60	242.60	857.03	895.02	541.60
μg GAG/construct	378.92	111.89	492.80	887.17	975.80
	102.92	298.70	857.03	973.00	820.41
					389.58
Average	264.48	217.73	735.62	918.40	681.85
SEM	83.09	55.34	121.41	27.40	110.00

Table B.2. PCC versus CC experiment 1 (continued)

	47.24	54.07	231.07	968.75	804.73
μg collagen/construct	15.86	92.01	395.32	1272.52	997.48
	38.17	67.74	395.32	849.64	755.49
					536.38
Average	33.75	71.27	340.57	1030.30	773.52
SEM	9.32	11.09	54.75	125.90	63.95

Table B.3. PCC versus CC experiment 2

CC Bioreactor	Day 4	Day 7	Day 14	Day 21	Day 28
	2653207	2706348	7148326	5868303	7683035
Cells/construct	2260020	2783195	6917533	9232877	7243046
	2182906	3658691	7170459	6037568	6788227
Average	2365378	3049412	7078772	7046249	7238103
SEM	145626	305447	80872.7	1094405	258321
	286.79	942.11	1317.18	1150.68	1139.42
μg GAG/construct	487.06	511.35	1079.58	1698.77	1517.45
	330.63	423.66	741.84	1142.98	1326.66
Average	368.16	625.71	1046.20	1330.81	1327.85
SEM	60.78	160.22	166.92	183.99	109.13
	67.92	144.86	736.38	1157.98	1834.53
μg collagen/construct	55.19	171.25	750.88	1584.68	1932.22
	85.98	233.29	918.63	1195.33	1641.78
Average	69.70	183.13	801.96	1312.67	1802.84
SEM	8.93	26.21	58.48	136.44	85.32
PCC Bioreactor	Day 4	Day 7	Day 14	Day 21	Day 28
	185132^{b}	2257928^{b}	5493323^{b}	8744076^{b}	10814064^{b}
Cells/construct	405509^{b}	2846642^{t}	8630492^{t}	4169375^{t}	9562322^{t}
	70703^{t}	1473802^{t}	3035327^{b}	6896536^{t}	7097164^{t}
Average	220448	2192791	5719714	6603329	9157850
SEM	98250	397641	1619147	1328715	1091869
	309.06	289.79	448.74	854.89	796.45
μg GAG/construct	232.62	293.30	1070.53	360.50	790.03
	282.10	472.12	487.31	442.32	435.89
Average	274.59	351.74	668.86	552.57	674.12
SEM	22.38	60.20	201.14	153.00	119.13
	42.77	132.90	450.64	1712.92	1639.49
μg collagen/construct	30.89	86.84	1117.26	819.94	1484.39
	28.50	175.47	526.67	800.10	1484.68
Average	34.05	131.74	698.19	1110.99	1536.19
SEM	4.41	25.59	210.68	301.02	51.65

b: bottom row, t: top row

Table B.4. Perfusion+shear versus shear experiment 1

Perfusion+Shear	Day 4	Day 7	Day 14	Day 21	Day 28
	467758^{t}	1919472^{b}	8085956^{t}	10336068^{b}	13846829^{b}
Cells/construct	469595^{b}	2174417^{t}	9596421^{b}	10181725^{t}	12816990^{t}
	269569^{b}	423743^{t}	7748173^{b}	8785463^{t}	13391430^{t}
Average	402307	1505877	8476850	9767752	13351750
SEM	66371	546050	568215	493161	297950
	150.00	116.93	704.50	925.68	1355.18
μg GAG/construct	122.31	184.94	668.35	771.29	942.23
	57.22	4.20	468.00	529.27	1194.66
Average	109.84	102.02	613.62	742.08	1164.02
SEM	27.50	52.71	73.55	115.36	120.19
	39.62	120.10	648.58	1440.63	2875.62
μg collagen/construct	47.64	50.44	556.09	1137.18	2363.53
	69.81	24.46	484.94	921.25	3151.11
Average	52.36	65.00	563.20	1166.35	2796.76
SEM	9.03	28.55	47.37	150.64	230.75
Shear	Day 4	Day 7	Day 14	Day 21	Day 28
	590222^{t}	220746^{b}	4227764^{t}	4694056^{b}	4890157^{b}
Cells/construct	266165^{b}	181176^{t}	3879711^{b}	3995503^{t}	6404423^{t}
	280084^{b}	206897^{t}	2897795^{b}	6830726^{t}	768382^{t}
Average	378824	202940	3668423	5173428	4020987
SEM	105775	11593	398199	852833	1684026
	68.53	477.19	749.84	1173.21	1304.33
μg GAG/construct	64.85	440.43	726.56	1396.23	1714.22
	56.89	134.09	804.37	1350.28	583.19
Average	63.42	350.57	760.26	1306.57	1200.58
SEM	3.44	108.76	23.06	67.99	330.59
	80.07	138.30	541.36	860.70	1196.58
μg collagen/construct	52.27	164.61	432.82	1017.22	1429.05
	32.09	86.68	524.15	900.57	1067.35
Average	54.81	129.86	499.44	926.16	1230.99
SEM	13.91	22.89	33.68	46.96	105.82

b: bottom row, t: top row

Table B.5. Perfusion+shear versus shear experiment 2

Perfusion+Shear	Day 4	Day 7	Day 14	Day 21	Day 28
	185132^{t}	2257928^{b}	5493323^{b}	8744076^{b}	10814064^{b}
Cells/construct	405509^{b}	2846642^{t}	8630492^{t}	4169375^{t}	9562322^{t}
	70703^{b}	1473802^{t}	3035327^{b}	6896536^{t}	7097164^{t}
Average	220448	2192791	5719714	6603329	9157850
SEM	98250	397641	1619147	1328715	1091869
	309.06	289.79	448.74	854.89	796.45
μg GAG/construct	232.62	293.30	1070.53	360.50	790.03
	282.10	472.12	487.31	442.32	435.89
Average	274.59	351.74	668.86	552.57	674.12
SEM	22.38	60.20	201.14	153.00	119.13
	42.77	132.90	450.64	1712.92	1639.49
μg collagen/construct	30.89	86.84	1117.26	819.94	1484.39
	28.50	175.47	526.67	800.10	1484.68
Average	34.05	131.74	698.19	1110.99	1536.19
SEM	4.41	25.59	210.68	301.02	51.65
Shear	Day 4	Day 7	Day 14	Day 21	Day 28
	380993^{t}	1803698^{t}	743317^{t}	1959938^{b}	4553622^{t}
Cells/construct	53069^{b}	1233404^{t}	3960861^{b}	5348497^{t}	3472623^{t}
	51100^{b}	2282927^{b}	3532472^{b}	4946374^{t}	3387697^{b}
Average	161721	1773343	2745550	4084936	3804647
SEM	109638	303351	1008726	1068822	375289
	267.16	261.16	632.24	1020.86	463.94
μg GAG/construct	272.08	181.09	700.61	983.46	521.21
	271.43	472.70	878.27	578.48	382.71
Average	270.23	304.98	737.04	860.93	455.95
SEM	1.54	86.99	73.32	141.64	40.18
	42.54	87.86	443.98	767.08	831.96
μg collagen/construct	37.06	68.74	402.56	780.40	871.64
	49.10	116.39	322.18	641.66	667.01
Average	42.90	90.99	389.57	729.71	790.20
SEM	3.48	13.84	35.75	44.19	62.65

b: bottom row, t: top row

Table B.6. Perfusion+shear versus shear experiment 3: mechanical properties

Perfusion+Shear	Day 4	Day 7	Day 14	Day 21	Day 28
Compressive Modulus (MPa)	0.08	0.11	0.12	0.09	0.15
	0.12	0.17	0.05	0.06	0.10
	0.12	0.10	0.07	0.04	0.13
					0.23
Average	0.11	0.13	0.08	0.06	0.15
SEM	0.01	0.02	0.02	0.02	0.03
Permeability Constant ($m^4/(N*s)$)	1.66E-13	1.31E-13	9.84E-14	1.75E-13	2.67E-13
	1.29E-13	2.00E-13	5.30E-13	7.21E-13	3.39E-13
	5.67E-14	1.32E-13	3.71E-13	9.03E-13	1.27E-13
					1.58E-13
Average	1.17E-13	1.54E-13	3.33E-13	6.00E-13	2.23E-13
SEM	3.21E-14	2.27E-14	1.26E-13	2.19E-13	4.90E-14
Shear Modulus at 1Hz (Pa)	830540	632130	470550	72610	366130
	722020	897380	34144	115460	325290
	1548500		252320	159490	21183
	1255100	1418800	542150	112690	306980
	1208000	721790	611690	75712	93680
	1677400	1309000	803190	170900	103720
					539900
					485900
Average	1206927	995820	452341	117810	280348
SEM	154611	157170	111323	16736	67204
Phase Angle at 1 Hz (degree)	4.4	6.5	8.0	13.3	14.2
	4.4	7.7	15.0	12.8	18.7
	4.0		13.0	14.9	13.8
	3.9	4.6	11.5	14.8	15.1
	4.5	6.6	8.0	15.1	14.3
	4.2	5.7	6.7	16.0	15.5
					13.0
					12.1
Average	4.23	6.22	10.37	14.48	14.59
SEM	0.10	0.52	1.35	0.49	0.70

Table B.6. Perfusion+shear versus shear experiment 3: mechanical properties (continued)

Shear	Day 4	Day 7	Day 14	Day 21	Day 28
Compressive Modulus (MPa)	0.14	0.09	0.06	0.11	0.12
	0.22	0.21	0.11	0.08	0.20
	0.03	0.06	0.10	0.11	0.11
	0.07				
Average	0.12	0.12	0.09	0.10	0.14
SEM	0.04	0.05	0.02	0.01	0.03
Permeability Constant ($m^4/(N*s)$)	1.22E-13	4.85E-14	5.01E-13	1.93E-13	3.76E-13
	6.86E-14	5.80E-13	4.94E-13	3.24E-13	5.01E-14
	1.39E-14	1.33E-14	2.02E-13	1.57E-13	8.46E-14
	1.17E-12				
Average	3.45E-13	2.14E-13	3.99E-13	2.25E-13	1.70E-13
SEM	2.77E-13	1.83E-13	9.84E-14	5.08E-14	1.03E-13
Shear Modulus at 1 Hz (Pa)	494630	617380	70577	436420	778950
	378500	2000800	903270	1507000	
	1023200	641090	413180	432120	221830
	764020	796150	562330	368900	243480
	1379500	590990	958660	196600	431280
	560430	849740	783500	1007200	207100
	1902000				
	309930				
Average	851526	916025	615253	658040	376528
SEM	195876	221053	137779	203251	108462
Phase Angle at 1 Hz (degree)	5.3	6.0	8.1	6.1	9.9
	6.2	5.3	6.1	4.5	
	4.8	5.3	6.1	7.5	10.6
	4.7	5.4	5.9	6.7	12.8
	4.1	5.4	5.0	6.5	8.1
	5.2	5.2	5.0	5.8	12.9
	4.4				
	6.0				
Average	5.1	5.4	6.0	6.2	10.9
SEM	0.3	0.1	0.5	0.4	0.9

Table B.7. VS55 6/7 steps versus VS70 6/7 steps on native cartilage

	VS55 6/7 steps	VS70 6/7 steps
Viability (%)	8.12	22.49
	9.09	20.04
	7.13	23.40
	8.94	26.01
Average	8.32	22.99
SEM	0.45	1.23
p-value	0.0005	
Time (s) 4ºC → -100ºC	678	

Table B.8. Traditional freezing versus VS55 6/7 steps

	VS55 6/7 steps	Frozen
Viability (%)	12.47	38.51
	26.53	23.45
	17.08	20.77
	18.63	52.95
		28.26
Average	18.68	32.79
SEM	2.93	5.88
p-value	0.077	
Time (s) 4ºC → -100ºC	124	

Table B.9. VS55 6/7 steps versus VS70 6/7 steps – no cryopreservation

	VS55 6/7 steps		VS70 6/7 steps
Viability (%)	34.27		34.68
	40.12		19.95
	48.60		26.28
	42.84		23.83
Average	41.46		26.19
SEM	2.98		3.12
p-value		0.0122	
Time (s) at 4ºC		1416	
Viability (%)	53.32		49.46
	55.47		45.24
	42.41		39.60
	52.58		61.57
Average	50.94		48.97
SEM	2.91		4.66
p-value		0.7336	
Time (s) at 4ºC		1530	
Viability (%)	51.14		12.97
	41.89		14.38
	27.88		17.54
	10.41		16.72
Average	32.83		15.40
SEM	8.87		1.05
p-value		0.1437	
Time (s) at 4ºC		1757	
Viability (%)	56.30		35.67
	46.35		35.70
	67.54		22.48
	64.89		23.64
Average	58.77		29.37
SEM	4.78		3.65
p-value		0.0033	
Time (s) at 4ºC		1739	

Table B.10. VS55 6/7 steps versus VS70 6/7 steps

Day 6 or 7 samples	VS55 6/7 steps	VS70 6/7 steps
Viability (%)	26.76	21.23
	13.92	38.21
	19.92	66.67
	22.93	32.48
Average	20.88	39.65
SEM	2.71	9.67
p-value	0.1460	
Time (s) 4ºC → -100ºC	131	
Viability (%)	16.01	17.07
	9.00	14.04
	11.92	25.62
	6.72	22.54
Average	10.91	19.82
SEM	2.00	2.61
p-value	0.0378	
Time (s) 4ºC → -100ºC	437	
Viability (%)	8.34	30.51
	11.49	22.82
	8.85	29.75
	6.76	20.37
Average	8.86	25.86
SEM	0.98	2.52
p-value	0.0036	
Time (s) 4ºC → -100ºC	372	
Day 14 samples	VS55 6/7 steps	VS70 6/7 steps
Viability (%)	8.29	18.37
	14.79	27.78
	8.12	33.03
	12.31	35.26
Average	10.88	28.61
SEM	1.63	3.76
p-value	0.0118	
Time (s) 4ºC → -100ºC	687	

Table B.10. VS55 6/7 steps versus VS70 6/7 steps (continued)

Day 28 samples	VS55 6/7 steps	VS70 6/7 steps
Viability (%)	17.70	13.95
	6.37	18.54
	7.21	24.20
	7.76	29.98
Average	9.76	21.67
SEM	2.66	3.48
p-value	0.0370	
Time (s) 4ºC → -100ºC	198	

Table. B.11. VS55 6/7 steps versus VS83 6/7 steps

	VS55 6/7 steps	VS83 6/7 steps
Viability (%)	20.79	7.06
	11.30	6.15
	23.50	6.39
Average	18.53	6.53
SEM	3.70	0.27
p-value	0.08	
Time (s) 4ºC → -100ºC	225	

Table B.12. VS70 6/7 steps versus VS70 4/4 steps

	VS70 6/7 steps		VS70 4/4 steps
Viability (%)	21.23		39.66
	38.21		52.34
	66.67		44.48
	32.48		32.11
Average	39.65		42.15
SEM	9.67		4.25
p-value		0.82	
Time (s) 4ºC → -100ºC		131	
Viability (%)	5.54		13.17
	11.16		23.76
	15.46		11.46
	14.04		34.90
Average	11.55		20.82
SEM	2.19		5.42
p-value		0.16	
Time (s) 4ºC → -100ºC		1145	
Viability (%)	12.44		10.80
	7.08		6.41
	13.38		7.44
	10.43		4.60
Average	10.83		7.31
SEM	1.39		1.30
p-value		0.11	
Time (s) 4ºC → -100ºC		849	
Viability (%)	30.38		51.74
	57.15		46.87
	38.92		45.20
	51.43		56.26
Average	44.47		50.02
SEM	6.05		2.50
p-value		0.43	
Time (s) 4ºC → -100ºC		160	

Table B.13. Orbital Shaker versus PCC bioreactor (BR)

	PCC BR	Orbital Shaker
Viability (%)	21.92	6.31
	9.31	6.28
	6.25	7.78
	7.44	9.32
	5.52	
	8.80	
	8.32	
	6.93	
Average	9.31	7.42
SEM	1.86	0.72
p-value	0.37	
Time (s) 4ºC → -100ºC	374	
Viability (%)	21.99	54.08
	44.07	50.12
	46.14	54.44
	71.45	65.31
	63.36	
	32.82	
	54.54	
	47.84	
Average	47.78	55.99
SEM	5.60	3.26
p-value	0.23	
Time (s) 4ºC → -100ºC	213	

Table B.13. Orbital Shaker versus PCC bioreactor (BR) (continued)

	PCC BR	Orbital Shaker
Viability (%)	2.32	10.38
	14.73	6.68
	1.61	4.49
	2.66	6.54
	10.02	
	5.50	
	8.83	
	3.53	
Average	6.15	7.02
SEM	1.64	1.23
p-value	0.68	
Time (s) 4ºC → -100ºC	723	

REFERENCES

Adolphe, M., X. Ronot, et al. (1983). "Effects of Donor's Age on Growth Kinetics of Rabbit Articular Chondrocytes in Culture." Mechanisms of Aging and Development 23(2): 191-198.

Alsalameh, S., R. Amin, et al. (2004). "Identification of Mesenchymal Progenitor Cells in Normal and Osteoarthritic Human Articular Cartilage." Arthritis and Rheumatism 50(5): 1522-1532.

Angell, C. A. (2002). "Liquid Fragility and the Glass Transition in Water and Aqueous Solutions." Chem Rev 102(8): 2627-50.

Archer, C. W. and P. Francis-West (2003). "The Chondrocyte." The International Journal of Biochemistry and Cell Biology 35(4): 401-404.

Atkinson, B., M. P. Brocklebank, et al. (1969). "Low Reynolds Number Developing Flows." AIChE Journal 15: 548-553.

Bancroft, G. N., V. I. Sikavitsas, et al. (2002). "Fluid Flow Increases Mineralized Matrix Deposition in 3D Perfusion Culture of Marrow Stromal Osteoblasts in a Dose-Dependent Manner." Proc Natl Acad Sci U S A 99(20): 12600-5.

Barbero, A., S. Grogan, et al. (2004). "Age Related Changes in Human Articular Chondrocyte Yield, Proliferation and Post-Expansion Chondrogenic Capacity." Osteoarthritis Cartilage 12(6): 476-84.

Best, B. (2006). "Vitrification in Cryonics." Retrieved 2008, from http://www.benbest.com/cryonics/vitrify.html.

Bird, R. B., W. E. Stewart, et al. (2002). Transport Phenomena Second Edition. New York, John Wiley & Sons, Inc.

Blunk, T., A. Sieminski, et al. (2002). "Differential Effects of Growth Factors on Tissue Engineered Cartilage." Tissue Engineering 8(1): 73-84.

Bosnakovski, D., M. Mizuno, et al. (2006). "Chondrogenic Differentiation of Bovine Bone Marrow Mesenchymal Stem Cells (MSCs) in Different Hydrogels: Influence of Collagen Type II Extracellular Matrix on MSC Chondrogenesis." Biotechnology and Bioengineering 93(6): 1152-1163.

Both, S. K., A. J. van der Muijsenberg, et al. (2007). "A Rapid and Efficient Method for Expansion of Human Mesenchymal Stem Cells." Tissue Eng 13(1): 3-9.

Bravo, L. A. and M. Griffith (2005). "Characterization of Antifreeze Activity in Antarctic Plants." J Exp Bot 56(414): 1189-96.

Brighton, C. T. and R. B. Heppenstall (1971). "Oxygen Tension in Zones of the Epiphyseal Plate, the Metaphysis and Diaphysis. An in Vitro and in Vivo Study in Rats and Rabbits." The Journal of Bone and Joint Surgery American Volume 53(4): 719-728.

Brittberg, M., A. Lindahl, et al. (1994). "Treatment of Deep Cartilage Defects in the Knee with Autologous Chondrocyte Transplantation." The New England Journal of Medicine 331(14): 889-895.

Brockbank, K. G. M., J. C. Covault, et al. (2001). Cryopreservation Manual, A Guide to Cryopreservation Techniques. Marietta, OH, Thermo Fisher Scientific Inc.

Browning, J. A., K. Saunders, et al. (2004). "The Influence and Interactions of Hydrostatic and Osmotic Pressures on the Intracellular Milieu of Chondrocytes." Biorheology 41(3-4): 299-308.

Bruckner, P., I. Horler, et al. (1989). "Induction and Prevention of Chondrocyte Hypertrophy in Culture." The Journal of Cell Biology 109(5): 2537-2545.

Bulthuis, Y., K. W. Drossaers-Bakker, et al. (2007). "Arthritis Patients Show Long-Term Benefits from 3 weeks Intensive Exercise Training Directly Following Hospital Discharge." Rheumatology (Oxford) 46(11): 1712-7.

Caplan, A. I., M. Elyaderani, et al. (1997). "Principles of Cartilage Repair and Regeneration." Clinical Orthopaedics Related Research(342): 254-269.

Carsi, B., J. L. Lopez-Lacomba, et al. (2004). "Cryoprotectant Permeation through Human Articular Cartilage." Osteoarthritis Cartilage 12(10): 787-92.

Cartwright, T. (1994). Animal Cells as Bioreactors. New York, Cambridge University Press.

Carwile, L. C. K. and H. J. Hoge (1966). Thermal Conductivity of Pyrex Glass: Selected Values. Thermal Conductivity-1. U. S. A. N. Laboratories. Natick, MA, U.S. Army Material Command.

Caterson, B., C. Flannery, et al. (2000). "Mechanisms Involved in Cartilage Proteoglycan Catabolism." Matrix Biology 19: 333-344.

Cecil, R. and B. Archer (1925). "Arthritis of the Menopause." Journal of the American Medical Association 84: 75-89.

Chen, A. C., W. C. Bae, et al. (2001). "Depth- and Strain-Dependent Mechanical and Electromechanical Properties of Full-Thickness Bovine Articular Cartilage in Confined Compression." J Biomech 34(1): 1-12.

Cima, L. G., J. P. Vacanti, et al. (1991). "Tissue Engineering by Cell Transplantation using Degradable Polymer Substrates." Journal of Biomechanical Engineering 113(2): 143-151.

Cohen, B., G. S. Chorney, et al. (1994). "Compressive Stress-Relaxation Behavior of Bovine Growth Plate may be Described by the Nonlinear Biphasic Theory." J Orthop Res 12(6): 804-13.

Coimbra, I. B., S. A. Jimenez, et al. (2004). "Hypoxia Inducible Factor-1 Alpha Expression in Human Normal and Osteoarthritic Chondrocytes." Osteoarthritis Cartilage 12(4): 336-45.

Currey, C. J., MHA. (2005). "Cellular Organization of the Body: Part III Connective Tissue." Retrieved 2005, from http://medinfo.ufl.edu/pa/chuck/summer/handouts/connect.htm.

Darling, E. M. and K. A. Athanasiou (2003). "Articular Cartilage Bioreactors and Bioprocesses." Tissue Engineering 9(1): 9-26.

Davisson, T., R. L. Sah, et al. (2002). "Perfusion Increases Cell Content and Matrix Synthesis in Chondrocyte Three-Dimensional Cultures." Tissue Engineering 8(5): 807-816.

Davisson, T., S. Kunig, et al. (2002). The Effects of Perfusion and Compression on Modulation of Tissue Engineered Cartilage. 48th Annual Meeting of the Orthopaedic Research Society.

DeVries, A. L. and D. E. Wohlschlag (1969). "Freezing Resistance in Some Antarctic Fishes." Science 163(871): 1073-5.

Dewey, C. F., Jr., S. R. Bussolari, et al. (1981). "The Dynamic Response of Vascular Endothelial Cells to Fluid Shear Stress." J Biomech Eng 103(3): 177-85.

Erickson, G. R., L. G. Alexopoulos, et al. (2001). "Hyper-Osmotic Stress Induces Volume Change and Calcium Transients in Chondrocytes by Transmembrane, Phospholipid, and G-protein pathways." J Biomech 34(12): 1527-35.

Eyre, D. (2002). "Collagen of Articular Cartilage." Arthritis Research 4(1): 30-35.

Fahy, G. M., B. Wowk, et al. (2004). "Improved Vitrification Solutions based on the Predictability of Vitrification Solution Toxicity." Cryobiology 48(1): 22-35.

Fahy, G. M., D. I. Levy, et al. (1987). "Some Emerging Principles Underlying the Physical Properties, Biological Actions, and Utility of Vitrification Solutions." Cryobiology 24(3): 196-213.

Farina, G., R. Lemaire, et al. (2006). "Cartilage Oligomeric Matrix Protein is Overexpressed by Scleroderma Dermal Fibroblasts." Matrix Biology 25(4): 213-222.

Farndale, R., C. Sayers, et al. (1982). "A Direct Spectrophotometric Microassay for Sulfated Glycosaminoglycans in Cartilage Cultures." Connective Tissue Research 9(4): 247-248.

Felson, D. T. and M. C. Nevitt (1998). "The Effects of Estrogen on Osteoarthritis." Current Opinion in Rheumatology 10: 269-72.

Fernandes, J. C., J. Martel-Pelletier, et al. (2002). "The Role of Cytokines in Osteoarthritis Pathophysiology." Biorheology 39(1-2): 237-46.

Fitzgerald, J. B., M. Jin, et al. (2008). "Shear- and Compression-Induced Chondrocyte Transcription Requires MAPK Activation in Cartilage Explants." J Biol Chem 283(11): 6735-43.

Freed, L. and G. Vunjak-Novakovic (1997). "Microgravity Tissue Engineering." In Vitro Cellular and Developmental Biology. Animal 33(5): 381-385.

Freed, L. E., A. P. Hollander, et al. (1998). "Chondrogenesis in a Cell-Polymer-Bioreactor System." Experimental Cell Research 240(1): 58-65.

Freed, L. E., C. Vunjak-Novakovic, et al. (1993). "Cultivation of Cell-Polymer Cartilage Implants in Bioreactors." Journal of Cellular Biochemistry 51(3): 257-264.

Freed, L. E., G. Vunjak-Novakovic, et al. (1993). "Kinetics of Chondrocyte Growth in Cell-Polymer Implants." Biotechnology and Bioengineering 43: 597-604.

Freed, L. E., R. Langer, et al. (1997). "Tissue engineering of cartilage in space." Proc Natl Acad Sci U S A 94(25): 13885-90.

Freed, L., J. Marquis, et al. (1993). "Neocartilage Formation in vitro and in vivo Using Cells Cultured on Synthetic Biodegradable Polymers." Journal of Biomedical Materials Research 27(1): 11-23.

Frenkel, S. R. and P. E. Di Cesare (1999). "Degradation and Repair of Articular Cartilage." Frontiers in Bioscience 4: 671-685.

Gemmiti, C. V. and R. E. Guldberg (2006). "Fluid Flow Increases Type II Collagen Deposition and Tensile Mechanical Properties in Bioreactor-Grown Tissue-Engineered Cartilage." Tissue Eng 12(3): 469-79.

Genitrix. "Naturally Crosslinked Type II Triple Helix Collagen." Retrieved 2005, from http://www.genitrix.co.uk/products/collamenddata.htm.

Giannoni, P., A. Crovace, et al. (2005). "Species Variability in the Differentiation Potential of in vitro-Expanded Articular Chondrocytes Restricts Predictive Studies on Cartilage Repair using Animal Models." Tissue Eng 11(1-2): 237-48.

Giauque, W. F. and P. F. Meads (1941). "The Heat Capacities and Entropies of Aluminum and Copper from 15 to 300°K." Journal of the Amercian Chemical Society 63(7): 1897-1901.

Goldstein, A. S., T. M. Juarez, et al. (2001). "Effect of Convection on Osteoblastic Cell Growth and Function in Biodegradable Polymer Foam Scaffolds." Biomaterials 22: 1279-1288.

Gonzalez, R. J. and J. B. Tarloff (2001). "Evaluation of Hepatic Subcellular Fractions for Alamarblue and MTT Reductase Activity." Toxicol In Vitro 15(3): 257-9.

Grimshaw, M. J. and R. M. Mason (2001). "Modulation of Bovine Articular Chondrocyte Gene Expression in vitro by Oxygen Tension." Osteoarthritis Cartilage 9(4): 357-64.

Guan, J., J. P. Urban, et al. (2006). "Effects of Rapid Cooling on Articular Cartilage." Cryobiology 52(3): 430-9.

Guilak, F., R. A. Zell, et al. (1999). "Mechanically Induced Calcium Waves in Articular Chondrocytes are Inhibited by Gadolinium and Amiloride." J Orthop Res 17(3): 421-9.

Hardingham, T., T. Simon, et al. (2002). "Tissue Engineering: Chondrocytes and Cartilage." Arthritis Research 4(Suppl 3): S63-S68.

Hedbom, E., P. Antonsson, et al. (1992). "Cartilage Matrix Proteins. An Acidic Oligomeric Protein (COMP) Detected Only in Cartilage." J Biol Chem 267(9): 6132-6.

Heneghan, P. and P. E. Riches (2008). "Determination of the Strain-Dependent Hydraulic Permeability of the Compressed Bovine Nucleus Pulposus." J Biomech 41(4): 903-6.

Hines, A. L. and R. N. Maddox (1985). Mass Transfer: Fundamentals and Applications. Englewood Cliffs, NY, Prentics Hall.

Hodge, W. A., R. S. Fujan, et al. (1986). "Contact Pressures in the Human Hip Joint Measured in Vivo." Proceedings of the National Academy of Sciences of the United States of America 83(9): 2879-2883.

Holden, P., D. R. Keene, et al. (2005). "Secretion of Cartilage Oligomeric Matrix Protein is Affected by the Signal Peptide." J Biol Chem 280(17): 17172-9.

Holden, P., R. S. Meadows, et al. (2001). "Cartilage Oligomeric Matrix Protein Interacts with Type IX Collagen, and Disruptions to These Interactions Identify a Pathogenetic Mechanism in a Bone Dysplasia Family." J Biol Chem 276(8): 6046-55.

Holmes, M. H. and V. C. Mow (1990). "The Nonlinear Characteristics of Soft Gels and Hydrated Connective Tissues in Ultrafiltration." J Biomech 23(11): 1145-56.

Hunziker, E. B. (2000). "Articular Cartilage Repair: Problems and Perspectives." Biorheology 37: 163-164.

Hunziker, E. B., T. M. Quinn, et al. (2002). "Quantitative Structural Organization of Normal Adult Human Articular Cartilage." Osteoarthritis and Cartilage 10(7): 564-572.

Imhof, H., I. Sulzbacher, et al. (2000). "Subchondral Bone and Cartilage Disease." Investigative Radiology 35(10): 581-588.

Imhof, H., M. Breitenseher, et al. (1999). "Importance of Subchondral Bone to Articular Cartilage in Health and Disease." Topics in Magnetic Resonance Imaging 10(3): 180-192.

Jeffery, A. K., G. W. Blunn, et al. (1991). "Three-Dimensional Collagen Architecture in Bovine Articular Cartilage." The Journal of Bone and Joint Surgery 73(5): 795-801.

Jin, C. Z., S. R. Park, et al. (2007). "In vivo Cartilage Tissue Engineering using a Cell-Derived Extracellular Matrix Scaffold." Artif Organs 31(3): 183-92.

Jung, Y., S. H. Kim, et al. (2008). "Cartilaginous Tissue Formation using a Mechano-Active Scaffold and Dynamic Compressive Stimulation." J Biomater Sci Polym Ed 19(1): 61-74.

Khirabadi, B. S., Y. C. Song, et al. (2001). Method of Cryopreservation of Blood Vessels by Vitrification. United States, Organ Recovery Systems, Inc. (Chicago, IL).

Kim, H., M. Moran, et al. (1991). "The Potential for Regeneration of Articular Cartilage in Defects Created by Chondral Shaving and Subchondral Abrasion. An Experimental Investigation in Rabbits." The Journal of Bone and Joint Surgery. American volume 73(9): 1301-1315.

Kim, W. S., J. P. Vacanti, et al. (1994). "Cartilage Engineered in Predetermined Shapes Employing Cell Transplantation on Synthetic Biodegradable Polymers." Plastic and Reconstructive Surgery 94(2): 233-240.

Kim, Y., R. Sah, et al. (1988). "Fluorometric Assay of DNA in Cartilage Explants using Hoechst 33258." Analytical Biochemistry 174(1): 168-176.

Kisiday, J. D., M. Jin, et al. (2004). "Effects of Dynamic Compressive Loading on Chondrocyte Biosynthesis in Self-Assembling Peptide Scaffolds." J Biomech 37(5): 595-604.

Krishnan, R., S. Park, et al. (2003). "Inhomogeneous Cartilage Properties Enhance Superficial Interstitial Fluid Support and Frictional Properties, but do not Provide a Homogeneous State of Stress." J Biomech Eng 125(5): 569-77.

Kuettner, K. E., M. B. Aydelotte, et al. (1991). "Articular Cartilage Matrix and Structure: a Minireview." The Journal of Rheumatology. Supplement 27: 46-48.

Laasanen, M. S., J. Töyräs, et al. (2003). "Biomechanical Properties of Knee Articular Cartilage." Biorheology 40: 133-140.

Lai, W. M., V. C. Mow, et al. (1981). "Effects of Nonlinear Strain-Dependent Permeability and Rate of Compression on the Stress Behavior of Articular Cartilage." J Biomech Eng 103(2): 61-6.

Langer, R. and J. P. Vacanti (1993). "Tissue Engineering." Science 260(5110): 920-926.

Lee, C., S. Grad, et al. (2005). The Influence of Mechanical Stimuli on Articular Cartilage Tissue Engineering. Topics in Tissue Engineering. N. Ashammakhi and R. L. Reis. 2.

LeRoux, M. A., F. Guilak, et al. (1999). "Compressive and Shear Properties of Alginate Gel: Effects of Sodium Ions and Alginate Concentration." J Biomed Mater Res 47(1): 46-53.

Lewis, M. C., B. D. Macarthur, et al. (2005). "Heterogeneous proliferation within engineered cartilaginous tissue: the role of oxygen tension." Biotechnol Bioeng 91(5): 607-15.

Lipshitz, H., R. I. Etheredge, et al. (1975). "In Vitro Wear of Articular Cartilage." The Journal of Bone and Joint Surgery American Volume 57(4): 527-534.

Loeser, R. F. (2002). "Integrins and Cell Signaling in Chondrocytes." Biorheology 39(1-2): 119-24.

Lovelock, J. E. and M. W. H. Bishop (1959). "Prevention of Freezing Damage to Living Cells by Dimethyl Sulfoxide." Nature 183: 1394-1395.

Luan, Y., L. Kong, et al. (2008). "Inhibition of ADAMTS-7 and ADAMTS-12 Degradation of Cartilage Oligomeric Matrix Protein by Alpha-2-Macroglobulin." Osteoarthritis Cartilage.

Macpherson, J. V., D. O'Hare, et al. (1997). "Quantitative Spatially Resolved Measurements of Mass Transfer through Laryngeal Cartilage." Biophys J 73(5): 2771-81.

Malaviya, P. and R. M. Nerem (2002). "Fluid-Induced Shear Stress Stimulates Chondrocyte Proliferation Partially Mediated via TGF-b1." Tissue Engineering 8(4): 581-590.

Malda, J., P. van den Brink, et al. (2004). "Effect of oxygen tension on adult articular chondrocytes in microcarrier bioreactor culture." Tissue Eng 10(7-8): 987-94.

Mandl, E. W., S. W. van der Veen, et al. (2004). "Multiplication of Human Chondrocytes with Low Seeding Densities Accelerates Cell Yield without Losing Redifferentiation Capacity." Tissue Eng 10(1-2): 109-18.

Mansour, J. M. (2004). Biomechanics of Cartilage, Lippincott Williams & Wilkins.

Marion, N. W. and J. J. Mao (2006). "Mesenchymal Stem Cells and Tissue Engineering." Methods Enzymol 420: 339-61.

Maroudas, A. and P. Bullough (1968). "Permeability of Articular Cartilage." Nature 219(160): 1260-1261.

Martin, I., D. Wendt, et al. (2004). "The Role of Bioreactors in Tissue Engineering." Trends Biotechnol 22(2): 80-6.

Martin, I., V. P. Shastri, et al. (2001). "Selective Differentiation of Mammalian Bone Marrow Stromal Cells Cultured on Three-Dimensional Polymer Foams." Journal of Biomedical Materials Research 55(2): 229-235.

Mauck, R. L., C. C. Wang, et al. (2003). "The Role of Cell Seeding Density and Nutrient Supply for Articular Cartilage Tissue Engineering with Deformational Loading." Osteoarthritis Cartilage 11(12): 879-90.

Mazur, P. (1981). Fundamental Cryobiology and the Preservation of Organs by Freezing. New York, Marcel Dekker.

Millward-Sadler, S. J., M. O. Wright, et al. (1999). "Integrin-Regulated Secretion of Interleukin 4: A Novel Pathway of Mechanotransduction in Human Articular Chondrocytes." J Cell Biol 145(1): 183-9.

Millward-Sadler, S. J., M. O. Wright, et al. (2000). "Altered Electrophysiological Responses to Mechanical Stimulation and Abnormal Signaling through Alpha5Beta1 Integrin in Chondrocytes from Osteoarthritic cartilage." Osteoarthritis Cartilage 8(4): 272-8.

Millward-Sadler, S. J., M. O. Wright, et al. (2000). "Mechanotransduction via Integrins and Interleukin-4 results in Altered Aggrecan and Matrix Metalloproteinase 3 Gene Expression in Normal, but not Osteoarthritic, Human Articular Chondrocytes." Arthritis Rheum 43(9): 2091-9.

Milosevic, J., A. Storch, et al. (2005). "Cryopreservation does not affect proliferation and multipotency of murine neural precursor cells." Stem Cells **23**(5): 681-8.

Minas, T. and S. Nehrer (1997). "Current Concepts in the Treatment of Articular Cartilage Defects." Orthopedics 20(6): 525-538.

Mobasheri, A., S. D. Carter, et al. (2002). "Integrins and Stretch Activated Ion Channels; Putative Components of Functional Cell Surface Mechanoreceptors in Articular Chondrocytes." Cell Biol Int 26(1): 1-18.

Mow, V. C. and W. M. Lai (1980). "Recent Developments in Synovial Joint Biomechanics." Society of Industrial and Applied Mathematics Review 22: 275-317.

Mow, V. C. and X. E. Guo (2002). "Mechano-Electrochemical Properties of Articular Cartilage: Their Inhomogeneities and Anisotropies." Annual Review of Biomedical Engineering 4: 175-209.

Mow, V. C., A. Ratcliffe, et al. (1992). "Cartilage and Diarthrodial Joints as Paradigms for Hierarchical Materials and Structures." Biomaterials 13(2): 67-97.

Mow, V. C., M. H. Holmes, et al. (1984). "Fluid Transport and Mechanical Properties of Articular Cartilage: A Review." Journal of Biomechanics 17(5): 377-394.

Mow, V. C., S. C. Kuei, et al. (1980). "Biphasic Creep and Stress Relaxation of Articular Cartilage in Compression? Theory and Experiments." J Biomech Eng 102(1): 73-84.

Muir, H. (1995). "The Chondrocyte, Architect of Cartilage. Biomechanics, Structure, Function and Molecular Biology of Cartilage Matrix Macromolecules." Bioessays 17(12): 1039-1048.

Mukherjee, I. N. (2008). A Rational Design Approach for the Cryopreservation of Natural and Engineered Tissues. Chemical and Biomolecular Engineering. Atlanta, Georgia Institute of Technology. Doctor of Philosophy.

Mukherjee, I. N., Y. Li, et al. (2008). "Cryoprotectant Transport through Articular Cartilage for Long-Term Storage: Experimental and Modeling Studies." Osteoarthritis Cartilage.

Muldrew, K. and L. E. McGann (1998). Cryobiology - A Short Course. Chapter 6.2 - The Freezing Process. U. o. Alberta. Alberta, Canada.

Muldrew, K. and L. E. McGann (1998). Cryobiology - A Short Course. Chapter 8.1 – Cryoprotective Compounds. U. o. Alberta. Alberta, Canada.

Murphy, C. L. and S. Athanassios (2001). "Effect of Oxygen Tension and Alginate Encapsulation on Restoration of the Differentiated Phenotype of Passaged Chondrocytes." Tissue Engineering 7(6): 791-803.

National Center for Health Statistics. (2007). "National Health Interview Survey Arthritis Surveillance." Retrieved 2008, from http://www.cdc.gov/arthritis/data_statistics/national_data_nhis.htm#future.

Nawroth, F., G. Rahimi, et al. (2005). "Cryopreservation in Assisted Reproductive Technology: New Trends." Semin Reprod Med 23(4): 325-35.

Nenes, A. (2003). "Computational Fluid Dynamics Webpage." Retrieved January 2008, from http://nenes.eas.gatech.edu/CFD/1phase/PCCAV1/PCcav.htm.

Nerem, R. M. and A. Sambanis (1995). "Tissue Engineering: From Biology to Biological Substitutes." Tissue Engineering 1: 3-13.

Ochoa, E. R. and J. P. Vacanti (2002). "An Overview of the Pathology and Approaches to Tissue Engineering." Annals of the New York Academy of Sciences 979: 10-26, 35-38.

Orazizadeh, M., H. S. Lee, et al. (2008). "CD47 associates with Alpha 5 Integrin and Regulates Responses of Human Articular Chondrocytes to Mechanical Stimulation in an in vitro Model." Arthritis Res Ther 10(1): R4.

Park, S., C. T. Hung, et al. (2004). "Mechanical Response of Bovine Articular Cartilage under Dynamic Unconfined Compression Loading at Physiological Stress Levels." Osteoarthritis Cartilage 12(1): 65-73.

Passaretti, D., R. Silverman, et al. (2001). "Cultured Chondrocytes Produce Injectable Tissue-Engineered Cartilage in Hydrogel Polymer." Tissue Engineering 7(6): 805-815.

Pazzano, D., K. A. Mercier, et al. (2000). "Comparison of Chondrogensis in Static and Perfused Bioreactor Culture." Biotechnology Progress 16(5): 893-896.

Pearson, L. L. (2006). Total Knee and Hip Replacement Surgery Projections Show Meteoric Rise by 2030 Retrieved May 20, 2008, from http://www6.aaos.org/news/Pemr/press_release.cfm?PRNumber=442.

Pegg, D. E., L. Wang, et al. (2006). "Cryopreservation of Articular Cartilage. Part 3: the Liquidus-Tracking Method." Cryobiology 52(3): 360-8.

Pegg, D. E., M. C. Wusteman, et al. (2006). "Cryopreservation of Articular Cartilage. Part 1: Conventional Cryopreservation Methods." Cryobiology 52(3): 335-46.

Polge, C., A. Y. Smith, et al. (1949). "Revival of Spermatozoa after Vitrification and Dehydration at Low Temperatures." Nature 164: 666.

Poole, A. R., T. Kojima, et al. (2001). "Composition and Structure of Articular Cartilage: A Template for Tissue Repair." Clinical Orthopaedics Related Research(391 Suppl): S26-S33.

Puelacher, W. C., S. W. Kim, et al. (1994). "Tissue-Engineered Growth of Cartilage: The Effect of Varying the Concentration of Chondrocytes Seeded onto Synthetic Polymer Matrices." International Journal of Oral and Maxillofacial Surgery 23(1): 49-53.

Raimondi, M. T., M. Colombo, et al. (2003). Biomechanical Evaluation of Chondrocyte-Seeded Scaffolds for Cartilage Tissue Engineering. 2003 Summer Bioengineering Conference. Sonesta Beach Resort in Key Biscayne, FL: 277-278.

Raimondi, M. T., M. Moretti, et al. (2006). "The Effect of Hydrodynamic Shear on 3D Engineered Chondrocyte Systems Subject to Direct Perfusion." Biorheology 43(3-4): 215-22.

Rajpurohit, R., C. J. Koch, et al. (1996). "Adaptation of Chondrocytes to Low Oxygen Tension: Relationship Between Hypoxia and Cellular Metabolism." Journal of Cellular Physiology 168(2): 424-432.

Rangamani, P. (2005). Bioprocessing Conditions for Improving Material Properties of Tissue Engineered Cartilage. Chemical and Biomolecular Engineering. Atlanta, Georgia Institute of Technology.

Razaq, S., R. J. Wilkins, et al. (2003). "The Effect of Extracellular pH on Matrix Turnover by Cells of the Bovine Nucleus Pulposus." Eur Spine J 12(4): 341-9.

Richette, P., M. Corvol, et al. (2003). "Estrogens, Cartilage, and Osteoarthritis." Joint Bone Spine 70: 257-262.

Riesle, J., A. P. Hollander, et al. (1998). "Collagen in Tissue-Engineered Cartilage: Types, Structure, and Crosslinks." Journal of Cellular Biochemistry 71: 313-327.

Roos, E. M. and L. Dahlberg (2005). "Positive Effects of Moderate Exercise on Glycosaminoglycan Content in Knee Cartilage: a Four-Month, Randomized, Controlled Trial in Patients at Risk of Osteoarthritis." Arthritis and Rheumatism 52(11): 3507-14.

Roughley, P. J. (2001). "Articular Cartilage and Changes in Arthritis: Noncollagenous Proteins and Proteoglycans in the Extracellular Matrix of Cartilage." Arthritis Res 3(6): 342-7.

Roughley, P. J. (2006). "The Structure and Function of Cartilage Proteoglycans." Eur Cell Mater 12: 92-101.

Runstadler, P. W. (1992). "The Importance of Cell Physiology to the Performance of Animal and Cell Bioreactors." Annals of the New York Academy of Sciences 665: 380-390.

Saini, S. (2001). Bioreactor for the Production of Tissue Engineered Cartilage: Defining Operating Parameters for Optimal Construct Growth. Chemical Engineering. Atlanta, Georgia Institute of Technology. Doctor of Philosophy.

Saini, S. and T. M. Wick (2003). "Concentric Cylinder Bioreactor for Production of Tissue Engineered Cartilage: Effect of Seeding Density and Hydrodynamic Loading on Construct Development." Biotechnology Progress 19: 510-521.

Saini, S. and T. Wick (2004). "Effect of Low Oxygen Tension on Tissue-Engineered Cartilage Construct Development in the Concentric Cylinder Bioreactor." Tissue Engineering 10(5/6): 825-832.

Salter, D. M., M. O. Wright, et al. (2004). "NMDA Receptor Expression and Roles in Human Articular Chondrocyte Mechanotransduction." Biorheology 41(3-4): 273-81.

Schumann, S. C., J. G. Aston, et al. (1942). "The Heat Capacity and Entropy, Heats of Fusion and Vaporization and the Vapor Pressures of Isopentane." Journal of the Amercian Chemical Society 64(5): 1039-1043.

Seidel, J. O., M. Pei, et al. (2004). "Long-Term Culture of Tissue Engineered Cartilage in a Perfused Chamber with Mechanical Stimulation." Biorheology 41(3-4): 445-58.

Sharma, B. and J. H. Elisseeff (2004). "Engineering Structurally Organized Cartilage and Bone Tissues." Annals of Biomedical Engineering 32(1): 148-159.

Shieh, A. C. and K. A. Athanasiou (2003). "Principles of Cell Mechanics for Cartilage Tissue Engineering." Annals of Biomedical Engineering 31: 1-11.

Sikavitsas, V. I., G. N. Bancroft, et al. (2003). "Mineralized Matrix Deposition by Marrow Stromal Osteoblasts in 3D Perfusion Culture Increases with Increasing Fluid Shear Forces." Proc Natl Acad Sci U S A 100(25): 14683-8.

Silver, F. H., D. L. Christiansen, et al. (2001). "Transition from Viscous to Elastic-Based Dependency of Mechanical Properties of Self-Assembled Type I Collagen Fibers." Journal of Applied Polymer Science 79(1): 134-142.

Slivka, M. A., Neil C. Leatherbury, et al. (2001). "Porous, Resorbable, Fiber-Reinforced Scaffolds Tailored for Articular Cartilage Repair." Tissue Engineering 7(6): 767-780.

Soltz, M. A. and G. A. Ateshian (1998). "Experimental Verification and Theoretical Prediction of Cartilage Interstitial Fluid Pressurization at an Impermeable Contact Interface in Confined Compression." J Biomech 31(10): 927-34.

Song, Y. C., F. G. Lightfoot, et al. (2003). "Vitreous Preservation of Rabbit Articular Cartilage." Cell Preservation Technology 2(1): 1-8.

Spiteri, C. G., E. W. Young, et al. (2008). "Substrate Architecture and Fluid-Induced Shear Stress during Chondrocyte Seeding: Role of Alpha5Beta1 Integrin." Biomaterials 29(16): 2477-89.

Stading, M. and R. Langer (1999). "Mechanical Shear Properties of Cell-Polymer Cartilage Constructs." Tissue Eng 5(3): 241-50.

Steele, C. and P. Pinsky. (2008). "Thermal Conductivity: Aluminum." Retrieved 2008, from http://www.efunda.com/materials/elements/TC_Table.cfm?Element_ID=Al.

Stegemann, H. and K. Stalder (1967). "Determination of Hydroxyproline." Clin Chim Acta 18(2): 267-73.

Stockwell, R. A. (1979). Biology of Cartilage Cells. Cambridge, Cambridge University Press.

Stoop, R. (2008). "Smart Biomaterials for Tissue Engineering of Cartilage." Injury 39 Suppl 1: S77-87.

Sucosky, P., D. F. Osorio, et al. (2004). "Fluid Mechanics of a Spinner-Flask Bioreactor." Biotechnology and Bioengineering 85(1): 34-46.

Temenoff, J. S. and A. G. Mikos (2000). "Injectable Biodegradable Materials for Orthopedic Tissue Engineering." Biomaterials 21(23): 2405-2412.

Thur, J., K. Rosenberg, et al. (2001). "Mutations in Cartilage Oligomeric Matrix Protein causing Pseudoachondroplasia and Multiple Epiphyseal Dysplasia affect Binding of Calcium and Collagen I, II, and IX." J Biol Chem 276(9): 6083-92.

Tomchaney, A. P., J. P. Morris, et al. (1982). "Purification, Composition, and Physical Properties of a Thermal Hysteresis "Antifreeze" Protein from Larvae of the Beetle, Tenebrio Molitor." Biochemistry 21(4): 716-21.

U.S.CoastGuard (1999). Chemical Hazards Response Information System: Isopentane, United States Department of Transportation, United States Coast Guard.

Urban, J. P. (2000). "Present Perspectives on Cartilage and Chondrocyte Mechanobiology." Biorheology 37(1-2): 185-190.

Vacanti, C. A., R. Langer, et al. (1991). "Synthetic Polymers Seeded with Chondrocytes Provide a Template for New Cartilage Formation." Plastic and Reconstructive Surgery 88(5): 753-759.

Valhmu, W. B. and F. J. Raia (2002). "Myo-Inositol 1,4,5-Trisphosphate and Ca(2+)/Calmodulin-Dependent Factors Mediate Transduction of Compression-Induced Signals in Bovine Articular Chondrocytes." Biochem J 361(Pt 3): 689-96.

van Osch, G. J. V. M., E. W. Mandl, et al. (2002). "Growth Factors in Cartilage Tissue Engineering." Biorheology 39: 215-220.

Voet, D. and J. G. Voet (2004). Biochemistry, John Wiley and sons, Inc.

Vunjak-Novakovic, G., B. Obradovic, et al. (1998). "Dynamic Cell Seeding of Polymer Scaffolds for Cartilage Tissue Engineering." Biotechnology Progress 14(2): 193-202.

Vunjak-Novakovic, G., I. Martin, et al. (1999). "Bioreactor Cultivation Conditions Modulate the Composition and Mechanical Properties of Tissue-Engineered Cartilage." Journal of Orthopaedic Research 17(1): 130-138.

Vunjak-Novakovic, G., L. E. Freed, et al. (1996). "Effects of Mixing on the Composition and Morphology of Tissue-Engineered Cartilage." American Institute of Chemical Engineers Journal 42(3): 850-860.

Wakitani, S., T. Goto, et al. (1994). "Mesenchymal Cell-Based Repair of Large, Full-Thickness Defects of Articular Cartilage." The Journal of Bone and Joint Surgery 76-A(4): 579-592.

Watt, F. M. (1988). "Effect of Seeding Density on Stability of the Differentiate Phenotype of Pig Articular Chondrocytes in Culture." Journal of Cell Science 89(Pt 3): 373-378.

Wernike, E., Z. Li, et al. (2008). "Effect of Reduced Oxygen Tension and Long-Term Mechanical Stimulation on Chondrocyte-Polymer Constructs." Cell Tissue Res 331(2): 473-83.

Wheeless, C. R., III. (2005). "Chondroitin and Keratin Sulfate." Wheeless' Textbook of Orthopaedics Retrieved 2005, from http://www.wheelessonline.com/ortho/chondroitin_and_keratin_sulfate.

Wilkins, R. J., J. A. Browning, et al. (2000). "Chondrocyte regulation by Mechanical Load." Biorheology 37(1-2): 67-74.

Williams, K. A., S. Saini, et al. (2002). "Computational Fluid Dynamics Modeling of Steady-State Momentum and Mass Transport in a Bioreactor for Cartilage Tissue Engineering." Biotechnology Progress 18: 951-963.

Wiseman, M., D. L. Bader, et al. (2004). "Passage in Monolayer Influences the Response of Chondrocytes to Dynamic Compression." Biorheology 41(3-4): 283-98.

Woessner, J. F., Jr. (1961). "The Determination of Hydroxyproline in Tissue and Protein Samples Containing Small Proportions of this Imino Acid." Archives of Biochemistry and Biophysics 93: 440-447.

Wong, M., P. Wuethrich, et al. (1996). "Zone-specific Cell Biosynthetic Activity in Mature Bovine Articular Cartilage: a New Method Using Confocal Microscopic Stereology and Quantitative Autoradiography." Journal of Orthopaedic Research 14(3): 424-432.

Wright, M., P. Jobanputra, et al. (1996). "Effects of Intermittent Pressure-Induced Strain on the Electrophysiology of Cultured Human Chondrocytes: Evidence for the Presence of Stretch-Activated Membrane Ion Channels." Clin Sci (Lond) 90(1): 61-71.

Xie, J., Z. Han, et al. (2007). "Mechanical Loading-Dependence of mRNA Expressions of Extracellular Matrices of Chondrocytes Inoculated into Elastomeric Microporous Poly(L-Lactide-co-Epsilon-Caprolactone) Scaffold." Tissue Eng 13(1): 29-40.

Xu, X., J. P. Urban, et al. (2006). "Influence of Perfusion on Metabolism and Matrix Production by Bovine Articular Chondrocytes in Hydrogel Scaffolds." Biotechnol Bioeng 93(6): 1103-11.

Yamashita, I., T. Tojo, et al. (2001). "Low-Temperature Heat Capacity of Sodium Borosilicate Glasses at Temperature from 14 K to 300 K." The Journal of Chemical Thermodynamics 33: 535-554.

Yasuda, T. (2006). "Cartilage Destruction by Matrix Degradation Products." Mod Rheumatol 16(4): 197-205.

Youn, J. I., S. A. Telenkov, et al. (2000). "Optical and Thermal Properties of Nasal Septal Cartilage." Lasers Surg Med 27(2): 119-28.

Zachariassen, K. E. and E. Kristiansen (2000). "Ice Nucleation and Antinucleation in Nature." Cryobiology 41(4): 257-79.

Zaucke, F., R. Dinser, et al. (2001). "Cartilage Oligomeric Matrix Protein (COMP) and Collagen IX are Sensitive Markers for the Differentiation State of Articular Primary Chondrocytes." Biochem J 358(Pt 1): 17-24.

Zhang, Y., T. E. McAlindon, et al. (1998). "Estrogen Replacement Therapy and Worsening of Radiographic Knee Osteoarthritis: The Framingham Study." Arthritis and Rheumatism 41(10): 1867-1873.

Zhu, W., V. C. Mow, et al. (1993). "Viscoelastic Shear Properties of Articular Cartilage and the Effects of Glycosidase Treatments." J Orthop Res 11(6): 771-81.